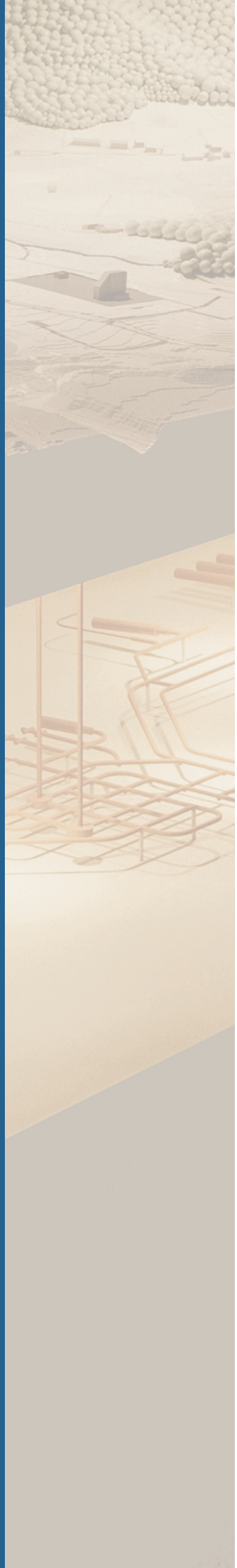

nagra.

TECHNICAL REPORT 23-07

Radionuclide Retention in the Cementitious Near-field of a Repository for Low- and Intermediate-level Waste: Development of the Cement Sorption Database

December 2023

Nagra | National Cooperative for the Disposal of Radioactive Waste
Hardstrasse 73 | 5430 Wettingen | Switzerland
T. +41 56 437 11 11 | info@nagra.ch | nagra.ch

nagra.

TECHNICAL REPORT 23-07

Radionuclide Retention in the Cementitious Near-field of a Repository for Low- and Intermediate-level Waste: Development of the Cement Sorption Database

December 2023

J. Tits[1] & E. Wieland[2]

[1]Paul Scherrer Institute, Villigen PSI, Switzerland

[2]CWL Solutions GmbH, Kleindöttingen, Switzerland

Nagra | National Cooperative for the Disposal of Radioactive Waste
Hardstrasse 73 | 5430 Wettingen | Switzerland
T. +41 56 437 11 11 | info@nagra.ch | nagra.ch

ISSN 1015-2636

Abstract

This report documents the cement sorption database (SDB) for the cementitious near-field of Switzerland's future deep geological repository for low- and intermediate-level waste (L/ILW repository). The current update of sorption values is based on earlier SDBs prepared within the framework of the Swiss waste management programme. The updated cement SDB is intended for use in safety assessment calculations. Sorption values were selected based on the values and procedures reported in earlier SDBs, taking into account the results from in-house experimental studies and from work published in the open literature. In contrast to previous SDBs, sorption values were also assigned to the radionuclides considered for safety analysis in the fourth stage of the cement degradation process.

In addition to the sorption values, this report also includes a compilation of sorption reduction factors resulting from the presence of cement-derived colloids and important complexing ligands as well as from sorption competition with iron-corrosion products and stable isotopes present in the cementitious near-field. The sorption reduction factors linked to colloids and complexing ligands were assigned on the basis of information on their concentrations in the near-field and their complexing properties, while sorption reduction due to sorption competition was assessed by estimating the effect of the solubility-limited concentrations of key radionuclides on the sorption capacity of calcium silicate hydrates (C-S-H).

Zusammenfassung

Dieser Bericht umfasst die Zusammenstellung einer Zement-Sorptionsdatenbank (SDB) für das zementhaltige Nahfeld des Schweizer Tiefenlagers für schwach- und mittelaktive Abfälle (SMA-Lager). Die vorliegende Aktualisierung der Sorptionswerte basiert auf früheren Datenbanken, die im Rahmen des schweizerischen Entsorgungsprogramms erstellt wurden. Die aktualisierte Zement-SDB ist für Berechnungen für den Langzeitsicherheitsnachweis vorgesehen. Die Sorptionswerte wurden auf der Grundlage der in den früheren Datenbanken angegebenen Werte und Verfahren ausgewählt, wobei die Ergebnisse aus eigenen experimentellen Studien und aus Arbeiten, die in der freien Literatur veröffentlicht worden sind, mitberücksichtigt wurden. Im Unterschied zu den früheren Datenbanken wurden auch Sorptionswerte für die dosisrelevanten Radionuklide in der vierten Stufe des Zementabbaus zugeordnet.

Zusätzlich zu den Sorptionswerten enthält dieser Bericht auch eine Zusammenstellung von Sorptionsminderungsfaktoren durch die Anwesenheit von zementartigen Kolloiden sowie wichtigen komplexbildenden Liganden und durch Sorptionskonkurrenz mit Eisenkorrosionsprodukten und stabilen Isotopen, die im Nahfeld vorhanden sind. Die Sorptionsminderungsfaktoren durch Kolloide und komplexbildende Liganden wurden auf der Grundlage der verfügbaren Informationen über ihre Konzentrationen im SMA-Nahfeld und ihre komplexbildenden Eigenschaften zugewiesen. Die Sorptionsminderung durch Sorptionskonkurrenz wurde bewertet, indem die Auswirkungen der löslichkeitsbegrenzten Konzentrationen der wichtigsten Radionuklide auf die Sorptionskapazität von Kalziumsilikathydraten (C-S-H Phasen) beurteilt wurden.

Table of Contents

Abstract I

Zusammenfassung II

Table of Contents III

List of Tables VI

List of Figures VIII

List of Acronyms IX

1 Introduction 1

1.1 Deep geological repositories for low- and intermediate level waste 1

1.2 Objective of this report – a cement sorption database 2

1.3 Composition of hydrated cement and cement porewater at different stages of cement degradation 4

1.4 Update on sorption values and sorption reduction factors 5

1.5 Considered dose-relevant radionuclides for safety analysis 6

2 Cement porewaters and phase assemblage 9

2.1 Thermodynamic modelling of the porewater composition and phase assemblage for cementitious systems 9

2.2 Model description 10

2.3 Consequences of the compositions of HCP and CPW for SDB development 14

3 Selected sorption data for cement degradation stages I to III 23

3.1 Not re-assessed, not revised sorption values 23

3.2 Re-assessed, not revised sorption values 23

3.2.1 Lanthanides and actinides 23

3.2.2 Alkaline and earth alkaline metals 28

3.2.3 Transition and other metals 33

3.2.4 Anions 40

3.3 Re-assessed, revised sorption values 41

3.3.1 Actinides and lanthanides 41

3.3.2 Alkaline and earth alkaline metals 44

3.3.3 Transition and other metals 45

3.3.4 Anions 47

3.4 New dose-relevant elements 61

3.4.1 Lanthanides and actinides 61

3.4.2 Alkaline and earth alkaline metals 62

3.4.3 Transition and other metals 62

3.4.4 Anions 65

4 Shared solubility and isotopic exchange processes 67
4.1 Definition of operational R_d values 67
4.2 $^{59/63}Ni$ and $^{14}CO_3^{2-}$ retention 68
4.3 ^{41}Ca, ^{26}Al and ^{32}Si retention 72

5 Selected sorption data for stage IV of the cement degradation process 75
5.1 Composition of near-field mineralogy and porewater 75
5.2 Methodology 75
5.3 Recommended sorption values 77

6 Sorption reduction factors 79
6.1 Sorption reduction by cementitious colloids 79
6.2 Sorption reduction by complexing ligands 79
6.3 Sorption reduction factors associated with complexing agents 89
6.3.1 Sorption reduction due to the presence of ISA 89
6.3.2 Sorption reduction due to the presence of GLU 91
6.3.3 Sorption reduction due to the presence of EDTA 92
6.3.4 Sorption reduction by minor complexing ligands 94
6.4 Sorption competition 94

7 Compilation of sorption values and sorption reduction factors 97

8 References 111

App. A Assessment of sorption reduction factors A-1
A.1 List of abbreviations A-1
A.2 Derivation of reduction factors accounting for aqueous complexation, sorption onto dispersed colloids and sorption competition A-2
A.2.1 Effect of complexation with aqueous organic ligands, L, on radionuclide uptake by cement paste A-4
A.2.2 Effect of dispersed colloids on radionuclide uptake by cement paste in the presence and absence of complexing ligands A-6
A.2.3 Overall effect of metal complexation and metal sorption on dispersed colloids on radionuclide uptake by cement paste A-9
A.2.4 Overall effect of metal complexation, metal sorption on dispersed colloids and sorption competition on radionuclide uptake by cement paste A-11

App. B Sorption competition B-1
B.1 Introduction B-1
B.2 Conceptual approach B-1
B.3 Near-field parameters B-2
B.4 Cement phases and radionuclides involved B-3
B.5 Interaction of corrosion products with C-S-H phases B-6
B.6 Sorption competition of Fe(II,III) with dose-relevant radionuclides B-11
B.7 Maximum loadings of dose-relevant radionuclides and stable isotopes B-13

B.8 Comparison of elemental loadings and sorption capacity on C-S-H phases ... B-23
B.9 Recommendation for an appraisal of sorption competition in the cementitious near-field of an L/ILW repository ... B-27

App. C Influence of EDTA on radionuclide speciation ... C-1
C.1 Database and code ... C-1
C.2 Porewater compositions ... C-1
C.3 Operational approach for deriving "EDTA solubility enhancement factors" ... C-1

App. D Cement sorption values for the cement-based near-field for Nagra's safety analysis ... D-1
D.1 Introduction ... D-1
D.1.1 Data basis for deriving the cement sorption values ... D-1
D.1.2 Influence of the composition of C-S-H phases on the sorption behaviour of HCP ... D-3
D.1.3 Complexing ligands ... D-3
D.2 Derivation of the sorption values for the cement-based near-field for the safety analysis ... D-4
D.2.1 Approach ... D-4
D.3 Extended assumptions for the derivation of the sorption values ... D-6
D.4 Derivation of lower pessimistic limits for waste groups 1 and 2 based on the solubility calculations of dose-relevant nuclides in the cement porewater ... D-7
D.5 Derived sorption values for the safety analysis ... D-9

List of Tables

Tab. 1-1: Considered dose-relevant radionuclides for safety analysis 6

Tab. 1-2: Redox states of redox-sensitive elements in aqueous media under highly alkaline conditions considered in this study 7

Tab. 2-1: Composition of CEM I 52.5 R 11

Tab. 2-2: NL-ZNO-22 porewater composition 12

Tab. 2-3: Geochemical conditions (solids, porewater composition) in DS-I, DS-II, DS-III assuming a hydrated cement porosity of ~ 20%, oxic/ reducing conditions in DS-I and reducing conditions in DS-II and DS-III 13

Tab. 2-4: Geochemical conditions (solids, porewater composition) for cement paste, CEM I 52.5 N HTS in DS-I, DS-II, DS-III used in the SDB for Stage 2 of the Sectoral Plan 15

Tab. 2-5: Mineral composition of cement paste, CEM I 52.5 N HTS, after about 3 years of hydration (w/c = 1.3) considered in the development of the CEM-14 SDB for Stage 2 of the Sectoral Plan 18

Tab. 3-1: R_d values measured by Lange et al. (2020) for Mo(VI) sorption on various cement phases as well as aged HCP under three different chemical conditions 60

Tab. 4-1: Characteristic parameters of the L/ILW repository per metre of cavern length 68

Tab. 4-2: Input data used to calculate distribution ratios for $^{59,63}Ni$ and $^{14}CO_3^{2-}$ on HCP 70

Tab. 4-3: Estimated R_d values for $^{59,63}Ni$ and $^{14}CO_3^{2-}$ for the three stages of cement degradation of the L/ILW repository 71

Tab. 4-4: Input data used to calculate distribution ratios for ^{41}Ca, ^{26}Al and ^{32}Si on HCP 73

Tab. 4-5: Estimated operational R_d values for ^{41}Ca, ^{26}Al and ^{32}Si for the three stages of cement degradation in the L/ILW repository 74

Tab. 5-1: Geochemical conditions (solids, porewater composition) for DS-IV of cementitious materials (provisional container concrete, mortar M1, container-filling cement) modelled by assuming the degradation of the HCP by carbonation or the dissolution of siliceous aggregates 76

Tab. 6-1: Maximum concentration and concentration limit for the waste group assignment of complexing ligands in near-field porewater 80

Tab. 6-2: Recommended sorption reduction factors in the presence of ISA and GLU 92

Tab. 6-3: Summary of solubilities without and with 0.025 M EDTA for selected elements in CPW expected in DS-II 93

Tab. 6-4: Recommended sorption reduction factors in the presence of EDTA, CN^- and NO_3^-/NO_2^- 93

Tab. 7-1: Sorption values for unperturbed HCP (m^3/kg) in cement degradation stages I – III under oxidising (oxid.) and reducing (red.) conditions 97

Tab. 7-2: Lower and upper limits of the sorption values ($m^{3/}$kg) for cement degradation stages I – III (lower and upper limits as reported by Wang et al. 2012 and Ochs et al. 2011 except where indicated) 99

Tab. 7-3: Sorption reduction factors (realistic and upper bound (pessimistic) values), $F_{red,1}$, for uptake by HCP in the presence of cement-derived near-field colloids assuming a typical colloid concentration of 10^{-4} kg/m^3 101

Tab. 7-4: Sorption reduction factors for waste group 1, $F_{red,2}$, due to the presence of important complexing ligands in the porewater for cement degradation stages I – III under oxidising (oxid.) and reducing (red.) conditions 103

Tab. 7-5: Sorption reduction factors for waste group 2, $F_{red,2}$, due to the presence of important complexing ligands in the porewater for cement degradation stages I – III under oxidising (oxid.) and reducing (red.) conditions 105

Tab. 7-6: Sorption reduction factors by sorption competition in the porewater for cement degradation stages I – III of the under oxidising (oxid.) and reducing (red.) conditions, $F_{red,3}$ 107

Tab. 7-7: Sorption values for cement degradation stage IV under oxidising (oxid.) and reducing (red.) conditions in m^3/kg 108

Tab. B-1: Characteristic parameters of the L/ILW repository B-2

Tab. B-2: Concentrations of the stable counterparts of radionuclides present as impurities in unhydrated (Wieland 2014) and hydrated CEM I 52.5 N HTS and the porewater assuming DS-II, reducing conditions B-14

Tab. B-3: Maximum aqueous concentrations of the elements in cementitious environments at pH 12.5 based on solubility limits calculated by taking into account the CPW composition under anoxic conditions in DS-II B-16

Tab. B-4: Loading of C-S-H phases under near-field conditions in DS-I B-19

Tab. B-5: Loading of C-S-H phases under near-field conditions in DS-II B-20

Tab. B-6: Loading of C-S-H phases under near-field conditions in DS-III B-21

Tab. B-7: Upper bound of the loading of C-S-H phases under near-field conditions in DS-II B-22

Tab. B-8: Comparison of C-S-H loadings in the three stages of cement degradation with the maximum sorption capacity of interlayer and surface sites for the base case B-26

Tab. C-1: GEMS recipe of the anoxic all-in-one system in the presence of 0.025 M EDTA C-2

Tab. C-2: Composition of composition object “CEMIPWDS2ZrE20” C-3

Tab. C-3: Composition of composition object “RedoxMtPy” equivalent to 1 mol of magnetite and 1 mol of pyrite C-3

List of Figures

Fig. B-1: a) Schematic diagram of the tobermorite-based structure of a C-S-H phase with a C/S ratio of 1.5 obtained by removing the bridging tetrahedra and neutralising the negative charges of the silanol groups by Ca^{2+} ions. b) Schematic diagram of the tobermorite-based structure of a C-S-H phase with a C/S ratio of 0.66 and a maximum degree of protonation of the silica chains B-4

Fig. B-2: Sorption isotherms of Fe(III) on C-S-H with a target C/S ratio of 1.5 (a), and C-S-H with a target C/S ratio of 0.8 (b). The experimental data correspond to linear sorption B-7

Fig. B-3: Fe(II) sorption isotherms on C-S-H phases (target C/S ratios = 0.8 and 1.5) B-10

Fig. B-4: Np(IV) sorption into the interlayers of C-S-H phases with low (a) and high (b) C/S ratios B-24

List of Acronyms

BFS	Blast furnace slag
C-(A)-S-H	Calcium (aluminium) silicate hydrate (phases)
CDP	Cellulose degradation product
CEM I 52.5 N HTS	Sulphate-resisting Portland cement (Lafarge, France)
CPW	Cement porewater
C/S	Calcium to silica ratio of C-S-H phases
DS-I, -II, -III, -IV	Degradation stages I, II, III, IV
EDTA	Ethylenediaminetetraacetic acid
EXAFS	Extended X-ray absorption fine structure
GEM(S)	Gibbs energy minimisation (selektor)
GGBFS	Ground granulated blast furnace slag
GLU	Gluconic acid
HCP	Hardened cement paste
HLW	High-level waste
hyd	Hydrous
ILW	Intermediate-level waste
IS	Ionic strength
ISA	Isosaccharinic acid
LDH	Layered double hydroxide
L/ILW	Low- and intermediate-level waste
LLW	Low-level waste
LS	Lignosulphonates
Meth	Methacrylate
M-S-H	Magnesium silicate hydrate
mt	Redox potential imposed by the presence of magnetite (Fe_3O_4(cr)) and Fe/Al siliceous hydrogarnet
mt-py	Redox potential imposed by the presence of magnetite (Fe_3O_4(cr)) and pyrite
ncr	Nanocrystalline
NL	Nördlich Lägern
NMR	Nuclear magnetic resonance
NRVB	Nirex reference vault backfill
NTA	Nitrilotriacetic acid
OPA	Opalinus Clay
OPC	Ordinary Portland cement

PAE	Polyaryl ethers
PC	Polycarboxylate
PCE	Polycarboxylate ether
PEG	Polyacrylic or polymaleic polymers with polyethylene glycol sidechains
PFA	Pulverised fly ash
PMS	Sulphonated melamine-formaldehyde condensates
PNS	Sulphonated naphthalene-formaldehyde condensates
PSI	Paul Scherrer Institute
RBG	General licence application (*Rahmenbewilligungsgesuch*)
SA	Safety analysis
SDB	Sorption database
SF	Spent fuel
SGT-E2 and 3	Sectoral Plan for Deep Geological Repositories – Stages 2 and 3 (*Sachplan geologische Tiefenlager – Etappen 2 und 3*)
SIT	Specific ion-interaction theory
S/L	Solid-to-liquid ratio
SP	Superplasticiser
TDB	Thermodynamic database
w/b	Water-to-binder ratio
w/c	Water-to-cement ratio
XANES	X-ray absorption near-edge spectroscopy
XRD	X-ray diffraction
ZNO	Zürich Nordost

1 Introduction

1.1 Deep geological repositories for low- and intermediate level waste

In Switzerland, the Nuclear Energy Act requires the disposal of all types of radioactive waste in deep geological repositories (KEG 2003). The basic feasibility of the safe disposal of radioactive waste in a deep geological repository in a clay host rock was demonstrated by Nagra in Project *Entsorgungsnachweis* (the term translates into English as "demonstration of disposal feasibility") at the end of 2002. This feasibility study was based on the potential Opalinus Clay (OPA) host rock in the Zürcher Weinland area in Northern Switzerland and was supported by a detailed safety case (Nagra 2002b, 2002c, 2002a). At the time, two types of repositories were foreseen in Switzerland:

- a repository for the disposal of low- and intermediate-level waste (L/ILW) arising from the operation and decommissioning of Swiss nuclear power plants, from medicine, industry and research and from those reprocessing operations that produce only low-level technological waste,
- a repository for the disposal of high-level waste (HLW), comprising spent nuclear fuel (SF) and vitrified HLW, as well as long-lived intermediate-level waste (ILW), primarily resulting from fuel reprocessing.

Project *Entsorgungsnachweis* considered only the repository for SF/HLW/ILW, referred to in the following as the HLW repository.

The choice of both the Opalinus Clay and the Zürcher Weinland was the result of a preliminary, safety-based evaluation of potential host rocks, in which other possible options were also evaluated but set aside by Nagra; host-rock and site selection were later carried out in a more systematic manner following the Sectoral Plan for Deep Geological Repositories.

In September 2022, as part of Stage 3 of the siting procedure, Nagra formally proposed the Nördlich Lägern (NL) siting region, which lies within Cantons Zürich and Aargau, as the site for a combined repository for all waste types, with Opalinus Clay as the selected host rock. Nagra is currently in the process of preparing a general licence application for this site, supported by a safety case. The documentation will be submitted at the end of 2024. The present report is one of several required to demonstrate that the geological and engineered barrier systems of deep geological repositories meet all safety requirements over the time period under consideration (KEG 2003).

This report contains the cement sorption database required for the dose calculations for radionuclide release from the L/ILW near-field to be performed within the scope of the safety analyses. By design, a large amount of cementitious material will be used for the construction of the L/ILW section of the repository as well as for the conditioning of the waste and the backfilling of the caverns. The cementitious material contains a high proportion of ordinary Portland cement (OPC). A large fraction of the waste is conditioned with cementitious materials. The waste drums are placed in concrete disposal containers and the void space will be filled with cementitious material. Metallic decommissioning waste, such as activated metal parts or activated concrete blocks, will be disposed of directly in the disposal containers and filled with a cementitious suspension. The disposal containers will be stacked in the L/ILW caverns and the void space will be filled with a backfill mortar.

Cementitious materials influence the geochemical conditions in the near-field and contribute to the retention and slow release of radionuclides: 1) They create a high-pH environment that ensures low solubility for much of the radionuclide inventory and contributes to the passivation of the steel contributing to low metal corrosion rates. 2) The alkaline near-field creates hostile conditions for microbial activity. 3) Many radionuclides are strongly bound to cement minerals, reducing the concentrations in the cement porewater (CPW) and thus radionuclide mobility.

The sorption values on hardened cement paste (HCP) for the radionuclides considered for safety analysis (hereafter referred to as dose-relevant radionuclides) are therefore key input data for the calculation of the radionuclide release from the L/ILW near-field as part of the dose calculations that Nagra will perform for the safety analysis (SA) within the framework of the general licence application (RBG).

1.2 Objective of this report – a cement sorption database

The aim of this report is to develop a sorption database (SDB) containing sorption values for dose-relevant radionuclides on cementitious materials for the SA calculations to be performed by Nagra for a deep geological repository. Data from the open literature combined with results from in-house research were used to select the sorption values, taking into account current information on the waste inventories and the repository design. This cement SDB is the latest in a series that has been published over the last almost three decades and updated each time to reflect the latest state of the art. Wieland (2014) developed an SDB (CEM-14 SDB) for cementitious systems for use in the SA of a deep geological repository for L/ILW within the framework of Stage 2 of the Sectoral Plan for Deep Geological Repositories ("*Sachplan geologische Tiefenlagerung – Etappe 2, SGT-E2*") of the Swiss waste management programme for radioactive waste. The latter report was an update of previous SDBs prepared by Wieland & van Loon (2002) (referred to as CEM-02), Bradbury & van Loon (1997) (referred to as CEM-96) and Bradbury & Sarott (1994) (referred to as CEM-94) for the cementitious near-field of L/ILW and ILW repositories.

Already for the previous cement SDBs, the sorption values were selected on the basis of in-house experimental data and literature data. In-house sorption studies were carried out with the sulphate-resisting Portland cement CEM I 52.5 N HTS (Lafarge, France), which is currently used for the conditioning of L/ILW in Switzerland. In the case of the previous SDBs, the sorption values were selected by taking into account the three main stages of cement degradation.

Briefly, the stages can be characterised as follows. In stage I of cement degradation, the composition of cement porewater (CPW) is dominated by the release of alkali hydroxides (NaOH, KOH), which results in a pH of > 13. In stage II, the chemical composition of the alkali-depleted CPW is controlled by the solubility of portlandite, which fixes $[Ca]_t$ at ~ $2 \cdot 10^{-2}$ M and the pH at ~ 12.5. Stage III is reached when the portlandite is completely dissolved. In stage III, calcium silicate hydrate (C-S-H) phases dissolve incongruently, which results in a pH decrease from 12.5 to 10 and varies the Ca and Si concentrations in CPW depending on the chemical composition of the C-S-H phases, in particular the Ca/Si (C/S) ratio.

In the present study, stage IV of the cement degradation is also considered. Stage IV is reached when all Ca-bearing cement phases (portlandite, C-S-H, AFt, AFm) are dissolved. The matrix is dominated by carbonate or clayey minerals. Recent modelling showed that a cementitious near-field could be significantly altered as a result of internal and external degradation processes (Kosakowski et al. 2020, Kosakowski et al. 2023).

The compositions of the cementitious materials in the different stages of the cement degradation and the corresponding porewaters have been discussed in several reports (e.g., Wieland & Kosakowski 2020, Kosakowski et al. 2023). The most important findings from these reports are briefly summarised in Chapter 2. The composition of the cementitious materials and the corresponding CPWs in equilibrium are used as key data for the evaluation of radionuclide sorption in the different stages of cement degradation.

The sorption values listed in the tables are defined in terms of a distribution ratio, with R_d, accounting for the partitioning as follows:

$$R_d = \frac{\text{Quantity of a radionuclide sorbed per unit mass cement}}{\text{Equilibrium concentration of the radionuclide in porewater}} \left(\frac{m^3}{kg}\right) \quad (1)$$

The above equation corresponds to the disappearance of the radionuclide from solution due to uptake by the solid. The amount of a radionuclide sorbed is given by the difference between the initial radionuclide activity added to the cementitious system and the final activity in solution. An experimental approach such as this does not provide specific information on the uptake mechanism. The latter information can only be obtained on the basis of additional parameter variations in wet chemistry investigations, such as measurements at increasing solute concentrations (isotherms) and reversibility tests, or spectroscopic investigations on the coordination environment of the sorbate, which are often missing in sorption studies. Therefore, the mechanisms of the radionuclide sorption on cement paste and cement phases are often poorly known and, for some radionuclides, several mechanisms have been proposed to explain their uptake by cement paste. In this study, an attempt is made not only to assign R_d values to each radionuclide, but also to consider the radionuclide uptake process itself and the cement phases responsible for the uptake process, i.e., the uptake-controlling cement phase.

Sorption reduction due to the presence of complexing ligands (formation of water-soluble complexes), colloids (association of radionuclides with colloids, leading to an increased radionuclide mobility) or due to sorption competition can have an effect on radionuclide sorption and thus reduce the R_d value. The relationship between sorption value and sorption reduction factors is represented by the following equation (see App. A for the detailed derivation):

$$R_d^{eff} = \frac{R_d^0}{F_{red,1} \cdot F_{red,2} \cdot F_{red,3}} \quad (2)$$

$F_{red,1}$ is the factor accounting for the sorption reduction caused by dispersed colloids, $F_{red,2}$ accounts for sorption reduction due to the presence of complexing ligands in certain waste forms designated as waste groups 1 and 2 in Nagra's waste inventory, and $F_{red,3}$ accounts for sorption reduction due to sorption competition.

The methodology followed for the dose calculations within the scope of the consequence analysis is based on a so-called mixing tank approach with a homogenised, fully saturated near-field (Nagra NTB 24-18 *planned*). It should be noted that partially saturated conditions within the L/ILW near-field dominate the time period under consideration as shown by Papafotiou & Senger (2016) and explained in Martin et al. (2023). However, as thermodynamic calculations can only be performed for fully saturated conditions and as these conditions are a conservative abstraction of the repository, a full mixing tank assumption is considered for the waste group classification. Therefore, by analogy, the sorption values derived within the scope of this report are related to fully saturated conditions. The derived sorption values are therefore conservative values with regard to the mixing tank approach.

This study provides a compilation of sorption values for stages I to IV of the cement degradation (Tab. 7-1 and Tab. 7-7:) and sorption reduction factors (Tab. 7-3 to Tab. 7-6) recommended for use in the safety analysis for the RBG. The appraisal of sorption values and reduction factors is documented by briefly summarising essential considerations and thoughts in the course of the data selection.

1.3 Composition of hydrated cement and cement porewater at different stages of cement degradation

Cement degradation in the cementitious near-field of an L/ILW repository is the consequence of various processes, such as the decomposition of organic matter, the dissolution of siliceous aggregates in hyperalkaline CPW, and groundwater ingress from the surrounding host rock (Kosakowski et al. 2014, Kosakowski et al. 2020, Kosakowski et al. 2023). Cement degradation accounts for the time-dependent evolution of the mineral composition of cementitious materials in the near-field of the cement-based repository and the composition of the corresponding near-field porewater in equilibrium with these materials (Wieland & Kosakowski 2020). The degradation of cement in three main stages was predicted by earlier modelling studies (Berner 1992, Hoch et al. 2012, Jacques et al. 2010, Kosakowski et al. 2014, Neall 1994) that were developed on the basis of experimental data (e.g. Faucon et al. 1996). The three main stages with a progressively lowering pH of the porewater with time are the main feature of the diffusion-controlled models of cement degradation and can be generically summarised as follows:

Degradation stage I (DS-I): The first stage accounts for freshly hydrated cement with a pH of the porewater between 12.5 and 13.5 at 25 °C. The solution composition is dominated by high concentrations of free alkali metal ions, which are released from the clinker minerals during cement hydration. Equivalent OH^- concentrations are generated to fulfil charge balance.

Degradation stage II (DS-II): The pH of the porewater is controlled by portlandite solubility. The large inventory of the mobile alkalis has been significantly reduced due to uptake by alkali-binding minerals or due to exchange with the solutes of the porewater of the surrounding host rock. Solubility of portlandite fixes the total Ca concentration $[Ca]_{tot}$ at ~ $2 \cdot 10^{-2}$ M and the pH at ~ 12.5. This stage is characterised by the presence of portlandite and C-S-H phases with a high C/S ratio, along with other cement phases, in HCP.

Degradation stage III (DS-III): This stage follows when portlandite has completely dissolved and the incongruent dissolution of C-S-H phases occurs and dominates the evolution of the cementitious materials. As a result, the C/S ratio of the C-S-H phase changes from initially ~ 1.65 at pH ~ 12.5 to ~ 0.8 at pH ~ 10 (Atkins & Glasser 1992). Congruent dissolution of the C-S-H phases occurs at the end of DS-III, thus buffering the pH at ~ 10 (Ochs et al. 2016).

These three main stages of cement degradation are characterised by the presence of typical cement phases, such as portlandite, AFt phases (calcium aluminate ferrite trisubstituted or calcium aluminate trisubstituted), AFm phases (calcium aluminate ferrite monosubstituted or calcium aluminate monosubstituted), hydrotalcite, siliceous hydrogarnet and C-S-H. Progressing degradation of the cementitious materials results in the complete dissolution of all Ca-bearing cement phases, which is often designated as the stage IV of the cement degradation.

Degradation stage IV (DS-IV): The final stage of cement degradation is reached when all Ca-bearing cement phases (portlandite, C-S-H, AFt, AFm) have dissolved. The pH is controlled by incoming water and by equilibrium with carbonates (calcite) (Ochs et al. 2016). It should be noted that the mineralogy in this stage resembles a geological formation mainly containing clay-type minerals and carbonates rather than a cementitious environment (Jacques et al. 2010, Kosakowski et al. 2020). This final stage can only be reached if the cement is carbonated with considerable amounts of CO_2, or if Ca is leached by high fluxes of incoming formation water.

The latter process can be excluded as a possible degradation mechanism for a repository placed in a low-permeability clay formation such as OPA (Kosakowski et al. 2014, Kosakowski et al. 2023), while carbonation due to the internal production of CO_2 from degradation of organics is conceivable.

This report focuses on the first three stages of cement degradation, which are characterised by specific phase compositions of HCP and the corresponding porewaters in equilibrium with these cement phases. Information on DS-IV, including the compilation of sorption values, is added for "what-if" scenario calculations in the safety analysis.

1.4 Update on sorption values and sorption reduction factors

The present update on sorption values has been made with reference to the previous reports, CEM-94 (Bradbury & Sarott 1994), CEM-96 (Bradbury & van Loon 1997), CEM-02 (Wieland & van Loon 2002) and CEM-14 SDBs (Wieland 2014). Sorption values were revised when new information and/or data became available that allowed changes or re-appraisals of the data compared to previous SDBs. The sorption values have been selected either on the basis of i) available in-house experimental data, ii) a survey of sorption values in the open literature, or iii) chemical analogy.

The sorption values were re-assessed and divided into three categories for the development of the updated cement SDB:

Not re-assessed, not revised: No new information and experimental data are available that allow a re-evaluation of the sorption values previously recommended in NTB 14-08 (Wieland 2014). Sorption values as listed in NTB 14-08 were not revised.

Re-assessed, not revised: New and relevant information and experimental data are available that allow a re-evaluation of the sorption values previously recommended in NTB 14-08 (Wieland 2014). However, the new information and data do not require a revision of the sorption values as listed in NTB 14-08. The values compiled in NTB 14-08 are retained and, if necessary, only modified according to the different porewater compositions of the reference systems for Stage 2 of the Sectoral Plan and the RBG.

Re-assessed, revised: New and relevant information and experimental data are available that allow a re-evaluation of the sorption values previously recommended in NTB 14-08 (Wieland 2014). The values are revised in accordance with the new experimental data and/or based on a more in-depth knowledge of the sorption process. If necessary, the values are further adjusted according to the different porewater compositions of the reference systems for Stage 2 of the Sectoral Plan and the RBG.

The present evaluation of sorption values is based on the reference CPW chemistries in the different cement degradation stages as outlined in Section 1.3. In the earlier SDBs (CEM-94, CEM-96, CEM-02, CEM-14), degradation products of bitumen and cellulose, concrete admixtures and cement-derived near-field colloids were taken into account as perturbing factors that could reduce radionuclide retention in the near-field. For this purpose, possible impacts on radionuclide mobility were considered and quantified in terms of sorption reduction factors. In the current update, a re-appraisal of the sorption reduction factors is undertaken with reference to the earlier cement SDBs. To add a new aspect, the updated cement SDB also considers the possibility of the effect of sorption competition on the radionuclide uptake in cementitious systems.

1.5 Considered dose-relevant radionuclides for safety analysis

The considered dose-relevant radionuclides for safety analysis were selected on the basis of an analysis of the waste streams including a re-assessment of radionuclide inventories and simplified transport calculations. The radionuclides belong to the element groups listed in Tab. 1-1. Most radionuclides have been classified as dose-relevant in the previous stages of the Swiss waste management programme. New elements have been added to the list of dose-relevant radionuclides (^{26}Al, ^{41}Ca, $^{249/251}$Cf, ^{60}Fe, ^{194}Hg, ^{166m}Ho, ^{32}Si) due to a new selection procedure resulting from transport calculations for the RBG. The selection process for the sorption values of the new radionuclides is documented in detail. The dose-relevant radionuclides in L/ILW include all actinides and their daughters with long half-lives, as well as activation and fission products.

Tab. 1-1: Considered dose-relevant radionuclides for safety analysis*

Element groups 1, 2 and 13	Cs, Ca, Sr, Ra, Al
Transition elements (first to third period)	Ti, Fe, Ni, Zr, Nb, Mo, Tc, Ag, Hg
Element groups 14, 16 and 17	C, Si, Sn, Pb, Se, Po, Cl, I
Lanthanoids and actinoids	Ho, Ac, Th, Pa, U, Np, Pu, Am, Cm, Cf

* Some radionuclides considered in previous SDBs are not discussed in this report due to their lower priority at the current stage of safety analysis.

The sorption behaviour of a radionuclide is influenced by the redox state of the dominant aqueous species. In this study, sorption values for reduced and oxidised species of a radionuclide are given to account for possible variability of the redox potential in the cementitious near-field of a repository. Although all realistic scenarios predict strongly reducing conditions in a cement-based L/ILW repository in the long term (Kosakowski et al. 2023), sorption values for both reducing and oxidising conditions in the first three stages of cement degradation are selected in this SDB for the sake of completeness. It should be noted that oxidising conditions prevail in the early phase of a repository, while reducing conditions are expected to establish soon after repository closure mainly due to the large amount of steel in the near-field that binds oxygen by oxic steel corrosion. Wersin et al. (2003) recommended a reference E_H potential of -230 mV for reducing conditions. Kosakowski et al. (2023) give an E_H range between 445 mV for cement degradation stage I and ≈ -604 mV in stage II and up to -379 mV in cement degradation stage III (see also Tab. 2-3). Tab. 1-2 shows the oxidation states of the redox-sensitive radionuclides under the oxidising and reducing conditions of an L/ILW repository as considered in this study.

Tab. 1-2: Redox states of redox-sensitive elements in aqueous media under highly alkaline conditions considered in this study

Element	Oxidising conditions	Reducing conditions
Se	+VI	+IV/-II
Mo	+VI	+VI
Tc	+VII	+IV
Ag	+I	0
Hg	+II	0
Sn	+IV	+IV
Po	+IV	+II
Pa*	+V	+V
U	+VI	+IV
Np	+VI/+V	+IV
Pu	+VI/+V	+IV

* The same Pa redox state has been assigned to oxidising and reducing conditions as no evidence for Pa(IV) under alkaline, reducing conditions exists (Hummel et al. 2022).

2 Cement porewaters and phase assemblage

2.1 Thermodynamic modelling of the porewater composition and phase assemblage for cementitious systems

Within the framework of the general licence application, cement porewater compositions and compositions of the cement materials have been defined for the three stages of cement degradation of the cementitious systems representative for the near-field of an L/ILW repository. These data define the chemical reference conditions for various subsequent modelling studies (e.g., solubility limits for dose-relevant radionuclides, complexation of radionuclides by ethylenediaminetetra-acetic acid (EDTA)) carried out for the development of the cement SDB. The properties of the cementitious systems should adequately represent the expected chemical conditions of the near-field over the time period under consideration for an L/ILW repository.

The general description of the three stages of cement degradation has been presented above (Section 1.3). Nevertheless, the specific conditions in these stages have to be determined for a particular repository system based on thermodynamic calculations. The thermodynamic model used to calculate the reference porewaters and the phase assemblage of HCP for the L/ILW near-field is based on the equilibrium of a cement representative of a cement-based near-field in three stages of cement degradation with representative porewaters, in particular OPA porewater in later stages of degradation (see Section 2.3). It can be assumed that the initial composition of the OPA porewater is strongly altered in equilibrium with cement paste, which is why the initial OPA water composition plays only a minor role for the modelling. A detailed description of the approach used to define the HCP compositions and their equilibrium cement porewaters in the three stages of cement degradation can be found in Kosakowski et al. (2023). In the following, a summary is provided, which includes the description of the model and the modelling approach as well as the resulting HCP and porewater compositions in the three different cement degradation stages.

In a realistic scenario, it is assumed that the redox state is mainly reducing during the lifetime of the cementitious near-field because the available oxygen is rapidly consumed by oxic metal corrosion and microbiological activity after closure of the repository. The redox potential is then determined by Fe-containing minerals resulting from anoxic corrosion of steel present in the cement barrier. This scenario is also applied in the thermodynamic calculations of the cement porewaters in the three degradation stages of HCP. The present cement SDB therefore contains radionuclide sorption values for the reducing conditions to be expected during the period of concern for the repository. Oxidising conditions were predicted by Kosakowski et al. (2023) only for the porewater in DS-I, as they are not relevant in the later degradation stages of HCP in a deep geological repository. For the selection of sorption values under oxidising redox conditions in DS-II and DS-III, it is assumed that the same cement minerals control sorption as under reducing conditions.

2.2 Model description

Selection of a representative cement

A CEM I-type cement is currently foreseen for the production of the in-situ concrete elements, the cavern filling mortar and the concrete containers, and it could also be used in container-filling mortar. A CEM I 52.5 R (from Jura Cement, Switzerland) is provisionally considered as a representative cement for the porewater calculations (see Kosakowski et al. 2023 for more details). The composition of CEM I 52.5 R is listed in Tab. 2-1.

Selection of the OPA porewater

For equilibration with concrete in DS-II and DS-III, the OPA in-situ porewater from the Nördlich Lägern and Zürich Nordost (NL-ZNO) siting regions was defined as the reference OPA porewater (OPAw-NL-ZNO-22 in Kosakowski et al. 2023) (Tab. 2-2). It is to be noted that OPAw_NL-ZNO-22 is assumed to be representative for the repository in the NL siting region selected for the repository by Nagra.

GEMS version, database and model implementation

All calculations were carried out using the updated PSI-Nagra thermodynamic database (TDB) 2020 (Hummel & Thoenen 2023), implemented in the GEM-Selektor version 3.9.3, and the CEMDATA18.1 TDB for cement phases (Lothenbach et al. 2019). They were adjusted by G.D. Miron for compatibility with the PSI-Nagra TDB 2020 at the level of equilibrium constants, i.e., 1 bar and 25 °C. Activity coefficients of aqueous species were calculated based on the specific ion-interaction theory (SIT) for aqueous species using parameters compiled in the PSI-Nagra TDB 2020.

The CSHQ solid solution model of C-S-H (Kulik 2011) is used and also integrated in the CEMDATA18.1 TDB (Lothenbach et al. 2019), which reproduces the water content of C-S-H including the gel porewater of C-S-H. In this report, information on the mass (volume) of gel porewater in C-S-H was needed to create a workaround that avoids an underestimation of the accessible porosity and the mass/volume of the aqueous phase per given mass of concrete, which in turn could lead to an overestimation of the ionic strength.

Porewater and solid phase compositions were modelled for the three representative cement degradation stages (DS-I, DS-II, DS-III) (Kosakowski et al. 2023) (Tab. 2-3). For use in the present SDB, the reference variants with an average porosity of 20% as defined by Kosakowski et al. (2023) are used, i.e., during the early DS-I phase, oxidising redox conditions are characterised by a pe value of 7.5 (E_H = 443 mV, “oxic” conditions). Reducing conditions at a later stage in DS-I are assumed to be imposed by the presence of magnetite (Fe_3O_4(cr)) and Fe/Al siliceous hydrogarnet (SHG; $C_3(AF)S_{0.84}H$) at equilibrium (pe = -6.76, E_H = -399 mV, “reducing conditions”). During cement degradation stages II and III, redox conditions are assumed to be buffered by the presence of magnetite and pyrite (FeS_2)(cr) (DS-II: pe = -10.2, E_H = -604 mV. DS-III: pe = -6.4, E_H = -379 mV, “reducing conditions”).

The different redox states are implemented in the GEMS project by removing more oxygen from the bulk composition to mimic the influence of iron corrosion, which would form iron oxide (e.g., magnetite). Increasing the removal of oxygen moves the redox state from oxidising, via a suboxic state, to a strongly reducing state (cf. the “negative addition” of O_2 in Tab. 2-3). A detailed discussion of the applied modelling procedures can be found in Kosakowski et al. (2023).

Tab. 2-1: Composition of CEM I 52.5 R

From Wieland & Kosakowski (2020), Tab. 8, with extensions

Chemical composition		**Elemental composition Compos CEM_I_52.5R**		**Normative phase composition**[******]	
	[g/100g]		[mol/100g]		[g]
SiO_2	20.0	Al	$9.61 \cdot 10^{-2}$	Alite	64.7
Al_2O_3	4.9	Ba	$6.52 \cdot 10^{-5}$	Belite	14.5
Fe_2O_3	3.3	Br	$1.25 \cdot 10^{-6}$	Aluminate	5.9
CaO	63.5	C	$2.27 \cdot 10^{-2}$	Ferrite	8.5
MgO	1.8	Ca	1.13	Gypsum	3.0
MnO	0.1	Cl	$2.54 \cdot 10^{-4}$	Hemihydrate	0.6
SrO	0.059[*]	F	$1.58 \cdot 10^{-3}$	Anhydrite	0.1
BaO	0.01[**]	Fe	$4.13 \cdot 10^{-2}$	Periclase	0.3
K_2O	0.7	H	$1.33 \cdot 10^{-1}$	Calcite	1.8
Na_2O	0.2	K	$1.49 \cdot 10^{-2}$	Dolomite	1.7
LOI[***] 2.0 g/100g	0	Mg	$4.47 \cdot 10^{-2}$	Quartz	0.4
CO_2	1.0[***]	Mn	$1.41 \cdot 10^{-3}$	CaO_{free}	0.64
H_2O	1.1946[***]	Na	$6.45 \cdot 10^{-3}$		
SO_3	3.2	O	2.29		
Br	0.0001[**]	S	$4.00 \cdot 10^{-2}$		
Cl	0.009[*]	Si	$3.33 \cdot 10^{-1}$		
F	0.03[**]	Sr	$5.69 \cdot 10^{-4}$		
P_2O_5	0.2[****]				
TiO_2	0.3[****]				
O_2 (mol)	-0.00264[*****]				
Total (without LOI, P_2O_5, TiO_2)	97.8				102.14
Total (with SrO, BaO, Br, Cl, F; no P_2O_5,TiO_2), g	100.0				

[*] Average content in clinkers from Moir & Glasser (1992)

[**] Minimum values for clinkers using data from Bhatty (2003) available from the website https://www.cementequipment.org/home/everything-you-need-to-know-about-minor-elements-in-cement-manufacturing (accessed 11th January 2022)

[***] LOI = loss on ignition, assumed to be 1.0 g/100 g CO_2 and 1.0 g/100 g H_2O. Set to ½ of LOI, H_2O content modified to achieve 100.0 g total

[****] Ignored

[*****] O_2 removed to make O_2-rich gas phase unstable, yet remain at oxidising redox conditions

[******] Normative cement composition from Caruso et al. (2017)

Tab. 2-2: NL-ZNO-22 porewater composition

Described in Kosakowski et al. (2023) (OPAw_NL-ZNO-22; Tab. A-2)

Porewater composition OPAw_NL-ZNO-22	
log $p(CO_2)$ [bar]	-2.20
pH	7.10
pe	-2.83
Ionic strength [mol/kg_w]	0.319
	Molality [mol/kg_w]
Al	$2.09 \cdot 10^{-8}$
Ba	$1.57 \cdot 10^{-7}$
C	$2.21 \cdot 10^{-3}$
Ca	$2.03 \cdot 10^{-2}$
Cl	0.240
F	$1.74 \cdot 10^{-4}$
Fe	$2.56 \cdot 10^{-5}$
K	$2.13 \cdot 10^{-3}$
Mg	$1.45 \cdot 10^{-2}$
Mn	$8.24 \cdot 10^{-5}$
Na	0.215
S	$2.29 \cdot 10^{-2}$
Si	$1.72 \cdot 10^{-4}$
Sr	$3.70 \cdot 10^{-4}$

Tab. 2-3: Geochemical conditions (solids, porewater composition) in DS-I, DS-II, DS-III assuming a hydrated cement porosity of ~ 20%, oxic/reducing conditions in DS-I and reducing conditions in DS-II and DS-III

Kosakowski et al. (2023)

Parameters	**DS-I (oxic)**	**DS-I-mt (reducing)**	**DS-II-mt-py (reducing)**	**DS-III-mt-py (reducing)**
Porosity [%]	20.14	20.599	19.73	20.51
pH	13.11	13.113	12.682	9.89
pe	7.5	-6.659	-10.236	-6.42
E_H [mV]	445	-393.2	-604.36	-379.0
Ionic strength [m]	0.184	0.182	0.288	0.327
Solutes [mol/L]				
Na	$3.64 \cdot 10^{-2}$	$3.64 \cdot 10^{-2}$	0.187	0.113
K	$1.44 \cdot 10^{-1}$	$1.44 \cdot 10^{-1}$	$6.68 \cdot 10^{-2}$	$8.92 \cdot 10^{-3}$
Ca	$2.76 \cdot 10^{-3}$	$2.76 \cdot 10^{-3}$	$1.37 \cdot 10^{-2}$	$7.10 \cdot 10^{-2}$
S (sulphate)	$9.04 \cdot 10^{-4}$	$9.02 \cdot 10^{-4}$	$8.91 \cdot 10^{-4}$	$1.34 \cdot 10^{-2}$
Cl	$4.41 \cdot 10^{-3}$	$4.41 \cdot 10^{-3}$	0.209	0.238
C_{inorg}	$5.74 \cdot 10^{-5}$	$5.74 \cdot 10^{-5}$	$1.58 \cdot 10^{-5}$	$8.41 \cdot 10^{-6}$
Si	$3.60 \cdot 10^{-5}$	$3.60 \cdot 10^{-5}$	$8.91 \cdot 10^{-4}$	$5.88 \cdot 10^{-4}$
Al	$2.63 \cdot 10^{-5}$	$2.63 \cdot 10^{-5}$	$1.62 \cdot 10^{-4}$	$7.7 \cdot 10^{-7}$
Fe	$3.23 \cdot 10^{-8}$	$3.22 \cdot 10^{-8}$	$2.60 \cdot 10^{-8}$	$1.5 \cdot 10^{-9}$
Mg	$1.89 \cdot 10^{-9}$	$1.88 \cdot 10^{-9}$	$4.78 \cdot 10^{-9}$	$9.06 \cdot 10^{-6}$
Major solids of hardened / degraded cement paste [weight (wt.) %]				
C-S-H - C/S ratio	33.3 1.58	33.3 1.58	36.67 1.59	67.53 0.70
Portlandite	17.6	17.6	17.33	0
Ettringite	9.9	9.9	10.12	0
Al/Fe siliceous hydrogarnet	10.2	10.2	0	0
OH-hydrotalcite	2.75	2.75	2.75	0
Calcite	26.1	26.1	24.46	17.19
Monocarbonate	0	0	6.39	0
Friedel's salt	0	0	0.37	0
Gypsum	0	0	0	2.60
Ferrihydrite	0	0	0	0
Magnetite	0	0.025	1.73	1.15

Tab. 2-3: Cont.

Parameters	DS-I (oxic)	DS-I-mt (reducing)	DS-II-mt-py (reducing)	DS-III-mt-py (reducing)
Pyrite	0	0	0.02	0.01
M-S-H	0	0	0	2.56
Chabazite (zeolite)	0	0	0	8.865

2.3 Consequences of the compositions of HCP and CPW for SDB development

In this section, the differences in the compositions of the porewaters and the cementitious materials are briefly discussed with respect to possible consequences for the development of the cement SDB for the RBG. A comparison is made with the composition of the porewater and the cement paste (CEM I 52.5 N HTS) used for the development of the previous cement SDB for Stage 2 of the Sectoral Plan (reference system in NTB 14-08, Wieland 2014) (Tab. 2-4). The most important parameters to be considered in the appraisal of sorption values are: 1) the concentrations of Na and K, 2) the Ca concentration, 3) the pH, 4) the concentrations of anions (in particular Cl^-), 5) the mineral composition of the cementitious material.

Effect of alkalis and Ca^{2+}

The alkalis influence Cs(I) sorption, while Ca(II) has an influence on the sorption of the alkaline earth metals (Sr(II), Ra(II)) and the anion sorption onto C-S-H phases. Several studies report that aqueous Ca concentrations below $\sim 2 \cdot 10^{-3}$ M give rise to negative surface charges (e.g., Labbez et al. 2007, Pointeau et al. 2006, Viallis-Terrisse et al. 2001). Above this treshold of Ca concentration, a charge reversal occurs at the C-S-H surfaces, which promotes the sorption of negatively charged anions.

Effect of pH

The pH values of the reference system used for NTB 14-08 (Wieland 2014) and the anticipated systems modelled for the RBG documentation are similar for DS-I and DS-II, but about an order of magnitude lower for DS-III (Tab. 2-3 and Tab. 2-4). Differences in the pH can be attributed to differences in the total alkali concentrations controlled by alkali uptake by C-S-H phases and zeolites. The lower pH for the anticipated system in DS-III modelled for the RBG is a consequence of the higher margin assumed for this degradation stage (C-S-H degraded to C/S 0.7 instead of C/S ~ 0.8).

In the case of strongly hydrolysed metal cations in alkaline conditions, e.g., Pb, U(VI) and Np(V), the variations in the pH may change the proportions of the concentrations of the hydroxyl species in solution. These changes give rise to variations in the extent of uptake of strongly hydrolysed cations by cementitious matrices in relation to the pH and thus account for the differences in the sorption values recommended in the cement SDB. However, it should be noted that uncertainty ranges by a factor of 2 for the moderately sorbing metal cations and a factor of 10 for the very weakly and strongly sorbing cations, respectively, were already assigned in the CEM-14 SDB (Wieland 2014). This is therefore considered to already take into account the small pH deviations in DS-I and DS-II. For DS-III, the reference pH 11.07 used in the CEM-14 SDB is retained in the appraisal of sorption on degraded HCP, as pH = 9.89 (Tab. 2-3) represents conditions at the very end of the degradation stage. Hence, it may be assumed that the hydrolysis behaviour of the dose-

relevant radionuclides is comparable to the reference and anticipated systems at each stage of cement degradation, indicating similar species distributions in the systems and negligible effects on sorption. Furthermore, it is assumed that the uncertainty ranges assigned to the sorption values already cover changes in the speciation of the metal cations caused by the small difference in the pH between the reference and the anticipated systems.

Tab. 2-4: Geochemical conditions (solids, porewater composition) for cement paste, CEM I 52.5 N HTS in DS-I, DS-II, DS-III used in the SDB for Stage 2 of the Sectoral Plan Wieland (2014)

Parameters	**Stage I**	**Stage II**	**Stage III**
Porosity [%]	20	20	18
pH	13.1	12.54	11.07
E_H [mV]	-529.9	-498.1	-180.7
Ionic strength [m]	0.168	0.098	0.150
Solutes [mol/L]			
Na	$9.68 \cdot 10^{-2}$	$4.21 \cdot 10^{-2}$	0.104
K	$7.27 \cdot 10^{-2}$	$3.30 \cdot 10^{-3}$	$2.55 \cdot 10^{-2}$
Ca	$2.43 \cdot 10^{-3}$	$1.80 \cdot 10^{-2}$	$5.35 \cdot 10^{-3}$
S (sulphate)	$6.24 \cdot 10^{-4}$	$4.70 \cdot 10^{-5}$	$7.81 \cdot 10^{-3}$
Cl	$2.46 \cdot 10^{-4}$	$3.74 \cdot 10^{-2}$	0.123
C_{inorg}	$4.46 \cdot 10^{-5}$	$8.04 \cdot 10^{-6}$	$1.67 \cdot 10^{-5}$
Si	$4.34 \cdot 10^{-5}$	$3.42 \cdot 10^{-5}$	$3.45 \cdot 10^{-4}$
Al	$2.61 \cdot 10^{-5}$	$6.89 \cdot 10^{-6}$	$1.15 \cdot 10^{-4}$
Fe	$2.11 \cdot 10^{-7}$	$5.58 \cdot 10^{-8}$	$3.86 \cdot 10^{-8}$
Mg	-	-	-
Major solids			
	C-S-H	C-S-H	C-S-H
	Portlandite	Portlandite	
	Ettringite	Ettringite	
	Monocarbonate	Monocarbonate	
	Calcite	Calcite	Calcite
	OH-hydrotalcite	OH-hydrotalcite	OH-hydrotalcite

Effect of SO_4^{2-} and CO_3^2

Differences in the pH (OH^- concentration) and the concentrations of Cl^-, SO_4^{2-} and CO_3^{2-} could have an effect on the speciation of cations (e.g., actinides, etc.) and consequently on the extent of uptake of metal cations by the cementitious materials. However, it has been noted that hydrolysis dominates the speciation under high pH conditions, which allows to largely ignore the complexation of the dose-relevant metal cations by SO_4^{2-} and CO_3^{2-} present at much lower concentrations compared to OH^-. The concentrations of SO_4^{2-} and CO_3^{2-} show notable differences in all three stages of cement degradation. These anions could potentially act as complex-forming ligands with metal cations such as actinides and lanthanides. However, speciation calculations performed for a selection of important metal cations in the context of Stage 2 of the Sectoral Plan revealed that even at the lowest OH^- concentration (pH = 11.07), variations in anion concentrations (SO_4^{2-}, CO_3^{2-}) only negligibly affect speciation (Wieland 2014). For example, the calculations showed that the concentrations of metal-sulphate complexes of dose-relevant metal cations (Co, Ni, Ag, Sn(IV), Pb, Th, U(VI), Np(IV), Pu(III), Pu(IV), Am) are negligibly low at an SO_4^{2-} concentration of $7.88 \cdot 10^{-3}$ M and a pH of 11.07 as hydroxo complexes dominate and make up more than 99% of the aqueous species. The calculations further showed that the proportions of metal-carbonate complexes is negligibly small at a pH of 11.07 as compared to the concentration of the hydroxo complexes for all the above-mentioned metal cations (cf. Wieland 2014). We therefore believe that even the lower pH value (pH = 9.89) calculated for CPW at the end of DS-III and the slightly higher SO_4^{2-} concentration ($1.3 \cdot 10^{-2}$ M) would not significantly change the metal speciation and that metal-hydroxo complexes still dominate speciation under these conditions. It can be assumed that SO_4^{2-} has no significant effect on the speciation of metal cations in any stages of cement degradation due to the significantly higher stability of the hydroxo complexes. This further applies to metal-carbonate complex formation under the carbonate concentrations expected in DS-III ($8.41 \cdot 10^{-6}$ M).

Effect of Cl^-

A maximum Cl^- concentration of up to ~ 0.24 M has been predicted for the porewater of the reference system in equilibrium with the NL-ZNO-22 porewater (Tab. 2-3). In Wieland (2014) the speciation of the dose-relevant metal cations (Co, Ni, Ag, Sn(IV), Pb, Th, U(VI), Np(IV), Pu(III), Pu(IV), Am) at an elevated salinity (with assumed Cl^- concentrations ranging between 0.124 M and 1.282 M) and a pH of 11.07 has been modelled. These calculations showed that the formation of aqueous chloro complexes changes the speciation of only very few radionuclides at a pH of 11.07. For example, the speciation of Ag is dominated by AgCl, $AgCl_2^-$, $AgCl_3^{2-}$ and $AgCl_4^{3-}$ complexes, while for other metal cations, such as Zr, Sn, Pb and in particular all the actinides, hydroxo complexes are thermodynamically more stable than chloro complexes. Hence, hydrolysis of metal cations determines the species distribution even at the highest Cl^- concentration in the pH range > 11. As a result of this finding, reduced sorption should be considered at an elevated Cl^- concentration in the case of Ag (and Hg), while for all the other cationic radionuclides, the effect of enhanced Cl^- concentration on the uptake by HCP is considered negligibly small (Wieland 2014). We therefore assume that Cl^- has only a negligibly small effect on the speciation of most metal cations even in the pH range between 9.89 (end of DS-III) and 11.07 (reference state of DS-III). Note, however, that Cl^- must be considered as a competing anion for the uptake of anions (e.g., I- and Se-oxyanions) by cementitious materials (Wieland 2014).

In summary, there is evidence that the effect of metal complexation by Cl^-, SO_4^{2-}, CO_3^{2-} on speciation can be ignored in all stages of cement degradation as the thermodynamic stability of the hydrolysis products dominates. The formation of chloro complexes with Ag and Hg is the only exception, for which $R_d = 0$ is assumed in this cement SDB for all stages of cement degradation.

Effect of Si

The Si concentrations of the CPWs are ~ $3.6 \cdot 10^{-5}$ M in DS-I, ~ $9 \cdot 10^{-4}$ M in DS-II and ~ $6 \cdot 10^{-4}$ M in DS-III (Tab. 2-3). These values are comparable (difference less than a factor of 5) to those used for the development of the CEM-14 SDB (NTB 14-08, Wieland 2014). Speciation calculations performed for a selection of important radionuclides under the conditions of a low-pH shotcrete porewater with a pH value and Si concentration similar to those calculated for DS-III in this report revealed that Si concentrations in the given range cannot compete with OH^- for complexation. Their effect on the speciation is therefore negligible (Thoenen 2012 cited in Wieland 2014). The thermodynamic complexation constants used for these earlier calculations do not significantly deviate from those selected in the more recent PSI-Nagra TDB 2020 (Hummel & Thoenen 2023) used in the present report. Therefore, the conclusion of Wieland (2014) that the formation of silicate complexes is negligible in low pH shotcrete porewaters is also valid for the radionuclide speciation in DS-I, DS-II and DS-III. Furthermore, Hummel et al. (2022) performed speciation calculations to determine the solubilities of the metal cations included in the present SDB under the porewater conditions in DS-II. These calculations confirm that silicate complexes do not play a significant role under DS-II conditions.

Effect of HCP composition

In addition to the composition of the porewater, the composition of the cementitious materials, i.e., the cement phases present in the three stages of cement degradation, also has an effect on the uptake of metal cations and anions. Therefore, the composition of HCP must be taken into account in all stages of cement degradation when assigning sorption values. It has been found that the same cement phases are present in DS-I as modelled for the present cement SDB (Tab. 2-3) and previously used for the development of the cement SDB in Stage 2 of the Sectoral Plan, with the exception of the AFm phases (monocarbonate). The absence of AFm phases in the current modelling for the RBG can be attributed to the new thermodynamic data available for Al/Fe siliceous hydrogarnet. These data have been determined experimentally in recent years (Dilnesa et al. 2014a, Lothenbach et al. 2019) and were therefore not available for the earlier modelling in Stage 2 of the Sectoral Plan and NTB 14-08 (Wieland 2014). The modelling shows that Al/Fe siliceous hydrogarnet is the most thermodynamically stable Al/Fe-containing cement phase, which is formed at the expense of AFm phases. AFm phases are only present in the form of monocarbonate in DS-II and are not present at all in DS-I and DS-III (Tab. 2-3). It should be noted that thermodynamic modelling determines the most thermodynamically stable composition of HCP, which is considered representative of the long-term near-field evolution of a deep geological repository. This means that AFm phases can be observed experimentally in fresh HCP due to kinetic control of phase formation, which may affect the sorption values determined in short-term sorption experiments. However, these AFm phases are not expected to be present in HCP aged for hundreds or thousands of years.

In DS-III, C-S-H phases, calcite and zeolites are the predominant solid phases according to the current model of the cementitious system (Tab. 2-3). In contrast to previous modelling, ettringite is predicted to be thermodynamically stable in DS-I and DS-II, while it is unstable in DS-III as Al is preferentially accommodated by zeolites. This is related to the fact that the porewater composition for DS-III has been selected to represent the final stage to include cement phases. The porewater compositions selected in Stage 2 of the Sectoral Plan implied a less degraded cementitious material. It should be noted that C-S-H phases and calcite are the only solid phases present in all three stages of cement degradation.

AFm phases were considered an important cement phase for anion retention in previous cement SDBs (Wieland 2014). In the current evaluation of sorption values for the RBG, AFm phases are only considered to be present in DS-II in the form of monocarbonate. It is known that AFm phases show a strong preference for CO_3^{2-} anions in their interlayers compared to other anions (Aimoz

et al. 2012, Appelo 2021, Mesbah et al. 2011, Mesbah et al. 2012, Nedyalkova et al. 2020). Thus, monocarbonate is not considered a good sorbent for anions and, in the present SDB, is therefore not considered further in the selection of sorption values for the long-term retention of anionic radionuclides in a deep geological repository.

The new assessment of the composition of the cement materials requires C-S-H phases and ettringite rather than the AFm phases to be considered as the relevant cement phases contributing to anion retention. The other cement phases present in the cement materials at the different stages of cement degradation such as portlandite, Al/Fe siliceous hydrogarnet, calcite, zeolites, hydrotalcite, etc. are presently not considered when evaluating anion retention due to limited experimental information. The main solid phase relevant to the sorption process of the dose-relevant cations, C-S-H, was observed in all stages of cement degradation in the reference systems used for NTB 14-08 (CEM 52.5 N HTS) and the RBG (Tab. 2-3), irrespective of the degradation process by carbonation or reaction with silica (Wieland & Kosakowski 2020). The retention of cations in the cementitious near-field in the three stages of the cement degradation can thus be evaluated according to NTB 14-08 (Wieland 2014). However, improved knowledge of the long-term evolution of the mineral composition of degrading cementitious materials, in particular the absence of AFm phases, requires a re-evaluation of anion retention for the development of the new cement SDB compared to NTB 14-08 (Wieland 2014). The re-evaluation of anion retention is essentially based on the idea that C-S-H phases also play a key role for anion sorption in a deep geological repository.

Tab. 2-5: Mineral composition of cement paste, CEM I 52.5 N HTS, after about 3 years of hydration (w/c = 1.3) considered in the development of the CEM-14 SDB for Stage 2 of the Sectoral Plan

Wieland (2014)

Cement phase	**Portion in CEM I 52.5 N HTS** [wt -%]
C-S-H	51
Portlandite	20
AFt phases (ettringite)	8.9
AFm phases (i.e., monocarbonate)	9.7
OH-hydrotalcite	1.6
Calcium carbonate	1.1
Non-hydrated clinker minerals	7.7

The following paragraphs summarise the specific considerations for each stage of cement degradation and are based on a comparison of porewater and cement mineral compositions presented in Tab. 2-3 for the RBG and in Tab. 2-4 and Tab. 2-5 for Stage 2 of the Sectoral Plan.

DS-I

Alkalis: The total alkali concentrations of the porewaters used for the development of the CEM-14 SDB (NTB 14-08, Wieland 2014) and those calculated for the RBG are comparable (difference within a factor of 2). This suggests that sorption values for Cs uptake by HCP previously recommended in NTB 14-08 can be retained.

Calcium: The Ca concentration of the porewater used for the development of the CEM-14 SDB (NTB 14-08, Wieland 2014) and that calculated for the RBG are similar. This suggests that sorption values previously recommended in NTB 14-08 for the uptake of Sr and Ra by HCP can be retained.

pH: The pH values of the porewaters considered for the development of the CEM-14 SDB (NTB 14-08, Wieland 2014) and those calculated for the RBG are similar (pH 13.1 and ~ 13.2, respectively), indicating that, at the given high OH^- concentrations, hydrolysis determines the speciation of the metal cations.

SO_4^{2-} and CO_3^{2-}: The concentrations of SO_4^{2-} and CO_3^{2-} in the porewater modelled for the RBG are similar to those of the porewater used for the development of the cement SDB in NTB 14-08. The concentrations of both anions are in the submillimolar range and therefore well below the OH^- concentration. As a consequence of this, the effect of both anions on the speciation of metal cations can be neglected under the given conditions, so that no effect on their uptake by HCP is to be expected.

Cl^-: The Cl^- concentration of the porewater considered for the development of the CEM-14 SDB (NTB 14-08, Wieland 2014) is about a factor of ~ 20 lower than that calculated for the RBG. The Cl^- concentration is in the millimolar range and thus has no effect on the speciation of metal cations (Wieland 2014). Nevertheless, a possible effect of Cl^- on the uptake of other anions (e.g., I^-) needs to be addressed in the current appraisal of sorption values.

HCP: The phase composition of HCP considered for the development of the CEM-14 SDB (NTB 14-08, Wieland 2014) (Tabs. 2-4 and 2-5) and that predicted for the RBG (Tab. 2-3) are similar with C-S-H phases, portlandite, ettringite and calcite as the main cement phases. Only monocarbonate is absent in the new cement composition and replaced by Al/Fe siliceous hydrogarnet, which is a result of the new CEMDATA18.1 TDB for cement phases (Lothenbach et al. 2019). The proportions differ for some minerals, which is taken into account when assigning sorption values when appropriate. Note again that the thermodynamic data for SHG are new and therefore, this mineral did not appear in the modelling of the cementitious system considered for NTB 14-08 (Wieland 2014). Overall, however, the same sorption-relevant cement phases are present.

DS-II

Alkalis: The total concentrations of the alkalis in the porewaters used for the development of the CEM-14 SDB (NTB 14-08, Wieland 2014) are significantly lower (~ 0.045 M) than those calculated for the RBG (~ 0.25 M). This difference in concentration, which is higher by a factor of ~ 5, must be taken into account when assigning sorption values for Cs uptake by HCP in DS-II. This is related to the fact that the composition of the CEM I 52.5 R used for the calculation of the CPW has a higher alkali content in comparison to the CEM I HTS considered as the reference cement in Stage 2 of the Sectoral Plan.

Calcium: The Ca concentration of the porewater used for the development of the CEM-14 SDB (NTB 14-08, Wieland 2014) is similar to that of the porewater calculated for the RBG (difference by a factor of < 2). This suggests that sorption values previously recommended in NTB 14-08 for the uptake of Sr and Ra by HCP can be retained.

pH: The pH of the porewaters considered for the development of the CEM-14 SDB (NTB 14-08, Wieland 2014) and calculated for the RBG are comparable, indicating that hydrolysis determines the speciation of the metal cations of both porewaters.

SO_4^{2-} and CO_3^{2-}: The SO_4^{2-} concentration of the porewater modelled for the RBG is higher (by a factor of ~ 20) compared to that of the porewater used for the development of the CEM-14 SDB (NTB 14-08, Wieland 2014). However, the CO_3^{2-} concentrations are similar in both porewaters. Nevertheless, as with DS-I, the concentrations of both anions are in the submillimolar range and thus well below the OH^- concentration. As a consequence of this, it is assumed that the effects of both anions on the speciation of metal cations can be neglected under the given conditions, so that no effects on their uptake by HCP are to be expected.

Cl^-: The Cl^- concentration of the porewater considered for the development of the CEM-14 SDB (NTB 14-08, Wieland 2014) is about a factor of ~ 7 – 10 lower than that of the porewater calculated for the RBG. The Cl^- concentration is in the submolar range (≤ 0.238 M) but has no influence on the speciation of metal cations under the given hyperalkaline conditions (Wieland 2014). Nevertheless, a more detailed appraisal of the effect of Cl^- on the sorption of dose-relevant anions is necessary.

HCP: The phase composition of HCP considered for the development of the CEM-14 SDB (NTB 14-08, Wieland 2014) and that predicted for the RBG are similar insofar as the C-S-H phases, portlandite, ettringite, monocarbonate and calcite are the main cement phases. While the proportions of these cement phases may vary, this is taken into account for the assignment of the sorption values when appropriate. Overall, the same sorption-relevant cement phases are present. Note, however, that a possible contribution of AFm phases to the long-term retention of anions in a deep geological repository is not further considered in the current evaluation of sorption values.

DS-III

Alkalis: The total alkali concentrations of the porewaters used for the development of the CEM-14 SDB (NTB 14-08, Wieland 2014) and calculated for the RBG are comparable (difference less than a factor of 2). This suggests that sorption values for Cs uptake by HCP previously recommended in NTB 14-08 can be retained.

Calcium: The Ca concentration of the porewater used for the development of the CEM-14 SDB (NTB 14-08, Wieland 2014) is lower (factor of ~ 10) than that of the porewater calculated for the RBG. This suggests that the enhanced Ca concentration must be taken into account when assigning sorption values for the uptake of Sr and Ra by HCP in the updated cement SDB. In addition, high Ca concentrations create a positive charge on the surface of the C-S-H phases, resulting in a higher affinity for anions and thus stronger anion sorption.

pH: For the development of the updated SDB, the same reference pH value of the porewater in DS-III (pH 11.07) is considered as previously for the CEM-14 SDB (NTB 14-08, Wieland 2014). The pH at the end of DS-III as calculated for the RBG differs by 1.2 pH units (pH 9.89) as a result of the selection process of the DS-III porewater composition. This has been chosen to correspond to the final stage of DS-III. Yet even under these conditions, hydrolysis still determines the speciation of the metal cations in the porewater, with some exceptions such as Fe(II), Ni(II) and Np(V). For these latter metal cations, speciation may be influenced by other complexing ligands, particularly carbonate and sulphate. As a reference pH value of 11.07 is assumed for the appraisal of the sorption values in this SDB (see the discussion on the effect of pH, above), the effect of carbonate and sulphate complexes on the R_d values for Fe(II), Ni(II) and Np(V) is not taken into account.

SO_4^{2-} and CO_3^{2-}: The SO_4^{2-} concentrations of the porewaters used for the development of the CEM-14 SDB (NTB 14-08, Wieland 2014) and calculated for the RBG are comparable (difference less than a factor of 2), while the CO_3^{2-} concentration of the RBG porewater is even lower by a factor of ~ 2. SO_4^{2-} forms only weak complexes with metal cations and, therefore, significant effects on the speciation of metal cations are not to be expected under the given high pH conditions. This also applies to the complexation of metal cations by carbonate, which is expected to be present at concentrations in the submillimolar range.

Cl^-: The Cl^- concentration of the porewater considered for the development of the CEM-14 SDB (NTB 14-08, Wieland 2014) is lower by about a factor of ~ 2 than calculated for the RBG. The Cl^- concentration is in the submolar range (~ 0.240 M), which corresponds to the chlorine content of the reference OPA porewater from the NL-ZNO region (see Mäder & Wersin 2023), but does not impact the speciation of metal cations under the given hyperalkaline conditions (Wieland 2014). However, as with DS-II, a more detailed appraisal of the effect of Cl^- on the sorption of dose-relevant anions is required in DS-III.

HCP: The phase composition of HCP considered in the development of the CEM-14 SDB (NTB 14-08, Wieland 2014) differs from the composition predicted for the RBG, as the new thermodynamic data for Al/Fe siliceous hydrogarnet have been considered in the current modelling. The current modelling for the RBG implies that C-S-H phases, calcite and zeolites are the main sorption-relevant cement phases in DS-III. The modelling for NTB 14-08 showed that, besides C-S-H phases and calcite, ettringite and hydrotalcite are present. The difference in the composition of the cementitious system does not affect the sorption values of metal cations recommended in the CEM-14 SDB, as C-S-H phases were considered to be the uptake-controlling sorbent in the development of the CEM-14 SDB. However, a possible effect on anion sorption due to the absence of ettringite must be taken into account.

3 Selected sorption data for cement degradation stages I to III

3.1 Not re-assessed, not revised sorption values

There are no sorption values in the category "not re-assessed, not revised sorption values" in the updated cement SDB because new experimental data have been published for all dose-relevant radionuclides in recent years or because new information on the sorption properties of the radionuclides became available.

3.2 Re-assessed, not revised sorption values

This section includes all radionuclides for which a re-assessment of the sorption values has been made because new experimental data have been published in recent years or because new considerations have been made about the sorption properties of the radionuclides. However, based on the available information, it was not necessary to revise the sorption values recommended in NTB 14-08, while adjustments have been made in accordance with changes of the porewater chemistry of the reference systems in Stage 2 of the Sectoral Plan and the general licence application.

3.2.1 Lanthanides and actinides

Previously not considered sorption data for lanthanides and actinides (An(IV), An(V), An(VI)) on HCP are available from wet chemistry studies, such as the uptake of actinides by C-S-H phases (Häussler et al. 2018, Tits & Wieland 2018, Wolter et al. 2019a, Wolter et al. 2019b), as well as studies on degraded Nirex reference fault backfill (NRVB) (Baston et al. 2012) and on lanthanide and actinide uptake by NRVB (Felipe-Sotelo et al. 2012) and Pu sorption on HCP in the absence and presence of isosaccharinic acid (ISA) (Tasi et al. 2021). NRVB is a highly porous cementitious material, containing ~ 26 wt.% ordinary Portland cement (OPC), ~ 10 wt.% hydrated lime (primarily calcium hydroxide), and ~ 29 wt.% fine limestone aggregate (primarily calcite) as the solid components of the raw mix and reacted with ~ 35 wt.% water. NRVB is produced at a relatively high w/c ratio of 1.37. It was estimated that HCP contributes ~ 50 wt.% to the bulk weight of NRVB.

All new sorption data reported in the past years corroborate strong interaction of lanthanides and actinides with HCP.

Lanthanides and trivalent actinides

The neutral aqueous species, i.e., $Ln(OH)_3(aq)$ and $An(OH)_3(aq)$, are the dominant hydrolysis products in the pH range relevant to cementitious systems (pH ~ 11- 13.5) (e.g., Ochs et al. 2016, Tits & Wieland 2018, Wang et al. 2012). Therefore, as hydrolytic species are present, hydrolysis is expected to have a constant effect on Ln/An(III) uptake by cementitious materials in the given pH range.

In-house sorption studies with Am(III), Eu(III), and Cm(III) on HCP made from HTS cement and C-S-H phases (effective C/S ratio = 0.75 – 1.25) indicate strong uptake of these elements with R_d values typically ranging from 100 to 1,000 m^3/kg at solid contents of the experimental systems (solid-to-liquid (S/L) ratios) ranging from 0.1 to 1 g/L. Uptake was observed to be linear over a large concentration range (equilibrium concentration in solution from $10^{-12} – 2 \cdot 10^{-7}$ M) (Tits & Wieland 2018).

Häussler et al. (2018) studied Am sorption onto C-S-H phases with target C/S ratios ranging from 0.7 to 1.8 and S/L ratios varying between 0.5 and 20 g/L. The pH varied between 10.5 in the equilibrium solution with a C-S-H phase with an effective C/S of 0.75 and up to 12.5 in the equilibrium solution with a C-S-H phase with an effective C/S of 1.65. The authors determined sorption values for Am(III) ≥ 100 m^3/kg at an S/L ratio of 5 g/L on all C-S-H phases irrespective of the C/S ratio. Furthermore, the measured R_d values reveal no dependence on the S/L ratio above 1 g/L. Hence, the work of Häussler and co-workers supports earlier findings of a strong sorption of lanthanides and trivalent actinides onto C-S-H phases (e.g., Tits et al. 2003, Tits & Wieland 2018) and HCP (Stumpf et al. 2004).

Felipe-Sotelo et al. (2012) determined an R_d value of 662 ± 23 m^3/kg for Eu uptake by HCP made from OPC and in equilibrium with an artificial NRVB porewater with a pH of 12.8. Comparison with sorption values determined on NRVB suggested that the limestone flour, which is one of the three main components of NRVB, is the main uptake-controlling component for Eu retention in NRVB. The latter finding is supported by earlier work showing strong interaction of trivalent lanthanides and actinides (e.g., Eu^{3+}, Am^{3+}, Cm^{3+}) with calcite in wet chemistry studies (e.g., Curti et al. 2005, Lakshtanov & Stipp 2004, Tits et al. 2005). This is due to specific coordination in the calcite structure by Ca^{2+} substitution as indicated from spectroscopic investigations (e.g., Hellebrandt et al. 2016, Marques Fernandes et al. 2008, 2008b, Stumpf & Fanghänel 2002, Stumpf et al. 2006, Wolter et al. 2019a). It should be noted that the limestone content in NRVB is ~ 29 wt.%, whereas the calcite content in HPC made from OPC (e.g., sulphate-resisting HTS cement) is significantly lower (~ 4 wt.%) (e.g., Lothenbach & Wieland 2006). Thus, a cautious approach is taken by assigning the sorption value of trivalent actinides for use in SA solely on the basis of sorption measurements on HCP, as calcite may also contribute to the retention of trivalent actinides in calcite-enriched cementitious environments.

Wolter et al. (2019a) studied Cm(III) uptake by C-S-H phases (target C/S ratios = 1.0 and 2.0) and portlandite as well as Cm(III) uptake by the alteration products calcite, vaterite, and aragonite formed during carbonation of the two cement phases. R_d values of 1.2 and 2.7 m^3/kg were reported for the two C-S-H phases with target C/S values of 1.0 and 2.0, respectively, which is almost two orders of magnitude lower than values recently reported by Häussler et al. (2018) and Tits & Wieland (2018). The authors noted that incomplete phase separation during centrifugation may give rise to the presence of Cm(III)-carrying colloidal material, which eventually enhances the apparent aqueous Cm(III) concentration. The efficiency of phase separation, in particular the degree to which colloidal matter is removed from solution, clearly determines the quantification of the partitioning between solid and liquid phases in case of strongly sorbing radionuclides such as lanthanides and trivalent actinides (Cowper et al. 2006, Wieland 2014). The luminescence studies reported by Wolter et al. (2019a) further corroborated earlier findings (Tits et al. 2003) that two non-equivalent Cm(III) species exist in the C-S-H structure with a C/S ratio of 1.0. These have been assigned to Cm(III) taken up in the interlayer of C-S-H phases and Cm(III)-Ca replacement in the polyhedral CaO sheet of the C-S-H structure (Tits et al. 2003). Nevertheless, the authors observed a weak signal in the excitation spectrum of the C-S-H phase with a C/S ratio of 2.0, which was red-shifted as compared to the signals of the two Cm(III) species associated with C-S-H. It should be noted that the latter phase was synthesised at a high target C/S ratio of 2.0, thus leading to a mixture of ~ 82 wt.% C-S-H (effective C/S ratio ~ 1.65) and ~ 18 wt.% portlandite (Tits et al. 2014a). The additional signal observed in the excitation spectrum was assigned to Cm(III) uptake by portlandite. Note that the same signal was previously observed in luminescence investigations on Cm(III) uptake by HCP (Stumpf et al. 2004).

The new wet chemistry studies support the notion of a strong retention of lanthanides and trivalent actinides by cementitious materials. Thus, retaining an R_d of 100 m^3/kg for lanthanides (e.g., Ho) and trivalent actinides (e.g., Ac, Cm, Am) for use in safety analysis calculations in all stages of cement degradation (Tab. 7-1) is supported by all these studies.

The following sorption values are recommended for the uptake of lanthanides and trivalent actinides by cementitious systems (see also Tab. 7-1):

Stages I, II and III: The sorption values are retained as previously recommended in NTB 14-08 (Wieland 2014), i.e., an R_d of 100 m^3/kg, for all stages of cement degradation.

Th and tetravalent actinides

The neutral aquo species $An(OH)_4(aq)$ is the dominant hydrolysis product in the pH range relevant to cementitious systems (pH > 10) (e.g., Ochs et al. 2016, Tits & Wieland 2018, Wang et al. 2012). There is evidence to suggest that the aqueous Th-silicate species $(Th(OH)_3(SiO(OH)_3)_3^{2-}$ might exist at high silica concentrations ($\geq 10^{-3}$ M) and low Ca concentrations ($\leq 10^{-3}$ M) (Tits & Wieland 2018). However, such conditions are hardly even achieved in DS-III for which $[Ca]_{aq}$ ~ 0.07 M and $[Si]_{aq} \sim 5.88 \cdot 10^{-4}$ M is reported (Tab. 2-3). For this reason, it is currently assumed that the concentration of Th-silica complexes is negligible even in DS-III and further that hydrolysis has no effect on the uptake of Th and tetravalent actinides by cementitious materials as only one hydrolysis product exists over the pH range of interest.

Felipe-Sotelo et al. (2012) determined an R_d of $(5.8 \pm 1.0) \cdot 10^3$ m^3/kg for Th(IV) uptake by HCP prepared from OPC and in equilibrium with an artificial NRVB porewater of pH 12.8. Comparison with the sorption values determined for NRVB indicated that, in NRVB, HCP was the main sorbing component in the case of Th, as Th uptake by limestone flour and hydrated lime, the other main components of NRVB, was found to be about an order of magnitude lower. Baston et al. (2012) previously reported unconsidered sorption data on the uptake of Np(IV) by untreated NRVB (pH 12.2) and NRVB aged to DS-III by leaching with deionised water (pH ~ 10.5). Very strong uptake of Np(IV) was observed with R_d values > $5 \cdot 10^4$ m^3/kg by untreated NRVB and in the leached state. The authors noted that, in most experiments, the final Np(IV) concentrations were close to or below the analytical detection limit, indicating a maximum measurable R_d value of 100 m^3/kg.

Häussler et al. (2018) reported an R_d of 200 m^3/kg for Th(IV) uptake by C-S-H phases with C/S ratios ranging from 0.76 to 1.46 and S/L ratios varying between 0.7 and 19 g/L. The authors further assigned the same R_d value to Pu(IV) uptake by these C-S-H phases (R_d = 200 m^3/kg). Tasi et al. (2021) observed significantly stronger uptake of Pu(IV) by HCP at S/L ratios between 2 and 4 g/L ($\log°R_d = (3.3 \pm 0.6)$ m^3/kg). Neither of the two studies reported more specific information on the uptake mechanism of Th(IV) and Pu(IV) by C-S-H phases and HCP.

The in-house sorption data with Th(IV) and Np(IV) on C-S-H phases compiled in Tits & Wieland (2018) indicate R_d values ranging from 200 to 1,000 m^3/kg. The large scatter is believed to be a consequence of experimental challenges associated with the quantification of the R_d values of strongly sorbing radionuclides at a low content of C-S-H phases (S/L ratio = $2 \cdot 10^{-4}$ kg/L). Kinetic studies indicate neither time-dependence of the sorption values nor a dependence of the sorption values on the C/S ratio of the C-S-H phases (C/S ranging from 0.75 to 1.6) and the equilibrium pH (pH ranging from 10.4 to 13.3). In the case of Th, high sorption values (R_d > 200 m^3/kg) were also determined in conditions representative of DS-III (C/S = 0.75, pH = 10.4), indicating that $Th(OH)_4(aq)$ dominates Th speciation under these conditions. This further supports the idea that Th-silica complexes have only a negligible effect on the uptake of Th by C-S-H phases even in DS-III.

All above studies clearly indicate very strong sorption of Th and tetravalent actinides onto HCP and C-S-H phases, the main component of HCP. Th uptake by HCP can be rationalised based on the assumption that C-S-H is the uptake-controlling cement phase for Th and the tetravalent actinides in HCP. The large variation in R_d values can further be explained by the experimental challenges associated with the quantification of the sorption of strongly sorbing metal cations in cementitious systems. We thus conclude that the new experimental data support earlier appraisals

indicating very strong interaction of Th and tetravalent actinides with cementitious materials (Wieland 2014, Wieland & van Loon 2002), which allows an R_d of 100 m^3/kg to be retained for Th and other tetravalent actinides (U(IV), Np(IV), Pu(IV)) in the three cement degradation stages (Tab. 7-1).

The following sorption values are recommended for the uptake of Th and tetravalent actinides by cementitious systems (see also Tab. 7-1):

Stages I, II and II: The sorption values are retained as previously recommended in NTB 14-08 (Wieland 2014), i.e., an R_d of 100 m^3/kg, for all stages of cement degradation.

Hexavalent actinides (DS-I and DS-II)

Several studies have reported new sorption data on the U(VI) uptake by cementitious materials (Baston et al. 2012, Felipe-Sotelo et al. 2012, Häussler et al. 2018, Ochs et al. 2018, Tits & Wieland 2018) and investigations into the sorption mechanism of U(VI) binding to C-S-H phases by using spectroscopic techniques and performing molecular dynamics simulations (Androniuk & Kalinichev 2020, Kremleva et al. 2020, Wolter et al. 2019b). In contrast, information on Np(VI) retention by cementitious materials is sparse. To the best of the authors' knowledge, the in-house compilation of sorption studies with Np(VI) on C-S-H phases is the only new source of information currently available (Tits & Wieland 2018).

Baston et al. (2012) reported R_d values for U(VI) uptake by untreated and leached NRVB, while Felipe-Sotelo et al. (2012) quantified U(VI) sorption onto untreated NRVB and the main components of NRVB, i.e., HCP prepared from OPC, limestone flour and hydrated lime. The sorption values listed by Baston et al. (2012) range from 42 to 95 m^3/kg for untreated NRVB in equilibrium with an artificial NRVB-porewater with a pH of 12.9 and from 120 to 190 m^3/kg for leached NRVB in equilibrium with leach solution with a pH of 10.5. The sorption values given in Felipe-Sotelo et al. (2012) are as follows: $R_d = 33.7 \pm 0.5$ m^3/kg for U(VI) sorption onto NRVB and $R_d = 20.0 \pm 0.2$ m^3/kg for U(VI) uptake by HPC prepared from OPC, both determined at pH 12.8 – 12.9. The sorption values for NRVB and HCP agree very well as HCP is the main component of NRVB (~ 50 wt.%). Felipe-Sotelo et al. (2012) concluded that HCP is the uptake-controlling component in NRVB on the basis of a comparison of the sorption values determined with U(VI) on the individual components. The results reported by Baston et al. (2012) further suggest that U(VI) uptake by NRVB, or HCP, respectively, increases with a decreasing pH, i.e., from pH 12.9 corresponding to DS-II to pH 10.5 corresponding to DS-III.

High sorption values were also determined for U(VI) uptake by C-S-H phases (Häussler et al. 2018, Tits & Wieland 2018). Häussler and co-workers assigned an R_d of 100 m^3/kg to U(VI) uptake by C-S-H phases with C/S ratios ranging from 0.76 to 1.46, thus indicating no pH dependence of the sorption process. This result is in contrast to those reported by Tits & Wieland (2018). These authors observed a decrease of the R_d value for U(VI) sorption onto C-S-H from ~ 1,000 m^3/kg at pH 10 (C/S = 0.75) to ~ 30 m^3/kg at pH 13.3 (C/S = 1.82). The latter sorption value is somewhat higher than the one determined in the case of U(VI) uptake by untreated HCP in artificial CPW of pH 13.3 (R_d = 2 m^3/kg, Wieland 2014), assuming the presence of 50 wt.% C-S-H in HCP (Tab. 2-5). Overall, there is clear evidence that the extent of U(VI) uptake by cementitious materials depends on pH, i.e., uptake decreases with increasing pH, which further indicates the importance of hydrolysis. It should be noted that the concentration of the hydrolysis species $UO_2(OH)_3^-$ and $UO_2(OH)_4^{2-}$ increases with increasing pH. This means that U(VI) sorption by HCP is likely to increase during its degradation from DS-I to DS-II, and eventually to DS-III. This trend in U(VI) uptake was already evident in previous studies reviewed by Ochs et al. (2016). Previous appraisals of U(VI) uptake by HCP led to the following recommended values: R_d = 2 m^3/kg for DS-I and R_d = 20 m^3/kg for DS-II and DS-III (Ochs et al. 2018, Wieland 2014). The new set of sorption data allows a re-evaluation of U(VI) uptake by HCP in DS-III, while the

sorption values for DS-I and DS-II are retained. An increase in the R_d value for DS-III from 20 m^3/kg to 100 m^3/kg is justified given the consistently strong uptake of U(VI) by cementitious materials observed under conditions representative of DS-III, as reported in the above-mentioned studies.

Earlier spectroscopic investigations suggested U(VI) incorporation into the C-S-H structure with a coordination environment of U(VI) comparable to that in uranyl silicates (Harfouche et al. 2006, Macé et al. 2013, Tits et al. 2011). Nevertheless, unequivocal discrimination between surface-bound U(VI) and U(VI) species hosted in the interlayer of C-S-H phases is challenging on the basis of evidence provided by synchrotron-based or laser-induced, luminescence-based studies. It is conceivable that both types of species exist in U(VI)-containing C-S-H systems. Quantum chemical modelling studies in combination with conventional geometry optimisation as reported by Kremleva et al. (2020) and molecular dynamics simulations in combination with the potential of mean field calculations published by Androniuk & Kalinichev (2020) enabled investigations on the binding mechanism of U(VI) on C-S-H phases. The study of Kremleva et al. (2020) supports the hypothesis that interlayer bonding of U(VI) can exist and considerably contribute to U(VI) uptake by C-S-H phases. However, the coexistence of several sorption complexes was indicated as no single sorption complex exhibited all geometry features in a comparison between modelled structural parameters and those determined in spectroscopic investigations (Kremleva et al. 2020). Androniuk & Kalinichev (2020) showed that ternary complex formation between $UO_2(OH)_3^-$ and Ca^{2+} at the C-S-H surface plays an important role in the overall sorption process of U(VI). The two main mechanisms controlling U(VI) uptake by C-S-H phases are UO_2^{2+} binding to unoccupied deprotonated silanol groups, a mechanism likely to prevail under near-neutral conditions, and the formation of ternary surface complexes between the uranyl hydrolysis products and Ca^{2+} under strongly alkaline conditions. The latter conclusion is supported by the wet chemistry studies reported by Tits & Wieland (2018). These authors showed that Np(VI) sorption onto a TiO_2 surface is significantly increased under alkaline conditions in the presence of Ca^{2+}, thus supporting the idea of the formation of ternary surface complexes between the hydrolytic species of hexavalent actinides and Ca^{2+}.

The following sorption values are recommended for the uptake of hexavalent actinides by cementitious systems (see also Tab. 7-1):

Stages I and II: The sorption values are retained as previously recommended in NTB 14-08 (Wieland 2014); i.e., an R_d of 2.0 m^3/kg for DS-I and an R_d of 20 m^3/kg for DS-II.

Stage III: see Section 3.3.1.

3.2.2 Alkaline and earth alkaline metals

Caesium – DS-I and DS-II

García-Gutiérrez et al. (2018) investigated Cs migration by carrying out in-diffusion experiments on cylindrical mortar samples prepared from several cement types (CEM I, CEM II, CEM IV)[1]. The presence of different pathways for Cs diffusion in the different cement pastes was postulated in accordance with a double porosity system of the matrices. Apparent diffusion coefficients, D_a, were determined, ranging in value between $6.0 \cdot 10^{-13}$ m/s and $1.0 \cdot 10^{-14}$ m/s. Sorption values for Cs^+ could not be extracted from this study as porosity data for the cementitious materials were not reported.

Felipe-Sotelo et al. (2014) investigated Cs diffusion through NRVB. The authors determined through-diffusion of Cs in a radial configuration under equilibrium conditions using NRVB-equilibrated water as solvent (pH 12.4 – 13). They estimated the partition ratios (R_d values) of Cs on NRVB at $0.2 – 2.3 \cdot 10^{-3}$ m^3/kg from modelling the elution profiles recorded in the diffusion experiments. The R_d value for Cs on HCP was estimated on the assumption that Cs is preferentially taken up by HCP rather than lime and limestone and further that the portion of HCP in NRVB amounts to ~ 50 wt.%. The R_d values range from 0.4 to $4.6 \cdot 10^{-3}$ m^3/kg. These values correspond to previously recommended sorption values for Cs uptake by HCP in DS-I and DS-II and thus support previously selected sorption values for use in SA.

Arayro et al. (2018) published a computational study of Cs sorption onto C-S-H phases. At Cs loadings below 0.19 mol/kg, Cs adsorption in the interlayer was preferred to Cs adsorption on the nanopore surface, while Cs adsorption onto the surface preferentially occurred at higher loadings. Furthermore, Cs uptake into the interlayer of C-S-H phases was found to increase with a decreasing C/S ratio. The conclusions are in line with experimental data and corroborate the current selection of R_d values for the different stages of cement degradation (Tab. 7-1).

Tamura et al. (2017) studied the uptake of Cs by C-S-H phases (C/S ratios = 0.4, 0.8, 1.2 and 1.6) in the presence of carbonate (0, 10 mM, 100 mM, 1,000 mM). The authors observed no effect on the Cs^+ uptake at the lowest carbonate concentrations, while an increase of Cs^+ uptake was indicated at carbonate concentrations ≥ 100 mM. Similarly, Park & Jang (2018) observed a positive carbonation-induced weathering effect on the Cs^+ uptake by a paste prepared from Portland cement. Carbonation gave rise to decalcification of the binder gel (presumably C-S-H phases), while adsorption of carbonate resulted in a negatively charged surface of the binder gel. A completely carbonated paste showed the highest Cs^+ uptake. In these conditions, C-S-H phases had been converted into silica gel and the Al-containing phases (AFm, AFt) into an alumina gel. Both gels carrying a negative charge under alkaline conditions can enhance Cs^+ uptake in a strongly carbonated HCP as compared to pristine C-S-H phases. It should be noted that the carbonate concentrations of the cementitious systems relevant to the Swiss disposal programme range in value between ~ 0.008 and ~ 0.06 mM in the three stages of cement degradation (see Tab. 2-3). Hence, we infer that the effect of carbonate on Cs^+ uptake by C-S-H phases is limited in these systems and can therefore be ignored in the current assessment of sorption values in stages I – III of cement degradation.

[1] See https://www.beton.wiki/index.php?title=Zementarten, accessed 25 September 2023.

Jang et al. (2017) investigated Cs uptake by alkali-activated cements (i.e., fly ash- and slag-containing binders activated by a sodium hydroxide and sodium silicate solution) in comparison to a reference prepared from Portland cement. Batch sorption experiments were carried out with crushed materials in Cs-containing solutions, whose compositions were not in equilibrium with the cementitious material. The authors determined sorption values of 0.23 m^3/kg for Cs sorption onto HCP, while sorption values were even higher in case of the alkali-activated materials (0.41 – 1.47 m^3/kg). The experimental set-up and the measured zeta potentials of the suspended materials indicate that the sorption properties of Cs correspond to those observed on C-S-H phases with a low C/S ratio. Thus, the experimental conditions chosen by Jang et al. (2017) correspond to those of a strongly altered cementitious environment, i.e., typically observed in DS-III. The sorption values reported by Jang and co-workers are about two orders of magnitude higher than the recommended value for DS-III in NTB 14-08 (Wieland 2014). We refrain from adjusting the sorption value for Cs on the basis of the new experimental data reported by Jang et al. (2017) because the experimental conditions, especially the compositions of the pore solutions, were not reported in the required level of detail and cannot be reconstructed.

Li & Pang (2014) investigated the uptake of Cs by a mortar containing a slag cement and quartz aggregates (0.08 – 2 mm particle size). The blended binder contained 30% OPC, 65% ground and granulated blast furnace slag (GGBFS) and 5% silica fume. The binder was reacted at a water/binder (w/b) ratio of 0.45. The mortar was prepared with a binder/aggregate ratio of 0.47. The weight content of HCP was estimated at ~ 52 wt.% on the assumption that the total amount of slag reacted, while the content of the paste only amounts to ~ 32 wt.% if 50% of the slag had reacted. Reactivity of the slag was not reported by Li & Pang (2014). Sorption studies were carried out by immersing crushed mortar into an artificial solution (pH 13.4), which had a composition of a porewater in close equilibrium with the solid. The authors determined the uptake kinetics. They observed a fast uptake of Cs by the mortar as sorption equilibrium was attained within 20 days. The distribution coefficient (K_d) was determined to be $1.4 \cdot 10^{-3}$ m^3/kg for Cs^+. Sorption values for Cs on HCP can be estimated to range in value between 2.8 and $4.4 \cdot 10^{-3}$ m^3/kg. The sorption values for Cs estimated based on the study of Li & Pang (2014) are about a factor of 5 to 9 higher than the values recommended for DS-I in NTB 14-08. The estimated values are based on the assumption that the experimental conditions established in the study of Li & Pang (2014) correspond to those in non-degraded HCP and that the proportions of reacted slag correspond to the values estimated as above. Overall, the sorption values estimated on the basis of the new experimental data are in good agreement with the values recommended in NTB 14-08, which refer to uptake by HCP prepared from OPC. This is presently the reference scenario for the safety analysis.

The following sorption values are recommended for Cs uptake by cementitious systems (see also Tab. 7-1):

Stage I: We retain the values recommended in NTB 14-08 ($R_d = 5 \cdot 10^{-4}$ m^3/kg) because the alkali concentrations are similar for the reference system considered in NTB 14-08 (Wieland 2014) and the anticipated system for the RBG (Tab. 7-1).

Stage II: In NTB 14-08, an R_d of $5 \cdot 10^{-3}$ m^3/kg was assigned in view of the low alkali concentrations (~ $4.5 \cdot 10^{-2}$ M). The alkali concentrations of the porewaters of the cementitious system modelled for the RBG, however, are higher by about a factor of 5 (~ 0.25 M). As a result of the higher alkali concentrations, the R_d value is correspondingly reduced by a factor of 5 (R_d = 10^{-3} m^3/kg) (Tab. 7-1).

Stage III: see Section 3.3.2.

Strontium

Bar-Nes et al. (2018) studied the effect of irradiation and carbonation under atmospheric conditions on the leaching of Sr from cement paste prepared from OPC. The authors observed that irradiation of the paste (dose rate = 24 Gy/min, total dose = $5.0 \cdot 10^6$ Gy) had no effect on Sr uptake by the paste. In contrast, carbonation enhanced Sr uptake due to the formation of carbonated zones. Carbonation results in the decalcification of C-S-H phases, AFt, and AFm phases, which further causes the precipitation of silica and alumina gels. Park & Jang (2018) postulated such a conversion, which led to enhanced Sr^{2+} uptake by a strongly carbonated HCP. Silica and alumina gels carry a negative surface charge under alkaline conditions, which is higher than that of C-S-H phases. Thus, the observations reported by Bar-Nes and co-workers may explain higher sorption values for Sr^{2+} in DS-IV of cement degradation compared to Sr^{2+} uptake by calcite. Nevertheless, the observation has no consequences for the appraisal of the sorption values, which are assigned to stages I – III of cement degradation.

Jang et al. (2017) also investigated Sr uptake in addition to Cs uptake by alkali-activated cements in comparison to an OPC reference. The experimental conditions were identical to those previously described for the sorption studies with Cs. Sorption values for Sr were determined at 0.5 m^3/kg for OPC and ranged in value between 0.77 and 1.27 m^3/kg in the case of the alkali-activated cements. The sorption properties of Sr correspond to those observed on C-S-H phases with a low C/S ratio. As previously mentioned, the experimental conditions selected by Jang et al. (2017) correspond to those of a strongly altered cementitious environment, i.e., typically observed in DS-III. The sorption values reported by Jang and co-workers are about two orders of magnitude higher than the recommended value for DS-III. As with Cs, we refrain from adjusting the sorption value for Sr based on the new experimental data reported by Jang et al. (2017) due to lack of detailed information on the experimental conditions.

Li & Pang (2014) also investigated the uptake of Sr by the mortar containing a slag cement and quartz aggregates (0.08 – 2 mm particle size). The system was identical to the one used for the sorption studies with Cs as described above. The authors observed a fast uptake of Sr by the mortar as sorption equilibrium was attained within 20 days. The distribution coefficient (K_d) for Sr was determined to be $7.58 \cdot 10^{-2}$ m^3/kg. Sorption values for Sr on HCP can be estimated to range in value between 0.15 and 0.24 m^3/kg. The sorption values for Sr estimated from the study of Li & Pang (2014) is less than a factor of 3 higher than the value recommended for DS-I in NTB 14-08 (Wieland 2014). Overall, the sorption values estimated on the basis of the new experimental data are in good agreement with the values recommended in the previous SDB. Note again that the sorption values recommended in Tab. 7-1 refer to uptake by an HCP prepared from OPC, which is presently the reference scenario for the safety analysis.

The following sorption values are recommended for Sr uptake by cementitious systems (see also Tab. 7-1):

Stage I: We retain the values recommended in NTB 14-08 (R_d = 0.1 m^3/kg) because the Ca concentrations are similar for the reference system considered in NTB 14-08 (Wieland 2014) and the anticipated system for the RBG (Tab. 7-1).

Stage II: In NTB 14-08, an R_d of 10^{-2} m^3/kg was assigned in view of the higher Ca concentration in DS-II compared to DS-I (Tab. 2-3). The Ca concentration of the porewater considered in NTB 14-08 (Wieland 2014) and that of the cementitious system modelled for the RBG are similar (see Tab. 2-3 and Tab. 2-4). Therefore, an R_d of 10^{-2} m^3/kg is retained (Tab. 7-1).

Stage III: In the case of the cementitious system modelled for the RBG, the Ca concentration of the porewater in DS-III is about an order of magnitude higher than in DS-II (Tab. 2-3). As a consequence of this, an R_d of 10^{-2} m^3/kg, which was assigned to DS-II, is accordingly reduced by a factor of 10 ($R_d = 10^{-3}$ m^3/kg in DS-III) (Tab. 7-1).

Radium - DS-I and DS-II

Kittnerová et al. (2020) published a comparative study on Ra and Sr interaction with a C-S-H phase (target C/S ratio = 1.4), several HCPs prepared from CEM I, CEM II and CEM III cements, respectively, and two concretes made with the CEM I and III cements. CEM I is an OPC, while the CEM II Portland cement contains another component (here CEM II/A-S which contains a blast furnace slag) and CEM III refers to blast furnace slag cement (Kittnerová et al. 2020). The sorption studies were performed by contacting crushed materials with simulated (synthetic) CPW with pH 12.4 – 12.6, which, in the case of HCPs and concretes, corresponds to a porewater saturated with $Ca(OH)_2$, and the C-S-H phase was suspended in its mother solution (pH 12.1). Therefore, the sorption values reported by Kittnerová et al. (2020) are representative of the conditions in DS-II.

The sorption values reported for the CEM I HCP are considered to be relevant to the current appraisal. Rapid sorption was observed in line with other studies (e.g., Lange et al. 2018, Li & Pang 2014). Distribution ratios were found to range in value between 0.008 and 0.015 m^3/kg for Sr, with some dependency on the S/L ratio of the experimental system, while about an order of magnitude higher sorption values were determined for Ra (range 0.04 – 0.1 m^3/kg) (Kittnerová et al. 2020). Note that a difference of one order of magnitude was also observed for Sr and Ra uptake by the C-S-H phase with an C/S ratio of 1.4 (R_d ~ 0.1 m^3/kg for Sr; R_d ~ 2 m^3/kg for Ra) (Kittnerová et al. 2020). Nevertheless, sorption onto HCP cannot be correctly quantified based on the measured sorption values on the C-S-H phase and on the assumption of the proportion of C-S-H in HCP amounts to 50 wt.% (Sr: R_d ~ 0.05 m^3/kg (est.) and R_d ~ 0.008 – 0.015 m^3/kg (meas.); Ra: R_d ~ 1 m^3/kg (est.) and R_d ~ 0.04 – 0.1 m^3/kg (meas.). This discrepancy indicates that a C-S-H phase with a C/S ratio of 1.4 may not represent a C-S-H in HCP. Note that C-S-H phases with a C/S ratio ~ 1.6 are expected to dominate in HCP in DS-II.

The new experimental data on Sr and Ra sorption on HCP reported by Kittnerová et al. (2020) support the values recommended for use in the safety analysis (Tab. 7-1).

New experimental studies on the Ra uptake by cementitious materials were also published by Lange et al. (2018) and Olmeda et al. (2019). Olmeda et al. (2019) investigated the uptake of Ra by cement phases (C-S-H, C-A-S-H) and cement paste made from a cement-type CEM V containing 23 wt.% fly ash and slag. The sorption studies with Ra on the C-S-H phases (C/S ratios = 0.8, 1.0, 1.2, and 1.6) were carried out in their mother solutions, i.e., the solutions in equilibrium with the solids as achieved during synthesis (pH 10.4 for C/S = 0.8, pH 11.4 for C/S = 1.0, pH 12.19 for C/S = 1.2, and pH 12.37 for C/S = 1.6). Hence, the former two C-S-H phases are representative of DS-III, while the latter two C-S-H phases are representative of DS-II. The four C-A-S-H phases had C/S ratios of 0.8 and 1.2, respectively, while the Al/Si ratios were 0.05 and 0.2 for each of the two C/S ratios. The pH values of the mother solutions were pH 10.2 and 10.4 where the C-A-S-H phases had a C/S ratio of 0.8, and pH 11.4 and 11.0 where the C-A-S-H phases had a C/S ratio of 1.2. Uptake of Ra by the CEM V paste was determined in equilibrium with pore solutions of unperturbed cement (pH 13.2) and corresponding to DS-II (pH 12.2).

Olmeda and co-workers observed rapid adsorption on the cement phases and the HCP with sorption equilibria attained within approximately 14 days. For the present study, the distribution ratios for Ra uptake by C-S-H phases were estimated on the basis of the reported experimental data as follows: R_d ~ 14.5 ± 5.0 m^3/kg for C/S = 0.8, R_d ~ 7.1 ± 1.1 m^3/kg for C/S = 1.0, R_d ~ 5.8 ± 0.9 m^3/kg for C/S = 1.2, R_d ~ 0.6 ± 0.1 m^3/kg for C/S = 1.6. The distribution ratios for the C-A-S-H phases were estimated as follows: R_d ~ 8.9 ± 1.1 m^3/kg for C/S = 0.8 and Al/Si = 0.05, R_d ~ 21.9 ± 4.1 m^3/kg for C/S = 0.8 and Al/Si = 0.2, R_d ~ 9.3 ± 1.0 m^3/kg for C/S = 1.2 and Al/Si = 0.05, R_d ~ 128.8 ± 31.1 m^3/kg for C/S = 1.2 and Al/Si = 0.2. A comparison of the R_d values indicates a trend to stronger Ra uptake by C-A-S-H compared to C-S-H. Olmeda et al. (2019) reported the following sorption values for the HCP: R_d = 0.583 m^3/kg in the pH 13.2 porewater (DS-I) and R_d = 0.492 m^3/kg in the pH 12.2 porewater (DS-II).

Lange et al. (2018) carried out batch-type sorption studies with Ra on various cement phases (specifically C-S-H phases, ettringite, monosulphate, monocarbonate, hydrogarnet) and HCP prepared from OPC and a low-pH mortar made from a blended cement mix. Sorption studies were carried out by contacting weighted amounts of dried solids with a solution that had been pre-equilibrated with the respective solid material at the same S/L ratio. In the case of the cement phases, sorption measurements were also carried out on the solids in contact with the mother solution (equilibrium achieved during synthesis). Both experimental set-ups imply that the sorption measurements were carried out in conditions close to solid-liquid equilibrium. Eventually, sorption measurements were also carried out in an artificial, alkali-rich CPW (pH > 13), representing conditions in DS-I, and a $Ca(OH)_2$-saturated solution (pH = 12.3), representing conditions in DS-II. The C-S-H phases had target C/S ratios of 0.9 (pH = 11.9 of the mother solution) and 1.4 (pH = 12.1 of the mother solution). Thus, their compositions correspond to those of C-S-H phases in DS-II.

Lange and co-workers observed fast uptake kinetics under all conditions, with sorption equilibria typically attained within 30 days. Strong uptake of Ra by C-S-H phases (target C/S ratios = 0.9 and 1.4) was observed at pH 11.9 ($R_d = 22.5 \pm 4.0$ m^3/kg) and 12.1 ($R_d = 1.8 \pm 0.7$ m^3/kg), respectively, while slightly weaker uptake was observed at pH 13.2 ($R_d = 13.3 \pm 2.4$ m^3/kg for C-S-H 0.9 and $R_d = 0.95 \pm 0.38$ m^3/kg for C-S-H 1.4). It is to be noted that the uptake of Ra by the Al-containing cement phases (ettringite, monosulphate, monocarbonate, hydrogarnet) was much weaker with R_d values ranging between 0.004 and 0.139 m^3/kg. It is further to be noted that the differences in the R_d values between the Al-containing phases and C-S-H phases cannot be attributed to differences in the surface areas. The results support the idea that Ra is preferentially taken up by C-(A)-S-H phases in HCP. Lange et al. (2018) reported an R_d of~ 0.06 m^3/kg for Ra uptake by the HCP at an estimated pH of 12.6. Thus, the experimental conditions are representative of DS-II. However, significantly higher sorption values were determined on the low-pH cement paste (R_d > 10 m^3/kg at pH ≤ 11.8), which seem to correspond to the conditions in DS-III.

The sorption values listed in Tab. 7-1 have been selected based on earlier sorption studies with Ra on HCP reported by Bayliss et al. (1988), Holland & Lee (1991) and Tits et al. (2006). The experimental data suggest higher uptake of Ra by HCP in DS-I compared to DS-II in accordance with the higher Ca concentration in DS-II compared to DS-I. Therefore, C-S-H phases and in particular Ra-Ca competition is considered to play a decisive role in the uptake process. The new studies reported by Lange et al. (2018) and Olmeda et al. (2019) support the above rationale. Lange et al. (2018) show that Ra uptake is significantly stronger by C-S-H phase than by Al-containing cement phases, supporting the idea that C-S-H phases are the uptake-controlling cement phase in HCP. It should be noted that the study of Olmeda et al. (2019) indicates even stronger Ra uptake by C-A-S-H phases compared to C-S-H phases at the same C/S ratios of the solids. Lange et al. (2018) determined an R_d of ~ 0.06 m^3/kg for Ra uptake by an HCP made from Portland cement at pH 12.6, which corresponds to conditions relevant to DS-II. This value is in very good agreement with the presently recommended value $R_d = 0.05$ m^3/kg for DS-II (Wieland 2014). Note that, under conditions representative of DS-II, the R_d value was about an order of magnitude higher for HCP made from a cement blended with fly ash and slag ($R_d = 0.492$ m^3/kg at pH 12.2). Interestingly, Ra uptake by the blended cement was comparable for DS-I (R_d = 0.583 m^3/kg at pH 13.2) and DS-II ($R_d = 0.492$ m^3/kg at pH 12.2) (Olmeda et al. 2019). In view of these new data, the lower sorption value for Ra uptake by HCP in DS-II compared to DS-I as given in the CEM-14 SDB (Wieland 2014) is retained in accordance with differences in the Ca concentrations of the two CPWs and the idea that Ra-Ca exchange on C-S-H phases is the dominant sorption mechanism.

The studies of Lange et al. (2018) and Olmeda et al. (2019) disclose a controversial aspect in the reported sorption data. While both studies indicate C-(A)-S-H phases as the uptake-controlling cement phases for Ra in HCP, the high sorption values observed for Ra uptake by C-S-H phases

contradict the comparatively weak uptake observed on HCP in DS-II. Note that the weight content of C-S-H in HCP ranges between 46 and 60 wt.%. Therefore, we would expect sorption values on HCP (DS-II) > 0.3 m^3/kg using the sorption data on C-S-H 1.4 and 1.6 reported by Lange et al. (2018) and Olmeda et al. (2019), respectively. Direct measurements of Ra uptake by HCP in conditions relevant to DS-II, however, result in R_d values of ~ 0.05 m^3/kg. Note that agreement between measured R_d values on HCP and those estimated based on the Ra uptake by C-S-H phases is better in DS-I.

The studies of Lange et al. (2018) and Olmeda et al. (2019) also aimed at developing a mechanistic picture of Ra uptake by cementitious materials either by atomistic or thermodynamic simulations. Olmeda et al. (2019) modelled Ra uptake in terms of an Ra-Ca exchange process. Ra-Ca replacement may occur at negatively charge silanol sites on the surface and in the interlayer space of C-S-H phases. The results from the atomistic simulations reported by Lange et al. (2018) indicate that Ra-Ca replacement in the C-S-H interlayer space is a plausible sorption mechanism, especially for C-S-H phases with a low C/S ratio. This mechanism could explain the strong Ra uptake by HCP and C-S-H phases in DS-III of cement degradation.

Grambow et al. (2020) proposed a decreasing affinity of the alkaline earth elements in the order $Ra^{2+} > Ba^{2+} > Sr^{2+}$ for the interaction with C-S-H phases based on ion selectivity coefficients by also considering the recently published studies on Sr and Ra uptake by Kittnerová et al. (2020) and Ba uptake by C-S-H phases (Missana et al. 2017). This order anti-correlates with the binding energy of the water molecules in the coordination shell of the divalent earth alkaline metals, which increases with decreasing size of the metal cation ($Mg^{2+} > Ca^{2+} > Sr^{2+} > Ba^{2+}$) (Rodriguez-Cruz et al. 1999). The binding energy of water molecules bound to Ra^{2+} was found to be the weakest among the divalent alkaline earth metal ions (Matsuda & Mori 2014). This finding implies that replacement of the hydration shell by ionic bonding to structural coordination sites of C-S-H phases is facilitated with increasing size of the metal cation in the order $Ra^{2+} > Ba^{2+} > Sr^{2+}$.

The following sorption values are recommended for Ra uptake by cementitious systems (see also Tab. 7-1):

Stages I and II: We retain the values recommended in NTB 14-08 (Wieland 2014) (Stage I: R_d = 0.5 m^3/kg; Stage II: R_d = 0.05 m^3/kg) because the Ca concentrations are similar for the reference system considered in NTB 14-08 and the anticipated system for the RBG (Tab. 2-4 and Tab. 2-3).

Stage III: see Section 3.3.2.

3.2.3 Transition and other metals

Nickel

In NTB 14-08, the R_d value of Ni uptake by cementitious materials was estimated in terms of a "shared solubility" approach (see Chapter 4). This approach was chosen due to ample evidence showing that Ni uptake in cementitious materials is controlled by isotopic exchange with stable Ni present in the cementitious materials. The overall aqueous Ni concentrations (stable Ni^+ radioisotopes of Ni) control the solubility of the stable Ni phases, mainly in the $Ni(OH)_2$(s) and Ni-Al layered double hydroxide (LDH) phases (Scheidegger et al. 2000, Johnson & Glasser 2003, Vespa et al. 2006, Wieland et al. 2006, Wieland 2014). The majority of these studies was carried out on fresh HCP. To the best of the authors' knowledge, there is no information in the literature on the presence of solid Ni phases in DS-II and DS-III. Kosakowski et al. (2023) calculated the compositions of concrete in DS-I, DS-II and DS-III based on a representative composition of concrete possibly considered to be used in the L/ILW emplacement caverns according to the current concept. The calculations of the cement porewater and degradation are given in

Kosakowski et al. (2023). These calculations show that the solid phase composition of concrete in DS-III does not contain LDH phases (e.g., hydrotalcites or AFm phases) in contrast to the compositions in DS-I and DS-II. However, this does not necessarily also exclude minor amounts of Ni-AL LDH phases from being present in concrete in DS-III. The exact composition and thermodynamics of these Ni-Al LDH phases are still poorly understood. Hence, their stability during the concrete degradation process cannot be predicted.

Assuming isotopic exchange with stable Ni present as a solid phase in the concrete, the R_d value for Ni retention in concrete is estimated to be 0.41 m^3/kg (Section 4.2). This value is considered for the three stages of concrete degradation. Missana et al. (2022) measured R_d values of ~ 0.3 m^3/kg and ~ 6.3 m^3/kg for the ^{63}Ni uptake by C-S-H phases with a C/S of 1.6 and a C/S of 0.8, respectively. Taking into account that C-S-H phases make up approximately ~ 37% and 67% of the concrete composition in DS-II and DS-III, respectively, this would mean that the overall R_d values are ~ 0.1 m^3/kg (DS-II) and ~ 4.2 m^3/kg (DS-III). In case of DS-II, this R_d value is comparable to the R_d value obtained assuming isotopic exchange (0.41 m^3/kg), noting that the presence of LDH phases was predicted in the thermodynamic modelling for DS-II. In the case of DS-III, however, the C-S-H-based R_d value is much larger. For reasons of conservatism, the lower R_d value determined by isotopic exchange is assumed, which implies that the retention of ^{63}Ni by concrete in DS-III could be controlled by isotopic exchange, as in DS-I and DS-II.

The study of Felipe-Sotelo et al. (2012) on the Ni uptake by NRVB shows that the linear sorption range of Ni is very narrow, i.e., ranging from 10^{-8} M < $[Ni]_{aq}$ < 10^{-7} M, which is in accordance with the results published by Wieland et al. (2006). The authors concluded that the mechanism of removal of Ni under repository conditions is likely to be precipitation, thus corroborating the approach proposed earlier in NTB 14-08 (Wieland 2014). The R_d value estimated on the basis of shared solubility requires information on characteristic parameters of the L/ILW near-field, such as the amount of HCP and total volume per metre of cavern length as well as porosity, and on concentrations, such as the Ni content of HCP and the Ni concentration in solution. The Ni concentration in alkaline cement porewater in equilibrium with HCP was found to range in value between ~ 10^{-7} M (Felipe-Sotelo et al. 2012) and ~ 10^{-6} M (Felipe-Sotelo et al. 2016, García et al. 2018a, Wieland et al. 2006). In NTB 14-08 (Wieland 2014), the solubility of β-$Ni(OH)_2$(cr), a candidate mineral for solubility control of Ni, was calculated to be $3 \cdot 10^{-6}$ M at pH 12.5 using thermodynamic properties reported earlier (e.g., Hummel et al. 2005, Hummel et al. 2002). Note that this concentration was considered by Wieland (2014) for estimating the sorption value of Ni based on the shared-solubility approach. The presence of the hydrolytic species $Ni(OH)_3^-$ gives rise to the expected, relatively high Ni concentration of $3 \cdot 10^{-6}$ M in cement-type porewaters at pH 12.5. Studies by Palmer & Gamsjäger (2010) and, more recently, by Brown & Ekberg (2016) and by González-Siso et al. (2017), however, indicate the neutral species $Ni(OH)_2$(aq) as the only hydrolytic species, suggesting an absence of $Ni(OH)_3^-$ and thus lower Ni concentrations in the alkaline range. In fact, González-Siso et al. (2017) determined the solubility of β-$Ni(OH)_2$(cr) at pH > 10 in the range of $2 \cdot 10^{-8}$ M to 10^{-7} M. This range is more than an order of magnitude lower than the previously estimated solubility of β-$Ni(OH)_2$(cr) at pH 12.5, i.e., $3 \cdot 10^{-6}$ M. Note that in the shared-solubility approach, the R_d values increase with decreasing aqueous concentrations of the element of interest. In NTB 14-08, an R_d of 0.32 m^3/kg was reported as the best estimate for the R_d value of Ni applying the shared-solubility approach and using an Ni concentration of $3 \cdot 10^{-6}$ M. It should be noted that using the new experimental data for the β-$Ni(OH)_2$(cr) solubility in alkaline conditions would increase the R_d value by more than an order of magnitude. For the current appraisal, however, we take a cautious approach by retaining the R_d value reported in NTB 14-08 (Wieland 2014). A lower Ni concentration, however, was used to estimate the upper limit of the sorption value of Ni in the cementitious environment.

The following sorption values are recommended for Ni uptake by cementitious systems (see also Tab. 7-1):

Stages I to III: The "shared solubility" approach for estimating the sorption values of Ni was retained as detailed in NTB 14-08 (Wieland 2014) (see also Section 4.2). Recalculation resulted in an R_d of 0.41 m^3/kg based on the updated near-field parameters and solubility calculations.

Lead

The oxidation state +II dominates in the E_H-pH space relevant to a cement-based repository (Brookins 1988, Pourbaix 1974), and $Pb(OH)_2(aq)$ and $Pb(OH)_3^-$ are the main hydrolytic species above pH 10.

Ochs et al. (2016) published a comprehensive compilation of earlier sorption measurements with Pb on cement phases and HCP. These earlier data were also used to assign sorption values in NTB 14-08 (Wieland 2014). To the best of the authors' knowledge, no new experimental sorption data have been reported in recent years. Żak & Deja (2015) carried out a spectroscopic study of the microstructure of Pb-containing C-S-H phases and investigated the leaching behaviour of Pb. The authors concluded that Pb can be effectively immobilised by the C-S-H structure, which is in line with the notion of strong sorption as reflected by the R_d values assigned in this study (Tab. 7-1). However, no specific information on the uptake mechanism of Pb in C-S-H phases was reported by Żak & Deja (2015).

Therefore, the current appraisal of lead sorption to cementitious materials still has to be based on the earlier experimental sorption data compiled by Ochs et al. (2016) and Wieland (2014). Ochs et al. (2016) recommended the following R_d values for the different stages of the cement degradation: R_d = 0.5 m^3/kg for DS-I, R_d = 3 m^3/kg for DS-II, and R_d = 30 m^3/kg for DS-III. The values recommended by Ochs et al. (2011) are consistent with those recommended earlier in NTB 14-08 (Wieland 2014), and they are retained in the current appraisal (Tab. 7-1).

The following sorption values are recommended for Pb uptake by cementitious systems (see also Tab. 7-1):

Stages I to III: The sorption values recommended in NTB 14-08 (Wieland 2014) are retained, i.e., an R_d of 0.5 m^3/kg for DS-I, an R_d of 3 m^3/kg for DS-II, and an R_d of 30 m^3/kg for DS-III.

Niobium

The oxidation state +V is the most stable among the four oxidation states ranging from +II to +V, and +V was observed even under highly reducing conditions (Baes & Mesmer 1976, Brookins 1988). The principal chemical form under acidic conditions is NbO_2^+. Neutral species ($HNbO_3$ or $Nb(OH)_5$) dominate under slightly acid to neutral conditions. The anionic species $Nb(OH)_6^-$ or even $Nb(OH)_7^{2-}$ are the prevailing hydrolysis species above pH 7 (Baes & Mesmer 1976, Talerico et al. 2004). In highly alkaline solutions, several studies provide evidence for a significant decrease of the Nb(V) solubility in the presence of Ca, attributed to sparingly soluble ternary Ca-Nb(V)-OI/OH(s) solid phases (Talerico et al. 2004, Pointeau et al. 2004a, Yamaguchi et al. 2020, Tachi et al. 2020, Çevirim-Papaioannou et al. 2022) and for the existence of ternary Ca-Nb-OH complexes in Ca-containing alkaline solutions (Yamaguchi et al. 2020, Jo et al. 2022).

Wang et al. (2012) and Ochs et al. (2016) assigned sorption values for Nb(V) based on earlier studies already cited in NTB 14-08 (Wieland 2014). The authors recommended an R_d of 50 m^3/kg as a best estimate with an upper bound of R_d = 1,000 m^3/kg and a lower limit of R_d = 1 m^3/kg. Wieland (2014) chose a cautious approach by using the lower limit (R_d = 1 m^3/kg) for the base case, as only limited information is available on the Nb speciation in cementitious environments.

Ghosh and co-workers carried out sorption studies with Nb(V) on silica (Ghosh et al. 2015) and iron oxides (Ghosh et al. 2017), and further used spectroscopic techniques to explore the structural arrangement of Nb(V) bound to silica (Ghosh et al. 2019). Nb(V) sorption was determined in the pH range up to pH 12. On silica, the authors reported strong sorption of Nb(V) with > 96% uptake in the pH range between 2 and 11. Above pH 11, the percentage of sorbed Nb(V) decreased, indicating formation of the hydrolytic species $Nb(OH)_6^-$. Furthermore, the sorption behaviour of Nb was consistent on silica and iron oxides. The reported data did not allow exact quantification of the R_d value. An R_d of ~ 12 m^3/kg was estimated at pH 11, which results in an estimated R_d of ~ 1.2 m^3/kg at pH 12 on the assumption that $Nb(OH)_6^-$ is the dominant hydrolysis species that affects Nb(V) sorption above pH 11. This value is consistent with the one recommended for use in the safety analysis (Tab. 7-1), while it should be noted that sorption on silica may not account for sorption processes on cement phases, in particular C-S-H phases. The synchrotron-based spectroscopic studies reveal neighbouring Si atoms at a distance of ~ 3.05 Å from the central Nb absorber atom (Ghosh et al. 2019). This finding indicates inner-sphere coordination of Nb(V) with Si atoms of the silica surface, which is supported by the relatively high sorption value observed for Nb(V) on silica in the given pH range.

Only very recently, two new Nb(V) sorption studies on cementitious materials were published (Çevirim-Papaioannou et al. 2022, Jo et al. 2022). These authors report very strong uptake of Nb by pure C-S-H phases (C/S = 1.4) and fresh HCP (R_d value of ~ 100 m^3/kg) notwithstanding the presence of stable ternary Ca-Nb(V)-OH complexes in solution. Sorption isotherms were found to be linear in a solution concentration range covering almost 8 orders of magnitude in the case of C-S-H phases, and the R_d values appear to be largely independent of pH. In the case of fresh HCP, radioactive ^{95}Nb(V) sorption was found to be at least partially controlled by isotopic exchange with stable ^{93}Nb(V) present as an impurity in the otherwise pristine HCP. These two recent publications appeared too late for the preparation of the present cement SDB and could therefore no longer be taken into account for the assessment of the sorption behaviour of Nb on HCP. However, these more recent data indicate that the value proposed for the consequence analysis (R_d = 1 m^3/kg) probably underestimates the sorption of Np on HCP.

The presently available literature supports the idea of a strong uptake of Nb(V) by cement phases and HCP, which is reflected by an R_d of 1 m^3/kg in this study (Tab. 7-1). Nevertheless, the available information does not require revision of the currently selected value.

The following sorption values are recommended for the uptake of Nb by cementitious systems (see also Tab. 7-1):

Stages I to III: The sorption values recommended in NTB 14-08 (Wieland 2014) are retained, i.e., an R_d of 1 m^3/kg for DS-I, DS-II and DS-III of the cement degradation.

Technetium

The dominant technetium isotope present in radioactive waste is ^{99}Tc (half-life $2.14 \cdot 10^5$ years) originating from thermal fission of ^{235}U. In L/ILW, it is typically found on ion-exchange resins and filters as well as in sludge and decommissioning waste (Ochs et al. 2016). Tc is a redox-sensitive element occurring in redox state +VII as TcO_4^- under oxidising conditions and in redox state +IV as insoluble TcO_2 under reducing conditions (Guillaumont et al. 2003). The literature data reviewed in NTB 14-08 (Wieland 2014) revealed very weak sorption of TcO_4^- onto HCP characterised by R_d values in the range of ~ 0.001 to 0.002 m^3/kg. R_d values reported for Tc(IV) were found to range between 1 and 10 m^3/kg. The current understanding of the mechanisms controlling Tc uptake by cementitious materials is very limited.

Since 2014, only a few papers have been published dealing with Tc sorption onto cementitious materials. Bu (2018) investigated the surface adsorption of TcO_4^- by 14-Å tobermorite, jennite and ettringite with the help of molecular dynamics simulations. The author found that uptake on the octahedral CaO_6 surfaces of 14-Å tobermorite and ettringite was energetically favourable. Both inner-sphere and outer-sphere complex formation was predicted by the models. No adsorption was observed on the octahedral CaO_6 surface sites of jennite. Sorption on the tetrahedral SiO_4 surface sites of 14-Å tobermorite and jennite and on the tetrahedral SO_4 surface sites of ettringite was also energetically unfavourable.

Isaacs et al. (2020) performed wet chemistry batch sorption experiments with TcO_4^- on various synthetic cement phases, including C-S-H phases (C/S = 0.9 and 1.4), monosulphate (AFm-SO_4), monocarbonate (AFm-CO_3), ettringite, hydrogarnet, portlandite, and calcite in the presence of three different porewaters: a solution in equilibrium with the solid, a young artificial CPW (pH = 13.3) and a portlandite-saturated CPW. Sorption kinetics were very fast in all cases and TcO_4^- sorption was found to be very weak in all systems leading to R_d values in the range from $6 \cdot 10^{-4}$ m^3/kg to $4.5 \cdot 10^{-3}$ m^3/kg. Batch sorption measurements with TcO_4^- on HCP led to R_d values varying between 10^{-3} m^3/kg and $4 \cdot 10^{-3}$ m^3/kg, thus confirming the observations made in the sorption studies on the pure minerals. R_d values measured on an HCP prepared from a cement blended with blast furnace slag containing Fe(II) and sulphides were slightly higher ($\sim 10^{-2}$ m^3/kg), probably due to partial reduction of Tc(VII) to Tc(IV) followed by the formation of TcO_2(s) or Tc-sulphides. The new experimental results support the earlier appraisal given in NTB 14-08 (Wieland 2014).

Saslow et al. (2020) performed ab-initio molecular dynamics simulations and batch co-precipitation experiments to investigate TcO_4^- sorption during ettringite formation. Solid-phase characterisation techniques, including synchrotron-based absorption and fluorescence spectroscopy, and diffraction methods, showed that TcO_4^- can be incorporated into the ettringite crystal structure by an anion-exchange-driven process and further showed that one TcO_4^- and one OH^- substitute for one SO_4^{2-} anion and one H_2O molecule. The presence of TcO_4^- in the co-precipitation experiments, however, appeared to inhibit ettringite formation, thus promoting the formation of calcite, gypsum and amorphous material (> 65 wt.%). The partitioning of TcO_4^- was quantified based on the chemical analysis data of the filtrates recovered at the end of the batch sorption experiments and taking into account the ettringite content calculated from Rietveld refinement of the powder X-ray diffraction patterns. The partitioning ratios indicate very low uptake of TcO_4^- by precipitating ettringite. It should be noted that Isaacs et al. (2020) also conducted sorption experiments with TcO_4^- on ettringite instead of co-precipitation experiments. The authors observed no significant adsorption of TcO_4^- on ettringite.

Gillispie et al. (2021) investigated the role of ettringite as a possible mineralogical host for TcO_4^-. The authors investigated TcO_4^- uptake by ettringite in the presence of the competing oxyanions IO_3^- and CrO_4^{2-}. Solution analyses allowed the removal of the oxyanions to be quantified, and the solid was characterised by synchrotron-based bulk and microprobe X-ray diffraction in combination with analysis of pair distribution functions and microprobe X-ray fluorescence. Essentially, the study by Gillispie and co-workers confirms the results of Saslow et al. (2020), indicating incorporation by precipitating ettringite. Furthermore, it was observed that the incorporation of TcO_4^- by ettringite was completely inhibited in the presence of IO_3^-. These results suggest that incorporation of TcO_4^- into the ettringite structure may not be a preferred mode of TcO_4^- retention in cementitious environments.

Druteikienė et al. (2017) conducted batch-type sorption/desorption studies with TcO_4^- on a HCP made from CEM II/A cement with and without the addition of a reducing agent (sodium dithionite). In the absence of the reducing agent, consistently small sorption values were obtained (K_d value = $1.2 \pm 1.1 \cdot 10^{-3}$ m^3/kg (batch 1) and $1.5 \pm 1.2 \cdot 10^{-3}$ m^3/kg (batch 2)), indicating weak interaction of TcO_4^- with HCP. However, significantly stronger sorption was

observed in the presence of the reducing agent, thus suggesting the formation of Tc(IV) (K_d value = $6.2 \pm 0.8 \cdot 10^{-2}$ m^3/kg (batch 1) and $4.2 \pm 0.7 \cdot 10^{-2}$ m^3/kg (batch 2)). In addition, Tc sorption was partially irreversible, further supporting the idea of a strong interaction of Tc(IV) with HCP. However, Druteikiene and co-workers did not verify whether the total ^{99}Tc inventory added to the solution as TcO_4^- was reduced to Tc(IV) in the sorption experiments.

The following sorption values are recommended for Tc uptake by cementitious systems (see also Tab. 7-1):

The new results on Tc uptake by HCP support the estimates in NTB 14-08 (Wieland 2014), which assumed a very weak interaction of Tc(VII) and a stronger interaction of Tc(IV) with HCP. Competition with Cl^- could further reduce Tc(VII) uptake by HCP. However, data on this are currently lacking. It was therefore decided to retain the sorption values for Tc under reducing conditions as given in NTB 14-08 (Wieland 2014) (R_d = 1 m^3/kg) for the three stages of cement degradation. Tc(IV) is a non-anionic species and there is currently no evidence for the formation of Tc(IV)-chloro complexes. For oxidising conditions, the value assigned to DS-I in NTB 14-08 is retained, as no enhanced Cl^- concentration of the porewater is expected in DS-I. However, the R_d value for DS-II is reduced by a factor of 10 due to the expected high salinity of the porewater ($R_d = 10^{-4}$ m^3/kg instead of $R_d = 10^{-3}$ m^3/kg). The high Ca concentration in DS-III porewater, which provides positive C-S-H surface charges beneficial for anion sorption, and the high Cl^- concentration possibly leading to strong competition effects, prompted us to assign the same R_d values to DS-III and DS-II; i.e., an R_d of 10^{-4} m^3/kg (Tab. 7-1).

Zirconium

The oxidation state +IV is the dominant redox state of Zr in the E_H-pH space relevant to a cement-based repository (Brookins 1988). Different interpretations regarding the distribution of the hydrolysis products have been presented. In earlier work, $Zr(OH)_5^-$ was considered to be the main hydrolytic species in the alkaline pH range based on the hydrolysis constant reported by Baes & Mesmer (1976) and further accepted in the earlier Nagra/PSI TDB (Hummel et al. 2002). Recent reviews, however, suggest the presence of $Zr(OH)_4(aq)$ and $Zr(OH)_6^{2-}$ together with ternary Ca-Zr(IV)-OH complexes (Altmaier et al. 2008) as the dominant hydrolysis products in the neutral to strongly alkaline pH range, which has also been accepted in the updated Nagra/PSI TDB (Hummel & Thoenen 2023). Ochs et al. (2016) modelled Zr hydrolysis for a cementitious environment, which shows the existence of the neutral $Zr(OH)_4(aq)$ species in the alkaline pH range up to pH 13 and the formation of $Zr(OH)_6^{2-}$ above pH 13. Altmaier et al. (2008) reported the formation of very stable ternary $Ca_n[Zr(OH)_6]^{2n-2}$ complexes (n=1,2) in alkaline conditions containing Ca, which may dominate the aqueous Zr(IV) speciation in DS-I and DS-II. The chemical nature of the hydrolytic Zr species is expected to have an effect on the extent of Zr uptake by cement phases and HCP. If $Zr(OH)_4(aq)$ and $Zr(OH)_6^{2-}$ are the dominant aqueous species in neutral to alkaline conditions, a continuous decrease of the R_d value with increasing pH is anticipated. However, this effect might be strongly influenced by a reversal of the C-S-H surface charge from negative to positive due to increasing Ca sorption with increasing aqueous Ca concentrations expected at higher pH values. A positive surface charge could increase the affinity of the C-S-H phases for anionic $Zr(OH)_6^{2-}$ complexes but decrease the affinity for positively charged ternary $Ca_2[Zr(OH)_6]^{2+}$ complexes. Alternatively, this effect can also be explained by stronger sorption of the ternary $Ca_n[Zr(OH)_6]^{2n-2}$ complexes described by Altmaier et al. (2008) on negatively charged C-S-H surfaces. When only $Zr(OH)_4(aq)$ dominates Zr(IV) speciation in the alkaline pH range, Zr uptake by cement phases or HCP should not show a strong pH dependence up to pH 13. This appraisal is made on the assumption that competition between sorption of Zr on the solid phase and its stabilisation as an aqueous hydrolytic species governs Zr partitioning, and further that inner-sphere coordination of Zr on solids occurs, i.e., no effects of the surface charge, alkalis and Ca on Zr sorption.

A compilation of earlier sorption values was reported by Ochs et al. (2016). Baston et al. (2012) reported previously unconsidered sorption data on the uptake of Zr by untreated NRVB and NRVB aged to DS-III by leaching with deionised water (pH ~ 10.5). Very strong uptake of Zr was reported with R_d values > 10^4 m^3/kg in suspensions containing untreated NRVB (pH 12.2). From the study of Baston et al. (2012), it further appears that the presence of colloidal materials could have a pronounced effect on measurements of Zr partitioning between the aqueous phase and solid material. This finding supports the idea of a very strong interaction of Zr with solids even of colloidal nature. The authors reported a large scatter on the sorption data determined on leached NRVB. Sorption measurements in the pH range of 9.7 – 11.4 resulted in R_d values ranging from an R_d of 140 m^3/kg at pH 9.7 to an $R_d > 1.9 \cdot 10^4$ m^3/kg at pH 11.4. The reported lower bound of the R_d value implies that the sorption value tends to decrease by two orders of magnitude when the pH changes from 12.2 to 9.7. In contrast, the reported upper bound indicates no effect of the pH on sorption, resulting in an $R_d > 10^4$ m^3/kg irrespective of the pH. This large difference between R_d values determined at pH 9.7 and 11.4 can hardly be attributed to changes in the concentration of the hydrolysis products in this pH range. It should be noted that no dependence of the sorption value on pH is expected on the assumption that $Zr(OH)_4(aq)$ is the main hydrolysis product, while the difference should be less than two orders of magnitude if $Zr(OH)_5^-$ were the dominant hydrolytic species. Both potential effects of hydrolysis on Zr uptake by NRVB are not reflected in the experimental data.

Ochs et al. (2016) assigned higher sorption values to DS-III compared to DS-II, which corresponds to the idea of a pH-dependent Zr uptake by cement phases and HCP. No sorption value was assigned to DS-I by these authors. The trend of a pH dependence of Zr uptake by cement phases and HCP can hardly be justified in view of the very high sorption values reported in the literature and the expected hydrolysis behaviour of Zr under alkaline conditions. It should be noted that an R_d value of 10 m^3/kg was assigned to all stages of cement degradation in NTB 14-08 (Wieland 2014). We believe that Zr sorption in cementitious systems is very strong, i.e., comparable to that of tetravalent actinides (R_d = 100 m^3/kg). However, a conclusive line of argumentation that would justify an increase of the sorption value previously selected in NTB 14-08 cannot be presented at the present time.

Stable Zr inventories in cement reported in the literature vary between c_{cem} = ~ 10^{-5} mol/kg (Ochs et al. 2016) and $c_{cem} = 4 \cdot 10^{-4}$ mol/kg (Wieland 2014 and Tab. B-2 in this report). Isotopic exchange with stable Zr (IV) thus could control the uptake of the radioactive Zr(IV) isotopes in the repository. The aqueous concentration of stable Zr(IV) is either controlled by sorption on the cement minerals or by the solubility of Zr(IV)-containing solids. In the former case, the discussion above applies. In the latter case, an apparent R_d value can be estimated based upon the solubility of the dominating Zr(IV) solid phase under alkaline conditions. The PSI-Nagra chemical thermodynamic database (Hummel & Thoenen 2023) does not contain thermodynamic data on the solubility and hydrolysis of Zirconium. Altmaier et al. (2008) report solubilities for $ZrO_2 \cdot xH_2O(s)$ under highly alkaline conditions (c_{aq}) varying between ~ 10^{-8} M in the absence of Ca and in the presence of 0.1 M $CaCl_2$ at pH 10 and ~ $3 \cdot 10^{-5}$ M in the presence of 0.1 M $CaCl_2$ at pH ~ 12.0. Applying the "shared solubility" approach (Eq. 4, Section 4.1) with an accessibility factor (f) of 0.1, this would lead to R_d values based upon isotopic exchange with solid $ZrO_2 \cdot xH_2O(s)$ in the concrete varying between 4 m^3/kg and $1.3 \cdot 10^{-3}$ m^3/kg. These R_d values are significantly lower than the R_d values experimentally determined in sorption studies. Thus, there is evidence to suggest that surface sorption processes will control the uptake of radioactive Zr(IV) by HCP.

We therefore retain R_d = 10 m^3/kg for all stages of cement degradation. The selection is based on the assumption that hydrolysis of Zr under alkaline conditions does not depend on pH, i.e., $Zr(OH)_4(aq)$ is the dominant species in the pH range 11 – 13.3, and that Zr is strongly bound to cement phases, suggesting the formation of inner-sphere complexes, such as uptake into the interlayer of C-S-H phases.

The following sorption values are recommended for Zr uptake by cementitious systems (see also Tab. 7-1):

Stages I to III: The sorption values recommended in NTB 14-08 (Wieland 2014) are retained, i.e., an R_d of 10 m^3/kg for DS-I, DS-II and DS-III of cement degradation.

Polonium

Limited information is available on the thermodynamic properties of Po (Brookins 1988, Pourbaix 1974). Ram et al. (2019) published a detailed review of the aqueous chemistry of Po. All Po isotopes are radioactive and decay with time (longest half-life of ^{208}Po at $2.9 \cdot 10^3$ years). The E_H-pH space is dominated by Po(0) under reducing conditions above pH 10 according to the data published by Brookins (1988) and Ram et al. (2019), while Po(IV) dominates under oxidising conditions. On the basis of chemical analogy with Te(IV) and Se(IV), it was speculated that H_2PoO_3(aq), $HPoO_3^-$ and PoO_3^{2-} are important hydrolysis species under alkaline conditions (Ram et al. 2019). The two latter species, however, are only prevalent above pH 12.

No experimental sorption data with Po on cementitious materials have been reported to date, which leads to the earlier appraisal in NTB 14-08 (Wieland 2014) and the recommendation of using an R_d of 0. The sorption behaviour of Po can be re-assessed with a view to the dominant redox states under alkaline conditions. Po(IV) dominates under oxidising conditions, which anticipates significant sorption onto cement phases and cement paste. On the basis of a similarity of hydrolysis, one may speculate that the R_d value for Po(IV) uptake by HCP may range between those assigned to Pb(II) and tetravalent actinides (e.g., Th(IV)), i.e., ranging between 0.5 and 100 m^3/kg. Under reducing conditions, however, where Po(0) is the dominant species, the sorption behaviour is likely to be comparable to those of Ag and Hg with the dominant aqueous species Ag(0)(aq) (postulated) and Hg(0)(aq) (experimentally verified), thus implying the presence of the neutral Po(0)(aq) species. This analogy would suggest a nominal $R_d = 10^{-4}$ m^3/kg for Po under reducing conditions. Therefore, it is conceivable that Po uptake by HCP occurs under reducing conditions. However, it is still justified to assign an R_d of 0 due to very limited information on the hydrolysis behaviour of Po and due to the absence of sorption data for Po on cementitious materials.

The following sorption values are recommended for Po uptake by cementitious systems (see also Tab. 7-1):

Stages I to III: Assuming no sorption, as recommended in NTB 14-08 (Wieland 2014), is retained, i.e., an R_d of 0 m^3/kg for DS-I, DS-II and DS-III of cement degradation.

3.2.4 Anions

Small organic carbon compounds

Carbon-14 carrying small organic carbon compounds mainly originate from the corrosion of irradiated metals under reducing conditions and therefore potentially contribute to the long-term activity release rate from the cementitious near-field (Wieland et al. 2023). These compounds are either released as dissolved ^{14}C-bearing oxygenated carbon compounds, predominantly ^{14}C-bearing carboxylates, or as ^{14}C-bearing volatile hydrocarbons, such as methane, ethane, and ethene (Wieland & Hummel 2015, Guillemot et al. 2022).

Interaction of the gaseous carbon compounds with HCP is expected to be negligible, while the retention of oxygenated carbon compounds can occur by interaction with surface sites of cement minerals or by incorporation into the structure of specific cement minerals such as AFm phases. In the case of charged, dissolved species, such as carboxylates that are deprotonated in high-pH

solutions, interaction of the small molecules occurs by electrostatic attraction between the negatively charged anions and the positively charged surface sites of some cement phases, especially C-S-H phases. These have a positively charged surface due to adsorption of Ca^{2+} ions above pH ≈ 11. Therefore, the surface of C-S-H phases is positively charged in all stages of cement degradation, leading to weak interaction of negatively charged carboxylates with HCP. In the case of non-ionised, polar organic compounds such as alcohols and aldehydes, non-specific interaction with oxidic surface sites may occur through hydrogen bonding or van der Waals forces. In any case, surface bonding is expected to be very weak, thus leading to very weak retention of these small carbon compounds.

Wieland et al. (2016) conducted diffusion and sorption experiments with the small organic molecules methanol, ethanol, formaldehyde, acetaldehyde and formic and acetic acids on HCP under conditions representative of DS-I. The uptake of oxidised hydrocarbons by HCP was found to be very low with R_d values typically below 10^{-3} m^3/kg. Strongest uptake was observed in the case of formaldehyde, acetaldehyde and formic acid ($R_d \sim 3 \cdot 10^{-4}$ m^3/kg), while the R_d values of methanol, ethanol and acetic acid were significantly smaller (ranging from 10^{-5} to 10^{-4} m^3/kg). Nedyalkova et al. (2021) recently conducted sorption measurements with ^{14}C-labelled formate on an aged cement paste. The R_d value was determined to be $(8.9 \pm 4.4) \cdot 10^{-4}$ m^3/kg at most, which is in good agreement with the values reported previously.

In NTB 14-08 (Wieland 2014), an R_d of 10^{-5} m^3/kg was recommended as the best estimate for use in the safety analysis (lower limit: $R_d = 0$; upper limit: $R_d = 10^{-3}$ m^3/kg). This value is based on a cautious approach taking into account that a variety of carbon compounds can carry ^{14}C that only weakly sorbs to cement phases. This cautious approach is retained for the updated SDB.

The following sorption values are recommended for uptake of small organic compounds by cementitious systems (see also Tab. 7-1):

Stage I: The sorption values for the uptake of small organic compounds are retained for DS-I as given in NTB 14-08 ($R_d = 10^{-5}$ m^3/kg; lower limit: $R_d = 0$; upper limit: $R_d = 10^{-3}$ m^3/kg) as only moderate Cl^- concentrations are expected for the porewaters in this degradation stage (Tab. 2-3).

Stages II and III: The high Cl^- concentrations in DS-II and DS-III (Tab. 2-3) could significantly reduce the retention of small organic compounds due to sorption competition. At present, no data are available on the uptake of small organic molecules by HCP in highly saline porewaters. Due to lacking data and a cautious approach, no sorption is assumed for either DS-II or DS-III (R_d = 0 m^3/kg).

3.3 Re-assessed, revised sorption values

This section includes all radionuclides for which previously recommended sorption values have been revised because new experimental information has become available in recent years or because new considerations have been made on the sorption properties of the radionuclides.

3.3.1 Actinides and lanthanides

Pentavalent actinides

Calculations of the species distribution of Np(V) were reported by Tits & Wieland (2018). The calculations were based on the well-established thermodynamic data for the complexation of Np(V), also considering the formation of ternary Ca-NpO_2-OH complexes and Np-silica complexes. The thermodynamic calculations were performed for alkaline conditions (pH ≥ 10) and at Ca concentrations ranging between $4 \cdot 10^{-5}$ M and 0.02 M, thus covering the range of typical Ca concentrations in cementitious environments. The results show that the speciation is

dominated by the three hydrolytic species NpO_2^+, $NpO_2OH(aq)$ and $NpO_2(OH)_2^-$ in the absence of Ca and Si. The formation of ternary Ca-NpO_2-OH complexes, however, becomes important with increasing Ca concentration. At $[Ca]_{aq}$ = 0.02 M, $Ca[NpO_2(OH)_2]^+$ was predicted to be the dominant aqueous species in the pH range 11.5 – 12.5. The Np(V)-silica complexes that might predominantly exist in the low-pH region (e.g., $NpO_2SiO(OH)_3(aq)$) do not play a role in the Np(V) speciation distribution under alkaline conditions. Note that the existence of ternary Np(V)-hydroxy-silicate complexes expected to prevail in the alkaline pH region has not yet been demonstrated. The above findings suggest that, in addition to hydrolysis, the formation of ternary Ca-NpO_2-OH complexes could have an effect on Np(V) sorption in cementitious systems.

Häussler et al. (2018) and Tits & Wieland (2018) published new series of sorption data for Np(V) uptake by C-S-H phases, while Baston et al. (2012) had previously published an earlier unaccounted sorption study with Np(V) on NRVB. An R_d of 500 m^3/kg was determined by Häussler et al. (2018) irrespective of the S/L ratio, the C/S ratio of the C-S-H phase and pH of the equilibrium solution used. Baston et al. (2012) reported R_d values ≥ 50 m^3/kg both for untreated NRVB (pH ~ 12.5) and leached NRVB (pH ~ 10.5). Note that no pH dependence of the R_d values was observed in this study. The idea of very strong sorption of Np(V) onto C-S-H phases was further corroborated by Tits & Wieland (2018). Kinetic studies performed by these authors resulted in sorption values ranging from ~ 100 to ~ 1,000 m^3/kg on C-S-H phases with C/S ratios ranging from 0.65 to 1.65 and sorption values ranging from ~ 80 to ~ 200 m^3/kg on HCP at pH 13.3, i.e., conditions corresponding to DS-I. The slightly lower R_d value determined for Np(V) sorption onto fresh HCP can be explained by assuming that C-S-H is the only sorbing cement phase and that C-S-H phases make up only ~ 50 wt.% of fresh HCP.

Tits & Wieland (2018) carried out sorption studies with Np(V) on TiO_2 with the aim of illustrating the effect of pH, i.e., the formation of hydrolytic species, and Ca concentration, i.e., the formation of ternary Ca-NpO_2-OH complexes. The authors observed that Np(V) uptake by TiO_2 decreases with increasing pH, which could be attributed to the increasing dominance of the $NpO_2(OH)_2^-$ species in solution. This finding supports the idea that this hydrolytic species is a limiting hydroxy complex, which cannot form surface bonds with Ti-OH groups on TiO_2. At a constant pH of 13.3, where the $NpO_2(OH)_2^-$ species dominates in solution, Np(V) sorption was observed to increase with increasing aqueous Ca concentration up to an equilibrium Ca concentration of $\sim 5 \cdot 10^{-5}$ M. This Ca concentration corresponds to maximum site saturation of Ca on TiO_2 as Ca was found to sorb on the surface of TiO_2 (Tits et al. 2014b). Above this concentration, the sorbing Np(V) thus binds to a "Ca-OH"-like surface rather than to a "Ti-OH"-like surface. The effect of Ca sorption on Np(V) sorption can be explained either by neutralisation of the negative surface charge or by the formation of a very strong surface-stabilised, Ca-neptunate complex or Ca–neptunate ion pair. The same effect was observed with Np(V) on C-S-H phases. The C/S ratio of C-S-H phases is known to correlate with both the pH and Ca concentrations in solution. Np(V) uptake was strong irrespective of the C/S ratio. This finding suggests that the sorption value is affected simultaneously by two counteracting parameters: 1) a decrease in the R_d value with increasing pH due to increasing concentrations of the non-sorbing anionic $NpO_2(OH)_2^-$ species, as previously observed in TiO_2 sorption systems in the absence of Ca, and 2) an increase in the sorption value with increasing aqueous Ca concentration. Both effects may compensate each other, which results in an apparently constant R_d value irrespective of the pH and the aqueous Ca concentration in solution. It further explains why the measured sorption values are identical within the uncertainty for untreated and treated NRVB (Baston et al. 2012) and C-S-H phases with different C/S ratios.

Progress has been made in unravelling the uptake mechanism of Np(V) by HCP and C-S-H phases, while a conclusive picture is still lacking. Previous spectroscopic studies indicate that C-S-H is the uptake-controlling cement phase in HCP (Gaona et al. 2013). This implies that information on the Np(V) uptake mechanism on C-S-H is key to developing a mechanistic picture of Np(V) sorption on HCP. Evidence from the X-ray absorption spectroscopy investigations of

Gaona et al. (2013) suggests that Np(V) could be accommodated in the interlayer space of the C-S-H phases. However, this process cannot be explained by a simple cation exchange process in which Ca^{2+} is replaced by NpO_2^+ (Tits & Wieland 2018). It was further noted that the presence of Ca seems to stabilise sorbed Np(V) species as shown by the sorption experiments with TiO_2 (Tits & Wieland 2018), which could promote the existence of ternary surface complexes of $NpO_2(OH)_2^-$ and Ca^{2+} rather than interlayer bonding of Np(V).

In their literature review of radionuclide sorption onto cement, Ochs et al. (2016) compiled the experimental data from earlier sorption studies with Np(V) on various cement formulations (see references in Ochs et al. 2016). The ranges of sorption values in the different stages of cement degradation were as follows: $R_d \sim 1$ m^3/kg to ~ 30 m^3/kg for DS-I (pH 13.3), $R_d \sim 0.3$ m^3/kg to ~ 200 m^3/kg for DS-II (pH 12.5), and $R_d \sim 50$ m^3/kg to ~ 1,000 m^3/kg for DS-III (pH 12). The large scatter in the data indicates experimental challenges typically found with strongly sorbing radionuclides. Previous appraisals of Np(V) retention in HCP led to recommended values $R_d = 2$ m^3/kg for DS-I and $R_d = 20$ m^3/kg for DS-II and DS-III on the basis of chemical analogy with U(VI) and the comprehensive dataset published for U(VI) (Wieland 2014). Wieland (2014) also assigned the same sorption value to Np(V) and Np(VI), which are considered as the two possible redox states of Np under oxidising conditions. We revise the sorption values based on the idea that the sorption of Np(V) on C-S-H phases and HCP is very strong and not or only slightly affected by pH. However, we take a cautious approach by assigning R_d values corresponding to the lower limit of values reported in the literature.

The following sorption values are recommended for the uptake of pentavalent actinides by cementitious systems (see also Tab. 7-1):

Stages I and II: An increase of the sorption value for Np(V), and by analogy also for Pa(V), to $R_d = 50$ m^3/kg for DS-I and DS-II is recommended.

Stage III: $R_d = 100$ m^3/kg is assigned to DS-III in agreement with the stronger sorption observed for U(VI) in DS-III compared to DS-I and DS-II (see next paragraph). The same R_d value is assigned to Pa(V) in DS-III.

Hexavalent actinides – DS-III

Previous appraisals of U(VI), Np(VI) and Pu(VI) uptake by HCP led to recommended R_d values of 2 m^3/kg for DS-I and 20 m^3/kg for DS-II and DS-III (Ochs et al. 2018, Wieland 2014). Nevertheless, an increase of the R_d value from 20 m^3/kg to 100 m^3/kg is justified based on the consistently strong uptake of U(VI) and Np(VI) determined on cementitious materials under conditions representative of DS-III reported in the recent literature as discussed in Section 3.2.1.

The following sorption values are recommended for the uptake of hexavalent actinides by cementitious systems (see also Tab. 7-1):

Stage III: An increase of the sorption value by a factor of 5 is recommended in view of the now well-established effect of pH on the sorption behaviour of U(VI). Therefore, $R_d = 100$ m^3/kg has been assigned to the hexavalent actinides (U, Np, Pa, Pu) in DS-III (Tab. 7-1).

3.3.2 Alkaline and earth alkaline metals

Caesium – DS-III

Missana et al. (2018) carried out batch sorption experiments and modelling studies on the uptake of Cs^+ and Na^+ by C-S-H phases. C-S-H phases with target C/S ratios 0.8, 1.0, 1.2 and 1.6 were prepared in suspensions with an S/L ratio of 10 g/L. The sorption studies with Cs^+ and Na^+ were carried out directly in the synthesised C-S-H slurries. The pH of the suspensions ranged from pH 10.38 in the case of C-S-H with a target C/S ratio of 0.8 to pH 12.37 in the case of C-S-H with a target C/S ratio of 1.6. It should be noted that the competitive effect of Na^+ on Cs^+ sorption, which is characteristic for DS-I, was not addressed by Missana et al. (2018). The authors report K_d values for Cs^+ uptake ($[Cs]_{eq} \leq 10^{-6}$ M) by C-S-H phases as follows: $K_d \sim 0.1 – 0.2$ m^3/kg at C/S = 0.8 (pH 10.38), $K_d \sim 0.04 – 0.06$ m^3/kg at C/S = 1.0 (pH 11.41), $K_d \sim 0.015 – 0.025$ m^3/kg at C/S = 1.2 (pH 12.19), and $K_d \sim (3.2 – 10) \cdot 10^{-3}$ m^3/kg at C/S = 1.6. Thus, the two conditions obtained with the C-S-H systems with a C/S of 0.8 (pH 10.38) and with a C/S of 1.0 (pH 11.41) are representative of a C-S-H system relevant to DS-III. By contrast, the other two conditions represent C-S-H systems in DS-II. Sorption values can be estimated from the K_d values obtained for C-S-H systems on the assumption that the C-S-H content in HCP amounts to 50 wt.%. This results in estimated sorption values on HCP ranging between 0.02 and 0.1 m^3/kg in DS-III and $(1.6 – 12.5) \cdot 10^{-3}$ m^3/kg for DS-II. Thus, the sorption values estimated for DS-II based on the experimental data reported by Missana et al. (2018) are in good agreement with the recommended value ($R_d = 5 \cdot 10^{-3}$ m^3/kg Tab. 7-1). For DS-III, however, the value recommended in NTB-14-08 (Wieland 2014) ($R_d = 5 \cdot 10^{-3}$ m^3/kg) is about an order of magnitude lower than the estimated values (0.02 and 0.1 m^3/kg, respectively). It should be noted that C-S-H phases with C/S ratios ranging between 0.8 and 1 are considered as the uptake-controlling sorbents for metal cations in DS-III of HCP. Thus, the recommended sorption value for Cs^+ retention in DS-III has been increased from $5 \cdot 10^{-3}$ m^3/kg to 0.02 m^3/kg on the basis of the new experimental data reported by Missana et al. (2018). However, due to the high alkali concentration, the recommended R_d value is reduced accordingly.

The following sorption values are recommended for the uptake of Cs by cementitious systems in DS-III (see also Tab. 7-1):

Stage III: The new experimental data on the Cs uptake by C-S-H phases under conditions relevant to DS-III would allow an increase of the R_d value recommended in NTB 14-08 (Wieland 2014) from $5 \cdot 10^{-3}$ m^3/kg to 0.02 m^3/kg. However, the new data result from sorption studies carried out on C-S-H phases in the absence of alkalis. The presence of alkalis is taken into account for the current appraisal. We thus assign the same R_d value to DS-II and DS-III due to similar alkali concentrations in the two stages (Tab. 2-3) ($R_d = 5 \cdot 10^{-4}$ m^3/kg). Therefore, $R_d = 5 \cdot 10^{-4}$ m^3/kg is assigned to all three stages of cement degradation due to competition with alkalis.

Radium – DS-III

To date, only preliminary experimental data exist for Ra uptake by HCP in DS-III (Grambow et al. 2020). These data suggest a very strong uptake of Ra by HCP made from OPC and degraded to DS-III ($R_d > 10$ m^3/kg). Due to the preliminary nature of these data, the current sorption value for DS-III is still estimated on the basis of Ra uptake by C-S-H phases. In DS-III, all experimental data reported by Lange et al. (2018) and Olmeda et al. (2019) clearly indicate an increase in Ra uptake with a decreasing C/S ratio of C-S-H phases (see Section 3.2.2). Note that a C/S ratio < 1 is anticipated for C-S-H phases in DS-III. Therefore, a higher sorption was selected

compared to DS-II in accordance with the new experimental findings reported by Lange et al. (2018) and Olmeda et al. (2019) as well as the preliminary data reported for HCP in DS-III by Grambow et al. (2020).

The following sorption value is recommended for Ra uptake by cementitious systems in DS-III (see also Tab. 7-1):

Stage III: For the cementitious system modelled for the RBG, the Ca concentration of the pore-water in DS-III is about a factor of 5 higher than the one of the porewater in DS-II (Tab. 2-3). As a consequence of this, the R_d of $5 \cdot 10^{-1}$ m^3/kg that was assigned to DS-III based on the new experimental data, is reduced by a factor of 5 ($R_d = 10^{-1}$ m^3/kg (Tab. 7-1) due to the expected effect of Ca on Ra uptake.

3.3.3 Transition and other metals

Silver

Under oxidising conditions, Ag(I) is the only redox state of silver, while Ag(0) is the thermodynamically stable redox state under reducing conditions. The E_H-pH space is dominated by a very large field of metallic Ag(0) (Brookins 1988). Ag(I) is only present under moderately to strongly oxidising conditions. The hydrolysis of Ag(I) is very weak (Baes & Mesmer 1976). Therefore, Ag^+ is the only silver species in the acid and neutral pH range. The hydrolysis products Ag(OH)(aq) predominates above pH 11.7, while the second hydrolysis product $Ag(OH)_2^-$ only exists above pH 12.6 (Baes & Mesmer 1976, Brown & Ekberg 2016, Hummel 2017, Ochs et al. 2016). Under reducing conditions, however, silver speciation and the solubility behaviour of Ag(0)(s) can only be interpreted in a plausible manner if the formation of the neutral aqueous species Ag(0)(aq) is considered (Hummel 2017). For this reason, Hummel (2017) argued that the aqueous Ag(0) species might exist as indicated from solubility studies with metallic silver (see Dobrowolski & Oglaza 1963 referenced in Hummel 2017) and therefore should be included in the TDB. Hummel (2017) noted further that, in the case of the chemically similarly heavy metal mercury, the existence of the Hg(0)(aq) species was demonstrated and the solubility of metallic mercury via the equilibrium Hg(l) ⇌ Hg(aq) is well established (Clever et al. 1985).

To the best of the authors' knowledge, reliable experimental data on silver uptake by cement phases and cement paste have not yet been reported. Ochs et al. (2016) suggested that Ag sorption might diverge from zero based on circumstantial evidence. The authors proposed that the sorption values for Ag on HCP may be similar to those of the alkali and alkaline earth elements. The authors further noted that the hydrolysis behaviour of Ag appears to be closer to hydrolysis of the alkalis than the alkaline earth elements. This implies very weak uptake and sorption values ranging between 10^{-4} and 10^{-3} m^3/kg with a view to alkali sorption onto HCP. Ochs et al. (2016) recommended a supplemental R_d value of 10^{-3} m^3/kg.

A nominal sorption value for Ag can be estimated based on the assumption of a solubility-controlled process between Ag associated with HCP (presumably in the chemical form of Ag(0)) and the Ag concentration in solution. This approach is based on the "shared solubility" considerations previously reported by Wieland (2014). Ag is assumed to be present in solution as Ag(0) under reducing conditions ($c_{aq} = 3.16 \cdot 10^{-7}$ M as determined by Dobrowolski & Oglaza (1963)) and Ag(OH) under oxidising conditions at pH 12 ($c_{aq} = 1.85 \cdot 10^{-5}$ M according to Baes & Mesmer 1976). It is further assumed that 2% of the total Ag inventory of HCP ($c_{cem} = 2.32 \cdot 10^{-6}$ mol/kg) is in equilibrium with the aqueous Ag species in both conditions. The resulting operational R_d value for the reference case is 10^{-4} M m^3/kg under reducing conditions and $2 \cdot 10^{-6}$ m^3/kg under oxidising conditions. Note that the difference in sorption is a consequence of differences in the aqueous Ag concentrations. The estimated values support the idea of a very weak interaction of Ag with HCP in accordance with Ochs et al. (2016). For the current appraisal,

a cautious approach has been taken by retaining zero sorption under oxidising conditions (Ag(I)) for all stages of cement degradation and by assigning a nominal sorption value of 10^{-4} M m^3/kg under reducing conditions (Ag(0)) for all stages of cement degradation.

The following sorption values are recommended for the interaction of Ag with cementitious systems (see also Tab. 7-1):

Stages I to III: A nominal sorption is assigned to Ag retention under reducing conditions (Ag(0)) ($R_d = 10^{-4}$ m^3/kg), which is based on the "shared solubility" considerations previously reported in NTB 14-08 (Wieland 2014). An R_d of 0 m^3/kg is retained under oxidising conditions as given in NTB 14-08.

Tin

The oxidation state +IV dominates in the E_H-pH space relevant to a cement-based repository (Brookins 1988, Pourbaix 1974) with $Sn(OH)_6^{2-}$ as the dominant hydrolytic species above pH 10.5 (Hummel et al. 2002, Ochs et al. 2016, Wang et al. 2012). It should be noted that, analogous to Zr(IV) (see Section 3.2.3), the formation of ternary complexes with Ca, e.g., $(Ca_x[Sn(OH)_6])^{2x-2}$, is also conceivable and could eventually influence the sorption behaviour of Sn(IV) on cement phases.

To date, only a limited number of studies have reported on the uptake of Sn(IV) by cementitious materials (e.g., review in Ochs et al. 2016). Baston et al. (2012) published sorption data with Sn on untreated NRVB and NRVB that was aged to DS-III by leaching with deionised water (pH ~ 10.5). Note that the solution in equilibrium with untreated NRVB had a pH of 12.2. The composition of NRVB is given in Section 3.2.1. Sorption values were found to range between 130 and 690 m^3/kg on untreated NRVB, which results in estimated sorption values on HCP ranging from 65 to 345 m^3/kg. This estimate is based on the assumption that the proportion of HCP in NRVB is ~ 50 wt.%. On aged NRVB, i.e., corresponding to pH ~ 10.5 of the equilibrated water, sorption values were found to range between 130 and 280 m^3/kg. It is noteworthy that the sorption values were found to be similar at pH 12.2 and 10.5, indicating that uptake of Sn(IV) by NRVB does not depend on pH. This finding is not consistent with the idea that a hydrolytic species, i.e., $Sn(OH)_6^{2-}$, is the main aqueous Sn species that competes with surface sites for Sn complexation. An interpretation of sorption based on hydrolysis would imply an increase in sorption with decreasing pH, i.e., with decreasing $Sn(OH)_6^{2-}$ and eventually $(Ca_x[Sn(OH)_6])^{2x-2}$ concentration. Note, however, that the aqueous Ca concentration is higher at pH 12.2 and could cause a charge reversal on the C-S-H surfaces, which could affect Sn(IV) sorption. The resulting positive surface charge could increase the C-S-H affinity for $Sn(OH)_6^{2-}$, thus compensating the pH effect.

The study of Baston et al. (2012) corroborates the notion of strong uptake of Sn(IV) by HCP and justifies the previously selected R_d of 10 m^3/kg in NTB 14-08 (Wieland 2014) for all stages of cement degradation and the R_d of 20 m^3/kg recommended by Ochs et al. (2016) for DS-I and DS-II. As a consequence of the consistently high sorption values determined for Sn(IV) on cementitious materials and in accordance with the earlier review of sorption data by Ochs et al. (2016), the sorption values for Sn(IV) on HCP in DS-II and DS-III are increased to an R_d of 20 m^3/kg, while an R_d of 10 m^3/kg is retained for DS-I. This selection reflects that experimental data have been published for HCP in DS-I (Bonhoure et al. 2003) and DS-II (Ochs et al. 2016) of cement degradation, which further accounts for the idea of an increase in sorption with decreasing pH.

The following sorption values are recommended for the uptake of Sn by cementitious systems (see also Tab. 7-1):

Stage I: The sorption values recommended in NTB 14-08 (Wieland 2014) are retained.

Stages II and III: Higher sorption values are selected for DS-II and DS-III (R_d = 20 m^3/kg instead of R_d = 10 m^3/kg).

3.3.4 Anions

Chloride

In NTB 14-08 (Wieland 2014), precipitation as Friedel's salt, anion exchange on AFm phases (formation of AFm-type solid solutions) and physical sorption onto C-S-H phases via electrostatic attraction by positively charged C-S-H surfaces were considered as the main processes controlling the Cl^- retention by cementitious materials. The precipitation of Friedel's salt ($Ca_4Al_2(Cl)_{1.95}(OH)_{12.05}\cdot 4H_2O$) only occurs at very high Cl^- concentrations, i.e. > ~ 10 mM (Ochs et al. 2016). Cl^- was found to substitute for OH^-, SO_4^{2-} and CO_3^{2-} in hydroxyl-AFm, monosulphate and monocarbonate to form series of solid solutions (Balonis et al. 2010). The high concentration of Ca^{2+} in solution in equilibrium with C-S-H phases with high C/S ratios (C/S > 1.2) gives rise to charge reversal of their negatively charged surfaces, thus enhancing Cl^- binding (Plusquellec & Nonat 2016, Shi et al. 2017). Therefore, electrostatic surface sorption onto C-S-H phases is a potential binding mechanism for Cl^- in DS-I and DS-II. Cementitious materials generally contain significant amounts of stable Cl^- (Ochs et al. 2016, Wieland 2014). ^{36}Cl uptake thus takes places via an isotopic exchange with stable Cl^- sorbed onto the cement minerals.

Since the publication of NTB 14-08 (Wieland 2014), several new studies on chloride binding by pure cement phases and by HCP prepared from OPC and cement blends have been published. They are briefly discussed as follows.

Ipavec et al. (2013) investigated the effect of limestone and pozzolanic materials (granulated blast furnace slag, fly ash and silica fume) as mineral admixtures on the Cl^- uptake by HCP in the pH range between 12.8 and 13.5. NaCl was used as the chloride source, and Cl^- concentrations varied between 0.05 M and 2.0 M. The Cl^- sorption data shows a Freundlich-type adsorption isotherm. Chloride uptake appears to be a reversible process. Cl^- uptake was weaker under highly alkaline conditions (pH = 13.5), and uptake increased when the pH was reduced to 12.8. At high pH (13.5), limestone-blended cements exhibited lower Cl^- uptake compared with limestone-free cements due to competition of CO_3^{2-} with Cl^- for exchange sites in the AFm interlayers. At lower pH (12.8), this effect was less obvious. The observed effect of the presence of various pozzolanic materials was explained in terms of their Al contents: an increasing Al content of the cementitious materials increased Cl^- uptake. Characterisation of the solid phases at the end of the experiments by X-ray powder diffraction indicates that increased chloride binding is accompanied by increasing intensities of the reflections of chloro-aluminates such as (Cl^--OH^-)-AFm and (Cl^--CO_3^{2-})-AFm solid solutions and rhombohedral and monoclinic Friedel's salt.

R_d values derived from the experimental sorption isotherms reported by Ipavec and co-workers vary between a maximum of $4 \cdot 10^{-3}$ m^3/kg at the lowest Cl^- concentration in solution and a minimum of 10^{-4} m^3/kg at the highest Cl^- concentration in solution. Effects of pH and Al and carbonate contents are present, but relatively small (at most a factor of 5) in relation to the R_d value. The influence of the Cl^- concentration in the equilibrium solution has a much stronger influence on the R_d values (more than one order of magnitude).

Weerdt et al. (2015) studied the effect of the type of cations accompanying Cl^- uptake by cementitious materials. The authors performed sorption experiments by adding Cl^- to fresh HCP prepared from CEM I 42.5 in the form of NaCl, $MgCl_2$ or $CaCl_2$ in the concentration range between 0.5 M

and 3.5 M. They measured a much stronger binding of Cl^- added as $CaCl_2$ or $MgCl_2$ compared to experiments carried out with NaCl, confirming observations made earlier by other research groups (Arya et al. 1990, Tritthart 1989). The authors also found that this effect is related to the influence of Ca^{2+} and Mg^{2+} concentrations in solution on the pH. A thermodynamic model description of the experimental systems showed that the addition of Cl^- in the form of $CaCl_2$ or $MgCl_2$ resulted in the precipitation of $Ca(OH)_2$(s) or $Mg(OH)_2$(s) leading to a reduction of the pH, higher Ca concentrations in solution and thus to higher C/S ratios of the C-S-H phases. The thermodynamic models further showed that these changes in solution composition have no influence on Cl^- incorporation into AFm phases, but they do affect Cl^- adsorption onto C-S-H surfaces. The authors concluded that, in the presence of high concentrations of divalent cations, C-S-H phases play a major role in the binding of Cl^- in HCP even at very high aqueous Cl^- concentrations. At low concentrations of divalent cations, the constant amounts of bound Cl^- with increasing Cl^- concentrations in solution suggest that Cl^- binding is probably controlled by Cl-AFm formation in agreement with the conclusions of Ipavec et al. (2013).

A recent study published by Shi et al. (2017) corroborates the observations of Ipavec et al. (2013) and Weerdt et al. (2015). These authors investigated the influence of the type of cations (Ca^{2+} versus Na^+) on Cl^- uptake by OPC-metakaolin-limestone cements using Cl^- concentrations ranging between 0.125 M and 2.0 M. Two sinks were found to exist for Cl^- in cementitious materials: AFm phases and C-S-H phases. In pure OPC (CEM I), Cl^- is immobilised in the presence of Na mainly in Friedel's salt (and AFm solid solutions) and sorbed to a lesser extent onto C-S-H phases. In the presence of divalent Ca^{2+}, however, larger amounts of Cl^- are sorbed mainly to the C-S-H phases, while less Cl^- is incorporated into the Friedel's salt. In OPC blended with supplementary cementitious materials adding additional Al to the cement, Cl^- uptake increased significantly due to additional formation of Friedel's salt. The addition of Ca to such cements increased the Cl^- uptake even further, while the presence of Ca^{2+} promoted the transformation of monocarbonate to Friedel's salt by precipitating the released carbonate as $CaCO_3$(s).

Plusquellec & Nonat (2016) investigated the uptake of Cl^-, Br^- and NO_3^-, added as Ca-salts, onto C-S-H and C-A-S-H phases with different C/S ratios ($0.8 \leq C/S \leq 1.42$) in the concentration range between ~ 5 mmol/L and 170 mmol/L, using ion-selective Cl^- and Br^- electrodes. The authors found no difference in the potentials between C-S-H suspensions and reference solutions without C-S-H phases with identical Ca and anion concentrations, irrespective of the C/S ratio, the presence of Al in the C-S-H structure or the type of anion. Only the pH of the suspension was lower than the pH of the corresponding C-S-H solution. Ca, on the other hand, was taken up by the C-S-H phases. The authors concluded from these observations that the anions do not chemically sorb onto C-S-H phases irrespective of the C/S ratio and that they merely neutralise the positive C-S-H surface charge by accumulating in the diffuse double layer. The anion adsorption observed by other research groups was considered to be an artefact caused by anions adhering to the positively charged C-S-H surfaces during filtration or centrifugation. It should be noted that the observed weak retention of Cl^- on C-S-H phases supports the idea of a process by charge compensation and not by chemical sorption.

Nedyalkova et al. (2021) published data on HTO, ^{36}Cl, ^{125}I and ^{14}C-formate uptake by fresh HCP and cement pastes aged in situ by interaction with formation waters from the Opalinus Clay and granite for more than 10 years. The fresh HCP was prepared from a Holcim Protego 4R (CEM I 42.5 R-SR0) sulphate-resistant cement. One aged cement sample was an OPC mortar drill core from the Grimsel Test Site (Switzerland) (equilibration with granite formation water) and the other one was an OPC drill core from the Mont Terri Rock Laboratory (Switzerland) (equilibration with Opalinus Clay formation water). The pH of the equilibrated suspensions varied between 13.37 (fresh HCP and Grimsel samples) and 13.0 for the Mont Terri sample indicating that all cement phases were still in DS-I. Both sorption kinetics and sorption isotherms were determined. In the case of ^{36}Cl sorption, sorption equilibrium was reached within 3 – 5 days except

for the fresh HCP only reached sorption equilibrium after ~ 10 days. Cl^- sorption was highly non-linear, and R_d values decreased with increasing Cl^- concentration of the porewater from a value of ~ 0.025 m^3/kg at a Cl^- equilibrium concentration of $7 \cdot 10^{-5}$ M (stable Cl^- + $^{36}Cl^-$) to a value of ~ 10^{-4} m^3/kg at a Cl^- equilibrium concentration of 0.5 M. Note that in the original publication, the authors did not account for the stable Cl^- concentration present as impurity in the cementitious material.

Very recently, Jo et al. (2022) published a study on Cl^- uptake by HCP under conditions relevant to DS-I. The authors also observed sorption isotherms that are highly non-linear taking into account stable Cl^- present in pristine HCP. R_d values decreased from ~ 0.04 m^3/kg at $[Cl^-]_{tot} = 1.5 \cdot 10^{-4}$ M, to ~ $3 \cdot 10^{-4}$ m^3/kg at $[Cl^-]_{tot} = 2.0$ M in agreement with the observations of Nedyalkova et al. (2021). The uptake at lower Cl^- concentrations was attributed to a surface adsorption process whereas the precipitation of Friedel's salt and the formation of solid solutions was considered to be the controlling immobilisation mechanism at high Cl^- concentrations.

The diffusion behaviour of Cl^- in cementitious materials was the subject of few more recent studies. Van Es et al. (2015) performed radial diffusion experiments to investigate the effect of the presence of cellulose degradation products (CDPs) on Cl^- diffusion through NRVB (see Section 3.2.1). The authors found that the presence of CDPs enhances the migration of Cl^- due to weaker Cl^- retention. It was postulated that the blocking of Cl^- sorption sites was caused by anionic CDPs. However, it should be noted that the concentration of the CDPs in the system was not reported, making it difficult to assess whether or not competitive sorption of CDPs (e.g., ISA) and Cl^- occurred. Savoye et al. (2018) published a study on Cl^- diffusion through partially saturated, fresh HCP prepared from CEM-V/A at different degrees of saturation (S_w) that varied between 0.18 and 1. The Cl^- concentration was 30 mmol/L. The results show a decrease of the effective diffusion coefficient (D_e) by a factor of 10, when the degree of saturation decreased from 1.0 to 0.85. Further decrease of S_w from 0.74 to 0.41 caused only a very small additional reduction of D_e. Strong reduction of S_w from 0.41 to 0.18 resulted in a further sharp reduction of D_e. R_d values derived from these diffusion experiments were not significantly affected by the degree of saturation and varied between $8 \cdot 10^{-5}$ m^3/kg and $5 \cdot 10^{-4}$ m^3/kg.

In summary, the new research published since NTB 14-08 (Wieland 2014) confirms that Cl^- is mainly bound to cement phases by three processes: precipitation of Friedel's salt, exchange with anions in AFm phases or possibly hydrotalcite, and electrostatic adsorption onto positively charged C-S-H phases with C/S ratios ≥ 1.1. Cl^- sorption is influenced by the type of cations present in solution: divalent cations improve sorption compared to monovalent cations due to the promotion of positively charged surface sites on C-S-H phases. Higher Al contents in the cementitious materials improve Cl^- uptake by promoting AFm formation. $^{36}Cl^-$ sorption by cement phases is assumed to take place by isotopic exchange with the stable Cl^- in the cementitious near-field. Therefore, the stable Cl^- concentration is a key parameter to consider when assessing Cl^- retention. Stable Cl^- is introduced by cement (content between 0.005 and 0.3 wt.%), as Cl^- is supplied with the raw materials and fuel during clinker production (Locher 2006). In addition, Cl^- is supplied by the porewater intruding from the OPA host rock into the L/ILW caverns from DS-II onwards for the applied model approach. It should be noted that the latter source of Cl^- is more important than the supply from the clinker (Tab. 2-1 and Tab. 2-2).

With respect to Cl^- sorption, there are three important differences between the cement mineral and porewater compositions used in NTB 14-08 (Wieland 2014) and in the present SDB:

- Cl^- concentration is one order of magnitude higher in the CPWs assumedly due to intruding NL-ZNO-22 OPA porewater.
- Almost complete absence of AFm phases in all degradation stages of the HCP as new thermodynamic data for Al/Fe siliceous hydrogarnet have been introduced in the CEMDATA 18.1 database. This cement phase appears to be the most thermodynamically stable Al/Fe-

containing cement phase with respect to the time period under consideration for a deep geological repository. Note that in NTB 14-08 it was assumed that AFm phases are an important component of HCP. The virtual absence of AFm phases means that the selection of R_d values for the cement SDB has to be based on Cl^- retention by C-S-H phases in all three stages of cement degradation.

With this information, together with the process understanding obtained from the new literature summarised above and with the information from earlier literature summarised in NTB 14-08 (Wieland 2014), it is proposed to select Cl^- R_d values for the new cement SDB as follows:

During all three stages of cement degradation, electrostatic surface sorption onto C-S-H phases is the only sorption mechanism considered. The C/S ratio of the C-S-H phases present in DS-I and DS-II is ~ 1.6 and the aqueous Ca concentration in the CPW is ~ $3 \cdot 10^{-3}$ M for DS-I and ~ 10^{-2} M for DS-II. In DS-III, the C/S ratio of the reference systems is assumed to be ~ 1.1, while the C/S ratio at the end of DS-III is calculated to be ~ 0.7 and the aqueous Ca concentration is ~ $7 \cdot 10^{-2}$ M (Tab. 2-3). It should be noted that the surface charge of C-S-H phases is not directly determined by the C/S ratio, but rather by the Ca concentration in solution. It was reported that aqueous Ca concentrations below ~ $2 \cdot 10^{-3}$ M give rise to negative surface charges (Labbez et al. 2007, Pointeau et al. 2006, Viallis-Terrisse et al. 2001). The above discussion of the new literature has confirmed the observation that higher aqueous Ca^{2+} concentrations enhance Cl^- sorption due to the higher positive charge of the C-S-H surfaces. Consequently, we can assume that the C-S-H phases have a neutral to positive surface charge in all stages of cement degradation. Such electrostatic properties are favourable for Cl^- adsorption. Knowing that AFm phases are virtually absent under the assumption that Al/Fe siliceous hydrogarnet is present and that C-S-H phases make up the majority of cement mineralogy (~ 33 wt.% in DS-I and DS-II and ~ 67 wt.% in DS-III), it can be safely assumed that Cl^- sorption is controlled by electrostatic attraction on the C-S-H fraction. The stable Cl^- concentration in the porewater of DS-I is ~ $4 \cdot 10^{-3}$ M whereas the Cl^- concentrations for DS-II and DS-III are approximately a factor of 50 higher; i.e., ~ 0.2 M (Tab. 2-3). High concentrations of stable Cl^- of the porewaters in DS-II and DS-III are expected to lead to very weak sorption of ^{36}Cl based on the isotopic exchange process that controls ^{36}Cl retention.

The following sorption values are thus recommended for Cl^- uptake by cementitious systems (see also Tab. 7-1):

Stage I: In NTB 14-08 (Wieland 2014), an R_d value of $5 \cdot 10^{-3}$ m^3/kg was recommended for DS-I. This value corresponds to the R_d value (~ $1 \cdot 10^{-2}$ m^3/kg) determined by Nedyalkova et al. (2021) for Cl^- sorption onto three different cement pastes at an aqueous Cl^- concentration of ~ 10^{-4} M. At the higher Cl^- porewater concentrations found for Stage 3 of the Sectoral Plan ($4 \cdot 10^{-2}$ M), Nedyalkova et al. (2021) measured Cl^- R_d values that are a factor of 10 lower (~ $3 \cdot 10^{-4}$ m^3/kg) (non-linear sorption isotherm). Note that this value is at the lower limit of the R_d values reported by Ochs et al. (2016). Thus, the R_d value previously selected in NTB 14-08 (Wieland 2014) ($5 \cdot 10^{-3}$ m^3/kg) for DS-I is lowered by a factor of 5 ($R_d = 10^{-3}$ m^3/kg), which is justified by the expected, significantly higher Cl^- concentration of the porewater in DS-I ($4 \cdot 10^{-3}$ M) and the absence of AFm phases.

Stage II: It can be assumed that Cl^- sorption is also controlled by electrostatic attraction on the C-S-H surface in this degradation stage. The Ca concentration is ~ $2 \cdot 10^{-2}$ M, thus providing a positively charged C-S-H surface favourable for Cl^- sorption. On the other hand, the Cl^- concentration of the porewater is expected to be a factor of 50 higher than in DS-I. Thus, it is recommended to reduce the R_d value for this stage by a factor of 10 compared to DS-I. An R_d of 10^{-4} m^3/kg is in agreement with the observations of Nedyalkova et al. (2021). This compares to an R_d value of $5 \cdot 10^{-2}$ m^3/kg as given previously in NTB 14-08.

Stage III: AFm phases are absent, and the C/S ratio of the C-S-H fraction is very low (C/S = ~ 0.7 – ~ 1.5). The Ca concentration of the CPW in DS-III is very high; i.e., ~ 0.07 M (Tab. 2-3), suggesting an at least partially positively charged C-S-H surface. However, the Cl^- concentration is also very high (~ 0.23 M), suggesting very weak sorption of ^{36}Cl (isotopic exchange process). Therefore, due to similar compositions of the CPWs, the same R_d values are assigned to DS-III and DS-II ($R_d = 10^{-4}$ m^3/kg).

Iodide

In L/ILW, ^{129}I is mainly bound to ion-exchange resins used for decontamination during reactor operation (Hummel 2017). The main degradation products of anion-exchange resins (such as Lewatite M-500 and Powdex PAO) are ammonia, methylamine, dimethylamine and trimethylamine (van Loon & Hummel 1999b), whereas the degradation products of cation exchange resins (like Lewatite S-100 and Powdex PCH) produce mainly sulphate and dissolved organic carbon (van Loon & Hummel 1999a). The most important organic ligand is oxalate (10 – 20 wt.% of the organic carbon found in solution after degradation). Iodide is expected to be sorbed on the ion-exchange resins and rapidly desorb upon conditioning the spent ion-exchange resins in cementitious matrices. Therefore, release of I^- is not due to the degradation of the spent ion-exchange resins. The interaction of I^- with the organic degradation products is not yet clear.

In NTB 14-08 (Wieland 2014), it was assumed that I^- is the dominant redox species in the cementitious near-field of an L/ILW repository in the long term. Sorption processes identified in NTB 14-08 are very similar to those controlling Cl^- sorption, i.e., anion exchange on AFm phases (formation of AFm-type solid solutions) and physical sorption onto C-S-H phases via electrostatic attraction by positively charged C-S-H surfaces. Precipitation as a pure I^--containing AFm phase, i.e., monoiodide (AFm-I_2). Is not expected at the low I^- concentrations present in L/ILW. I^- easily exchanges for SO_4^{2-} in AFm-SO_4, forming a solid solution. The presence of high concentrations of carbonate and chloride promotes the conversion of AFm-SO_4 to AFm-CO_3 or AFm-Cl_2, thus making it much more difficult for I^- to become incorporated into the AFm interlayer. These considerations led the authors to select R_d values for I^-, which are a factor of 5 lower than those for Cl^-.

Since the publication of NTB 14-08 (Wieland 2014), new research results have been published in the open literature, including a review by Ochs et al. (2016) that broadly confirms the conclusions presented in NTB 14-08.

Ait Mouheb et al. (2017) performed batch sorption experiments with I^- at a concentration of $5.9 \cdot 10^{-5}$ M on three different low-pH cements consisting of mixtures of OPC (CEM I 52.5 N), silica fume, limestone filler and superplasticiser at three different wt.% ratios: 39:39:19:3, 40:40:20:0, and 50:50:0:0. The characterisation of the HCPs reveals the presence of mainly amorphous phases (hypothesised to be C-S-H phases, calcite, and very small amounts of ettringite). Portlandite and AFm phases were not detected. The Ca concentration of the CPW was $3.56 \cdot 10^{-3}$ M. The anion composition of the solution was dominated by SO_4^{2-} ($5.75 \cdot 10^{-3}$ M) and Cl^- ($3.84 \cdot 10^{-3}$ M), and the pH was 11.0. According to the authors, the C/S ratio of the C-S-H fraction was between 0.6 and 0.8. R_d values for I^- sorption on these three low-pH cements were found to reach a mean value of $(1.3 \pm 0.1) \cdot 10^{-4}$ m^3/kg. Such low R_d values can only be explained by strong competition of SO_4^{2-} and Cl^- anions for sorption on the positively charged surface sites on the C-S-H phases.

Guo et al. (2020) showed that I^- is only weakly incorporated into the ettringite structure whereas IO_3^- uptake by ettringite is strong and takes place by substitution of SO_4^{2-} anions in the structure. The authors carried out co-precipitation experiments and determined the mean R_d values to be $6.6 \cdot 10^{-4}$ m^3/kg for I^- uptake and 17.2 m^3/kg for IO_3^- uptake after a very short reaction time of 24 hours.

Nedyalkova et al. (2020) published a detailed study of the "solid solution" formation between AFm-I_2 (monoiodide) and the OH- and CO_3-containing AFm phases. AFm-I_2 (monoiodide) and AFm-OH (monohydrate) as well as AFm-I_2 and AFm-(OH,CO_3) (hemicarbonate) form extensive solid solutions, whereas AFm-I_2 and AFm-CO_3 (moncarbonate) do not show end-member mixing. AFm-OH, AFm-(OH,CO_3) and AFm-(I,OH,CO_3) are metastable and transform to katoite and AFm-CO_3 with release of I^- from the interlayer of the AFm phases in the long term. In a subsequent study, Nedyalkova et al. (2020) could show that AFm-I_2 forms discontinuous solid solutions with AFm-HS (with miscibility gaps at AFm compositions close to both pure end-members) and with AFm-(OH,CO_3) (with one miscibility gap at $x_I > 0.9$). The authors also report I^- sorption isotherms onto AFm-SO_4 (monosulphate), AFm-(OH,CO_3) and AFm-HS (mono-sulphide) in the I^- concentration range between $2 \cdot 10^{-6}$ M and 0.1 M. Sorption values for I^- on all three AFm-phases were found to be very similar. The strongest sorption was observed on hemicarbonate with a mean calculated R_d value of $(4.8 \pm 1) \cdot 10^{-2}$ m^3/kg, followed by mono-sulphide with a mean R_d of $(3.5 \pm 0.7) \cdot 10^{-2}$ m^3/kg. Monosulphate showed the lowest affinity for I^- with an R_d of $(2.7 \pm 0.5) \cdot 10^{-2}$ m^3/kg, thus confirming previous in-house data reported in NTB 14-08 (Wieland 2014). The I^- sorption isotherms onto AFm-SO_4, AFm-OH and AFm-(OH,CO_3) could be well reproduced thermodynamically by assuming solid solution formation as described above and applying a subregular solid solution model with end-member definitions based upon the Vanselov convention. Model simulations further showed that in OPC with low carbonate content (< 2 wt.% $CaCO_3$), the addition of I^- leads to the formation of an AFm-(I_2,OH,CO_3) solid solution, resulting in a strong I^- retention. In OPC with higher carbonate content (> 2 wt.% $CaCO_3$), however, AFm-CO_3 formation takes place at the expense of AFm-(I_2,OH,CO_3) formation, resulting in reduced I^- immobilisation and thus lower I^- R_d values.

In their publication on HTO, ^{36}Cl, ^{125}I and ^{14}C-formate sorption on fresh and aged HCP (see previous section), Nedyalkova et al. (2021) published data from measurements of the I^- sorption kinetics and sorption isotherms. Overall, I^- sorption on theses HCPs was very similar to that of Cl^-. Sorption equilibrium was reached after up to 5 days except for fresh HCP where the time needed to reach sorption equilibrium was ~ 10 days. The sorption isotherms were highly non-linear. R_d values were found to be similar to those determined for Cl^-, i.e., ranging between $5 \cdot 10^{-3}$ m^3/kg and $1.5 \cdot 10^{-2}$ m^3/kg at the lowest I^- aqueous concentrations ($5 \cdot 10^{-7}$ M to 10^{-6} M) and between $2 \cdot 10^{-4}$ m^3/kg and $2 \cdot 10^{-3}$ m^3/kg at the highest I^- aqueous concentrations ($2 \cdot 10^{-3}$ M). In contrast to Cl^- sorption, however, no difference in I^- sorption behaviour was found between the different HCPs.

Kaplan et al. (2019) reported on the influence of organic iodine compounds on the uptake of iodine by grouts consisting of cement (25%) and fly ash (75%). This effect was not observed for the same grout containing additional slag (cement: 8%; fly ash: 47%; slag: 45%). The effect was attributed to the formation of organic-iodine species, which leads to increased leaching (i.e., lower sorption values) of iodine from the cementitious material. The authors postulated that organic compounds that are aromatic in nature react with iodine within the 3 months of hydration of the iodine-amended grouts, significantly changing the iodine speciation in the cementitious system. The reducing conditions established in the presence of slag promoted the formation of I^- and therefore prevented the presence of iodine in oxidation state 0 (such as HOI, I_2, or I(0)), which is the oxidation state of iodine species required to form covalent bonds with organic molecules (Kaplan et al. 2019). It has further been postulated that fly ash is the source of the aromatic organic compounds. However, the authors did not identify the organic-iodine complexes that could be present in the fly-ash-containing grout, so their presence was assumed on the basis of circumstantial evidence. The results reported by Kaplan et al. (2019) cannot be directly applied to cementitious systems prepared from OPC, which is the main source material for the conditioning of radioactive waste and the construction material for a cement-based deep geological repository in Switzerland. OPC contains only a limited amount of small organic molecules added as grinding aids during cement production, such as triethanolamine, or ethylene glycol. To the authors'

knowledge, naturally occurring or synthetic aromatic organic compounds that show increased reactivity with iodine in oxidation state 0 are not expected in OPC. The reactivity of cement admixtures, such as polynaphthalene-sulphonate- and lignin-sulphonate-based superplasticisers, which commonly have been used in concrete production and are aromatic in nature, is currently unknown. The development of the current cement SDB is based on the assumption that poly-carboxylate ether-based superplasticisers (PCEs) will be used for concrete production in the construction of the planned deep geological repository, which, for structural reasons, seem to be less susceptible to the formation of organically bound iodine.

In summary, the new data published since 2014 largely confirm the process understanding obtained for I^- binding by cementitious materials presented in NTB 14-08 (Wieland 2014). Similar to Cl^-, mainly two processes are considered to control I^- binding by cementitious materials: 1) exchange with anions in AFm phases, and 2) electrostatic adsorption onto the positively charged surface sites of C-S-H phases. I^- sorption is influenced by the type of cations present in solution: divalent cations improve sorption compared to monovalent cations. Higher Al contents of the cementitious materials improve Cl^- as well as I^- uptake by increased AFm formation. In contrast to $^{36}Cl^-$ binding, however, the $^{129}I^-$ binding does not take place by an isotopic exchange process with its stable counterpart because the stable I^- content of cementitious system is generally very low. Both possible sources of stable I^-, i.e., cement clinker and formation water, have very low I^- concentrations. In the case of cement, I^- is only present at low concentrations in the raw materials and fuel used for clinker production (Locher 2006). The high concentrations of stable Cl^- in CPWs probably lead to strong competition for sorption on the positively charged C-S-H surface sites. R_d values reported by different authors and in-house data (Wieland 2014) agree that I^- exhibits a similar or even a slightly higher affinity for cement surfaces than Cl^-. For example, R_d values for I^- were found to be similar to, or even a factor of 2 larger than those for Cl^- (Nedyalkova et al. 2021, Pointeau et al. 2008).

The difference in the cement mineralogy between NTB 14-08 (Wieland 2014) and the updated cement SDB also plays an important role in the selection of I^- R_d values, as previously discussed for Cl^-. The content of AFm phases in the cement materials calculated with the new CEMDATA 18.1 database is negligible. It can therefore be assumed that AFm phases do not play a role in anion sorption in aged cementitious systems. In NTB 14-08, AFm phases were assumed to be an important component of the cementitious materials and therefore contribute to I^- retention. This means that the selection of R_d values for I^- uptake by HCP for the updated cement SDB has to be based on uptake by C-S-H phases.

Based on this information and the process understanding from the new literature summarised above, as well as the information from previous literature summarised in NTB 14-08 (Wieland 2014), the following sorption values are recommended for I^- uptake by cementitious systems (see also Tab. 7-1):

Stage I: The amount of AFm phases is negligible, and electrostatic surface sorption to C-S-H phases is considered to be the main sorption mechanism. As discussed in the previous section on the selection of R_d values for Cl^-, we can assume that the C-S-H phase of the cementitious system in DS-I carries a neutral to positive surface charge and that the C-S-H content is approximately 33 wt.%. Therefore, it can be safely assumed that I^- sorption occurs due to electrostatic attraction by the C-S-H fraction of the HCP. It is known that I^- uptake takes place at the same mineral fraction and is controlled by the same process as Cl^- and that I^- has a similar affinity for HCP as Cl^-. Therefore, we select the same R_d values for $^{129}I^-$ sorption as previously assigned to $^{36}Cl^-$ sorption, which means that the R_d value of 10^{-3} m^3/kg previously selected for DS-I in NTB 14-08 (Wieland 2014) can be retained.

Stage II: AFm phases make up only ~ 6.4 wt.% of the cementitious material in DS-II, and therefore I^- sorption is assumed to take place on the C-S-H fraction of HCP. The Ca concentration of the CPW is ~ 10^{-2} M (Tab. 2-3). This means that C-S-H phases are positively charged favouring

I^- sorption. However, the Cl^- concentration of the DS-II porewater is expected to be high (~ 0.20 M) (Tab. 2-3). It is further assumed that the sorption behaviour of $^{36}Cl^-$ and $^{129}I^-$ is similar at high salinity. As a consequence, it is recommended to reduce the R_d value for DS-II given in NTB 14-08 ($R_d = 10^{-3}$ m^3/kg) by a factor of 10 to 10^{-4} m^3/kg, which corresponds to the R_d value of Cl^-.

Stage III: AFm phases are also absent in the cementitious materials in DS-III, and the C/S ratio of C-S-H phases is low (C/S ~ 0.7 at the end of DS-III and ~ 1.1 for the reference case in DS-III). The Ca concentration of the CPW is high, ranging from ~ 0.06 to ~ 0.1 M (Tab. 2-3). This implies that C-S-H phases carry a positive surface charge. However, the Cl^- concentration of the DS-III porewater is also high (~ 0.23 M), which could have a competing effect of Cl^- on I^- sorption. At present, there are no experimental data on the uptake of I^- by HCP at high salinity. Although experimental evidence for at least weak sorption at high salinity is lacking, we assign the same sorption values to $^{36}Cl^-$ and $^{129}I^-$ for DS-III ($R_d = 10^{-4}$ m^3/kg). Thus, the previously selected R_d value of zero in NTB 14-08 for DS-III (Wieland 2014) is revised in the current version of the cement SDB due to the high Ca concentration and the related positive surface charge of C-S-H phases under the expected near-field conditions.

Selenium

Selenium is mainly found as ^{79}Se in L/ILW and originates predominantly from neutron activation of Se traces in stainless reactor steel (Hummel 2017). Selenium is a strongly redox-sensitive element, and its mobility is strongly influenced by its redox speciation. In alkaline cementitious environments under oxidising and weakly reducing conditions, Se is present in the oxidation state +VI (SeO_4^{2-} oxyanion) and +IV (SeO_3^{2-}). Under strongly reducing conditions, Se can be reduced to metallic Se(0) or even to the oxidation state –II as HSe^- anion. Hummel (2017) showed that the current thermodynamic speciation models for Se predict unreasonably low solubilities for this element down to 10^{-15} M under conditions close to an E_H of 0 and a pH of 7.0. The author also noted that the current models for the aqueous speciation of Se are incomplete and do not account for a dissolved Se(0) species, as is the case for the speciation of the chemically similar element sulphur. However, experimental evidence for the existence of such an aqueous Se(0) species is currently unavailable.

In their recent review of the PSI-Nagra Chemical Thermodynamic database, Hummel & Thoenen (2023) concluded that under highly alkaline, reducing conditions, the redox state "zero" can also be stable in solution (Se(0)(aq)) and provided a rough estimate of solubility (Se(cr) ⇔Se(aq)(0)): $\log_{10}K°(298.15\ K) = -(6\pm1)$. In addition, polymeric aqueous polyselenides (mainly Se_4^{2-}) may be stable and could be taken into account in the assessment of Se sorption behaviour. At present, there are no data available in the literature on the sorption behaviour of aqueous zero-valent Se and of polyselenides. Therefore, due to the lack of experimental evidence in the literature, interaction of Se(0) and polyselenides with HCP is not considered in this SDB. A preliminary assessment based upon the charge of these species suggests that sorption is likely to be very weak in the case of the zero-valent Se(0) and comparable to Se(-II) in the case of the polyselenides.

In the CEM-14 SDB (Wieland 2014), only the sorption of Se(VI) and Se(IV) was taken into account. The retention of Se(0) and Se(-II) was not discussed because experimental data were not available in the literature and because the solubility of Se(-II) in cementitious environments was considered to be very low due to the formation of insoluble metal-selenide solids. Hummel (2017), however, noted that "all thermodynamic data for metal-selenide solids were obtained from calorimetric studies, thus not taking into account the corresponding aqueous metal-selenide complexes" and that "solubilities calculated with these data may be wrong by orders of magnitude".

In NTB 14-08 (Wieland 2014), it was assumed that the substitution of SO_4^{2-} anions in ettringite and AFm-SO_4 are the main sorption processes controlling the uptake of Se(VI) in cementitious materials, while the uptake of Se(IV) mainly occurs by anion exchange on the AFm fraction and by electrostatic attraction on the surfaces of the C-S-H phases.

Since the publication of NTB 14-08, a wealth of new research results have appeared in the open literature (Grambow et al. 2020, Grangeon et al. 2020, Guo et al. 2017, Ma et al. 2018, Ma et al. 2020, Missana et al. 2019, Nedyalkova 2019, Rojo et al. 2018), which are briefly discussed in the following paragraphs.

Guo et al. (2017) investigated the sorption of SeO_3^{2-} and SeO_4^{2-} on ettringite. The authors observed that the former anion sorbs on this cement mineral via inner-sphere complexation with Ca-OH_2 sites in the channel edges, whereas SeO_4^{2-}forms outer-sphere complexes by replacing SO_4^{2-} anions.

Ma et al. (2018) published Se(IV) sorption data onto AFm-SO_4 (monosulphate) and AFm-Cl_2 (Friedel's salt). The authors showed that at low Se(IV) loadings, sorption takes place through inner-sphere complexation on the AFm surface. With increasing Se(IV) loading, an AFm-SeO_3 phase was found to precipitate together with $CaSeO_3$(s). Se(IV) surface sorption on AFm-SO_4 was found to be much weaker (R_d = ~ 0.70 m^3/kg) than on AFm-Cl_2 (17.8 m^3/kg).

Nedyalkova (2019) confirmed the existence of two pure AFm-SeO_3 hydrates with interlayer distances of 11.05 Å and 9.65 Å and determined the mean solubility product to be a log K of -28.4 ± 0.8 ($3CaO \cdot Al_2O_3 \cdot CaSeO_3 \cdot 11H_2O$). The authors also characterised an AFm-SeO_4 phase with an interlayer distance of 10.18 Å. The mean solubility product of this AFm phase was found to be a log°K° of -29.2 ± 1.5 ($3CaO \cdot Al_2O_3 \cdot CaSeO_4 \cdot 13H_2O$). Nedyalkova (2019) further reported the uptake of Se(VI) and Se(IV) on several AFm phases, i.e., AFm-SO_4, AFm-CO_3 and AFm-(OH,CO_3). The results from co-precipitation experiments were used to construct thermodynamic models assuming the formation of a solid solution between Se(IV)- and Se(VI)-AFm end-members as well as AFm-SO_4 and AFm-(OH,CO_3) end-members with the aim of allowing an adequate reproduction of the experimentally obtained sorption isotherms. Only in the case of AFm-CO_3 was solid solution formation suppressed by the rigid structure and the narrow interlayer distance. Nevertheless, the low Se(IV) and Se(VI) sorption values that were measured on this phase is due to surface sorption by electrostatic attraction (outer-sphere complexation). Se(VI) sorption isotherms were found to be linear on all three AFm phases up to the Se(VI) concentration in solution of ~ 10^{-3} M. The strongest Se(VI) sorption was measured on AFm-(OH,CO_3) with a mean R_d value of 0.9 ± 0.2 m^3/kg, followed by AFm-SO_4 with a mean R_d value of 0.09 ± 002 m^3/kg. The lowest sorption was obtained on AFm-CO_3 with an R_d value of 0.005 ± 0.001 m^3/kg. The Se(IV) sorption isotherm on AFm-SO_4 was found to be linear up to an aqueous Se(IV) concentration of ~ 10^{-4} M. Se(IV) sorption was strong with a constant R_d value of ~ 0.7 ± 0.1 m^3/kg, which is identical to R_d values determined by Ma et al. (2018). Sorption isotherms for Se(IV) on AFm-CO_3 and AFm-(OH,CO_3) were not measured by Nedyalkova (2019). R_d values of ~ 0.77 m^3/kg on AFm-CO_3 were previously reported in NTB 14-08 (Wieland 2014).

Grangeon et al. (2020) studied the uptake of SeO_4^{2-} by Friedel's salt in flow-through reactors using a combination of wet chemistry analyses as well as spectroscopic and microscopic investigations of the resulting solid phases. The authors found that SeO_4^{2-} is capable of reversibly replacing Cl^- in the AFm interlayer at the same crystallographic site. The wet chemistry results could be well described with an ideal binary solid solution model with the end-member AFm-Cl and AFm-SeO_4. A Gaines-Thomas ion-exchange model considering only the exchange of anions in the interlayers without taking into account the entire AFm stability, however, was not capable of reproducing all experimental data. This work thus shows that AFm phases can efficiently

immobilise SeO_4^{2-} in cementitious materials. The authors further argued that previous studies identifying ettringite as a key mineral in immobilising SeO_4^{2-} can be attributed to SeO_4^{2-} immobilisation by AFm phases.

Studies carried out within the framework of the European CEBAMA project (Grambow et al. 2020) confirmed that retention of both SeO_4^{2-} and SeO_3^{2-} in cement matrices takes place predominantly on AFm phases and to a lesser extent onto ettringite, thus corroborating the results of the previous studies by Baur & Johnson (2003) and Grangeon et al. (2020). Moreover, uptake of SeO_4^{2-} and SeO_3^{2-} by AFm-SO_4 was found to be stronger than the uptake by AFm-CO_3. Finally, uptake of both Se-redox species was found to be higher on CEM-I than on a low-pH CEBAMA reference cement paste due to the higher aluminate content of the former HCP, which promotes the formation of AFm phases. The results demonstrate the importance of the AFm phases for selenate and selenite sorption and suggest that sorption of these radionuclides may be weaker in the absence of AFm phases, such as in low-pH cement where only C-S-H phases are the main sorbing mineral.

Missana et al. (2019) published the results from batch sorption experiments with Se(IV) on C-S-H phases with different C/S ratios ($0.8 \leq C/S \leq 1.6$). The results from the determination of sorption isotherms show that Se(IV) sorption is non-linear and R_d values increase slightly when the C/S ratio increases from 0.8 to 1.0. Furthermore, sorption remains virtually constant within the uncertainties at higher C/S ratios. At low Se(IV) loadings, the R_d values range from ~ 0.05 m^3/kg (C/S = 0.8) to ~ 0.1 m^3/kg ($C/S \geq 1.0$). This increase in the R_d value is considered to be due to charge reversal of the C-S-H surfaces with increasing C/S ratio as a result of an increase in the Ca concentration in solution and Ca adsorption on the C-S-H surface. The charge reversal is indicated by the zeta potential changing from ~ -15 mV (C/S = 0.8) to ~ 0 mV (C/S = 1.0) and ~ +15 mV (C/S = 1.6). Therefore, the study of Missana et al. (2019) confirms the assumption that Se(IV) sorbs onto C-S-H phases by electrostatic attraction, as previously postulated in NTB 14-08 (Wieland 2014).

To simulate Se retention in steel-reinforced concrete systems, Ma et al. 2020 carried out SeO_3^{2-} sorption studies on hydrated CEM-V/A cement (cement blended with blast furnace slag and fly ash) mixed with powders of nano-zero-valent-iron (NZVFe) and several iron corrosion products (magnetite, hematite and goethite) at a CEM-V to total Fe element mass ratio of 4:1. Measured R_d values were found to be very similar for all systems and ranged between $\sim 3 \cdot 10^{-5}$ m^3/kg and $\sim 7 \cdot 10^{-5}$ m^3/kg. Only in the presence of NZVFe were the Se R_d values a factor of ~ 100 higher ($R_d = 4.0 \cdot 10^{-3}$ m^3/kg). Analysis of XANES spectra showed that SeO_3^{2-} was only reduced in the presence of NZVFe, forming FeSe(s) and metallic Se(0). In all other systems, SeO_3^{2-} was immobilised mainly by the formation of inner- or outer-sphere complexes on the hydrated cement minerals, and immobilisation by reductive precipitation was < 1%. The similar R_d values obtained on HCP prepared from pure CEM-V and from CEM-V mixed with Fe corrosion products indicate that SeO_3^{2-} sorption on Fe corrosion phases or reductive precipitation does not play a quantitatively significant role in these systems.

Due to the lack of reliable data in the literature on the solubility of Se(0) and metal selenides, the mobility of Se(-II) can only be estimated taking into account sorption processes. However, Se(-II) sorption data on cementitious materials are very rare in the literature. Rojo et al. (2018) published the first study attempting to quantify the sorption of HSe^- on cement phases under strongly reducing conditions. The authors carried out batch sorption experiments with HSe^- on AFm-CO_3 and AFm-(OH,CO_3) in electrochemical cells, which allowed Se in the –II redox state to be stabilised in the sorption experiments. HSe^- was found to sorb much more strongly on AFm-(OH,CO_3) ($R_d = 0.1 \pm 0.05$ m^3/kg) than on AFm-CO_3 ($R_d = (4 \pm 2) \cdot 10^{-3}$ m^3/kg). Synchrotron-based spectroscopic studies reveal that the larger interlayer space of AFm-(OH,CO_3) allows HSe^- to intercalate in the interlayer, whereas in the case of AFm-CO_3 the smaller interlayer space hinders access of HSe^- into the interlayer, thus limiting the sorption of HSe^- mostly to the outer

planar surface and edges. The study of Rojo and co-workers suggests that surface adsorption of Se(-II) on AFm phases is very weak, which could also be true for other cement phases (e.g., C-S-H phases).

In summary, the new data on Se sorption in cementitious environments that have become available in the open literature since the publication of NTB 14-08 (Wieland 2014) have not significantly changed the process understanding in this field. Ma et al. (2019) summarised this process understanding very well in a recently published extensive literature review of the retention of redox-sensitive radionuclides by the various barrier materials of radioactive waste repositories: C-S-H phases, AFm phases and ettringite are the main sinks for Se in cementitious barriers. Se sorption onto C-S-H phases was found to be restricted to Se(IV) and only takes place in the presence of high aqueous Ca concentrations leading to positively charged surfaces, whereas Se(VI) does not sorb at all on this cement phase. In addition, Se(IV) and Se(VI) sorb onto AFm phases by surface adsorption (electrostatic attraction and inner-sphere complexation) as well as anion exchange in the interlayers of AFm-SO_4 and AFm-(OH,CO_3) and the formation of pure AFm-SeO_3 and AFm-SeO_4 phases at very high Se loadings. Anion exchange in the interlayers of monocarbonate (AFm-CO_3) does not take place. Sorption on ettringite takes place via adsorption in the inter-channels of already formed ettringite. In addition, small quantities of hydrotalcite can be present in cementitious matrices. The literature discussed by Ma et al. (2019) reveals that hydrotalcite also shows some affinity for oxyanions such as SeO_3^{2-} and SeO_4^{2-}. The oxyanions substitute for the easily replaceable CO_3^{2+} anions present in the interlayers of this layered double hydroxide, which is indicated by changes in the interlayer distance upon intercalation. Finally, Ma and co-workers further pointed out that SeO_3^{2-} is known to substitute for CO_3^{2-} in calcite during recrystallisation of the mineral leading to the formation of a $Ca(SeO_3)_x(CO_3)_{(1-x)}$ solid solution.

The large body of new data on the interaction of AFm phases with Se in its various redox states cannot be considered in the selection of R_d values for the updated SDB because AFm phases were found to be almost completely absent in the cement compositions (Tab. 2-3) or, if present, in the form of monocarbonate, which is practically inert in terms of anion uptake. Therefore, the current selection of R_d values has to be based on Se interaction with C-S-H phases or ettringite.

The following sorption values are recommended for Se uptake by cementitious systems (see also Tab. 7-1):

Stage I: Anion exchange with SO_4^{2-} anions in ettringite and electrostatic surface sorption onto C-S-H phases are considered as potential sorption mechanisms. Both cement phases are present in DS-I (Tab. 2-3). Under oxidising conditions, Se(VI) does not sorb on C-S-H phases, and Ochs et al. (2002b) measured an R_d value for Se(VI) uptake by pre-formed (primary) ettringite of 0.1 m^3/kg. Ettringite makes up approximately ~ 10 wt.% of the cementitious materials in DS-I. Hence, we assign an R_d value of 0.01 m^3/kg for Se(VI) sorption onto HCP under oxidising conditions. As Cl^- does not sorb on ettringite, a competing effect of stable Cl^- can be neglected. Under reducing conditions, Se(IV) and Se(-II) (under strongly reducing conditions) are the relevant redox species. In the literature, Se(IV) data on C-S-H phases measured by Missana et al. (2019) are available, while no data have been reported for Se(-II) uptake by C-S-H phases. In-house single-point measurements of Se(IV) sorption onto ettringite revealed only weak sorption with R_d values of ~ 0.01 m^3/kg (Wieland 2014). Hence, this sorption mechanism is not further considered. The R_d values determined by Missana et al. (2019) for C-S-H phases with a C/S ratio > 1.0 (R_d = 0.1 m^3/kg) are used and divided by a factor of 10 to account for the calculated C-S-H content of the considered cementitious system (~ 30 wt.%) and for Cl^- competition at the moderately high aqueous Cl^- concentration (~ $4 \cdot 10^{-3}$ M). This leads to an R_d value of 0.01 m^3/kg. Note, however, that Se(-II) could exist under strongly reducing conditions, while no sorption data on

ettringite and C-S-H phases are presently available. In this case, based on the sorption measurements on AFm phases (Rojo et al. 2018), an R_d of ~ 10^{-3} m^3/kg is provisionally assumed for strongly reducing conditions.

Stage II: C-S-H phases and ettringite are expected to control Se uptake by the cementitious system modelled in DS-II. For both oxidising and reducing conditions, the same considerations as for DS-I can be made. In addition, however, a strong competitive effect of Cl^- due to the high Cl^- concentration (~ 0.2 M) must be considered in DS-II. Under oxidising conditions, an R_d value of 0.01 m^3/kg similar to DS-I is selected assuming Se(VI) sorption onto ettringite and competition with Cl^- does not exist on ettringite. Under reducing conditions, an R_d value of 0.03 m^3/kg is selected based on the assumption that Se(IV) sorption occurs onto C-S-H phases with a C/S ratio > 1.0 and that C-S-H phases make up ~ 30 wt.% of HCP. Sorption competition at high Cl^- concentrations, however, might reduce Se(IV) uptake by C-S-H phases (assuming surface adsorption), while no experimental information is presently available. Therefore, the R_d value for Se(IV) is reduced by a factor of 10 in view of potential sorption competition with Cl^- ($R_d = 3 \cdot 10^{-3}$ m^3/kg). As for DS-I, Se(-II) could exist under strongly reducing conditions, while no sorption data on ettringite and C-S-H phases are presently available. A provisional assignment would result in an R_d of ~ 10^{-4} m^3/kg based on sorption measurements on AFm phases (Rojo et al. 2018) and in view of a possible competitive effect of Cl^-.

Stage III: C-S-H phases have been predicted to be the main cement mineral in DS-III (67 wt.%) (Tab. 2-3). Therefore, they are considered to be responsible for Se retention by HCP, although C-S-H phases have a low C/S ratio (reference C/S ~ 1.1, C/S =0.7 at end of DS-III). In addition, significant amounts of calcite may be present in this stage but, in accordance with the SDB for calcareous rocks compiled by Baeyens et al. (2014), it is assumed that Se(VI) and Se(IV) sorption on this mineral is negligible. Furthermore, Cl^- is present at high concentrations, which implies a potential competitive effect on Se uptake by cementitious materials. For oxidising conditions, R_d = 0 m^3/kg is assigned due to the absence of ettringite and as no sorption of Se(VI) on C-S-H phases was reported. Under reducing conditions and high Cl^- concentration (~ 0.2 M), the R_d value for Se(IV) sorption onto C-S-H phases with a C/S ratio of 0.8 measured by Missana et al. (2019) (0.05 m^3/kg) is selected and divided by a factor of 2 to account for its content (67 wt.%) (Tab. 2-3). This results in an R_d value of 0.025 m^3/kg. Sorption competition with Cl^-, however, might reduce Se(IV) uptake by C-S-H phases (assuming surface adsorption), while no experimental information is presently available. For this reason, the sorption value is further reduced by a factor of 10 in view of a potential sorption competition with Cl^- ($R_d = 2.5 \cdot 10^{-3}$ m^3/kg instead of $R_d = 2.5 \cdot 10^{-2}$ m^3/kg). In the case of Se(-II), the sorption value assigned to DS-II (R_d ~ 10^{-4} m^3/kg) is also assigned to DS-III due to similar porewater conditions (competitive effect of Cl^-).

Molybdenum

In L/ILW, molybdenum is present as ^{93}Mo, and, like ^{79}Se, originates from activated reactor steel components in which it is produced by neutron activation of stable ^{92}Mo (Lidmann et al. 2017). Speciation calculations show that the redox speciation of molybdenum is dominated by Mo(VI) (molybdate, MoO_4^{2-}) (Ochs et al. 2016). In the previous cement SDB NTB 14-08 (Wieland 2014), it has been noted that Mo(VI) could have similar chemical properties to Se(VI) as both are hexavalent anions in tetrahedral coordination with four oxygen atoms. Mo(VI), however, has a larger ionic radius than Se(VI), which could explain why it is less easily incorporated into ettringite (Zhang & Reardon 2003). On the other hand, Paikaray et al. (2013) observed that Mo(VI) has a higher affinity towards hydrotalcite-like layered double hydroxides than Se(VI), suggesting that the former may also sorb more strongly onto AFm phases. Because of the limited literature data available in 2014, an R_d of 0 was assigned to this element in all stages of cement degradation. In their review of the radionuclide sorption data on cement and concrete, Ochs et al.

(2016) referred to a Japanese cement SDB published in 2002 in which R_d values for Mo(VI) on OPC paste are listed. According to this study, the sorption values of Mo(VI) are in good agreement with those of Se(VI). Therefore, Ochs et al. (2016) concluded that R_d values for Se(VI) on HCP (R_d = 0.003 m^3/kg) are a good initial estimate for Mo(VI) R_d values.

Meanwhile, several new studies have been reported on Mo(VI) uptake by cementitious materials. Ma et al. (2017) investigated the uptake of Mo(VI) by AFm-SO_4 and AFm-Cl_2 by determining sorption isotherms. These authors identified three different sorption mechanisms for Mo(VI) interaction with AFm phases: 1) layer edge sorption, 2) anion exchange in the AFm interlayers, and 3) $CaMoO_4$(s) precipitation at the highest loadings. The layer edge sorption was characterised by R_d values of 0.032 m^3/kg and 9.4 m^3/kg on AFm-SO_4 and AFm-Cl_2, respectively. The anion exchange part of the isotherm could be modelled as a solubility-controlled system assuming the dissolution of the original AFm phase and the formation of AFm-MoO_4. The authors concluded that AFm phases can immobilise Mo(VI) by surface complexation on interlayer edges rather than via anion exchange in their interlayers. Marty et al. (2018) continued the work of Ma and co-workers by performing flow-through experiments with Mo(VI) and AFm-Cl_2 under alkaline conditions at intermediate Mo(VI) loadings, thus allowing to differentiate between precipitation and anion-exchange processes. It was observed that Mo(VI) is taken up by AFm-Cl_2 by replacing two Cl^- anions in the interlayers and that OH^- competes with MoO_4^{2-} for the same interlayer anion-exchange sites.

Lange et al. (2020) investigated several cement minerals with respect to Mo(VI) sorption, including C-S-H phases (C/S = 0.9 and 1.4), AFm-SO_4 (monosulphate), AFm-CO_3 (mono-carbonate), ettringite, hydrogarnet, portlandite, calcite and aged HCP (pH = 12.6). Lange and co-workers performed batch sorption experiments to determine the Mo(VI) sorption kinetics under anoxic conditions at initial molybdate concentrations between $5 \cdot 10^{-6}$ and 10^{-7} M. The equilibrium R_d values given in this publication are summarised in Tab. 3-1. Strong sorption was observed on all cement phases, but in particular on both AFm phases and on hydrogarnet. Mo(VI) sorption on the latter mineral was found to take place by dissolution of the hydrogarnet followed by neoformation of AFm-MoO_4. The R_d values determined by these authors for Mo(VI) sorption on AFm phases are up to a factor of 50 higher than the values published by Ma et al. (2017). Furthermore, significant sorption was observed onto portlandite and onto C-S-H phases. For these cement minerals, the R_d values were found to increase slightly with increasing aqueous Ca concentration in accordance with an increase of the positive surface charge. This indicates surface sorption of Mo(VI) by electrostatic attraction. It should be noted that Lange and co-workers determined R_d values for Mo(VI) sorption on C-S-H phases in artificial CPW with a pH > 13, which are a factor of 3 (C/S = 0.9) to 8 (C/S = 1.4) lower than the values determined in the equilibrium solution, despite the aqueous Ca concentrations reported in the supplementary information differing by less than a factor of 2. This observation was not further elaborated by Lange et al. (2020), and it is currently unclear what could have caused this difference in sorption. Ettringite, portlandite and calcite can also sorb Mo(VI) with sorption values depending on the porewater composition. An R_d of ~ 0.4 m^3/kg was determined for Mo(VI) sorption on HCP prepared from CEM I under conditions representative of DS-II. It should be noted that all Mo(VI) R_d values reported by Lange et al. (2020) are significantly higher than the values previously reported by Ochs et al. (2016).

In summary, molybdenum is predominantly present as an MoO_4^{2-} oxyanion under both oxidising and reducing, alkaline conditions. This oxyanion can be retained quite well by virtually all cement minerals with R_d values depending on the chemical conditions. In addition, MoO_4^{2-} can exchange for Cl^- in the interlayer of AFm-Cl_2 and it can precipitate as AFm-MoO_4 or $CaMoO_4$(s).

Tab. 3-1: R_d values measured by Lange et al. (2020) for Mo(VI) sorption on various cement phases as well as aged HCP under three different chemical conditions

Cement phase	**R_d** [m^3/kg]		
	ES*	**ACW***	**CH***
C-S-H (C/S = 0.9)	0.43 ± 0.03	0.143 ± 0.009	
C-S-H (C/S = 1.4)	0.78 ± 0.04	0.098 ± 0.005	
AFm-SO_4	1.6 ± 0.1	0.055 ± 0.002	0.24 ± 0.22
AFm-CO_3	1.56 ± 0.09		0.53 ± 0.48
Ettringite	0.120 ± 0.004	0.122 ± 0.004	0.02 ± 0.02
Hydrogarnet	3.1 ± 0.4	1.91 ± 0.14	0.59 ± 0.43
Portlandite	0.79 ± 0.03		0.044 ± 0.028
Calcite	0.32 ± 0.02		0.003 ± 0.00
Aged HCP	0.4 ± 0.2		

* ES: equilibrium solution, ACW: young artificial CPW, pH > 13, CH: portlandite equilibrated porewater, pH = 12.5

Wieland (2014) reports that cement may contain as much as 2.58 ppm of stable Mo in unhydrated CEM I 52.5N HTS; i.e., $2.1 \cdot 10^{-5}$ mol /kg HCP, thus suggesting that the actual sorption process for trace concentrations of ^{93}Mo could be isotopic exchange with stable Mo in the cementitious materials. As in the case of Zr, this ion-exchange process can either take place with stable Mo sorbed onto cement minerals or with stable Mo solid phases; i.e., $CaMoO_4$(s). In the former case, ^{93}Mo sorption values and stable Mo sorption values are identical and the discussion above applies. In the latter case, an apparent R_d value can be estimated based upon the solubility of $CaMoO_4$(s). Taking the aqueous Ca concentrations and pH values calculated for DS-I, DS-II and DS-III, the solubilities of $CaMoO_4$(s) are $7 \cdot 10^{-3}$ M, $1.6 \cdot 10^{-6}$ M and $1.2 \cdot 10^{-6}$ M, respectively. Applying the "shared solubility" approach (Eq. 4, Section 4.1) and assuming an accessibility factor (f) of 0.1, apparent R_d values can be calculated leading to ~ $4 \cdot 10^{-7}$ m^3/kg, $2 \cdot 10^{-3}$ m^3/kg and $2.6 \cdot 10^{-3}$ m^3/kg for DS-I, DS-II and DS-III, respectively. These R_d values are significantly lower than the R_d values determined experimentally in sorption studies. Thus, there is evidence to suggest that surface sorption processes likely control the uptake of radioactive Mo(VI) by HCP.

The following sorption values are recommended for Mo uptake by cementitious systems (see also Tab. 7-1):

- Stage I: Electrostatic surface sorption on C-S-H phases with a C/S ratio of 1.6 under conditions representative of DS-I is considered to be the dominant sorption mechanism. Sorption on hydrogarnet is not considered because the data available in the literature have been interpreted in terms of precipitation processes (Lange et al. 2020). The only sorption data for Mo(VI) on C-S-H phases published in the open literature are from Lange et al. (2020). The sorption value for Mo(VI) on HCP is estimated to be 0.1 m^3/kg based on the R_d value measured by Lange et al. (2020) on a C-S-H phase with a C/S ratio of 1.4 under conditions relevant to DS-I. This value is divided by a factor of 3 to account for the weight fraction of C-S-H phases in HCP in DS-I and by an additional factor of 2 to account for competition with Cl^- at the moderately high aqueous Cl^- concentration (~ $4 \cdot 10^{-3}$ M) of DS-I porewater

(Tab. 2-3). This results in an R_d value of $1.67 \cdot 10^{-2}$ m^3/kg. The R_d value based on this and selected for the updated cement SDB is $1.5 \cdot 10^{-2}$ m^3/kg for sorption under both oxidising and reducing conditions.

- Stage II: C-S-H phases are expected to control Mo(VI) sorption on HCP in DS-II. The C/S ratio of the C-S-H phases is 1.58 (Tab. 2-3). The high Ca concentration of the CPW in DS-II leads to a positive surface charge of C-S-H phases. The selection of the Mo(VI) R_d value of 0.8 m^3/kg for DS-II is thus based on the value measured by Lange et al. (2020) for C-S-H phases with a C/S of 1.4 under equilibrium conditions. This R_d value is divided by a factor of 3 to account for the C-S-H weight fraction of the cementitious material in DS-II (see Tab. 2-3) and by another factor of 10 to account for competition with Cl^- at the high Cl^- concentration of DS-II porewater (Tab. 2-3), resulting in an R_d of $2.67 \cdot 10^{-2}$ m^3/kg. The R_d value based on this and selected for Mo(VI) sorption in DS-II is $2.50 \cdot 10^{-2}$ m^3/kg (Tab. 7-1).
- Stage III: C-S-H phases account for ~ 67 wt.% of the HCP in DS-III and are therefore the main cement mineral (Tab. 2-3). C-S-H phases are considered to play a key role in Mo(VI) sorption in DS-III, although these phases have a reference C/S ratio of 1.1 in the reference state of DS-III and a low C/S ratio of 0.7 at the end of DS-III. However, in both cases, the high Ca concentration of DS-III porewater indicates a positive surface charge of the C-S-H phases. The R_d value measured by Lange et al. (2020) on a C-S-H phase with a low C/S ratio of 0.9 in equilibrium solution (R_d = 0.43 m^3/kg) was used to estimate the sorption value under both oxidising and reducing conditions. Taking into account the C-S-H weight fraction in DS-III and competition with Cl^- at the high aqueous Cl^- concentrations of DS-III porewater (Tab. 2-3), the R_d value selected for DS-III is $2.0 \cdot 10^{-2}$ m^3/kg.

3.4 New dose-relevant elements

This section contains an assessment of the sorption properties of new dose-relevant radionuclides and a justification for the selected sorption values.

3.4.1 Lanthanides and actinides

Holmium

Holmium (Ho(III)) is a lanthanide and therefore Eu(III) can be used as a suitable chemical analogue. Assessments of Eu retention by cementitious materials have been made in previous versions of the cement SDB (Wieland 2014, Wieland & van Loon 2002). There is substantial experimental evidence that Eu uptake by HCP and C-S-H phases is very strong and that the C-S-H phases are the uptake-controlling cement phase for the lanthanides in HCP. These findings allowed an R_d of 100 m^3/kg to be assigned to all stages of cement degradation (Wieland 2014). The recommended values are retained as no new information is available that would justify a re-appraisal of the sorption values for lanthanides.

The following sorption values are recommended for Ho uptake by cementitious systems (see also Tab. 7-1):

- Stages I to III: The sorption values recommended for Eu(III) in NTB 14-08 (Wieland 2014) are also assigned to Ho(III) (R_d = 100 m^3/kg).

Californium

Curium (Cm(III)) is considered a suitable chemical analogue for Cf (Hummel & Thoenen 2023). In Section 3.2.1, a re-appraisal of the sorption values for trivalent actinides has been made in light of new experimental information showing that the high sorption values recommended in previous versions of the cement SDB (Wieland 2014, Wieland & van Loon 2002) can be retained (R_d = 100 m^3/kg). Therefore, due to chemical similarity with Cm(III), these high sorption values are also assigned to Cf(III) for all stages of cement degradation.

The following sorption values are recommended for Cf uptake by cementitious systems (see also Tab. 7-1):

- Stages I to III: The sorption values recommended in NTB 14-08 (Wieland 2014) for trivalent actinides are also adopted for Cf(III) (R_d = 100 m^3/kg).

3.4.2 Alkaline and earth alkaline metals

Calcium: see Chapter 4

3.4.3 Transition and other metals

Aluminium: see Chapter 4

Iron

A radioisotope of iron (^{60}Fe) is new on the list of dose-relevant radionuclides. The oxidation states +II and +III are relevant in cementitious environments. The stability ranges of the two oxidation states and the hydrolysis reactions are well known and have been described elsewhere (Baes & Mesmer 1976, Brookins 1988, Hummel et al. 2002, Hummel & Thoenen 2023). It should be noted that, in the alkaline pH range, aqueous Fe(II) species are only stable under very reducing conditions and the stability field of pure Fe(II) hydroxide under the same conditions is very narrow.

In-house sorption studies with Fe(II,III) on C-S-H phases have recently been reported (Mancini et al. 2020, 2021). Very strong uptake of Fe(III) was observed on C-S-H phases with R_d values of ~ 700 m^3/kg (Mancini et al. 2020). The results show that neither the C-S-H composition nor the pH have any notable effect on Fe(III) sorption. Furthermore, Fe(III) uptake by C-S-H was found to be linear in the aqueous Fe(III) concentration range from 10^{-10} to 10^{-6} M. On the basis of structural parameters deduced from extended X-ray absorption fine structure (EXAFS) spectroscopy which were further supported by ^{29}Si nuclear magnetic resonance (NMR) data, the authors proposed a structural model for Fe(III) coordination in the interlayer of the C-S-H phases with C/S values of 1.2 and 1.5, respectively. Substitution of Ca by Fe in the interlayer of C-S-H phases was considered as the dominant sorption mechanism. Atomic distances and numbers of neighbouring atoms indicate that Fe(III) is directly bonded to Si tetrahedra of the "Dreierketten" silica chains adjacent to the interlayer space. However, the structural information did not allow an unambiguous interpretation of the Fe(III) uptake by a C-S-H phase with a low C/S ratio of 0.8. ^{29}Si NMR data indicated that Fe(III) uptake by the interlayer is not a dominant process. The coordination shell of Fe(III) derived from a multi-shell fit of the EXAFS data contain less neighbouring Si and Ca atoms compared to the C-S-H phases with higher C/S ratios and further suggest the presence of neighbouring Fe atoms. Mancini et al. (2020) interpreted the structural parameters provided by EXAFS spectroscopy in terms of the formation of a secondary phase or clusters, presumably on the surface of the C-S-H phase. For the current appraisal, a strong uptake of Fe(III) by HCP is assumed. An R_d of 100 m^3/kg has been selected in agreement with the experimentally determined sorption values on C-S-H phases.

The complexation of Fe(III) by silicate ions could have an effect on the sorption of Fe(III) in cementitious environments. This effect is determined by the concentration of silicate ions and the stability of Fe(III)-silicate complexes. Patten & Byrne (2017) reported an assessment of Fe(III) and Eu(III) complexation by silicate ions in acidic to slightly alkaline conditions with a view to identifying the dominant complexes of the two metal cations in seawater. The formation constant of $FeSiO(OH)_3^{2+}$ was determined and used for compilations of the Fe(III) speciation in seawater. The results show that ferric silicate complexes in seawater are present at much lower concentrations than ferric hydroxide complexes. Thus, it seems likely that silicate ions have only a negligible effect on Fe(III) speciation in cementitious environments (pH > 10) due to the weak stability of Fe(III)-silicate complexes and with a view to the much higher concentration of hydroxyl ions compared to silicate ions in these conditions.

The study of Mancini et al. (2021) shows that Fe(II) uptake by C-S-H phases, as in the case of Fe(III), is also independent of the C/S ratio of the C-S-H phases and thus of pH. Fe(II) sorption was found to be linear in the studied Fe(II) concentration range from 10^{-7} to 10^{-3} M, and the investigations showed that no Fe(II)-hydroxide precipitation occurred in this concentration range. The K_d value was estimated to be ~ 0.1 m^3/kg irrespective of the C/S ratio of the C-S-H phases and pH, suggesting that hydrolysis and Ca could have an opposite effect on the extent of Fe(II) uptake by C-S-H phases. X-ray diffraction (XRD) studies of samples from co-precipitation experiments indicated the uptake of a small portion of Fe(II) into the interlayer of the C-S-H phases, as evidenced by an increase in the interlayer spacing. EXAFS spectroscopy showed that Fe(II) is bound by C-S-H phases in an octahedral coordination environment, while Fe(II) uptake into the interlayer was not supported by the structural parameters determined by this spectroscopic technique. The number of neighbouring Ca and Si atoms (total Ca+Si atoms ~ 6) was much lower than in the case of Fe(III) (total Ca + Si > 10), where the incorporation into the interlayer of C-S-H phases with a high C/S ratio could be clearly demonstrated by ^{29}Si NMR and EXAFS spectroscopy. However, the total of ~ 6 Ca + Si neighbouring atoms also rules out the formation of a single surface-bound, inner-sphere-coordinated Fe(II) species. Instead, the structural data suggest the presence of Fe(II) in a structurally bound entity or the presence of equal proportions of both surface- and interlayer-bound Fe(II) species.

The K_d value of ~ 0.1 m^3/kg is comparable to the value of other bivalent metal cations, in particular the alkaline earth metals, at a high C/S ratio, while, in the case of alkaline earth metals, the K_d value is much lower at a low C/S ratio. The R_d value for Fe(II) on cement paste is estimated to be 0.05 m^3/kg on the assumption that the portion of C-S-H in cement paste amounts to 50%. An R_d of 0.05 m^3/kg is assigned to all stages of cement degradation as no obvious pH dependence of the sorption values was observed by Mancini et al. (2021).

The cementitious materials planned to be used in the near-field of a deep geological repository for L/ILW contain significant amounts of stable Fe; e.g., the provisional representative cement considered in the present study (CEM I 52 R from Jura Cement, Switzerland) contains 0.413 mol Fe/kg (Tab. 2-1) (c_{cem}), which implies that isotopic exchange with the stable Fe inventory could be considered as a potential process controlling the sorption of ^{60}Fe by HCP. As in the case of Ni, Zr and Mo, this isotopic exchange process may either take place with stable Fe cations sorbed onto cement minerals or with stable Fe-containing solid phases, i.e., siliceous hydrogarnet under oxidising conditions and, presumably, magnetite and/or pyrite under reducing conditions. In contrast to Ni, Zr and Mo, however, where only one oxidation state dominates over the E_H-pH space relevant to a deep geological repository and an identical chemical environment can be anticipated irrespective of the redox conditions, the situation might be very different in the case of iron. The studies by Mancini et al. (2020), (2021) clearly show that the chemical coordination environments of Fe(II) and Fe(III) on C-S-H phases are very different. It can thus be assumed that the two oxidation states of iron also have very different coordination environments in HCP, which severely limits the approach to consider the retention of Fe by isotopic exchange. The approach was tested in the case of Fe(III), since it can be assumed that stable Fe is present as Fe(III) in fresh

HCP that has not yet been exposed to reducing conditions. The sorption value determined by isotopic exchange was found to be a factor of 10 higher than the R_d values reported by Mancini et al. (2020). Therefore, for Fe(III) under oxidising conditions, the R_d value of 100 m^3/kg was retained as a conservative value for all degradation stages.

It should be noted that in addition to the Fe-containing cement minerals, other Fe-containing minerals are also likely to be present in the near-field of a repository in the long term, such as magnetite and pyrite formed by steel corrosion. It can therefore be assumed that isotopic exchange of radioactive Fe(II) and Fe(III) with the stable Fe of these minerals will significantly contribute to the long-term retention of these radionuclides in the cementitious near-field. However, these minerals are not currently assumed to contribute to retention, as cementitious systems are considered to be the only sorbent for radionuclides in the cementitious near-field. Therefore, it can be assumed that the R_d values for Fe(II) and Fe(III) as recommended in this study are based on very conservative considerations.

The following sorption values are thus recommended for Fe uptake by cementitious systems (see also Tab. 7-1):

- Stages I to III: An R_d of 100 m^3/kg is assigned to all stages of cement degradation under oxidising conditions (i.e., presence of Fe(III)), while an R_d of 0.05 m^3/kg is assigned to all stages of cement degradation under reducing conditions (i.e., presence of Fe(II)).

Mercury

A radioisotope of mercury (^{194}Hg) is new to the list of dose-relevant radionuclides. Metallic Hg(0) occupies the majority of the E_H-pH diagram under moderately oxidising to reducing conditions in the pH range > 10 (Brookins 1988). Hg(II) occupies the stability field under strongly oxidising conditions. The Hg^{2+} ion is hydrolysed to $Hg(OH)_2$(aq) in dilute, neutral to strongly alkaline solutions (Baes & Mesmer 1976).

To the best of the authors' knowledge, no reliable sorption measurements on Hg uptake by cement phases and cement paste are available. The only study dealing with the interaction of Hg with cement phases was reported by Serrano et al. (2012). The authors investigated the immobilisation of Hg during formation of Al- and Fe-ettringite and related solid products using synchrotron-based spectroscopic and microscopic spatial analysis methods. With this approach, it was possible to determine microscale mechanisms of Hg(II) uptake by the cement phases. The results suggest physical encapsulation of polynuclear chloromercury(II) salt during Hg(II) co-precipitation with ettringite as the primary immobilisation process. It should be noted that Hg(II) concentrations ranged between 0.01 and 0.25 mM with Cl^- present in the same concentration range due to Hg(II) addition as $HgCl_2$. No quantitative wet chemistry data on the interaction of Hg(II) with the cement phases were reported by Serrano et al. (2012).

The complexation properties of Hg and Ag are similar, and the chemical analogy between these two elements is generally accepted. The analogy between Ag and Hg is based on the similarity of the chemical properties of the two elements, such as the oxidation state of the dominant species in the E_H-pH range (Brookins 1988), hydrolysis behaviour (Baes & Mesmer 1976) and complexation with important ligands. For example, Hg(II) and Ag(I) form strong complexes with Cl^- and HS^- (Hummel et al. 2002). As a result of the chemically analogous complexation properties, Wieland (2019) assigned the same nominal sorption value for Hg and Ag on HCP. Therefore, analogous to Ag (see Section 3.3.3), zero sorption is assumed for all stages of cement degradation under oxidising conditions (Hg(II)), while a nominal sorption value of 10^{-4} M m^3/kg accounts for Hg uptake under reducing conditions (Hg(0)) for all stages of cement degradation.

The following sorption values are recommended for the retention of Hg in cementitious systems (see also Tab. 7-1):

- Stages I to III: A nominal sorption is assigned to Hg retention under reducing conditions (Hg(0)) ($R_d = 10^{-4}$ m^3/kg), which is based on the "shared solubility" considerations previously reported for Ag. An R_d of 0 m^3/kg is assigned to the retention of Hg under oxidising conditions.

Titanium

^{44}Ti is an exotic radionuclide present in the Switzerland's L/ILW and originates from Swiss accelerator facilities (the spallation source, SINQ at the Paul Scherrer Institute). It is produced from ^{50}Cr in stainless steel by neutron-induced reactions (Dressler et al. 2012). The oxidation state +IV is the dominant redox state of Ti in the E_H-pH space relevant to a cement-based repository (Brookins 1988). $Ti(OH)_4(aq)$ is the dominant hydrolysis species above pH 4 (Baes & Mesmer 1976). Hence, the hydrolysis behaviour is similar to that of the tetravalent actinides, e.g., Th(IV), and Zr(IV).

To the best of the authors' knowledge, no sorption studies with Ti on cement phases or HCP have been published. Therefore, nominal sorption values have to be assigned for the three stages of cement degradation. It can be assumed that a strong interaction of Ti with cementitious materials occurs similarly to Th (R_d = 100 m^3/kg in NTB 14-08 (Wieland 2014) or Zr (R_d = 10 m^3/kg in NTB 14-08). In addition, $Ti(OH)_4(aq)$ is the main hydrolytic species, indicating that there is no pH-induced effect on sorption in the alkaline pH range. For the current appraisal of Ti sorption on HCP, a cautious approach is taken in line with the assessment presented for Zr uptake by HCP by assigning a nominal, presumably excessively low sorption value of an R_d of 10 m^3/kg to all stages of cement degradation.

The following sorption values are recommended for the retention of Ti in cementitious systems (see also Tab. 7-1):

- Stages I to III: A nominal sorption is assigned to Ti uptake by HCP under oxidising and reducing conditions (R_d = 10 m^3/kg) based on the notion of a chemical similarity with Zr.

3.4.4 Anions

Silicon: see Chapter 4

4 Shared solubility and isotopic exchange processes

In NTB 14-08 (Wieland 2014), the uptake of CO_3^{2-} and Ni by HCP was considered to most probably not be controlled by an adsorption-type process. Instead, currently available experimental data indicate a solubility-limiting process by an Ni-containing cement phase in the case of Ni and calcite in the case of CO_3^{2-}. Therefore, retention of $^{59,63}Ni$ and $^{14}CO_3^{2-}$ in the cementitious near-field was estimated on the assumption that the distribution of radioisotopes ($^{59,63}Ni$ and $^{14}CO_3^{2-}$) between porewater and HCP is identical to that of stable isotopes (Ni and CO_3^{2-}) and that the aqueous concentrations of the stable isotopes and the radioisotopes correspond to the aqueous concentrations in equilibrium with HCP. The underlying concept thus implies an isotopic exchange process between stable isotopes and radioisotopes.

Isotopic exchange between stable isotopes and radioisotopes can also be assumed as a possible mechanism for ^{41}Ca, ^{26}Al and ^{32}Si uptake by HCP. The approach to evaluate the sorption behaviour of these dose-relevant radionuclides is based on the hypothesis that their retention by cementitious materials occurs through isotopic exchange with stable Al, Si and Ca during recrystallisation of the main cement minerals, such as C-(A)-S-H phases (Ca, Si, Al), portlandite (Ca), ettringite (Ca, Al) and AFm phases (Ca, Al) (Tits et al. 2023). Note that Ca, Al and Si are the most important structure-forming elements of most cement phases.

In this chapter, the concept of "shared solubility", respectively isotopic exchange, is applied as previously described in NTB 14-08 (Wieland 2014) and adapted for the scope of this report. In this way, R_d values for $^{59,63}Ni$, $^{14}CO_3^{2-}$, ^{41}Ca, ^{26}Al, and ^{32}Si were estimated based on the aqueous concentrations of the stable isotopes in cement-type porewater and their content in HCP and by assuming isotopic exchange as a potential uptake mechanism. It should be noted that R_d values derived in this manner are based on system parameters and can therefore not be considered equivalent to R_d values determined from sorption processes.

4.1 Definition of operational R_d values

In NTB 14-08 (Wieland 2014), the following approach was proposed to estimate the operational distribution ratio (R_d) for isotopic exchange:

$$R_d = \frac{m_{cem} \cdot f}{m_{aq}} \cdot \left(\frac{V_{sol}}{M_{cem}} \right) \quad (3)$$

m_{cem}: number of moles of an element (stable isotope) in the repository associated with HCP (mol)

m_{aq}: number of moles of the element (stable isotope) in porewater at equilibrium (mol)

V_{sol}: total volume of porewater in the cavern unit (m^3/m)

M_{cem}: total mass of cement in the cavern unit (kg/m)

f: fraction of the stable isotope inventory accessible to isotopic exchange [-]

The basic system parameters for the L/ILW repository (M_{cem}, V_{sol}), derived from the current, preliminary design of an L/ILW cavern are summarised in Tab. 4-1.

For fresh, i.e., non-degraded HCP, the operational distribution ratio R_d can be calculated directly with the measured concentration of an element in HCP (c_{cem}, mol/kg) and the concentration of this element in solution in equilibrium with HCP (c_{aq}, mol/L):

$$R_d = \frac{c_{cem} \cdot f}{c_{aq}} \ (m^3/kg) \qquad (4)$$

The proportion of the stable isotope inventory accessible to isotopic exchange, f, depends on the recrystallisation rate of the solid. For Ni, for example, it was shown that after 30 days reaction time, only a small portion of the inventory of stable Ni in the cement matrix is accessible for isotopic exchange with ^{63}Ni (range ~2 – ~ 5%, Wieland et al. 2006). In the case of $^{14}CO_3^{2-}$, it has been postulated that there is a relationship between the grain size of calcite crystals and the fraction of CO_3^{2-} accessible for isotopic exchange (Pointeau 2004, Pointeau et al. 2003). In the case of ^{41}Ca, ^{26}Al and ^{32}Si, isotopic exchange experiments recently showed that recrystallisation of the main Ca-, Al-, and Si-containing cement phases in HCP occurs, i.e., C-S-H phases, AFm phases and ettringite, and that this is a fast process leading to almost 100% recrystallisation within a few years (Tits et al. 2023).

Tab. 4-1: Characteristic parameters of the L/ILW repository per metre of cavern length

Kosakowski et al. (2023)

Parameter	Notation	Value
Total volume [m^3/m]*	V_{tot}	144
Average porosity [-]	ε	0.2
Total volume of solution** [m^3/m]	V_{sol}	29
Mass of sorption-effective HCP [kg/m]	M_{cem}	$4.02 \cdot 10^4$

* Based on the description of the dead-end caverns in NTB 23-03: internal width = ~ 11.5 m, height = 12.5 m. 11.5 × 12.5 = 143.75 m^3/m.

** $V_{sol} = \varepsilon V_{tot}$

4.2 $^{59/63}Ni$ and $^{14}CO_3^{2-}$ retention

Experimental evidence was provided that ^{63}Ni uptake by HCP should be interpreted in terms of an isotopic exchange process rather than an adsorption process on HCP because measured sorption isotherms could not be interpreted in terms of a Langmuir- or Freundlich-type sorption isotherm. Furthermore, a dependence of the R_d value on the S/L ratio of the cementitious system was observed (Wieland et al. 2006) (see discussion in Section A1.1.1 of NTB 14-08 (Wieland 2014)). For these reasons, it was proposed that a solubility-controlled mechanism governs Ni uptake by HCP as spectroscopic investigations further indicated that a mixed Ni-Al layered double hydroxide (LDH) phase might form in cement systems (Wieland et al. 2006, Scheidegger et al. 2000, Vespa et al. 2006). The Ni concentrations in cementitious systems were determined

to range in value between ~$2 \cdot 10^{-8}$ M and ~10^{-7} M at a pH of 13.3 (Wieland et al. 2006, Engelsen et al. 2010), which is lower than the aqueous Ni concentration predicted in equilibrium with $Ni(OH)_2$ or $Ni_4Al_2(OH)_{12}CO_3 \cdot 2H_2O$, a Ni-containing LDH (~$3 \cdot 10^{-6}$ M at pH 12.5; Berner 2014).

The predominant inorganic ^{14}C species is $^{14}CO_3^{2-}$, which can either (co)precipitate as $CaCO_3$ or sorb to the mineral phases of HCP. Isotopic exchange with calcium carbonate in HCP is commonly considered the most important process of ^{14}C immobilisation. In addition, isotopic exchange could occur with CO_3^{2-} bound in calcium monocarbonate ($Ca_4Al_2(CO_3)(OH)_{12} \cdot 5H_2O$; AFm-$CO_3$) or hemicarbonate ($Ca_4Al_2(CO_3)_{0.5}(OH)_{13} \cdot 5.5H_2O$; AFm-(OH,$CO_3$)), respectively. It is also conceivable that $^{14}CO_3^{2-}$ is adsorbed on C-S-H phases (Noshita et al. 1995). At present, however, conclusive evidence is lacking as to which of the possible mechanisms is responsible for $^{14}CO_3^{2-}$ uptake by HCP, i.e., isotopic exchange with CO_3^{2-}-containing cement phases (monocarbonate, hemicarbonate, calcite) or adsorption onto C-S-H phases.

The current assessment of $^{14}CO_3^{2-}$ immobilisation in the cementitious near-field is therefore still based on the idea that isotopic exchange of $^{14}CO_3^{2-}$ with solid calcium carbonate ($CaCO_3$) in HCP is responsible for $^{14}CO_3^{2-}$ uptake by HCP (Bradbury & Sarott 1994). An uptake mechanism based on isotopic exchange implies that $^{14}CO_3^{2-}$ is bound in the $CaCO_3$ structure and that uptake is largely controlled by the recrystallisation process of $CaCO_3$. The possibility of isotopic exchange of $^{14}CO_3^{2-}$ with finely divided calcium carbonate in HCP has been suggested previously based on the studies of Allard et al. (1981), Bayliss et al. (1988) and Pointeau et al. (2003). Pointeau et al. (2003) showed that isotopic exchange of $^{14}CO_3^{2-}$ with stable CO_3^{2-} of calcite occurs, while the aqueous CO_3^{2-} concentration is controlled by calcite solubility. Furthermore, Pointeau and co-workers provided an empirical relationship used to correlate the fraction of calcite available for isotopic exchange with the particle size of calcareous aggregates. The replacement of CO_3^{2-} by $^{14}CO_3^{2-}$ in the $CaCO_3$ structure was found to be a slow process in laboratory experiments. However, it is reasonable to assume that the recrystallisation of calcium carbonate can effectively retard the release of $^{14}CO_3^{2-}$ over longer timescales, such as in a deep geological repository. In this report, the "shared solubility" approach is applied to estimate $^{14}CO_3^{2-}$ retention in the cementitious near-field, i.e., by considering the replacement of CO_3^{2-} by $^{14}CO_3^{2-}$ in the $CaCO_3$ structure according to isotopic exchange and control of the aqueous CO_3^{2-} concentration by calcite solubility. Furthermore, only $CaCO_3$ present in HCP is considered to control $^{14}CO_3^{2-}$ retention in the near-field, although the formation of additional $CaCO_3$ is expected to occur at the interface between the cementitious near-field and the host rock due to diffusion-controlled mixing of Ca-rich porewater emanating from the alkaline near-field and CO_3^{2-}-rich porewater intruding from the host rock formation.

The input data used to estimate the operational distribution ratios for $^{59,63}Ni$ and $^{14}CO_3^{2-}$ are listed in Tab. 4-2.

Estimating an operational R_d value for the different stages of cement degradation on the basis of Eq. (4) requires that the concentration of the element in HCP and in solution, respectively, does not significantly change over time. A comparison of the total inventories of stable Ni and CO_3^{2-} in HCP with their concentrations in CPW (Tab. 4-2) shows that after about 1,000 exchange cycles of the near-field porewater, the inventories of the stable isotopes in HCP will decrease by ~ 18% in the case of Ni and by < 1% in the case of CO_3^{2-} (pH ~ 12.8). This indicates that the distribution ratio will not significantly change with time. However, assuming the upper bound of aqueous concentrations for Ni (Tab. 4-2), the reduction of the distribution ratio of Ni should already be significant (> 50%) after 100 exchange cycles. In this context, it should be noted that in the concrete of a deep geological repository located in the Opalinus Clay, fewer than two pore volumes are expected to be exchanged within 100,000 years (Kosakowski et al. 2014). As discussed in Martin et al. (2023), complete saturation of the L/ILW cavern will hardly be reached within 100,000 years. This implies that such assumptions are very conservative.

Tab. 4-2: Input data used to calculate distribution ratios for $^{59,63}Ni$ and $^{14}CO_3^{2-}$ on HCP

Parameter	**Notation**	**Ni**	**CO_3^{2-}**
Used in equation (4)			
Concentration of stable elements in HCP* [mol/kg]	c_{cem}	$4.1 \cdot 10^{-4}$	DS-I: 2.61 DS-II: 2.61 DS-III: 1.72
Concentration of elements in solution in equilibrium with HCP** [mol/L]	c_{aq}	10^{-7}	DS-I: $5.7 \cdot 10^{-5}$ (suboxic, pH ~ 13.11) DS-II: $1.58 \cdot 10^{-5}$ (anoxic, pH ~ 12.68) DS-III: $8.41 \cdot 10^{-6}$ (anoxic, pH ~ 9.89)
Accessibility factor	f	0.1	0.01
Upper bound for c_{aq}:			
Concentration of elements in solution in equilibrium with HCP** [mol/L]	c_{aq}	$5.7 \cdot 10^{-6}$	$2 \cdot 10^{-3}$
Used in equation (4) related to near-field			
Total inventory of stable elements in HCP*** [mol/m]	m_{cem}	15.78	DS-I: $1.0 \cdot 10^{5}$ (suboxic) DS-II: $9.4 \cdot 10^{4}$ (anoxic) DS-III: $6.6 \cdot 10^{4}$ (anoxic)
Total inventory of stable elements in solution**** [mol/m]	m_{aq}	$2.2 \cdot 10^{-3}$	DS-I: 1.26 (suboxic) DS-II: 0.35 (anoxic DS-III: 0.18 (anoxic)
Upper bound for m_{aq}			
Total inventory of stable elements in solution**** [mol/m]	$m_{aq,max}$	$6.6 \cdot 10^{-2}$	44

* Assuming the following concentrations in unhydrated cement: Ni = 24.32 ppm (NTB 14-08, Tab. 2.3). The $CaCO_3$ content of HCP is taken from Tab. 2-3 for the three stages of cement degradation.

** Aqueous Ni concentrations in line with those reported by Wieland & van Loon (2002), Wieland et al. (2006) and Engelsen et al. (2010). The upper bound is based on Hummel et al. (2022). The concentrations of total carbonate are taken from Tab. 2-3 for the three stages of cement degradation. For DS-I, suboxic conditions are considered, for DS-II and DS-III, anoxic conditions are considered.

*** $m_{cem} = M_{cem} \cdot c_{cem}$. ($M_{cem}$: Tab. 4-1)

**** $m_{aq} = V_{sol} \cdot c_{aq}$. (V_{sol}: Tab. 4-1)

The operational R_d values calculated according to Eq. (4) are listed in Tab. 4-3. The lower bounds of the R_d values for $^{59,63}Ni$ have been estimated using the upper limit of the aqueous Ni concentration. The accessibility factors are set to f = 0.1 in the case of $^{59,63}Ni$ and to f = 0.01 in the case of $^{14}CO_3^{2-}$ for reasons of conservatism. Note that the selected values expected to be valid in the long run are only slightly higher than those determined in short-term experiments, i.e., f = 0.02 – 0.05 for ^{63}Ni (Wieland et al. 2006) and f = 0.005 for $^{14}CO_3^{2-}$ (Pointeau et al. 2003). Assigning accessibility factors f of 0.1 and 0.01 implies that only a small amount of the Ni-containing LDH and calcium carbonate are assumed to be accessible to isotopic exchange in the cementitious near-field, i.e., 10% in the case of $^{59,63}Ni$ retention and 1% in the case of $^{14}CO_3^{2-}$ retention. It should be noted that assuming isotopic exchange with the total stable Ni and CO_3^{2-} inventories in the near-field, i.e., f = 1, the R_d values listed in Tab. 4-3 would increase by an order of magnitude in the case of $^{59/63}Ni$ and by two orders of magnitude in the case of $^{14}CO_3^{2-}$.

Tab. 4-3: Estimated R_d values for $^{59,63}Ni$ and $^{14}CO_3^{2-}$ for the three stages of cement degradation of the L/ILW repository

Accessibility factors f = 0.1 for $^{59,63}Ni$ and f = 0.01 for $^{14}CO_3^{2-}$

Radionuclide	**R_d value** [m^3/kg]	
	Best estimate*	**Lower bound****
$^{59,63}Ni$ – all stages	0.41	0.01
$^{14}CO_3^{2-}$		
Stage I	0.46 (suboxic)	10^{-1}
Stage II	1.55 (anoxic)	1.0
Stage III	2.04 (anoxic)	1.0

* Estimated with Eq. (3) using the parameters given in Tab. 4-2.
** Estimated based on uncertainty ranges of the parameters.

In NTB 14-08, operational R_d values were compared with experimental data reported in the literature (Wieland 2014). Sorption values for Ni determined in batch sorption experiments were found to range between ~ 0.03 and ~ 0.2 m^3/kg. From through-diffusion data of Ni on HCP, R_d values between 0.02 and 0.04 m^3/kg were determined, which is a factor of 5 – 10 lower than the values obtained in batch sorption experiments. This indicates that the operational R_d value for Ni listed in Tab. 4-3 is within the range of sorption values determined in laboratory experiments.

Sorption measurements with $^{14}CO_3^{2-}$ on HCP and concrete show a strong uptake of $^{14}CO_3^{2-}$ with R_d values ranging between ~0.7 m^3/kg and 30 m^3/kg (Wang et al. 2012). However, the distribution ratio was found to depend on the degradation stage of HCP and the S/L ratio of the cementitious system. For DS-II, Wang et al. (2012) recommended an R_d value (best estimate) of 5 m^3/kg (lower limit: 2 m^3/kg, upper limit : 20 m^3/kg), while slightly lower values were selected for DS-I (best estimate : 2 m^3/kg, lower limit : 0.7 m^3/kg, upper limit : 3 m^3/kg). The sorption values determined in the sorption tests fall within the range of the operational R_d values derived in this report.

The following sorption values are recommended for the retention of $^{59,63}Ni$ in cementitious systems (Tab. 7-1):

- Stages I to III: An operational sorption value is assigned to Ni retention under both oxidising and reducing conditions for all stages of cement degradation (R_d = 0.41 m^3/kg).

The following sorption values are recommended for the retention of $^{14}CO_3^{2-}$ in cementitious systems (see also Tab. 7-1):

- Stages I to III: The following operational R_d values are assigned to the retention of radiolabelled carbonate under both oxidising and reducing conditions: DS-I: R_d = 0.45 m^3/kg, DS-II: R_d = 1.5 m^3/kg, DS-III: R_d = 2.0 m^3/kg.

4.3 ^{41}Ca, ^{26}Al and ^{32}Si retention

Tits et al. (2023) investigated the uptake of ^{45}Ca and ^{32}Si by HCP and several cement phases (C-S-H phases, portlandite AFm phases, ettringite) with the aim of assessing the retention of the dose-relevant radionuclides ^{41}Ca, ^{26}Al and ^{32}Si in the cementitious near-field. The authors could explain the long-term uptake kinetics by assuming isotopic exchange with stable Ca, Al and Si in the cement phases during their recrystallisation. The uptake kinetics of ^{45}Ca and ^{32}Si by various cement phases were modelled with the help of homogeneous recrystallisation models (Curti et al. 2010, Heberling et al. 2018), assuming either constant bulk recrystallisation rates (AFm phases and ettringite) or decreasing bulk recrystallisation rates with time (C-S-H phases, portlandite, HCP).

For the calculation of R_d values for ^{26}Al, ^{32}Si and ^{41}Ca under near-field conditions, isotopic equilibrium of the radioisotopes and the stable isotopes between the solid and liquid phases is assumed. This isotopic equilibrium is reached by isotopic exchange with the respective stable isotopes during recrystallisation as experimentally demonstrated on C-S-H phases, portlandite, AFm phases, ettringite and intact HCP by Tits et al. (2023). It is further assumed that the same isotopic exchange process takes place on Al/Fe siliceous hydrogarnet, zeolites and calcite. It should be noted that recrystallisation studies on calcite showed that calcite also exhibits a ^{45}Ca isotopic exchange behaviour similar to that of C-S-H phases (e.g., Curti et al. 2005, Heberling et al. 2016). No evidence was found in the literature for the occurrence of recrystallisation processes in zeolites and Al/Fe siliceous hydrogarnets. Here, we assume that these minerals are subject to long-term recrystallisation processes similar to those of other cement minerals.

The following processes are considered to calculate the R_d values:

- ^{41}Ca: exchange with stable Ca associated with C-S-H phases with C/S ratios 1.6 (DS-I and DS-II) and 0.7 (DS-III), portlandite (DS-I and DS-II), ettringite (DS-I and DS-II) calcite (all stages) and zeolites (DS-III)
- ^{26}Al: exchange with stable Al associated with ettringite (DS-I and DS-II), Al/Fe siliceous hydrogarnet (DS-I) and zeolites (DS-III)
- ^{32}Si: exchange with stable Si associated with C-S-H phases with C/S ratios 1.6 (DS-I and DS-II) and 0.7 (DS-III), Al/Fe siliceous hydrogarnet (DS-I) and zeolites (DS-III)
- The above-mentioned isotopic exchange reactions reach complete isotopic equilibrium within timescales relevant for radioactive waste disposal.

The mineral contents of the cementitious systems are listed in Tab. 2-3. Note that using this approach to calculate the inventories of stable isotopes corresponds to a simplifying approach as only the predominant cement phases contributing to the inventory of an element of interest are considered. Thus, smaller elemental inventories associated with other minerals have been neglected, such as gypsum in the case of Ca, C-A-S-H phases and hydrotalcite in the case of Al, and quartz in the case of Si. Furthermore, only two C/S ratios of C-S-H phases were considered, which correspond to upper and lower bounds of Ca and Si contents. Finally, Ca-chabazite was assumed to represent zeolites.

The R_d values listed in Tab. 4-5 were estimated based on the near-field parameters compiled in Tab. 4-4 and the assumption that only 10% of the inventory of the stable elements are accessible to isotopic exchange (accessibility factor f = 0.1). The value for the accessibility factor was chosen in agreement with the value assumed for the isotopic exchange of ^{59,63}Ni in the L/ILW repository (Tab. 4-3). It should be noted that the experimental studies by Tits et al. (2023) on the ^{45}Ca and the ^{32}Si uptake by single cement phases and degraded HCP in dilute suspension show that an accessibility factor f of 1 can be achieved within a few years in dispersed systems used in

laboratory experiments. This result suggests that the selected value (f = 0.1) is probably a conservative estimate of the accessible mineral fraction and is valid even for compact cement systems under near-field conditions, where mineral accessibilities are expected to be lower than in dispersed systems. Note, however, that the same recrystallisation rate and the same accessible fraction were assumed for all cement phases.

Tab. 4-4: Input data used to calculate distribution ratios for ^{41}Ca, ^{26}Al and ^{32}Si on HCP

Parameter	**Notation**	**Ca**	**Al**	**Si**
Used in Equation (4)				
Concentration of stable elements in HCP* [mol/kg]	c_{cem}	DS-I: 8.86 DS-II: 8.16 DS-III: 7.49	DS-I: 0.67 DS-II: 0.16 DS-III: 0.35	DS-I: 1.88 DS-II: 1.83 DS-III: 8.70
Concentration of elements in solution in equilibrium with HCP* [mol/L]	c_{aq}	DS-I: $2.76 \cdot 10^{-3}$ DS-II: $1.37 \cdot 10^{-2}$ DS-III: $7.10 \cdot 10^{-2}$	DS-I: $2.63 \cdot 10^{-5}$ DS-II: $1.62 \cdot 10^{-4}$ DS-III: $7.7 \cdot 10^{-7}$	DS-I: $3.60 \cdot 10^{-5}$ DS-II: $8.91 \cdot 10^{-4}$ DS-III: $5.88 \cdot 10^{-4}$
Accessibility factor	f	0.1	0.1	0.1
Upper bound for c_{aq}				
Concentration of elements in solution in equilibrium with HCP** [mol/L]	c_{aq}	0.10	$5 \cdot 10^{-4}$	10^{-3}
Near-field				
Total inventory of stable elements in HCP*** [mol/m]	m_{cem}	DS-I: $3.41 \cdot 10^{5}$ DS-II: $3.05 \cdot 10^{5}$ DS-III: $2.88 \cdot 10^{5}$	DS-I: $2.58 \cdot 10^{4}$ DS-II: $6.21 \cdot 10^{3}$ DS-III: $1.35 \cdot 10^{4}$	DS-I: $7.24 \cdot 10^{4}$ DS-II: $6.48 \cdot 10^{4}$ DS-III: $3.35 \cdot 10^{5}$
Total inventory of stable elements in solution**** [mol/m]	m_{aq}	DS-I: 60.7 DS-II: 301 DS-III: 1560	DS-I: 0.58 DS-II: 3.56 DS-III: 0.017	DS-I: 0.79 DS-II: 19.6 DS-III: 12.9
Upper bound for m_{aq}				
Total inventory of stable elements in solution**** [mol/m]	$m_{aq,max}$	5,000	2.2	22

* The content of Ca-, Al, and Si-containing minerals of the cementitious systems are taken from Tab. 2-3 for the three stages of cement degradation. DS-I, DS- II and DS-III: reducing conditions are considered.

** Arbitrarily set upper limits based on the aqueous concentrations of the corresponding elements (Ca, Al, Si) listed in Tab. 2-3 for the three stages of cement degradation.

*** $m_{cem} = M_{cem} \cdot c_{cem}$. ($M_{cem}$: Tab. 4-1)

**** $m_{aq} = V_{sol} \cdot c_{aq}$. (V_{sol}: Tab. 4-1)

Tab. 4-5: Estimated operational R_d values for ^{41}Ca, ^{26}Al and ^{32}Si for the three stages of cement degradation in the L/ILW repository

Accessibility factor f = 0.1 for all radionuclides

Radionuclide	**R_d value** [m^3/kg]	
	Best estimate*	**Lower bound****
^{41}Ca		
Stage I	$3.2 \cdot 10^{-1}$	$9 \cdot 10^{-3}$
Stage II	$5.8 \cdot 10^{-2}$	$8 \cdot 10^{-3}$
Stage III	$1.0 \cdot 10^{-2}$	$7 \cdot 10^{-3}$
^{26}Al		
Stage I	2.5	0.13
Stage II	0.1	0.03
Stage III	45	0.07
^{32}Si		
Stage I	5.2	0.18
Stage II	0.2	0.18
Stage III	1.5	0.90

* Estimated with Eq. (3) using the near-field parameters given in Tab. 4-4 and on the assumption of accessibility factors f = 0.1.

** Estimated based on the upper limits for the aqueous concentrations given in Tab. 4-4.

5 Selected sorption data for stage IV of the cement degradation process

Stage IV of the cement degradation process is reached when all Ca-bearing cement minerals (C-S-H phases, portlandite, AFm phases, ettringite) are dissolved and replaced by calcite (Ochs et al. 2016). Although Kosakowski et al. (2023) stated that such a scenario is quite unrealistic for a repository placed in a low-permeability clay host rock such as OPA, this report includes a selection of sorption values for this late stage of cement degradation for the sake of completeness. To this end, a compilation of the typical mineralogy of the cementitious materials degraded to DS-IV and the corresponding porewater compositions is also included. These are the basic data required to derive a simplified SDB for DS-IV.

5.1 Composition of near-field mineralogy and porewater

Wieland & Kosakowski (2020) modelled the cement degradation process by carbonation and the pozzolanic reaction between dissolving siliceous aggregates and the cement matrix up to DS-IV for three cementitious materials (provisional container concrete, mortar M1 and a cement-based material termed reference cement in Stage 2 of the Sectoral Plan). The mineral compositions of these cementitious materials degraded to DS-IV and the corresponding porewaters are compiled in Tab. 5-1. The main characteristics are: i) calcite is the dominant mineral in all degraded materials (≥ 70 wt.%), while the quartz (< 10 wt.%) and clay contents (kaolinite < 9 wt.%) are significantly lower, ii) the porewater (pH ~ 8) contains K^+ and Mg^{2+} as the main cations, while SO_4^{2-} is the main charge-compensating anion. The presence of some additional minerals is predicted, e.g., gypsum (as the SO_4^{2-}-bearing mineral), ferrihydrite (as the Fe^{3+}-bearing mineral), natrolite (an Na-Ca-Al-Si-containing zeolite-type mineral), and magnesium-silicate hydrates (M-S-H) phases (as the Mg^{2+}-bearing mineral). It should be noted that the appearance of the minor minerals may be influenced by the selected geochemical set-up (dataset used to model the mineralogy). Nevertheless, it is safe to conclude that, in the given geochemical conditions, calcite will be present in the degraded cementitious materials in addition to quartz and clay minerals. As a consequence of this, the SDB for DS-IV was developed on the assumption that calcite is the only mineral controlling the retention of all radionuclides in DS-IV.

5.2 Methodology

Sorption databases for radionuclide retention calculations by calcite have previously been documented for the safety analysis within the framework of the Sectoral Plan for Deep Geological Repositories (e.g., Cloet et al. 2019, Nagra 2008, Schwyn 2008). The database for radionuclide retention by calcite was developed by Bradbury & Baeyens (1997) and later updated by Bradbury et al. (2008) and Baeyens et al. (2014). The current development of an SDB for radionuclide retention in DS-IV is based on these earlier studies, and no detailed review of the state-of-the-art literature has been performed. The most recent update of a calcite SDB was published within the framework of Stage 2 of the Sectoral Plan (Baeyens et al. 2014).

Tab. 5-1: Geochemical conditions (solids, porewater composition) for DS-IV of cementitious materials (provisional container concrete, mortar M1, container-filling cement) modelled by assuming the degradation of the HCP by carbonation or the dissolution of siliceous aggregates*

Parameters	Container concrete	Mortar M1	Container-filling cement
Porosity (%)	22.5	44.6	71.4
pH	7.84	8.02	7.99
pe**	2.76	10.76	12.79
Ionic strength (m)	1.02	0.41	0.70
Solutes (mol/kg$_{H2O}$)			
Na	$1.90 \cdot 10^{-2}$	$1.25 \cdot 10^{-2}$	$7.19 \cdot 10^{-3}$
K	0.264	0.111	0.307
Ca	$9.64 \cdot 10^{-3}$	$1.11 \cdot 10^{-2}$	$1.07 \cdot 10^{-2}$
Sulphate	0.584	0.194	0.202
Chloride***	n.d.	n.d.	$1.54 \cdot 10^{-2}$
Carbonate	$2.78 \cdot 10^{-3}$	$9.66 \cdot 10^{-4}$	$5.56 \cdot 10^{-4}$
Si	$1.83 \cdot 10^{-4}$	$1.84 \cdot 10^{-4}$	$1.86 \cdot 10^{-4}$
Al	$3.53 \cdot 10^{-8}$	$5.54 \cdot 10^{-8}$	$9.61 \cdot 10^{-8}$
Fe	$1.11 \cdot 10^{-10}$	$3.39 \cdot 10^{-11}$	$3.50 \cdot 10^{-11}$
Mg	0.434	0.121	$4.26 \cdot 10^{-2}$
Major solids			
Quartz	6.5 wt.%	9.8 wt.%	8.4 wt.%
Kaolinite	6.2 wt.%	7.9 wt.%	9.0 wt.%
Calcite	82.7 wt.%	76.4 wt.%	70.0 wt.%
Gypsum	0.6 wt.%	0.7 wt.%	4.6 wt.%
Ferrihydrite**	1.9 wt.%	1.9 wt.%	2.7 wt.%
Natrolite	0.5 wt.%	0.8 wt.%	0.8 wt.%
M-S-H phases	1.6 wt.%	2.5 wt.%	3.5 wt.%

* Degradation by carbonation or siliceous aggregates in the case of container concrete and mortar M1; the only degradation process of the container-filling cement is carbonation as this material does not contain siliceous aggregates.

** Redox conditions are largely determined by the composition of the cement and by selection of the stable Fe-containing mineral phases. Kosakowski et al. (2020) included ferrihydrite and magnetite, while other iron oxyhyroxides (e.g., goethite) were not considered. Only the oxidised form Fe^{3+} was considered, which potentially enforces oxidising conditions. Under real conditions, the presence and corrosion of Fe^0 in the repository will enforce reducing conditions in the long term.

*** The chlorine content of container concrete and mortar M1 was not available and therefore not used as an input parameter for the thermodynamic calculations. Small amounts of chlorine were added as modelling input to allow convergence of the GEMS calculations. The aqueous chloride concentrations are not realistic and thus denoted as "not determined" (n.d.). The chlorine content of the container-filling cement was known.

5.3 Recommended sorption values

The recommended sorption values for calcite listed in Tab. 7-7 were taken from NTB 12-04 (Baeyens et al. 2014). They are further consistent with values compiled in NAB 18-41 (Cloet et al. 2019). The sorption values proposed in NTB 12-04 for radionuclide retention by calcite were not reviewed. The values for DS-IV of a degraded cementitious near-field were estimated based on the sorption values reported for calcite and on the assumption that the degraded near-field in DS-IV consists of 70 wt.% calcite.

It should be noted that the sorption values listed in Tab. 7-7 do not account for sorption reduction caused by colloids and complexing ligands.

6 Sorption reduction factors

R_d values established for the dose-relevant radionuclides expected in the deep geological repository can be reduced due to the presence of complexing ligands or colloids in the CPWs or by sorption competition. These effects are accounted for with the help of sorption reduction factors. How these factors mathematically influence the R_d value is described in detail in App. A.

6.1 Sorption reduction by cementitious colloids

Laboratory-scale experiments and field studies showed that colloids are present in CPWs, which indicates that colloids will be present in the saturated cementitious near-field of the L/ILW repository (Wieland 2014). The low colloid concentration observed in CPWs is the consequence of the high ionic strength and the relatively high Ca concentration of CPWs. Both chemical parameters facilitate colloid-colloid interactions (aggregation-sedimentation process) or the attachment of colloids to the surface of the backfill material, respectively. Thus, high ionic strength and Ca concentrations in the millimolar range are capable of establishing favourable conditions for colloid destabilisation or colloid attachment to the surface of backfill material, respectively. These processes control the concentration of colloids dispersed in the porewater of the cementitious near-field. The low colloid concentration observed under the hyperalkaline conditions of a CPW is an important factor limiting radionuclide mobility in the cementitious near-field. A low inventory of dispersed colloids, however, requires low or stagnant water flow in the near-field of a repository in order to minimise colloid generation by re-dispersion. Under these conditions, the shear forces generated are expected to be too low to allow disaggregation and colloid detachment from the surface of the backfill material.

The effect of colloids on radionuclide uptake is expressed in terms of a sorption reduction factor, F_{red}, by analogy with the impact of complexing ligands on radionuclide uptake. Sorption reduction factors (realistic and upper-bound (pessimistic) values), F_{red}, for uptake by HCP in the presence of cement-derived near-field colloids, were estimated assuming a typical colloid concentration of 10^{-4} kg/m^3 (Wieland 2014). Sorption reduction factors are listed for those elements with sorption values different from zero. Values were either taken from Wieland & van Loon (2002) for DS-I and DS-II or they were estimated for DS-III and the new dose-relevant radionuclides following the approach presented in Wieland & van Loon (2002). The sorption reduction factors are listed in Tab. 7-3.

6.2 Sorption reduction by complexing ligands

Ethylenediaminetetraacetic acid (EDTA), nitrilotriacetic acid (NTA), cyanide (CN^-), gluconic acid (GLU) and isosaccharinic acid (ISA) are considered to be the most important complexing ligands of radionuclides in the cement-based L/ILW repository planned in Switzerland (Nagra 2023a). Nitrates/nitrites are oxidising agents, which are present in some waste forms and thus might have an influence on the redox potential, while their role in the complexation of radionuclides can be ignored under conditions representative of the cementitious near-field. The maximum concentrations of the main complexing ligands for the two waste groups 1 and 2, considered based on the chemical properties of the L/ILW and their potential consequences for the near-field evolution, were estimated on the basis of the MIRAM RBG inventories (Nagra 2023a) and are listed in Tab. 6-1. In addition to the aforementioned complexing ligands in the waste matrix, degradation products of polymeric organic materials (rubber, plastics etc.), bitumen and basic and acidic ion-exchange resins as well as concrete admixtures and degradation products could potentially act as complexing ligands for radionuclides.

Tab. 6-1: Maximum concentration and concentration limit for the waste group assignment of complexing ligands in near-field porewater

Nagra (2023a)

Material	**L/ILW maximum concentration** [M]	**Concentration limit** [M]
EDTA	$2.5 \cdot 10^{-2}$	10^{-5}
NTA	$6.5 \cdot 10^{-2}$	$2 \cdot 10^{-2}$
Cyanide	0.18	10^{-5}
Nitrate/Nitrite	0.48	0.05
Gluconic acid	$5.1 \cdot 10^{-6}$	10^{-5}
Isosaccharinic acid	$8.6 \cdot 10^{-4}$	10^{-4}

The environmental fate and impact of EDTA, NTA, ISA and cement additives on radionuclide migration have been discussed previously (Keith-Roach 2008, Keith-Roach et al. 2014). Several studies have been carried out with the aim of reviewing published thermodynamic data of the complexation of radionuclides with important organics present in waste forms and developing consistent sets of thermodynamic data for use in speciation calculations in connection with the safety analysis of radioactive waste disposal (e.g., Gaona et al. 2008, Hummel et al. 2005, Rai & Kitamura 2017). Sorption reduction due to the presence of complexing agents has further been assessed within the framework of the Japanese and Swedish waste management programmes (Keith-Roach et al. 2014, Tachi & Ochs 2018). In addition, a large number of experimental studies on the effect of EDTA, ISA (and other cellulose degradation products), GLU, and cement admixtures on the solubility and sorption of radionuclides have been carried out in the past. In the following sections, studies performed with the most important complexing agents, i.e., ISA, GLU, EDTA, NTA, CN^-, NH_3 and concrete admixtures, will be briefly discussed.

ISA and cellulose degradation products

A few waste forms contain cellulose, which degrades under alkaline conditions. The main degradation products of cellulose are α- and β-isosaccharinic acids, while the minor presence of other, currently not identified cellulose degradation products is conceivable. The kinetics of cellulose degradation and hence the formation of ISA is still disputed due to significant discrepancies observed in the rate constants determined from short- and long-term degradation experiments with those deduced from degradation studies at elevated temperatures (e.g., Glaus & van Loon 2008, Pavasars et al. 2003). ISA was found to be rapidly degraded by alkaliphilic microorganisms below a pH of ~ 11 (Bassil et al. 2015a, 2015b, Kuippers et al. 2015, 2018, Rout et al. 2015a, 2015b), which limits its impact as complexing agent for radionuclides under near-neutral conditions such as geological environments. However, under conditions relevant to a cement-based repository, i.e., above pH 11, ISA may persist in the repository environment due to inhibited microbial activity, thus acting as complexing agents. Under these conditions, the aqueous ISA concentration is controlled by its interaction with cementitious materials in the near-field. García et al. (2020) showed that HCP in DS-II has the highest ISA sorption capacity compared to HCP in DS-I or in the carbonated stage (DS-IV). ISA sorption is expected to take place on the surface of cement phases by interaction with positively charged surface sites, i.e., Ca^{2+} bound to silanol sites carrying a negative charge. While ISA sorption reduces its ability to act as a complexing agent for radionuclides, the formation of surface-bound ISA complexes may

exert two potential effects on the uptake of radionuclides by HCP: 1) ISA sorption may block cement sorption sites for radionuclides, thus increasing the aqueous concentration of radionuclides, or 2) ternary radionuclide-ISA surface complexes may form, which promotes radionuclide uptake by HCP.

In an initial approximation, it can be assumed that complexing ligands have the same effect on radionuclide solubility and sorption by cementitious materials. For example, an increase in the solubility of a radionuclide under the conditions of a cementitious near-field by one order of magnitude leads to a corresponding decrease in radionuclide sorption on HCP by the same ligand at the same concentration for the same element. For this reason, results from solubility measurements carried out in the presence of ISA, GLU, EDTA and superplasticisers therefore provide useful information on the potential effect of these ligands on sorption. Nevertheless, it is acknowledged that the aforementioned processes that can occur in cementitious systems with a complexing ligand, such as blocking of cement sorption sites for radionuclides and the formation of ternary radionuclide-ligand surface complexes, limits the possibility of a direct transfer of the observations made in solubility studies to sorption studies with the same complexing ligands. These processes can either enhance or reduce sorption of radionuclides on HCP.

New and previously not considered information is available on the effect of ISA on the solubility and sorption properties of several radionuclides (e.g., Felipe-Sotelo et al. 2017, González-Siso et al. 2017, Kobayashi et al. 2019, Kobayashi et al. 2017, Tasi et al. 2018a).

Felipe-Sotelo et al. (2017) observed an increase in the solubility of Th and U(VI) precipitates in NRVB solution containing cellulose degradation products (CDPs). Na-uranate or Ca-uranate were considered as the solubility-controlling U(VI) phases in either Na-containing alkaline solution or Ca-containing solutions and NRVB solution. The authors used a mixture of CDPs produced in contact with NRVB, but the nature and amounts of the different CDPs have not been reported.

By contrast, binary radionuclide-ISA systems were employed to determine the solubility of β–$Ni(OH)_2$(cr) (González-Siso et al. 2017), UO_2(am,hyd) (respectively $UO_2 \cdot xH_2O$) and $Na_2U_2O_7$(cr) (Kobayashi et al. 2019), $Zr(OH)_4$(am) (Kobayashi et al. 2017), and PuO_2(cr,hyd) (Tasi et al. 2018a). The solubility of β-$Ni(OH)_2$(cr) was found to significantly increase in alkaline conditions (pH 10 – 13) at total ISA concentrations above 10^{-2} M. However, no increase in solubility was observed at $[ISA]_{tot} \leq 10^{-3}$ M. The results are in line with previous studies on the formation of Ni-ISA complexes indicating weak complexation of Ni by ISA (Evans et al. 2012). The effect of ISA on the solubility of hexavalent U(VI) solid phases ($Na_2U_2O_7$(cr)) was found to increase with increasing ISA concentration (Kobayashi et al. 2019), while solubility enhancement was more pronounced in the pH range below 11. Above pH 11, no statistically significant effect was observed at an $[ISA]_{tot}$ of $3.98 \cdot 10^{-3}$ M, while an increase of about two orders of magnitude was reported at an $[ISA]_{tot}$ of $3.16 \cdot 10^{-2}$ M. The strong increase with increasing ISA concentration indicates the formation of a U(VI):ISA = 1:2 complex. Least-square fitting of the solubility data suggested the formation of the $UO_2(ISA)_2$(aq) complex in near-neutral solution and of the $UO_2(OH)_3(ISA)_2^{3-}$(aq) complex under alkaline conditions. The latter species may be deprotonated to $UO_2(OH)_2(ISA)(ISA_{-H})^{3-}$(aq) and $UO_2(OH)(ISA_{-H})_2^{3-}$(aq) depending on the pH and according to the acidity of the hydroxyl groups of the alkyl chain of ISA. The study of Kobayashi et al. (2019) suggests that an effect of ISA on the sorption of U(VI) is unlikely at an $[ISA]_{tot} \leq 10^{-3}$ M in the pH range above 11. Note again that ISA is considered to be readily degraded in the pH range ≤ 11 by microorganisms over the period of concern for a cement-based repository.

The solubility of the tetravalent metal cations Zr(IV), U(IV) and Pu(IV) was found to be enhanced under alkaline conditions in the presence of ISA. In the case of $Zr(OH)_4$(am), an increase in the solubility was observed at an $[ISA]_{tot} \geq 10^{-3}$ M in alkaline conditions above pH 10 with $Zr(OH)_4(ISA)(ISA_{-H})^{3-}$(aq) suggested as the dominant Zr species (Kobayashi et al. 2017). It

should be noted that similar observations were previously made in solubility studies with ThO_2(am), i.e., no measurable effect of ISA at an $[ISA]_{tot} \leq 10^{-3}$ M and the formation of a $Th(OH)_4(ISA)_2^{2-}$(aq) complex above this threshold concentration under alkaline conditions (Rai et al. 2009). In the presence of $1.99 \cdot 10^{-3}$ M ISA, the solubility of UO_2(am,hyd) (respectively $UO_2 \cdot xH_2O$) was comparable to that without ISA, indicating the limited effect of ISA on U(IV) solubility (Kobayashi et al. 2019). At higher ISA concentrations, however, solubility increased with the ISA concentration, thus indicating the formation of U(IV)-ISA complexes. Kobayashi et al. (2019) proposed a stoichiometry identical to the Th(IV)-ISA complex, i.e., $U(OH)_4(ISA)_2^{2-}$ as the dominant species formed under alkaline conditions. Tasi et al. (2018b) investigated the impact of α-ISA on the solubility and redox behaviour of nanocrystalline hydrous Pu(IV) oxide (PuO_2(ncr,hyd)). As in the studies of Kobayashi and co-workers, a significant effect of ISA on solubility was only observed above pH 11 and at an $[ISA]_{tot} \geq 10^{-3}$ M in Na-containing media. The authors proposed the formation of Pu-ISA = 1:1 aquo complexes both for Pu(III) and Pu(IV), i.e., $Pu(IV)(OH)_3(ISA_{-H})^-$, $Pu(IV)(OH)_3(ISA_{-2H})^{2-}$ and $Pu(III)(OH)(ISA_{-H})$. The thermodynamic calculations reported by Tasi and co-workers suggest that $Pu(IV)(OH)_3(ISA_{-2H})^{2-}$ is the dominant species above pH 11 at an $[ISA]_{tot} \geq 10^{-3}$ M. Additionally, the formation of quaternary Ca(II)-Pu(IV)-OH-ISA complexes was observed in Ca-containing media, such as CPWs, due to enhanced solubility of PuO_2(ncr,hyd) as compared to Ca-free solutions of analogous composition (Tasi et al. 2018b). The authors proposed the following aqueous quaternary complexes as the dominant species: $Ca(II)Pu(IV)(OH)_3(ISA_{-H})^+$ below pH ≈ 11 and $Ca(II)Pu(IV)(OH)_3(ISA_{-2H})$ above pH ≈ 11. However, a significant effect on solubility was only determined above pH 11 at an $[ISA]_{tot}$ of 10^{-3} M and a $[Ca]_{tot}$ of 10^{-2} M. This finding indicates that the formation of quaternary Ca-Pu-OH-ISA complexes may enhance the solubility in a CPW representative of DS-II ($[Ca]_{tot} \approx 1.37 \cdot 10^{-2}$ M) and DS-III ($[Ca]_{tot} \approx 7.10 \cdot 10^{-2}$ M), while the formation of these complexes is probably negligible in DS-I ($[Ca]_{tot} \approx 2.76 \cdot 10^{-3}$ M) (Tab. 2-3). No effect on the solubility was observed at $[ISA]_{tot} \leq 10^{-4}$ M, irrespective of pH (pH ≥ 10) and the Ca concentration of the solution.

Diesen et al. (2017), Ochs et al. (2018), and Tasi et al. (2021) investigated the sorption of various radionuclides by cementitious materials in the presence of ISA or CDPs, respectively. Diesen and co-workers degraded cellulosic materials under aerobic and anaerobic conditions in alkaline (pH 12.5) media. The CDPs were not characterised and therefore, no information was provided on the ISA concentration in the solutions. The products were found to enhance the solubility of freshly precipitated $Eu(OH)_3$(am), however only at the highest concentrations. A further assessment of the effect of the CDPs on Eu complexation under near-field conditions cannot be undertaken due to the lack of information on the concentrations of complexing ligands. Ochs and co-workers estimated the reduction of U(VI) sorption to HCP by ISA based on the earlier experimental work of Pointeau and co-workers (Pointeau et al. 2004a, Pointeau et al. 2004b). The authors concluded that no effect of ISA on U(VI) sorption onto HCP was observed in the ISA concentration range from 10^{-5} M to ~ $6 \cdot 10^{-3}$ M in all stages of cement degradation. A sorption reduction factor, however, was assigned at ISA concentrations above $6 \cdot 10^{-3}$ M as compared to an ISA-free system. Therefore, a sorption reduction factor of 10 was assigned to U(VI) sorption on HCP at ISA concentrations of 10^{-2} M, while a 100-fold reduction of sorption was assigned at an ISA concentration of 0.1 M.

Tasi et al. (2021) published new experimental data on the uptake of Pu(IV) by HCP in the presence of ISA in CPW at pH 12.5. The uptake of Pu(IV) by HCP was observed to decrease above an $[ISA]_{tot}$ of $3.16 \cdot 10^{-5}$ M (corresponding to an $[ISA]_{aq} \sim 2 \cdot 10^{-5}$ M). However, the mechanism responsible for sorption reduction is presently unknown. A simplified sorption model based on the formation of quaternary Ca-Pu-OH-ISA complexes, as previously observed in the solubility study with PuO_2(ncr,hyd) (Tasi et al. 2018b), did not allow a correct prediction of the effect of

increasing ISA concentrations on Pu(IV) uptake by HCP. The authors concluded that consistency between the trends in sorption and solubility data caused by the presence of ISA cannot be achieved simultaneously.

An additional complexing ligand formed during the degradation of wood and paper was found to have an impact on Ni sorption on HCP (van Loon & Glaus 1998). Complexation of Ni and Pb by the hitherto unknown, readily soluble organic ligand in wood and paper was considered in previous SDBs (Bradbury & Sarott 1994, Bradbury & van Loon 1997) and retained in the current assessment.

GLU

Solubility studies in the presence of GLU were reported for Th(IV) by Colàs et al. (2013b), for U(VI) by Colàs et al. (2013a) and for Zr by Kobayashi et al. (2017). The studies show that radionuclide complexes with GLU tend to be slightly more stable than those with ISA, which is in accordance with the complexation constants reported by Gaona et al. (2008). Dudás et al. (2017) stated that the structure of ISA and GLU is similar as both ligands contain one carboxylate group and several (4 or 5) alcoholic OH groups capable of coordinating with metal cations. However, the authors further inferred that GLU and ISA also exhibit structural differences, which imply that ISA and GLU do not behave identically (or even similarly) with respect to complexation with Ca and the higher-valent cations, such as various actinides and lanthanides. The solubility studies of Colàs et al. (2013a, 2013b), and Kobayashi et al. (2017) indicate that complexation constants with GLU are about an order of magnitude higher than the corresponding constants with ISA. For example, stronger complexation by GLU as compared to ISA was clearly illustrated in the case of Zr (Kobayashi et al. 2017).

To the best of the authors' knowledge, no new information on the effect of GLU on radionuclide uptake by HCP is available in addition to that previously reviewed in NTB 14-08 (Wieland 2014).

Sorption studies with GLU on C-S-H phases were reported by Androniuk et al. (2017), while molecular dynamics simulation of the interaction of U(VI) with C-S-H phases were carried out by Androniuk & Kalinichev (2020) with the aim of developing a mechanistic understanding of the effect of GLU on U(VI) uptake by C-S-H phases. The former study shows that GLU sorption to C-S-H phases is stronger at a higher C/S ratio. The latter study reveals that the formation of ternary surface complexes between U(VI) hydroxyl ions and Ca(II) at the C-S-H surface play an important role in the overall sorption process.

It should be noted that recalculation of the maximum GLU concentration in the near-field porewater on the basis of the updated MIRAM data gives a $[GLU]_{aq} \leq 5.1 \cdot 10^{-6}$ M for both waste groups. This means that the critical concentration limit for GLU (Tab. 6-1) is not impacted by the separation of L/ILW into two waste groups.

EDTA

The effect of EDTA on the solubility of Ni(II), Th(IV) and U(IV,VI) was studied by Felipe-Sotelo et al. (2015). The results show that EDTA may exert a significant effect on Ni(II) and U(IV) solubility in the EDTA concentration range between $5 \cdot 10^{-3}$ M and 0.1 M, while Th(IV) and U(VI) solubilities are only slightly affected by EDTA in the same concentration range. Sorption studies with Eu(III) on NRVB in the presence of EDTA further show that the complexing ligand reduced the extent of sorption at EDTA concentrations > 0.01 M (Telchadder et al. 2012). However, no effect was observed at an $[EDTA]_{aq}$ of 10^{-3} M. It should be noted that the maximum EDTA concentration in the near-field porewater of the deep geological repository was estimated to be 0.025 M for some L/ILW allocated to waste group 2 (Tab. 6-1), which is above the limit of 10^{-5} M for waste group 1. In this study, the effect of EDTA on radionuclide sorption was estimated

based on thermodynamic speciation calculations. Thermodynamic modelling reported by Hummel et al. (2022) and Ochs et al. (2014) show that EDTA exists nearly exclusively as a $CaEDTA^{2-}$ complex in CPW, i.e., strongly alkaline conditions and in the presence of Ca (≥ 1 mM). Under these conditions, EDTA has an effect on the speciation of only very few cations. More specifically, EDTA may affect the retention of Ni, Pb and Fe(III) by HCP. Recently performed speciation calculations support this finding and suggest that Fe(III) complexation by EDTA may reduce Fe(III) uptake by HCP solely at the highest EDTA concentration level (Hummel et al. 2022). Therefore, a provisional sorption reduction factor of 50 is assumed for Fe(III) and waste group 2. In NTB 14-08 (Wieland 2014), a sorption reduction factor of 5 was assigned to Pb in agreement with the previous cement SDBs. In the case of Ni, it is expected that the solubility limit may be enhanced in the presence of EDTA. An influence on actinide complexation (e.g., U, Np, Pu) is only expected if $[EDTA]_t > [Ca]_t$ under near-neutral pH conditions.

Recent studies carried out by DiBlasi et al. (2021) and DiBlasi et al. (2022) report on the existence of very stable ternary Ca-An(III)-EDTA complexes and/or quaternary Ca-An(III)-OH-EDTA complexes under highly alkaline conditions (An(III) = Cm(III) and Pu(III)) without being able to provide stoichiometries and stability constants of these complexes so far. Nevertheless, this work shows that Ca(II) may have a very stabilising effect on the speciation in trivalent actinide – EDTA systems and possibly also on the chemically analogous lanthanide – EDTA and Fe(III) – EDTA systems. The same authors could also show that Ca(II) strongly stabilises the Pu(IV) – EDTA system by forming very stable quaternary $CaPu(OH)_4EDTA^{2-}$ complexes characterised by a $\log_{10}K°$ value of ~ 64.9. Felipe-Sotelo et al. (2015) showed that, in the presence of 20 mM Ca, adding ~ $2 \cdot 10^{-3}$ M EDTA increases the solubility of U(IV) by almost two orders of magnitude. This observation can only be explained by the formation of ternary Ca-U(IV)-EDTA complexes as nearly all EDTA is present as $Ca\text{-}EDTA^{2-}$ under these conditions.

It can be assumed that the chemically analogous tetravalent actinides, Th(IV), Np(IV) and U(IV), form equally stable quaternary complexes. The formation of such stable complexes can greatly reduce the sorption of trivalent and tetravalent actinides as well as lanthanides on cement phases due to the effect of competition between the complexation reactions in solution and the sorption reactions. In the absence of experimental data on the influence of this competition effect on sorption R_d values, it is assumed, in a conservative scenario, that the effect of the above complexation reactions on sorption is as large as the effect on the solubility of the trivalent actinides and lanthanides reported by DiBlasi et al. (2021) and DiBlasi et al. (2022). To this end, solubility calculations for the Th(IV), U(IV) and Pu(IV) in CPW (Tab. 2-3) were carried out at varying EDTA concentrations in order to assess the impact on sorption reduction (see App. C; Hummel et al. 2022).

NTA

According to the MIRAM RBG inventories (Nagra 2023b), L/ILW also contains significant amounts of NTA. To the best of the authors' knowledge, no new studies on the complexation of radionuclides with this complexing agent have been published in recent years. Speciation calculations and linear free energy correlations show that metal – NTA complexes are generally much weaker than metal – EDTA complexes. Furthermore, the formation of ternary or quaternary metal complexes with Ca and NTA, as in the case of EDTA (see previous section), is unlikely due to the difference in structure: EDTA has six functional groups whereas NTA has only three functional groups. Based on the work of Hummel (1993) (cited in Wieland 2014) it is assumed that the effect of NTA on radionuclide sorption is negligible. Therefore, no sorption reduction factor is attributed to this complexing agent.

Cyanide

Cyanide (CN^-) is present in the chemical form of Prussian Blue ($FeIII_4[FeII(CN)_6]_3$), which is used as a caesium-ion exchanger in decontamination processes for liquid waste. Prussian Blue readily dissolves in alkaline solution, such as CPW (pH > 12) (Hummel 2004). Free cyanide is released when hexa-cyanoferrate ($Fe(CN)_6^{4-}$) decomposes. However, the compound is expected to be stable in the dark even under alkaline conditions (pH > 8), which limits the concentration of free cyanide. High CN^- concentrations are only expected in a very limited number of waste types based on the assumptions that hexacyanoferrate decomposes and that biotic or abiotic decomposition of free cyanide can be excluded. At the lower CN^- concentration anticipated in waste group 1 (Tab. 6-1), complex formation with CN^- has an effect on the speciation of only a very limited number of radionuclides, i.e., Fe(II), Ni(II), and Ag(I). The thermodynamic calculations published by Hummel (2004) and Hummel (2008) show that CN^- complexation of Fe(III) and Pb(II) in the alkaline region is weaker (i.e., needs more CN^- to reach 90% complexation) than the complexation of Fe(II) by CN^-. Ni(II)-CN complexes are slightly stronger than Fe(II)-CN complexes (Hummel 2004). In the case of Ag(I), even traces of CN^- will strongly affect its speciation (Hummel 2004). Therefore, it is considered that CN^- has no effect on radionuclide uptake except for Fe(II) and Ni(II). In the case of Ag(I), complexation by CN^- can be ignored as zero sorption on HCP is assumed (Tab. 7-1).

Nitrate/Nitrite

Various waste package types contain nitrate and nitrites, e.g., ammonium nitrate (NH_4NO_3), calcium nitrate ($Ca(NO_3)_2$), chromium-III-nitrate ($Cr(NO_3)_3$, iron-II-nitrate ($Fe(NO_3)_2$), potassium nitrate (KNO_3), potassium nitrite (KNO_2), sodium nitrate ($NaNO_3$) and silver nitrate ($AgNO_3$) (Nagra 2023b). It is to be assumed that all these salts are highly soluble and will be released once the waste gets in contact with water. NO_3^- will therefore be available as oxidant to oxidise other substances (e.g., chemical complexes, metals). Consequently, this may lead to a higher mobility of some redox-sensitive radionuclides. A concentration limit of 0.05 mol/L is recommended as the limit to be used to classify waste groups 1 and 2 in Nagra (Nagra 2023a) (Tab. 6-1).

Complexing ligands formed during the degradation of bitumen and acidic cation-exchange resins

Gamma irradiation decomposes strong acidic cation-exchange resins, while no evidence for decomposition was found in the absence of a radiation field. Sulphate and dissolved organic compounds were found to be the main degradation products, and oxalic acid and an unidentified ligand were found to be the most strongly complexing ligands formed upon decomposition of the exchange resin (van Loon & Hummel 1995, van Loon & Hummel 1999a). Nevertheless, both ligands are expected to have only a minor effect on radionuclide speciation (in particular Ni) under alkaline near-field conditions due to the limited total concentration of the ligands in the near-field porewater and due to the formation of strong Ca complexes of both ligands (van Loon & Hummel 1999a). In previous SDBs, it was assumed that the degradation products from bitumen and ion-exchange resins have no significant impact on radionuclide uptake by hydrated cement (e.g., Bradbury & Sarott 1994). This view is currently maintained as there is no evidence to support the relevance of these products for radionuclide complexation and mobility.

Polymeric organic matter

Earlier studies show that the effect of high-molecular-weight polymeric organic materials and their degradation products on radionuclide solubility and sorption is small compared to that of CDPs (see discussion in Wieland 2014). As no new information is available, it is assumed that an adverse effect of polymeric organic materials and their degradation products on radionuclide complexation, and therefore on radionuclide uptake by HCP and radionuclide mobility, can be ignored.

Concrete admixtures

Concrete admixtures will inevitably play an important role in the production of cement-based components for the near-field of a deep geological repository. For example, superplasticisers improve the flow properties of fresh cementitious materials and offer undeniable advantages for construction. Therefore, the role of SPs and possible degradation products on radionuclide mobility in the near-field is a matter of concern for the assessment of the safe disposal of radioactive waste. More specifically, it is important to understand the complexation properties of concrete admixtures and their degradation products on the solubility of radionuclides and radionuclide retention by cementitious materials in the near-field. Because of safety concerns, the fate of concrete admixtures in cementitious environments as well as their impact on radionuclide solubility and radionuclide sorption have been investigated in the last decade (see references below). Prioritisation of this topic is further documented in several review and overview reports that have been published by various waste management organisations (e.g., Baston et al. 2019, Keith-Roach & Höglund 2017, NDA 2015).

Several generations of polymeric organic compounds have been developed by the industry in the last decades for use as superplasticisers (SP). Earlier products comprised GLU-based suspensions, modified lignosulphonates (LS), vinyl maleic acid copolymers, sulphonated melamine-formaldehyde condensates (PMS) and sulphonated naphthalene-formaldehyde (PNS) condensates (Winnefeld et al. 2007). For the last 30 years, polycarboxylate (PC)-based superplasticisers in particular have been used to improve the flow properties of fresh cementitious materials, as well as to add strength and reduce the amount of clinker in the hardened materials (Winnefeld et al. 2007). The most commonly used PC superplasticisers are polycarboxylate ethers (PCE), polyacrylic or polymaleic polymers with polyethylene glycol (PEG) sidechains and polyaryl ethers (PAE), which belong to the latest generation of modern SPs. PCE SPs have a characteristic "comb" shape with a methacrylic-acid-based backbone and polyether side chains (Marchon et al. 2013, Winnefeld et al. 2007). PAE SPs combine the structural features of PNS SPs, i.e., aromatics in the backbone, with PEG sidechains (Chernyshev et al. 2018).

The degradation studies and investigations into the desorption of PMS, PNS and PC superplasticiser from HCP indicate that i) PNS SPs are chemically more stable in strongly alkaline solution (pH 14) than PMS SPs (Yilmaz et al. 1993), ii) PMS, PNS and PC SPs can be leached from HCP by wash-out processes in conditions corresponding to cement degradation by water (Märkl et al. 2017, Märkl & Stephan 2016), and iii) more than 90% of PCE SPs were found to remain on the paste and only 10% of SPs were quantified in pore solution squeezed from HCP (Fujita et al. 2008). Fujita and co-workers further showed that organic matter released to pore solution has a different chemical configuration compared to the original SP indicating that the organic residuals of low molecular weight have been desorbed during squeezing. Nevertheless, while the organic residuals have not been identified yet, it is very likely that they mainly consist of low-molecular-weight carboxylic acids or impurities or unreacted starting materials. It should be noted that the identification and quantification of SPs and their degradation products in cement leachates is difficult because concrete additives are usually introduced at low concentrations in materials (Guérandel et al. 2011). Keith-Roach & Höglund (2017) concluded in their review that

the long-term leaching of superplasticisers that bind to the cement during hydration is limited and expected to occur slowly although a significant portion of the initially added SPs remains in the CPW during hydration.

Recently, Chernyshev et al. (2018) showed that the decomposition of PAE SPs, which are under consideration for use as admixture for the concrete in the Swedish disposal concept, can be modelled in terms of first-order kinetics. Degradation occurs quite rapidly (half-life of degradation reaction ≈ 290 days) compared to the time period under consideration for a deep geological repository for radioactive waste (typically ≥ 10^5 years). The rate-limiting step of the degradation process involves the decomposition of charged organophosphate groups (phosphate ester dianion) into phosphate. This finding suggests that, using PAE as admixture, phosphate could be available as complexing ligand for radionuclides in the near-field in the long term.

Several experimental studies have investigated the effect of SPs on radionuclide solubility and sorption (Baston et al. 2019, Fröhlich et al. 2017, Fröhlich & Panak 2018, García et al. 2018a, Isaacs et al. 2018, Kitamura et al. 2013, NDA 2015, Young et al. 2013). In addition, García et al. 2018b carried out a modelling study to assess the effect of potential degradation products of PMS and PNS SPs on the solubility of Ni, Eu and U. In their study, Garcia and co-workers assumed the formation of small low-molecular-weight organic and inorganic compounds as proxy products from the degradation of PCE SPs, such as aliphatic compounds (e.g., acetate, urea), aromatic compounds (e.g., phthalate and phenol) and inorganic compounds, as they had previously been identified during hydrothermal degradation of PNS SPs or the biodegradation of lignin, naphthalene or melamine. Thermodynamic modelling showed that the presence of these proxy degradation products in alkaline conditions has no effect on the speciation of Ni(II), Eu(III) and U(VI) up to ligand concentrations of 10^{-2} M (García et al. 2018b). Nevertheless, an impact of the aqueous chemistry of the above radionuclides was predicted below pH 10 in the case of phthalate and acetate. This finding is further consistent with experimental investigations on Ni solubility in the presence of Glenium® 27, a PCE-type SP (García et al. 2018a). It was observed that the SP is mainly sorbed by the solid materials and only a small proportion is released to solution. Due to the overall low content of SP used in concrete formulations, the SP concentration in leachate is expected to be too low to exert any effect on radionuclide mobilisation.

This conclusion agrees with results reported by Isaacs et al. (2018) and Young et al. (2013). Young and co-workers determined the effect of the comb-type PCE SP ADVA Cast 551 on the uptake of two cement formulations (a BFS:OPC = 9:1 mix and a PFA:OPC = 3:1 mix, BFS: blast furnace slag, OPC: ordinary Portland cement, PFA: pulverised fly ash). Uptake of Ni and Eu by both cement formulations was not affected by the presence of the SP in the HCP, indicating that the concentration of the SP in pore solution is negligibly small and has no effect on radionuclide complexation. Furthermore, sorbed SP is not effective at blocking metal binding sites on the cement phases. Isaacs et al. (2018) carried out an experimental study on the effect of commercial and synthesised PCE SPs on the solubility of Ni(II), Am(III), Pu(IV) and U(VI). A more detailed presentation of the experimental data from this study has been published in an NDA report (NDA 2015). The authors found that the commercial products had a much greater effect on solubility than the adjuncts and bespoke, synthesised SPs and attributed this effect on the solubility to small molecules in the commercial products, primarily residual monomers present due to incomplete polymerisation. Furthermore, solubility enhancement was found to be negligibly small when the commercial SPs were present at concentrations anticipated in CPW.

The conclusions presented by Isaacs et al. (2018) were further substantiated by Kitamura et al. (2013). These authors observed no difference in Th(IV) and Am(III) solubilities in CPW squeezed from HCP that had been prepared with and without PCE-type SP. Similarly, Fröhlich et al. (2017) reported on the effect of Glenium® 517, another PCE-type SP, on Eu speciation in the neutral pH range. An effect was only observed at high SP dosages. Baston et al. (2019) investigated the stability of PCE SPs under conditions relevant to the UK concept of a deep geological repository

for high-level waste. For this purpose, the degradation process of SPs was investigated in alkaline solution and as a function of temperature and radiation. Furthermore, the sorption of SPs on a BFS/OPC mix and NRVB was measured with the aim of quantifying and understanding the partitioning between the solid and liquid phases. Pu(IV) solubility measurements were carried out to assess previous results of reported solubility increases due to the presence of SPs. An increase in Pu solubility was observed only at high dosage of the SP due to association of Pu with a high-molecular-weight fraction. However, it was further shown that this fraction is also preferentially sorbed onto cement phases, which mitigates the potential effect of PCE SPs on increasing Pu mobility. The PCE SP was found to be strongly bound to cement phases which limits its remobilisation to solution. Furthermore, the presence of sorbed SP had only little effect on Pu sorption, indicating that sorbed SP does not lead to substantial desorption of Pu from HCP. Leaching experiments with Pu-doped granules of grouted waste simulants revealed no measurable differences in Pu releases from samples with or without PCE SP. The radiolytic studies with the PCE SP show that radiolysis could reduce the impact of the SP by increasing Pu mobility. The overall conclusion from the comprehensive study on the role of PCE SP is that the use of PCE SPs is unlikely to significantly increase the mobility of Pu in conditions relevant to a deep geological repository.

In a series of spectroscopic investigations using luminescence and synchrotron-based techniques, Fröhlich and co-workers investigated the coordination of Eu(III) and Cm(III) to PCE SP, backbone components of SPs (e.g., methacrylate) and model compounds for organic additives based on PC SPs (Fröhlich et al. 2019, Fröhlich et al. 2017, Fröhlich & Panak 2018, 2019, Fröhlich et al. 2016). The spectroscopic studies with Eu(III), Gd(III) and Tb(III) in solutions (pH ~ 4, I = 0.1 mol/kg) containing Glenium® 51 at a concentration of 1 g/kg showed a non-chelate coordination of the trivalent metals through approximately three carbon atoms in the second coordination sphere (Fröhlich et al. 2017). A complementary study with the same lanthanides in a solution containing a synthetic acrylate-based PCE SP corroborated this finding (Fröhlich et al. 2019). The results from the two studies suggest that carboxylic groups of the polycarboxylate comb polymer are bound predominantly in a bidentate end-on fashion to the metal cations. In addition, Fröhlich & Panak (2019) studied the complexation of Eu(III) and Cm(III) with polyacrylate as a model compound for the complex polycarboxylate backbone of SPs. The results indicate that, also in the case of polyacrylate, one metal cation is coordinated to three carboxylic groups of the polymer in line with charge neutralisation. The thermodynamic constants for Eu(III) and Cm(III) coordination to polyacrylate were found to be at the lower end of the reported data for various polycarboxylic ligands. However, they are also in the range of constants expected for macromolecular carboxylic ligands that do not form chelate complexes (Fröhlich & Panak 2019). This finding suggests that an increased stability of metal-PC complexes due to chelate formation is unlikely, thus limiting modes of coordination to those with carboxylate groups of PC.

Fröhlich & Panak (2018) published a thermodynamic and spectroscopic study on the complex formation between Cm(III) and methacrylate (Meth), a potential degradation product of PC SPs that is typically synthesised using either acrylic or methacrylic acids. The formation of $[Cm(Meth)^{2+}]$ was found to dominate at a pH of ~ 4 below a ligand concentration of 0.02 g/kg, while the formation of $[Cm(Meth)_2^{+}]$ was only observed above this threshold concentration. The results from this study support earlier findings that coordination to methacrylate occurs via singly charged carboxylate groups. In another study, Fröhlich et al. (2016) explored the Cm(III) coordination to succinate, a dicarboxylic acid commonly used as model compound for humic substances and other natural organic matter, using luminescence spectroscopy and quantum chemical modelling. Interestingly, the stability constants suggest a binding mechanism with both carboxylic functions, which was supported by quantum-chemical calculations. Thus, in the case of succinate, the formation of a seven-membered chelate ring seems to be the favoured conformation, which may substantially increase the stability of metal-ligand complexes. Nevertheless, it is presently uncertain to what extent succinate is an appropriate surrogate for PC SPs.

Note that these studies were carried out under weakly acidic conditions and their conclusions therefore say little about the influence of SP under the highly alkaline conditions that prevail in a cementitious repository.

In summary, the structural investigations show that metal binding occurs via carboxylic groups to PCE SPs, mostly in a mono- or bidentate fashion, while the formation of a chelate ring is not indicated. This suggests the formation of relatively weak metal-ligand complexes, which are comparable in thermodynamic stability to the complexation of metal cations to small carboxylic acids, such as formic and acetic acids. Previous thermodynamic calculations show that the complexation capacity of small carboxylic acids, taken as proxies for the degradation products of PCE SPs and spent ion exchange-resins, towards metal cations (e.g., Ni, Eu, U) is almost negligible under alkaline conditions (García et al. 2018b, Hummel 2008, Hummel & van Loon 1999).

According to current knowledge, the application of modern concrete admixtures such as PNS, PMS, and PC SPs, in typical dosage (a few wt.% relative to cement) during concrete production leads to low concentrations of the polymeric and low-molecular-weight organic ligands in the near-field porewater due to the strong interaction of the concrete admixtures with HCP under the relevant repository conditions (e.g., HCP-to-porewater ratio of ~ 2 kg/L) (Wieland et al. 2014). Furthermore, in the case of PC SPs and their possible degradation products, the new literature shows that complexation of the radionuclides occurs via the carboxylic groups of these compounds, resulting in weak metal-ligand complexes that hardly exist in the alkaline pH range due to the formation of hydrolysis products. The earlier assessment in NTB 14-08 (Wieland 2014) that SPs have only a negligibly small effect on radionuclide retention in the cementitious near-field is retained and, with the exception of gluconic acid, sorption reduction by concrete admixtures is not taken into account in this study.

6.3 Sorption reduction factors associated with complexing agents

Sorption reduction factors have been assigned to waste group 1 (Tab. 7-4) and waste group 2 (Tab. 7-5) based on the concentration limits defined in Nagra (2023a) for the three different stages of cement degradation. They are estimated based on the concentration limits given in Tab. 6-1 for waste groups 1 and 2 (e.g., concentration limit in the case of ISA: 10^{-4} M to distinguish between waste group 1 and waste group 2). Sorption reduction is assessed with a view to currently available information on the impact of complexing ligands on solubility and sorption of the respective radionuclides (see Section 4.2). For strongly complexing ligands, the combined effect of all complexing ligands on the R_d values can be approximated as the sum of the reduction factors of each single complexing agent (see A.2, Eq. A-17).

6.3.1 Sorption reduction due to the presence of ISA

Ca, Al, Ni, Fe, Pb

Complexation of Ca(II) by ISA has been investigated extensively in the past (Dudás et al. 2017, Rai et al. 2003, Rai et al. 1998, van Loon et al. 1999, 2004, Vercammen et al. 1999). $CaISA^+(aq)$ and $CaISA_{-H}(aq)$ are considered to be the main complexes formed. The latter species dominates under alkaline conditions and involves deprotonation of an alcohol group. The Ca inventory in the near-field is dominated by stable Ca associated mainly with cement phases. The inventory of ^{41}Ca is comparatively low, and isotopic exchange between ^{41}Ca and stable Ca is the uptake mechanism. Isotopic dilution of stable Ca and radiocalcium implies that the concentration of the aqueous ISA complexes with ^{41}Ca is extremely low. No significant sorption reduction is anticipated at an $[ISA]_{aq} \leq 6.8 \cdot 10^{-4}$ M as a result of the formation of Ca-ISA complexes. Thus, no effect on ^{41}Ca sorption has been assigned (Tab. 6-2).

In addition, the influence of ISA on the uptake of other earth alkaline metals (e.g., Sr, Ba, Ra) and transition metals (e,g., Ni, Co) is also considered to be negligibly small in the concentration range of interest (Wieland 2014 and references therein). This conclusion is in line with solubility studies in the presence of ISA, such as in the case of Ni (González-Siso et al. 2017). To the best of the authors' knowledge, no thermodynamic data for Al-ISA complexes have been reported. Thus, a negligible effect on sorption is also assumed in the case of Al.

Rai et al. (2012) published thermodynamic data of the Fe(III)-ISA complex formation. The solubility of $Fe(OH)_3(s)$ was studied in the presence of ISA in the pH range from 2 to 14. Formation of Fe(III)-ISA complexes was observed at pH < 12, which significantly increased the $Fe(OH)_3(s)$ solubility at an $[ISA]_{aq}$ of 10^{-2} M, while no measurable effect within the experimental uncertainty was reported above pH 12. The thermodynamic calculations of Rai and co-workers further show that competition of Fe(III) with tetravalent cations for ISA does not significantly affect the solubilities of tetravalent hydrous oxides (e.g., Th and Np(IV)) in ISA solutions. This finding suggests that ISA forms stronger complexes with tetravalent actinides compared to Fe(III). Therefore, sorption reduction of Fe(III) by ISA is accounted for at the highest ISA concentration ($8.6 \cdot 10^{-4}$ M in waste group 2) and in DS-III (factor of 10 sorption reduction) (Tab. 6-2).

Complexation of Ni and Pb by a hitherto unknown, readily soluble organic ligand in wood and paper was considered in previous SDBs (Bradbury & Sarott 1994, Bradbury & van Loon 1997). The effect of this presently still unknown ligand on Ni and Pb uptake by HCP is taken into account and combined with the effect of EDTA in the sorption reduction factors listed in Tab. 7-4.

Ti, Zr, Sn

The influence of ISA on the uptake of Zr(IV), Sn(IV) and Ti(IV) is expected to be weak due to the limited thermodynamic stability of the ISA complexes. This conclusion is supported by solubility studies in the case of Zr (Kobayashi et al. 2017). A possible effect of ISA on Zr(IV) uptake by HCP is considered at the highest ISA concentration ($8.6 \cdot 10^{-4}$ M in waste group 2) (factor of 10 sorption reduction). Sorption reduction factors for Sn(IV) and Ti(IV) have been assigned on the basis of chemical analogy with Zr(IV) (Tab. 6-2).

Lanthanides and trivalent actinides

The sorption reduction factors previously proposed in NTB 14-08 (Wieland 2014) are retained as no new information is currently available that would require a re-appraisal of the ISA effect on the sorption by HCP. The factors given in NTB 14-08 were selected on the basis of in-house sorption studies with Eu(III) on HCP. Hence, based on chemical analogy, the same sorption reduction factors have been assigned to Ho(III), Ac(III), Am(III), Cm(III), Pu(III) and Cf(III) (Tab. 6-2).

Penta- and hexavalent actinides

The appraisal documented in NTB 14-08 (Wieland 2014) further shows that a reduction of U(VI) uptake by HCP due to the presence of aqueous ISA at concentrations $\leq 10^{-3}$ M is negligibly small. Therefore, no sorption reduction was considered for waste group 1 in any stages of cement degradation in NTB 14-08. The solubility studies with U(VI) in the presence of ISA reported by Kobayashi et al. (2019) indicate that U(VI)-ISA complexes could dominate at a pH ≤ 11. Hence, a cautious approach is taken by assigning a sorption reduction factor of 10 to all penta- and hexavalent actinides in waste group 1 ($[ISA]_{aq} \leq 10^{-4}$ M) in DS-III (Tab. 6-2, Tab. 7-4).

Sorption reduction is likely to occur at the enhanced ISA concentrations relevant to waste group 2 ($[ISA]_{aq} = 10^{-4}$ - $8.6 \cdot 10^{-4}$ M). For this reason, a sorption reduction factor of 10 was proposed in NTB 14-08 in DS-I and DS-II. This appraisal of the ISA effect is consistent with results obtained from the solubility studies with U(VI) by Kobayashi et al. (2019). Currently available information suggests that the complexes formed between penta- and hexavalent actinides by ISA are weaker than those with tetravalent actinides. The sorption reduction factors previously derived in NTB 14-08 are retained. A reduction in sorption by a factor of 10 is considered for waste group 2 at the highest ISA concentration (Tab. 6-2) in DS-I and DS-II. For the sake of consistency with the previous assessment for waste group 1, sorption reduction is increased to 100 for DS-III.

Tetravalent actinides

The studies of Tasi et al. (2018b) and Tasi et al. (2021) allow us to re-assess the sorption reduction factor proposed earlier for the tetravalent actinides in NTB 14-08 (Wieland 2014). The latter values were derived from in-house sorption studies with Th(IV) on HCP. Tasi et al. (2018b) observed an effect of ISA on the solubility of PuO_2(ncr,hyd) at pH 12 in the presence of an $[ISA]_{tot}$ of 10^{-4} M and a $[Ca]_{tot}$ of 10^{-2} M compared to a system in the absence of Ca. The formation of quaternary Ca-Pu-ISA-OH complexes was shown to enhance the solubility of PuO_2(ncr,hyd) at pH 12. Under these conditions, which are representative of DS-II, the solubility is enhanced by about an order of magnitude. However, the increase in solubility is negligible at pH 12 in the presence of an $[ISA]_{tot}$ of 10^{-4} M and an $[Ca]_{tot}$ of 10^{-3} M, which corresponds to the Ca concentration relevant to DS I (pH 13.3, $[Ca]_{tot} \approx 10^{-3}$ M). It should be noted that the in-house sorption studies performed with Th(IV) to derive sorption reduction factors in NTB 14-08 (Wieland 2014) were conducted under conditions representative of DS I, i.e., $[Ca]_{tot} \approx 10^{-3}$ M. Although a direct transfer of the observations made in the solubility studies for assessment of sorption processes is subject to great uncertainties for the reasons mentioned above (competition effects, formation of ternary surface complexes), the formation of quaternary Ca-Pu-ISA-OH complexes could lead to an increased sorption reduction in DS-II. As a consequence of the observed effect of Ca on Pu(IV)-ISA complexation and as a result of a cautious approach to the development of the cement SDB, the previously reported sorption reduction factors for tetravalent actinides in the different stages of cement degradation are revised as follows (Tab. 6-2):

Waste group 1 ($[ISA]_{aq} \leq 10^{-4}$ M):

- Stage I (pH 13.1, $[Ca]_{tot} \approx 10^{-3}$ M): 1
- Stage II (pH 12.5, $[Ca]_{tot} \approx 2 \cdot 10^{-2}$ M): 10
- Stage III (pH 9.9, $[Ca]_{tot} \approx 7 \cdot 10^{-2}$ M): 10

Waste group 2 ($[ISA]_{aq} = 10^{-4}$ - $8.6 \cdot 10^{-4}$ M):

- Stage I (pH 13.1, $[Ca]_{tot} \approx 10^{-3}$ M): 100
- Stage II (pH 12.5, $[Ca_{]tot} \approx 2 \cdot 10^{-2}$ M): 1,000
- Stage III (pH 9.9, $[Ca]_{tot} \approx 7 \cdot 10^{-2}$ M): 1,000

6.3.2 Sorption reduction due to the presence of GLU

Sorption reduction factors due to the presence of GLU were assigned in NTB 14-08 (Wieland 2014) under the assumption that the thermodynamic constants of radionuclide-GLU complexation are about one order of magnitude larger compared to radionuclide-ISA complexation and that the average and maximum concentrations of GLU in the near-field are about one order of magnitude lower. No influence of GLU is expected at a $[GLU]_{aq} \leq 5.1 \cdot 10^{-6}$ M), which is the maximum GLU concentration estimated for both waste groups.

Tab. 6-2: Recommended sorption reduction factors in the presence of ISA and GLU

Metal cation	**ISA***		**GLU**
	$\leq 10^{-4}$ M	10^{-4} M – $8.6 \cdot 10^{-4}$ M	**$\leq 5.1 \cdot 10^{-6}$ M**
Ca(II), Al(III), Ni(II), Pb(II)	1	1	1
Fe(III)	1	10	1
Zr(IV), Sn(IV), Ti(IV)	1	10	1
Ho(III)	1	10	1
Ac(III), Am(III), Cm(III), Pu(III)	1	10	1
Pa(IV), Th(IV), U(IV), Np(IV), Pu(IV)	1/10/10	100/1,000/1,000	1
Pa(V), Np(V), Pu(V)	1/1/10	10/10/100	1
U(VI)	1/1/10	10/10/100	1
Cf(III)	1	10	1

* First number assigned to DS- I, second number to DS-II and third number assigned to DS-III

6.3.3 Sorption reduction due to the presence of EDTA

All EDTA-containing L/ILW has been assigned to waste group 2 (Nagra 2023a). In NTB 14-08 (Wieland 2014), sorption reduction factors were assigned to some radionuclides under conditions anticipated in waste group 2: a factor 5 reduction in sorption for Fe(II), Pb and Ni due to the presence of EDTA, and a factor 50 reduction in sorption for Fe(III). The formation of Ca-EDTA complexes dominates Ca speciation in the alkaline pH range of a cement-type porewater (Hummel et al. 2022). The Ca inventory of the near-field is dominated by stable Ca associated mainly with cement phases. The inventory of ^{41}Ca is comparatively low suggesting that the concentration of ^{41}Ca-EDTA complexes is much lower than the concentration of Ca-EDTA. A cautious approach is taken by assigning ^{41}Ca a reduction in sorption by a factor of 10 at the highest EDTA concentration in waste group 2.

Given the new data available in the literature on the formation of apparently very stable ternary and quaternary Ca-An(III/IV)-OH-EDTA complexes under CPW conditions, the sorption reduction factors due to the presence of EDTA for trivalent and tetravalent actinides were re-evaluated. Hummel et al. (2022) calculated solubility limits for a series of 27 elements in a concrete porewater representative of DS-II using the PSI Chemical TDB 2020 (Hummel & Thoenen 2023) with the latest version of GEM software (GEMS, https://gems.web.psi.ch/). In the same report, the authors also modelled the influence of 0.05 M EDTA on the speciation and solubility of a selected subset of elements (Am, Fe, Hg, Ni, Np, Pb, Pu and U) for suboxic and reducing conditions. Note that 0.05 M EDTA is twice the maximum EDTA concentration indicated in Tab. 6-1. The effects were represented in terms of "solubility enhancement factors, "F_{enh}". For the present cement SDB, "EDTA solubility enhancement factors" were recalculated for an EDTA concentration of 0.025 M and under the chemical conditions representative of a DS-II porewater (see Appendix C). The results are summarised in Tab. 6-3. The enhancement factors clearly show that 0.025 M EDTA in the presence of Ca could strongly increase the solubilities of the tetravalent actinides. The experimentally observed effects of EDTA on the solubilities of trivalent actinides could not be taken into account, as stability constants for ternary and quaternary An(III)-EDTA complexes with Ca and OH are not yet available. The effect of the formation of the quaternary Ca-An(III/IV)-OH-EDTA complexes on An(III/IV) sorption have not yet been investigated experimentally. By taking a cautious approach, sorption reduction factors for EDTA

complexation with tetravalent actinides in all three stages of cement degradation have been estimated based on the solubility enhancement factors listed in Tab. 6-3. The sorption reduction factors assigned to EDTA are listed in Tab. 6-4 (values were rounded up to the nearest 5, 10 or 100 values; values > 1,000 are rounded to the thousand value). The effect of the quaternary Ca-EDTA-OH-An(IV) complexes on R_d values for Th(IV) and Pa(IV) was assumed to be identical to that of the R_d value for Np(IV); i.e., the reduction factor for Th(IV) and Pa(IV) was set to 1,000 (Tab. 6-4).

Although they could not yet report stability constants, the work of DiBlasi et al. (2021) and DiBlasi et al. (2022) convincingly shows that EDTA complexes with trivalent actinides are also strongly stabilised by the presence of Ca under alkaline conditions. Therefore, by taking a cautious approach, we also assign a reduction factor equal to 1,000 (i.e., the lowest F_{red} value assigned to the tetravalent actinides) to the trivalent actinides due to complexation with EDTA in the presence of Ca (Tab. 6-4 and Tab. 7-5).

Tab. 6-3: Summary of solubilities without and with 0.025 M EDTA for selected elements in CPW expected in DS-II

Hummel et al. (2022)

		Reducing conditions	
	No EDTA [mol/kg H_2O]	**With EDTA** [mol/kg H_2O]	**F_{enh}**
Am	$5.20 \cdot 10^{-10}$	$5.26 \cdot 10^{-10}$	1.01
Fe	$2.60 \cdot 10^{-8}$	$2.63 \cdot 10^{-8}$	1.02
Ni	$5.70 \cdot 10^{-6}$	$4.10 \cdot 10^{-5}$	7.00
Np	$9.70 \cdot 10^{-10}$	$1.00 \cdot 10^{-6}$	**811.0**
Pu	$2.40 \cdot 10^{-12}$	$2.33 \cdot 10^{-8}$	**7,800**
U	$4.40 \cdot 10^{-9}$	$1.60 \cdot 10^{-4}$	**31,900**

Tab. 6-4: Recommended sorption reduction factors in the presence of EDTA, CN^- and NO_3^-/NO_2^-

Metal cation	**EDTA***		**CN^-**		**NO_3^-/NO_2^-**	
	$\leq 10^{-5}$ M	10^{-5} – 0.025 M	$\leq 10^{-5}$ M	10^{-5} - 0.18 M	≤ 0.05M	0.04 – 0.48 M
Ca(II)	1	10	1	1	1	1
Fe(III)	1	50	1	1	1	1
Pb(II)	1	5	1	1	1	1
Fe(II)	1	5	1	100	1	1
Ni(II)	1	5	1	10	1	1
Ag(I)	1	1	1	1	1	1
Hg(I)	1	1	1	1	1	1

Tab. 6-4: Cont.

Metal cation	EDTA*		CN^-		NO_3^-/NO_2^-	
	$\leq 10^{-5}$ M	10^{-5} – 0.025 M	$\leq 10^{-5}$ M	10^{-5} - 0.18 M	≤ 0.05M	0.04 – 0.48 M
U(IV)	10	32,000	1	1	1	1
Np(IV)	1	1,000	1	1	1	1
Pu(IV)	5	8,000	1	1	1	1
Th(IV)	1	1,000	1	1	1	1
Ho, Ac, Am, Cm, Cf	1	1,000	1	1	1	1

* It should be noted that all EDTA-containing L/ILW will be assigned to waste group 2.

6.3.4 Sorption reduction by minor complexing ligands

Cyanide (CN^-) is an additional complexing agent present in some waste forms (Tab. 6-1). The presence of CN^- may affect Ni(II) and Fe(II) uptake by HCP. A slight sorption reduction is expected in the case of Ni, while the formation of strong complexes with CN^- was observed in the case of Fe(II). Accordingly, a sorption reduction factor of 10 has been assigned to Ni(II) and a reduction factor of 100 to Fe(II) in waste group 2 where high CN^- concentrations are expected.

Complexation of Ni and Pb by a hitherto unknown, readily soluble organic ligand in wood and paper has been considered in previous SDBs (Bradbury & Sarott 1994, Bradbury & van Loon 1997). The potential effect of this presently still unknown ligand on Ni and Pb uptake by HCP is retained and combined with the effect of EDTA in the sorption reduction factor listed in Tab. 7-5.

6.4 Sorption competition

An appraisal of sorption competition has been based on the assumption that HCP present in the cementitious near-field is the main source of impurity elements ("base case"), with the exception of a few elements whose content in cement is not known. This approach has been undertaken as the partitioning of the impurity elements between HCP and porewater determines the maximum loading of most elements on cement phases, in particular C-S-H phases. In order to undertake the appraisal by considering all elements present in the near-field, the maximum concentrations in the porewater were determined by means of solubility limits for those impurity elements for which the content in HCP is not known. It should be noted that this approach adds a lot of conservatism to the appraisal and increases the safety margin of the conclusions. The maximum concentrations were estimated in terms of the solubility limitation of the element of interest in alkaline CPW. The approach implies that i) the inventory of an element controlled by solubility is sufficiently large in the near-field in order to justify the notion of a solubility-limited concentration in the porewater, and ii) a solid phase precipitates above the threshold concentration, which limits the loading of the element of interest on C-S-H phases.

To place the effect of sorption competition in a broader framework, reference is made to the sorption competition effects in clay systems (OPA and MX-80 bentonite) (Bradbury et al. 2017). These authors found that competition effects mainly play a role for metals with similar chemical properties (valence state, hydrolysis behaviour). The authors distinguished three different groups of metals: divalent transition metals, trivalent lanthanides and actinides, and tetravalent metal ions. Competition was found to take place between members of the same group but was non-existent between members of different groups. The influence of these competitive sorption processes on the R_d values selected in the databases was modelled using the thermodynamic

"2SPNE SC/CE" sorption model, which takes into account both surface complexation and cation exchange processes of the metal ions on the clay surfaces and assumes "maximum limit" concentrations for the most important radionuclides in the bentonite backfill of a deep geological repository for HLW/SF. In the clay systems, reduction factors were found to vary between 30 and 100 in the case of the divalent transition metals, between a factor 20 and a factor 80 in the case of the trivalent lanthanides and actinides, and by approximately a factor of 10 in the case of the tetravalent metal ions.

The current, simplified assessment of sorption competition in the cementitious near-field is thus less detailed. In particular, it cannot account for the competitive effects of specific groups of metal cations. The assessment of sorption competition for the cementitious systems especially accounts for the possibility of a sorption competition between dose-relevant radionuclides and Fe(II,III). It should be noted that aqueous Fe(II,III) species are present in the near-field as a result of iron/steel corrosion. In particular, Fe(III) at maximum loadings may occupy a significant portion of the interlayer sites or surface sites, respectively. The maximum loading, however, depends on the Fe(III) concentration expected in the porewater of the cementitious near-field. It should be noted that the latter concentration was estimated to be much higher on the basis of laboratory studies than compared to the estimated solubility limits under near-field conditions. In addition to the corrosion products, the presence of stable isotopes may also contribute to sorption competition and reduce the uptake of the dose-relevant radionuclides.

The overall assessment of sorption competition for a cement-based near-field suggests that, on the basis of very conservative assumptions, i.e., high solubility of Fe(II,III) and the simultaneous presence of all solubility-limited radionuclides in the near-field, sorption competition with Fe(II,III) (corrosion products) and other stable isotopes present in the near-field can occupy a large portion of the sorption capacity of C-S-H phases. It is anticipated that, in a more realistic scenario, Fe(II,III) solubility is much lower under the conditions representative of the cementitious near-field due to control by Fe-bearing cement minerals instead of Fe-hydroxides. Furthermore, the simultaneous presence of all radionuclides at maximum concentrations is unlikely, as radionuclide release is most likely a time-dependent process related to the degradation of waste materials. A detailed assessment of sorption competition can be found in Appendix B.

For the above reasons, no sorption reduction (sorption reduction factor = 1) has been assigned in relation to sorption competition for the realistic base case ("real") (Tab. 7-6). An arbitrarily chosen sorption reduction factor of 10 is recommended for use in worst-case scenarios ("pess").

7 Compilation of sorption values and sorption reduction factors

Tab. 7-1: Sorption values for unperturbed HCP (m^3/kg) in cement degradation stages I – III under oxidising (oxid.) and reducing (red.) conditions

Element	Region of cement degradation*						
	Stage I		Stage II		Stage III		
	Oxid.	Red.	Oxid.	Red.	Oxid.	Red.	f_E **
Ca***	0.32	0.32	$5.8 \cdot 10^{-2}$	$5.8 \cdot 10^{-2}$	10^{-2}	10^{-2}	1.4
Al***	2.5	2.5	0.1	0.1	45	45	1.4/3.3
Si***	5.2	5.2	0.2	0.2	1.5	1.5	1.4
Cs	$5 \cdot 10^{-4}$	$5 \cdot 10^{-4}$	10^{-3}	10^{-3}	$5 \cdot 10^{-4}$	$5 \cdot 10^{-4}$	3.3
Sr	10^{-1}	10^{-1}	10^{-2}	10^{-2}	10^{-3}	10^{-3}	1.4
Ra	$5 \cdot 10^{-1}$	$5 \cdot 10^{-1}$	$5 \cdot 10^{-2}$	$5 \cdot 10^{-2}$	10^{-1}	10^{-1}	1.4
$^{14}CO_3^{2-}$***	0.46	0.46	1.6	1.6	2.0	2.0	1.4
Organics	10^{-5}	10^{-5}	0	0	0	0	3.3
Cl	10^{-3}	10^{-3}	10^{-4}	10^{-4}	10^{-4}	10^{-4}	3.3
I	10^{-3}	10^{-3}	10^{-4}	10^{-4}	10^{-4}	10^{-4}	3.3
Se****	10^{-2}	$10^{-2}/10^{-3}$	10^{-2}	$3 \cdot 10^{-3}/10^{-4}$	0	$2.5 \cdot 10^{-3}/10^{-4}$	1.4/3.3
Mo	$1.5 \cdot 10^{-2}$	$1.5 \cdot 10^{-2}$	$2.5 \cdot 10^{-2}$	$2.5 \cdot 10^{-2}$	$2 \cdot 10^{-2}$	$2 \cdot 10^{-2}$	1.4
Tc	10^{-3}	1	10^{-4}	1	10^{-4}	1	1.4/3.3
Fe	100	$5 \cdot 10^{-2}$	100	$5 \cdot 10^{-2}$	100	$5 \cdot 10^{-2}$	1.4/3.3
Ni***	0.41	0.41	0.41	0.41	0.41	0.41	1.4
Ti	10	10	10	10	10	10	3.3
Zr	10	10	10	10	10	10	3.3
Nb	1	1	1	1	1	1	1.4
Ag	0	10^{-4}	0	10^{-4}	0	10^{-4}	3.3
Hg	0	10^{-4}	0	10^{-4}	0	10^{-4}	3.3
Sn	10	10	20	20	20	20	3.3
Pb	$5 \cdot 10^{-1}$	$5 \cdot 10^{-1}$	3	3	30	30	1.4/3.3
Po	0	0	0	0	0	0	
Ho	100	100	100	100	100	100	3.3
Ac	100	100	100	100	100	100	3.3
Th	100	100	100	100	100	100	3.3
Pa****	50	100	50	100	100	100	3.3
U	2	100	20	100	100	100	1.4/3.3
Np****	50	100	50	100	100	100	3.3
Pu****	2	100	20	100	100	100	1.4/3.3

Tab. 7-1: Cont.

Element	Region of cement degradation*						
	Stage I		Stage II		Stage III		
	Oxid.	Red.	Oxid.	Red.	Oxid.	Red.	f_E **
Am	100	100	100	100	100	100	3.3
Cm	100	100	100	100	100	100	3.3
Cf	100	100	100	100	100	100	3.3

* Definitions of the regions of the cement degradation are given elsewhere (Kosakowski et al. 2023).

** Experimental uncertainty factors as derived in NTB 14-08 (Wieland 2014) are as follows: f_E = 3.3 for $R_d < 10^{-3}$ m^3/kg and > 10 m^3/kg, f_E = 1.4 for R_d ranging between 10^{-3} m^3/kg and 10 m^3/kg.

*** R_d value estimated based on isotopic exchange (see also NTB 14-08).

**** Sorption values estimated on the basis of Se(VI), Np(V), Pa(V) and Pu(VI) under oxidising conditions and on the basis of Se(IV), Np(IV), Pa(IV) and Pu(IV) under reducing conditions. In addition, sorption values are estimated for Se(-II) (strongly reducing conditions). Uptake of Np(III) and Pu(III) by HCP is treated in analogy to that of trivalent actinides, e.g., Am(III).

Tab. 7-2: Lower and upper limits of the sorption values (m^3/kg) for cement degradation stages I – III (lower and upper limits as reported by Wang et al. 2012 and Ochs et al. 2011 except where indicated)

Element	Region of cement degradation*					
	Stage I		Stage II		Stage III	
	Oxid.	Red.	Oxid.	Red.	Oxid.	Red.
Ca**	$10^{-1}/2$	$10^{-1}/2$	$10^{-2}/2 \cdot 10^{-1}$	$10^{-2}/2 \cdot 10^{-1}$	$10^{-3}/2 \cdot 10^{-2}$	$10^{-3}/2 \cdot 10^{-2}$
Al**	$10^{-1}/2$	$10^{-1}/2$	1/10	1/10	10/100	10/100
Si**	1/10	1/10	1/20	1/20	$5 \cdot 10^{-1}/5$	$5 \cdot 10^{-1}/5$
Cs**,***	$10^{-4}/10^{-2}$	$10^{-4}/10^{-2}$	$10^{-4}/5 \cdot 10^{-2}$	$10^{-4}/5 \cdot 10^{-2}$	$10^{-4}/10^{-2}$	$10^{-4}/10^{-1}$
Sr**,***	$3 \cdot 10^{-2}/3 \cdot 10^{-1}$	$3 \cdot 10^{-2}/3 \cdot 10^{-1}$	$5 \cdot 10^{-3}/10^{-1}$	$5 \cdot 10^{-3}/10^{-1}$	$5 \cdot 10^{-4}/10^{-2}$	$5 \cdot 10^{-4}/10^{-2}$
Ra**,***	$10^{-1}/1$	$10^{-1}/1$	$10^{-3}/1$	$10^{-3}/1$	$10^{-4}/10^{-1}$	$10^{-4}/10^{-1}$
$^{14}CO_3^{2-}$**	$10^{-2}/10^{-1}$	$10^{-2}/10^{-1}$	$3 \cdot 10^{-1}/3$	$3 \cdot 10^{-1}/3$	$5 \cdot 10^{-1}/10$	$3 \cdot 10^{-1}/10$
Organics**	$0/10^{-3}$	$0/10^{-3}$	n.a.	n.a.	n.a.	n.a.
Cl**	$10^{-4}/10^{-2}$	$10^{-4}/10^{-2}$	$10^{-5}/10^{-3}$	$10^{-5}/10^{-3}$	$0/10^{-4}$	$0/10^{-4}$
I**	$10^{-4}/10^{-2}$	$10^{-4}/10^{-2}$	$10^{-5}/10^{-3}$	$10^{-5}/10^{-3}$	$0/10^{-4}$	$0/10^{-4}$
Se**	$10^{-3}/2 \cdot 10^{-2}$	$10^{-3}/3$	$10^{-4}/5 \cdot 10^{-3}$	$10^{-4}/10^{-2}$	n.a.	$0/10^{-2}$
Mo**	$10^{-2}/3$	$10^{-2}/3$	$10^{-4}/10^{-2}$	$10^{-4}/10^{-2}$	$10^{-4}/10^{-2}$	$10^{-4}/10^{-2}$
Tc**	$0/10^{-3}$	$6 \cdot 10^{-2}/20$	$0/10^{-3}$	$6 \cdot 10^{-2}/20$	n.a.	$6 \cdot 10^{-2}/20$
Fe**	10/700	$10^{-2}/1$	10/700	$10^{-2}/1$	10/700	$10^{-2}/1$
Ni**	$10^{-2}/1$	$10^{-2}/1$	$10^{-2}/1$	$10^{-2}/1$	$10^{-2}/1$	$10^{-2}/1$
Ti**	$10^{-1}/100$	$10^{-1}/100$	$10^{-1}/100$	$10^{-1}/100$	1/1,000	1/1,000
Zr***	$10^{-1}/100$	$10^{-1}/100$	$10^{-1}/100$	$10^{-1}/100$	1/1,000	1/1,000
Nb***	1/1,000	1/1,000	1/1,000	1/1,000	1/1,000	1/1,000
Ag**	n.a.	$0/10^{-4}$	n.a.	$0/10^{-4}$	n.a.	$0/10^{-4}$
Hg**	n.a.	$0/10^{-4}$	n.a.	$0/10^{-4}$	n.a.	$0/10^{-4}$
Sn*	10/200	10/200	10/200	10/200	$3 \cdot 10^{-4}/100$	$3 \cdot 10^{-4}/100$
Pb**	$10^{-1}/1$	$10^{-1}/1$	1/10	1/10	1/100	1/100
Po**	0/100	$0/10^{-4}$	0/100	$0/10^{-4}$	0/100	$0/10^{-4}$
Ho**	$10^{-1}/5{,}000$	$10^{-1}/5{,}000$	1/5,000	1/5,000	3/5,000	3/5,000
Ac***	$10^{-1}/5{,}000$	$10^{-1}/5{,}000$	1/5,000	1/5,000	3/5,000	3/5,000
Th***	1/1,000	1/1,000	1/1,000	1/1,000	1/1,000	1/1,000
Pa***	$4 \cdot 10^{-1}/10$	1/1,000	3/300	1/1,000	1/1,000	1/1,000
U***	$4 \cdot 10^{-1}/10$	1/1,000	3/300	1/1,000	1/1,000	1/1,000
Np***	$4 \cdot 10^{-1}/10$	1/1,000	3/300	1/1,000	1/1,000	1/1,000
Pu***	$4 \cdot 10^{-1}/10$	1/1,000	3/300	1/1,000	1/1,000	1/1,000
Am***	$10^{-1}/5{,}000$	$10^{-1}/5{,}000$	1/5,000	1/5,000	3/5,000	3/5,000

Tab. 7-2: Cont.

Element	Region of cement degradation*					
	Stage I		Stage II		Stage III	
	Oxid.	Red.	Oxid.	Red.	Oxid.	Red.
Cm***	10^{-1}/5,000	10^{-1}/5,000	1/5,000	1/5,000	3/5,000	3/5,000
Cf**	10^{-1}/5,000	10^{-1}/5,000	1/5,000	1/5,000	3/5,000	3/5,000

* See Tab. 7-1. Presentation of the data: lower limit/upper limit; limits are only given for those oxidations states of radionuclides listed in Tab. 7-1 with $R_d \neq 0$.

** Estimated value (this study). Limits for Po based on discussion given in Section 3.2.3. Limits for Ho and Cf assigned in analogy to Eu (Wieland 2014) and Cm, respectively. Limits for Ti in analogy to Zr. Limits for Fe based on new experimental data (Section 3.4.3). Limits for Ni in analogy to Fe(II).

*** Limits as given in Wang et al. (2012) and Ochs et al. (2016), (2011) with the following exceptions: Zr: estimated limits for stage I; Tc: estimated limits for Tc(VII) (oxid.); Ac, Cm: limits corresponding to those given for Am; Pa, Np, Pu: limits corresponding to those given for Th (oxidation state IV) and U(VI).

n.a. not applicable

Tab. 7-3: Sorption reduction factors (realistic and upper bound (pessimistic) values), $F_{red,1}$, for uptake by HCP in the presence of cement-derived near-field colloids assuming a typical colloid concentration of 10^{-4} kg/m^3

Sorption reduction factors are listed for the elements with sorption values different from zero. Values were taken from Wieland & van Loon (2002) for cement degradation stages I and II and/or estimated for cement degradation stage III and the new dose-relevant radionuclides according to the procedure given in Wieland & van Loon (2002).

Element	**Region of cement degradation***					
	Stage I		**Stage II**		**Stage III**	
	Oxid.	**Red.**	**Oxid.**	**Red.**	**Oxid.**	**Red.**
	real./pess.	**real./pess.**	**real./pess.**	**real./pess.**	**real./pess.**	**real./pess.**
Ca	1/1	1/1	1/1	1/1	1/1	1/1
Al	1/1.01	1/1.01	1/1	1/1	1.12/1.5	1.12/1.5
Si	1.02/1.07	1.02/1.07	1/1	1/1	1/1.01	1/1.01
Cs	1/1	1/1	1/1	1/1	1/1	1/1
Sr	1/1	1/1	1/1	1/1	1/1	1/1
Ra	1/1	1/1	1/1	1/1	1/1	1/1
$^{14}CO_3^{2-}$	1/1	1/1	1/1.01	1/1.01	1/1.01	1/1.01
Organics	1/1	1/1	1/1	1/1	1/1	1/1
Cl	1/1	1/1	1/1	1/1	1/1	1/1
I	1/1	1/1	1/1	1/1	1/1	1/1
Se	1/1	1/1	1/1	1/1	1/1	1/1
Mo	1/1	1/1	1/1	1/1	1/1	1/1
Tc	1/1	1/1.01	1/1	1/1.01	1/1.01	1/1.01
Fe	1.2/2	1/1	1.2/2	1/1	1.2/2	1/1
Ni	1/1	1/1	1/1	1/1	1/1	1/1
Ti	1.02/1.07	1.02/1.07	1.02/1.07	1.02/1.07	1.02/1.07	1.02/1.07
Zr	1.02/1.07	1.02/1.07	1.02/1.07	1.02/1.07	1.02/1.07	1.02/1.07
Nb	1/1.01	1/1.01	1/1.01	1/1.01	1/1.01	1/1.01
Ag	n.a.	1/1	n.a.	1/1	n.a.	1/1
Hg	n.a.	1/1	n.a.	1/1	n.a.	1/1
Sn	1.02/1.07	1.02/1.07	1.04/1.12	1.04/1.12	1.04/1.12	1.04/1.12
Pb	1/1	1/1	1/1.02	1/1.02	1.07/1.2	1.07/1.2
Po	n.a.	n.a.	n.a.	n.a.	n.a.	n.a.
Ho	1.2/2	1.2/2	1.2/2	1.2/2	1.2/2	1.2/2
Ac	1.2/2	1.2/2	1.2/2	1.2/2	1.2/2	1.2/2
Th	1.2/2	1.2/2	1.2/2	1.2/2	1.2/2	1.2/2
Pa	1.12/2	1.2/2	1.12/1.5	1.2/2	1.2/2	1.2/2
U	1/1.01	1.2/2	1.04/1.12	1.2/2	1.2/2	1.2/2
Np	1.12/2	1.2/2	1.12/1.15	1.2/2	1.2/2	1.2/2

Tab. 7-3: Cont.

Element	Region of cement degradation*					
	Stage I		Stage II		Stage III	
	Oxid.	Red.	Oxid.	Red.	Oxid.	Red.
	real./pess.	real./pess.	real./pess.	real./pess.	real./pess.	real./pess.
Pu	1/1.01	1.2/2	1.04/1.12	1.2/2	1.2/2	1.2/2
Am	1.2/2	1.2/2	1.2/2	1.2/2	1.2/2	1.2/2
Cm	1.2/2	1.2/2	1.2/2	1.2/2	1.2/2	1.2/2
Cf	1.2/2	1.2/2	1.2/2	1.2/2	1.2/2	1.2/2

* See Tab. 7-1.

n.a. not applicable as no sorption (R_d = 0) is recommended in the corresponding stages of cement degradation (Tab. 7-1).

Tab. 7-4: Sorption reduction factors for waste group 1, $F_{red,2}$, due to the presence of important complexing ligands in the porewater for cement degradation stages I – III under oxidising (oxid.) and reducing (red.) conditions*

Element/ligand	Waste group 1**					
	Stage I		Stage II		Stage III	
	Oxid.	Red.	Oxid.	Red.	Oxid.	Red.
Ca	1	1	1	1	1	1
Al	1	1	1	1	1	1
Si	1	1	1	1	1	1
Cs	1	1	1	1	1	1
Sr	1	1	1	1	1	1
Ra	1	1	1	1	1	1
$^{14}CO_3^{2-}$	1	1	1	1	1	1
Organics	1	1	1	1	1	1
Cl	1	1	1	1	1	1
I	1	1	1	1	1	1
Se	1	1	1	1	1	1
Mo	1	1	1	1	1	1
Tc	1	1	1	1	1	1
Fe	1	1	1	1	1	1
Ni/L	1	1	1	1	10	10
Ti	1	1	1	1	1	1
Zr	1	1	1	1	1	1
Nb	1	1	1	1	1	1
Ag	n.a.	1	n.a.	1	n.a.	1
Hg	n.a.	1	n.a.	1	n.a.	1
Sn	1	1	1	1	1	1
Pb	1	1	1	1	1	1
Po	n.a.	n.a.	n.a.	n.a.	n.a.	n.a.
Ho/	1	1	1	1	1	1
Ac/	1	1	1	1	1	1
Th/ISA	1	1	10	10	10	10
Pa/ISA	1	1	1	10	10	10
U/EDTA, ISA	1	10	1	20	10	20
Np/ISA	1	1	1	10	10	10
Pu/EDTA, ISA	1	5	1	15	10	15
Am	1	1	1	1	1	1

Tab. 7-4: Cont.

Element/ligand	Waste group 1**					
	Stage I		Stage II		Stage III	
	Oxid.	Red.	Oxid.	Red.	Oxid.	Red.
Cm	1	1	1	1	1	1
Cf	1	1	1	1	1	1

* See Tab. 7-1.

** Concentration limits and maximum concentrations of the complexing ligands as listed in Tab. 6-1. Ligands affecting radionuclide uptake by HCP: CN = cyanide, ISA = isosaccharinic acid, GLU = gluconic acid, EDTA = ethylenediaminetetraacetic acid; L = unknown readily soluble organic ligand in wood and paper (Bradbury & Sarott 1994, Bradbury & van Loon 1997).

n.a. not applicable as no sorption (R_d = 0) is recommended in the corresponding stages of cement degradation (Tab. 7-1).

Tab. 7-5: Sorption reduction factors for waste group 2, $F_{red,2}$, due to the presence of important complexing ligands in the porewater for cement degradation stages I – III under oxidising (oxid.) and reducing (red.) conditions*

The values are rounded up to the nearest 5, 10 or 100 values. Values > 1,000 are rounded to the thousand value.

Element/ligand	**Waste group 2****					
	Stage I		**Stage II**		**Stage III**	
	Oxid.	**Red.**	**Oxid.**	**Red.**	**Oxid.**	**Red.**
Ca	10	10	10	10	10	10
Al	1	1	1	1	1	1
Si	1	1	1	1	1	1
Cs	1	1	1	1	1	1
Sr	1	1	1	1	1	1
Ra	1	1	1	1	1	1
$^{14}CO_3^{2-}$	1	1	1	1	1	1
Organics	1	1	1	1	1	1
Cl	1	1	1	1	1	1
I	1	1	1	1	1	1
Se	1	1	1	1	1	1
Mo	1	1	1	1	1	1
Tc	1	1	1	1	1	1
Fe/EDTA, ISA, CN***	50	105	50	105	60	105
Ni/EDTA, L, CN***	15	15	15	15	15	15
Ti/ISA, EDTA	10	10	10	10	10	10
Zr/ISA, EDTA	10	10	10	10	10	10
Nb	1	1	1	1	1	1
Ag	n.a.	1	n.a.	1	n.a.	1
Hg	n.a.	1	n.a.	1	n.a.	1
Sn/ISA, EDTA	10	10	10	10	10	10
Pb/EDTA, L***	5	5	5	5	5	5
Po	n.a.	n.a.	n.a.	n.a.	n.a.	n.a.
Ho/ISA, EDTA	1,010	1,010	1,010	1,010	1,020	1,020
Ac/ISA, EDTA	1,010	1,010	1,010	1,010	1,020	1,020
Th/ISA, EDTA	1,100	1,100	2,000	2,000	2,000	2,000
Pa/ISA, EDTA	10	1,100	10	2,000	100	2,000
U/ISA, EDTA	10	32,100	10	33,000	100	33,000
Np/ISA, EDTA	10	1,100	10	2,000	100	2,000
Pu/ISA, EDTA	10	8,100	10	9,000	100	9,000
Am/ISA, EDTA	1,010	1,010	1,010	1,010	1,020	1,020

Tab. 7-5: Cont.

Element/ligand	Waste group 2**					
	Stage I		Stage II		Stage III	
	Oxid.	Red.	Oxid.	Red.	Oxid.	Red.
Cm/ISA, EDTA	1,010	1,010	1,010	1,010	1,020	1,020
Cf/ISA, EDTA	1,010	1,010	1,010	1,010	1,020	1,020

* See Tab. 7-1.

** Concentration limits and maximum concentrations of the complexing ligands as listed in Tab. 6-1. Ligands affecting radionuclide uptake by HCP: CN = cyanide, ISA = isosaccharinic acid, GLU = gluconic acid, EDTA = ethylenediaminetetraacetic acid; L = unknown readily soluble organic ligand in wood and paper (Bradbury & Sarott 1994, Bradbury & van Loon 1997).

*** Sorption reduction factors for Ni and Pb as reported by Bradbury & van Loon (1997) for the reference case. For cement degradation Stage III, the effect of EDTA, L, and CN is taken into account in the case of Ni(II) and Fe(II).

n.a. not applicable as no sorption (R_d = 0) is recommended in the corresponding stages of cement degradation (Tab. 7-1).

Tab. 7-6: Sorption reduction factors by sorption competition* in the porewater for cement degradation stages I – III of the under oxidising (oxid.) and reducing (red.) conditions, $F_{red,3}$

Element	Region of cement degradation**					
	Stage I		Stage II		Stage III	
	Oxid.	Red.	Oxid.	Red.	Oxid.	Red.
	real./pess.	real./pess.	real./pess.	real./pess.	real./pess.	real./pess.
Cs	1/1	1/1	1/1	1/1	1/10	1/10
Sr	1/1	1/1	1/1	1/1	1/10	1/10
Ra	1/1	1/1	1/1	1/1	1/10	1/10
Fe	1/10	1/10	1/10	1/10	1/10	1/10
Ti	1/10	1/10	1/10	1/10	1/10	1/10
Zr	1/10	1/10	1/10	1/10	1/10	1/10
Nb	1/10	1/10	1/10	1/10	1/10	1/10
Ag	n.a.	1/1	n.a.	1/1	n.a.	1/10
Hg	n.a.	1	n.a.	1	n.a.	1
Sn	1/10	1/10	1/10	1/10	1/10	1/10
Pb	1/10	1/10	1/10	1/10	1/10	1/10
Po	n.a.	n.a.	n.a.	n.a.	n.a.	n.a.
Ho	1/10	1/10	1/10	1/10	1/10	1/10
Ac	1/10	1/10	1/10	1/10	1/10	1/10
Th	1/10	1/10	1/10	1/10	1/10	1/10
Pa	1/10	1/10	1/10	1/10	1/10	1/10
U	1/10	1/10	1/10	1/10	1/10	1/10
Np	1/10	1/10	1/10	1/10	1/10	1/10
Pu	1/10	1/10	1/10	1/10	1/10	1/10
Am	1/10	1/10	1/10	1/10	1/10	1/10
Cm	1/10	1/10	1/10	1/10	1/10	1/10
Cf	1/10	1/10	1/10	1/10	1/10	1/10

* Sorption competition is not effective in the case of Al, Ca, Si, Ni, $^{14}CO_3^{2-}$, Cl, I, Mo, Se, Tc and the organics.

** See Tab. 7-1.

n.a. not applicable as no sorption (R_d = 0) is recommended in the corresponding stages of cement degradation (Tab. 7-1).

Tab. 7-7: Sorption values for cement degradation stage IV under oxidising (oxid.) and reducing (red.) conditions in m^3/kg

Element	**Calcite***	**Degraded near-field in DS-IV** [70 wt.% calcite]	**f_E****	**Reference/comment**
Ca(II)	$5.0 \cdot 10^{-5}$	$3.5 \cdot 10^{-5}$	3.3	NTB 12-04
Al(III)	$5.0 \cdot 10^{-5}$	$3.5 \cdot 10^{-5}$	3.3	Nominal from Ca(II)
Si(IV)	0	0		This study
Cs(I)	0	0		NTB 12-04
Sr(II)	$5.0 \cdot 10^{-5}$	$3.5 \cdot 10^{-5}$	3.3	NTB 12-04
Ra(II)	$5.0 \cdot 10^{-5}$	$3.5 \cdot 10^{-5}$	3.3	NTB 12-04
C_{inorg} ($^{14}CO_3^{2-}$)	$5.0 \cdot 10^{-3}$	$3.5 \cdot 10^{-3}$	1.4	NTB 12-04
C_{org}(Organics)	0	0		NTB 12-04
Cl(-I)	0	0		NTB 12-04
I(-I)	0	0		NTB 12-04
Se(-II)	0	0		NTB 12-04
Mo(VI)	0	0		NTB 12-04
Tc(IV)	0	0		NTB 12-04
Fe(III)	$5.0 \cdot 10^{-4}$	$3.5 \cdot 10^{-4}$	1.4	Nominal from Ni(II)
Ni(II)	$5.0 \cdot 10^{-4}$	$3.5 \cdot 10^{-4}$	1.4	NTB 12-04
Ti(IV)	$8.5 \cdot 10^{-4}$	$6.0 \cdot 10^{-4}$	1.4	Analogy with Zr(IV)
Zr(IV)	$8.5 \cdot 10^{-4}$	$6.0 \cdot 10^{-4}$	1.4	NTB 12-04
Nb(V)	0	0		NTB 12-04
Ag(I)	0	0		NTB 12-04
Hg(II)	0	0		Analogy with Ag(I)
Sn(IV)	$3.8 \cdot 10^{-4}$	$2.7 \cdot 10^{-4}$	1.4	NTB 12-04
Pb(II)	$2.0 \cdot 10^{-2}$	$1.4 \cdot 10^{-2}$	1.4	NTB 12-04
Po(IV)	$4.0 \cdot 10^{-5}$	$2.8 \cdot 10^{-5}$	3.3	NTB 12-04
Ho(III)	0.13	$9.1 \cdot 10^{-2}$	1.4	NTB 12-04
Ac(III)	0.13	$9.1 \cdot 10^{-2}$	1.4	Analogy with Ho(III)
Th(IV)	$4.5 \cdot 10^{-2}$	$3.2 \cdot 10^{-2}$	1.4	NTB 12-04
Pa(V)	$4.6 \cdot 10^{-3}$	$3.2 \cdot 10^{-3}$	1.4	NTB 12-04
U(IV)	$9.5 \cdot 10^{-2}$	$6.7 \cdot 10^{-2}$	1.4	NTB 12-04
Np(IV)	$5.5 \cdot 10^{-2}$	$3.9 \cdot 10^{-2}$	1.4	NTB 12-04
Pu(III)	2.0	1.40	1.4	NTB 12-04
Am(III)	1.0	0.70	1.4	NTB 12-04

Tab. 7-7: Cont.

Element	Calcite*	Degraded near-field in DS-IV [70 wt.% calcite]	f_E**	Reference/comment
Cm(III)	0.87	0.61	1.4	NTB 12-04
Cf	0.87	0.61	1.4	Analogy with Cm(III)

* Data from NTB 12-04 (Tab. 7-2), including a lab-to-field transfer factor (0.05) owing to differences in the surface areas of calcite used in laboratory experiments (small grain size) and the calcite particles relevant to the field (coarser grain size).

** Estimated uncertainty factors in agreement with values listed in Tab. 7-1.

8 References

Aimoz, L., Wieland, E., Taviot-Guého, C., Dähn, R., Vespa, M. & Churakov, S.V. (2012): Structural insight into iodide uptake by AFm phases. Environmental Science & Technology 46/7, 3874-3881. DOI: 10.1021/es204470e.

Allard, B., Torstenfelt, B. & Andersson, K. (1981): Sorption studies of $H^{14}CO_3^-$ on some geologic media and concrete. MRS Symposium Proceedings 3, 465-472.

Altmaier, M., Neck, V. & Fanghänel, T. (2008): Solubility of Zr(IV), Th(IV) and Pu(IV) hydrous oxides in $CaCl_2$ solutions and the formation of ternary Ca-M(IV)-OH complexes. Radiochimica Acta 96/9-11, 541-550. DOI: 10.1524/ract.2008.1535.

Androniuk, I. & Kalinichev, A.G. (2020): Molecular dynamics simulation of the interaction of uranium (VI) with the C–S–H phase of cement in the presence of gluconate. Applied Geochemistry 113, 104496. DOI: 10.1016/j.apgeochem.2019.104496.

Androniuk, I., Landesman, C., Henocq, P. & Kalinichev, A.G. (2017): Adsorption of gluconate and uranyl on C-S-H phases: Combination of wet chemistry experiments and molecular dynamics simulations for the binary systems. Physics and Chemistry of the Earth, Parts A/B/C 99, 194-203. DOI: 10.1016/j.pce.2017.05.005.

Appelo, C. (2021): The anion exchange properties of AFm (hydrocalumite-group) minerals defined from solubility experiments and crystallographic information. Cement and Concrete Research 140, 106270. DOI: 10.1016/j.cemconres.2020.106270.

Arayro, J., Dufresne, A., Zhou, T., Ioannidou, K., Ulm, J.-F., Pellenq, R. & Béland, L.K. (2018): Thermodynamics, kinetics, and mechanics of cesium sorption in cement paste: A multiscale assessment. Physical Review Materials 2/5.
DOI: 10.1103/PhysRevMaterials.2.053608.

Arya, C., Buenfeld, N.R. & Newman, J.B. (1990): Factors influencing chloride-binding in concrete. Cement and Concrete Research 20/2, 291-300. DOI: 10.1016/0008-8846(90)90083-A.

Atkins, M. & Glasser, F.P. (1992): Application of portland cement-based materials to radioactive waste immobilization. Waste Management 12/2-3, 105-131. DOI: 10.1016/0956-053X(92)90044-J.

Atkinson, A., Everitt, N.M. & Guppy, R. (1987): Evolution of pH in a radwaste repository: experimental simulation of cement leaching. AERE-R 12594. United Kingdom Atomic Energy Authority UKAEA, Harwell.

Baes, C.F. & Mesmer, R.E. (1976): The Hydrolysis of Cations. John Wiley & Sons, New York, London, Sydney, Toronto 1976, 245-246.

Baeyens, B., Marques Fernandes, M. & Thoenen, T.M Bradbury, M.H. (2014): Sorption Data Bases for Argillaceous Rocks and Bentonite for the Provisional Safety Analyses for SGT-E2. Nagra Technical Report NTB 12-04.

Bar-Nes, G., Klein-Ben, D.O., Chomat, L., Macé, N., Arbel-Haddad, M. & Poyet, S. (2018): Sr immobilization in irradiated Portland cement paste exposed to carbonation. Cement and Concrete Research 107, 152-162. DOI: 10.1016/j.cemconres.2018.02.015.

Barzgar, S., Lothenbach, B., Tarik, M., Di Giacomo, A. & Ludwig, C. (2020): The effect of sodium hydroxide on Al uptake by calcium silicate hydrates (CSH). Journal of Colloid and Interface Science 572, 246-256. DOI: 10.1016/j.jcis.2020.03.057.

Bassil, N.M., Bewsher, A.D., Thompson, O.R. & Lloyd, J.R. (2015a): Microbial degradation of cellulosic material under intermediate-level waste simulated conditions. Mineralogical Magazine 79/6, 1433-1441. DOI: 10.1180/minmag.2015.079.6.18.

Bassil, N.M., Bryan, N. & Lloyd, J.R. (2015b): Microbial degradation of isosaccharinic acid at high pH. The ISME journal 9/2, 310-320. DOI: 10.1038/ismej.2014.125.

Baston, G., Cowper, M. & Marshall, T. (2012): Sorption properties of aged cements. Mineralogical Magazine 76/8, 3411-3423. DOI: 10.1180/minmag.2012.076.8.54.

Baston, G., Dawson, J., Farahani, B., Saunders, R., Schofield, J. & Smith, V. (2019): Further studies to underpin the use of PCE superplasticisers in the packaging of low-heat-generating wastes. Updates on the effects of radiolysis products on sorption and solubility in, NDA report RWM/Contr/19/035, Didcot, United Kingdom.

Baur, I. & Johnson, A.C. (2003): Sorption of selenite and selenate to cement minerals. Environmental Science & Technology 37/15, 3442-3447. DOI: 10.1021/es020148d.

Bayliss, S., Ewart, F.T., Howse, R.M., Lane, S.A., Pilkington, N.J., Smith-Briggs, J.L. & Williams, S.J. (1988): The solubility and sorption of radium and tin in a cementitious near-field environment. MRS Symposium Proceedings 127, 879-885. DOI: 10.1557/PROC-127-879.

Berner, U. (1992): Evolution of pore water chemistry during degradation of cement in a radioactive waste repository environment. Waste Management 12/2, 201-219. DOI: 10.1016/0956-053X(92)90049-O.

Berner, U. (2003): Project Opalinus Clay: Radionuclide Concentration Limits in the Cementitious Near-Field of an ILW Repository. Nagra Technical Report NTB 02-22.

Berner, U. (2014): Solubility of Radionuclides in a Concrete environment for Provisional Safety Analyses for SGT-E2. Nagra Technical Report NTB 14-07.

Bhatty, J.J. (2003): Effect of minor elements on clinker and cement manufacture: A laboratory analysis in: Association, P.C. (Ed.), PCA R&D Serial No. 2147.

Bonaccorsi, E., Merlino, S. & Kampf, A.R. (2005): The Crystal Structure of Tobermorite 14 A (Plombierite), a C-S-H Phase. Journal of the American Ceramic Society 88/3, 505-512. DOI: 10.1111/j.1551-2916.2005.00116.x.

Bonaccorsi, E., Merlino, S. & Taylor, H. (2004): The crystal structure of jennite, $Ca_9Si_6O_{18}(OH)_6 \cdot 8H_2O$. Cement and Concrete Research 34/9, 1481-1488. DOI: 10.1016/j.cemconres.2003.12.033.

Bonhoure, I., Wieland, E., Scheidegger, A., Ochs, M. & Kunz, D. (2003): EXAFS study of Sn(IV) immobilization by hardened cement paste and calcium silicate hydrates. Environmental Science & Technology 37/10, 2184-2191. DOI: 10.1021/es020194d.

Bradbury, M.H. & Sarott, F.A. (1994): Sorption Databases for the Cementitious Near-Field of a L/ILW Repository for Performance Assessment. Nagra Technical Report NTB 93-08.

Bradbury, M.H. & van Loon, L.R. (1997): Cementitious Near-Field Sorption Data Bases for Performance Assessment of a L/ILW Repository in a Palfris Marl Host Rock: CEM-94: Update 1, June 1996. Nagra Technical Report NTB 96-04.

Bradbury, M.H. & Baeyens, B. (1997): Far-field Sorption Data Bases for Performance Assessment of a L/ILW Repository in a Disturbed/Altered Palfris Marl Host Rock. Nagra Technical Report NTB 96-06.

Bradbury, M.H., Baeyens, B. & Thoenen, T. (2008): Sorption Data Bases for Generic Swiss Argillaceous, Crystalline and Calcareous Rock Systems. Nagra Arbeitsbericht NAB 08-50.

Bradbury, M.H., Marques Fernandes M. & Baeyens, B. (2017): Estimates of the Influence of Radionuclide Solubility Limits and Sorption Competition on the Sorption Values in the SDBs of MX-80 bentonite and Opalinus Clay, Nagra Technical Report NTB 17-11. Brookins, D.G. (1988): Eh-pH diagrams for Geochemistry. Springer-Verlag, Berlin.

Brown, P.L. & Ekberg, C. (2016): Hydrolysis of Metal Ions. Wiley-VCH Verlag GmbH Co., Weinheim, Germany, available online at https://onlinelibrary.wiley.com/doi/book/10.1002/9783527656189.

Brunauer, S., Emmett, P.H. & Teller, E. (1938): Adsorption of gases in multimolecular layers. Journal of the American Chemical Society 60/2, 309-319. DOI: 10.1021/ja01269a023.

Bu, J. (2018): Molecular Scale Interactions Between Hydrated Cement Phases and Radionuclides Using Molecular Dynamics Modeling, Environmental Engineering, Vanderbilt University, Nashville, Tennessee, USA.

Caruso, F., Mantellato, S., Palacios, M. & Flatt, R.J. (2017): ICP-OES method for the characterization of cement pore solutions and their modification by polycarboxylate-based superplasticizers. Cement and Concrete Research 91, 52-60. DOI: 10.1016/j.cemconres.2016.10.007.

Çevirim-Papaioannou, N., Jo, Y., Franke, K., Fuss, M., Blochouse, B. de, Altmaier, M. & Gaona, X. (2022): Uptake of niobium by cement systems relevant for nuclear waste disposal: Impact of ISA and chloride. Cement and Concrete Research 153, 106690. DOI: 10.1016/j.cemconres.2021.106690.

Chen, J.J., Thomas, J.J., Taylor, H. & Jennings, H.M. (2004): Solubility and structure of calcium silicate hydrate. Cement and Concrete Research 34/9, 1499-1519. DOI: 10.1016/j.cemconres.2004.04.034.

Chernyshev, A.N., Jonsson, M. & Forsberg, M. (2018): Characterization and degradation of a polyaryl ether based superplasticizer for use in concrete barriers in deep geological repositories. Applied Geochemistry 98, 172-181. DOI: 10.1016/j.apgeochem.2018.05.014.

Churakov, S.V., Labbez, C., Pegado, L. & Sulpizi, M. (2014): Intrinsic acidity of surface sites in calcium silicate hydrates and its implication to their electrokinetic properties. The Journal of Physical Chemistry C 118/22, 11752-11762. DOI: 10.1021/jp502514a.

Clever, H.L., Johnson, S.A. & Derrick, M.E. (1985): The solubility of mercury and some sparingly soluble mercury salts in water and aqueous electrolyte solutions. Journal of Physical and Chemical Reference Data 14/3, 631-680. DOI: 10.1063/1.555732.

Cloet, V., Lothenbach, B., Lura, P., Kosakowski, G., Curti, E., Wieland, E., Lanyon, G.W., Diomidis, N. & Leupin, O.X. (2019): Cementitious Backfill for a High-level Waste Repository: Impact of Repository-Induced Effects. Nagra Arbeitsbericht NAB 18-41.

Cloet, V., Schwyn, B. & Wieland, E. (2014): Geochemische Nahfeld-Daten zu den SMA und ATA für die provisorischen Sicherheitsanalysen in SGT Etappe 2. Nagra Arbeitsbericht NAB 14-52 Rev. 1.

Cocke, D.L. & Mollah, M. (1993): The chemistry and leaching mechanisms of hazardous substances in cementitious solidification-stabilization systems. In: Chemistry and microstructure of solidified waste forms, R.D.Spence (ed.), Lewis Publishers, Boca Raton, USA, 187-242.

Colàs, E., Grivé, M. & Rojo, I. (2013a): Complexation of uranium(VI) by gluconate in alkaline solutions. Journal of Solution Chemistry 42/7, 1545-1557. DOI: 10.1007/s10953-013-0048-0.

Colàs, E., Grivé, M., Rojo, M. & Duro, L. (2013b): The effect of gluconate and EDTA on thorium solubility under simulated cement porewater conditions. Journal of Solution Chemistry 42, 1680-1690. DOI: 10.1007/s10953-013-0054-2.

Cornelis, C., Johnson, C.A., van Gerven, T. & Vandecasteele, C. (2008): Leaching mechanisms of oxyanionic metalloid and metal species in alkaline solid wastes: A review. Applied Geochemistry 23/5, 955-976. DOI: 10.1016/j.apgeochem.2008.02.001.

Cowper, M.M., Baker, S., Chambers, A.V., Heath, T.G., Mihara, M. & Williams, S.J. (2006): The sorption of thorium and americium onto fresh and degraded ordinary Portland cement and onto green tuff. MRS Symposium Proceedings 932, 925-932.

Curti, E., Fujiwara, K., Iijima, K., Tits, J., Cuesta, C., Kitamura, A., Glaus, M. & Müller, W. (2010): Radium uptake during barite recrystallization at 23 ± 2 °C as a function of solution composition: An experimental ^{133}Ba and ^{226}Ra tracer study. Geochimica et Cosmochimica Acta 74/12, 3553-3570. DOI: 10.1016/j.gca.2010.03.018.

Curti, E., Kulik, D.A. & Tits, J. (2005): Solid solutions of trace Eu(III) in calcite: Thermodynamic evaluation of experimental data over a wide range of pH and pCO_2. Geochimica et Cosmochimica Acta 69/7, 1721-1737. DOI: 10.1016/j.gca.2004.06.027.

DiBlasi, N.A., Tasi, A.G., Gaona, X., Fellhauer, D., Dardenne, K., Rothe, J., Reed, D.T., Hixon, A.E. & Altmaier, M. (2021): Impact of Ca(II) on the aqueous speciation, redox behavior, and environmental mobility of Pu(IV) in the presence of EDTA. The Science of the Total Environment 783, 146993. DOI: 10.1016/j.scitotenv.2021.146993.

DiBlasi, N.A., Tasi, A.G., Trumm, M., Schnurr, A., Gaona, X., Fellhauer, D., Dardenne, K., Rothe, J., Reed, D.T., Hixon, A.E. & Altmaier, M. (2022): Pu(III) and Cm(III) in the presence of EDTA: aqueous speciation, redox behavior, and the impact of Ca(II). RSC Advances 12/15, 9478-9493. DOI: 10.1039/d1ra09010k.

Diesen, V., Forsberg, K. & Jonsson, M. (2017): Effects of cellulose degradation products on the mobility of Eu(III) in repositories for low and intermediate level radioactive waste. Journal of Hazardous Materials 340, 384-389. DOI: 10.1016/j.jhazmat.2017.07.008.

Dilnesa, B., Lothenbach, B., Renaudin, G., Wichser, A. & Wieland, E. (2012): Stability of monosulfate in the presence of iron. Journal of the American Ceramic Society 95/10, 3305-3316. DOI: 10.1111/j.1551-2916.2012.05335.x.

Dilnesa, B.Z., Lothenbach, B., Le Saoût, G., Renaudin, G., Mesbah, A., Filinchuk, Y., Wichser, A. & Wieland, E. (2011): Iron in carbonate containing AFm phases. Cement and Concrete Research 41/3, 311-323. DOI: 10.1016/j.cemconres.2010.11.017.

Dilnesa, B.Z., Lothenbach, B., Renaudin, G., Wichser, A. & Kulik, D. (2014a): Synthesis and characterization of hydrogarnet $Ca_3(Al_xFe_{1-x})_2(SiO_4)_y(OH)_{4(3-y)}$. Cement and Concrete Research 59, 96-111. DOI: 10.1016/j.cemconres.2014.02.001.

Dilnesa, B.Z., Wieland, E., Lothenbach, B., Dähn, R. & Scrivener, K.L. (2014b): Fe-containing phases in hydrated cements. Cement and Concrete Research 58, 45-55. DOI: 10.1016/j.cemconres.2013.12.012.

Dobrowolski, J. & Oglaza, J. (1963): Zastoswanie izotopu 110Ag do badania rozpuszczalnosci srebra metalicznego i chlorku srebra w roztworach wodnych siarczanu cynku [= use of the isotope 110Ag in studying the solubility of silver metal and silver chloride in aqueous solutions of zinc sulphide]. Nucleonika 8, 79-81.

Dressler, R., Ayranovm N, Bemmerer, D., Bunka, M., Dai, Y., Lederer, C., Fallis, J., Murphy, A., Pignatari, M., Schumann, D., Stora, T., Stowasser, T., Thielemenn, F.-K. & Woods, P.J. (2012): ^{44}Ti, ^{26}Al and ^{53}Mn samples for nuclear astrophysics: The needs, the possibilities and the sources. Journal of Physics G: Nuclear and Particle Physics 39/10, 105201. DOI: 10.1088/0954-3899/39/10/105201.

Druteikienė, R., Šapolaitė, J., Ežerinskis, Ž. & Juodis, L. (2017): Batch-type study of Cs, Co, and Tc binding with hydrated cement under hyperalkaline conditions. Journal of Radioanalytical and Nuclear Chemistry 313/2, 299-307. DOI: 10.1007/s10967-017-5303-1.

Dudás, C., Kutus, B., Böszörményi, É., Peintler, G., Kele, Z., Pálinkó, I. & Sipos, P. (2017): Comparison of the Ca^{2+} complexing properties of isosaccharinate and gluconate - is gluconate a reliable structural and functional model of isosaccharinate? Dalton Transactions 46/40, 13888-13896. DOI: 10.1039/c7dt03120c.

Engelsen, C.J., van der Sloot, H.A., Wibetoe, G., Justnes, H., Lund, W. & Stoltenberg-Hansson, E. (2010): Leaching characterisation and geochemical modelling of minor and trace elements released from recycled concrete aggregates. Cement and Concrete Research 40/12, 1639-1649. DOI: 10.1016/j.cemconres.2010.08.001.

Evans, N. (2008): Binding mechanisms of radionuclides to cement. Cement and Concrete Research 38/4, 543-553. DOI: 10.1016/j.cemconres.2007.11.004.

Evans, N., Warwick, P., Felipe-Sotelo, M. & Vines, M. (2012): Prediction and measurement of complexation of radionuclide mixtures by alpha-isosaccharinic, gluconic and picolinic acids. Journal of Radioanalytical and Nuclear Chemistry 293, 725-730. DOI: 10.1007/s10967-012-1828-5.

Faucon, P., Le Bescop, P., Adenot. F., Bonville, P., Jacquinot, J.F., Pineau, F. & Felix, B. (1996): Leaching of cement: Study of the surface layer. Cement and Concrete Research 26/11, 1707-1715. DOI: 10.1016/S0008-8846(96)00157-3.

Felipe-Sotelo, M., Edgar, M.L., Beattie, T., Warwick, P., Evans, N. & Read, D. (2015): Effect of anthropogenic organic complexants on the solubility of Ni, Th, U(IV) and U(VI). Journal of Hazardous Materials 300, 553-560. DOI: 10.1016/j.jhazmat.2015.07.060.

Felipe-Sotelo, M., Hinchliff, J., Drury, D., Evans. N.D.M., Williams, S.J. & Read, D. (2014): Radial diffusion of radiocaesium and radioiodide through cementitious backfill. Physics and Chemistry of The Earth 70-71, 60-70. DOI: 10.1016/j.pce.2014.04.001.

Felipe-Sotelo, M., Hinchliff, J., Evans, N., Warwick, P. & Read, D. (2012): Sorption of radionuclides to a cementitious backfill material under near-field conditions. Mineralogical Magazine 76/8, 3401-3410. DOI: 10.1180/minmag.2012.076.8.53.

Felipe-Sotelo, M., Hinchliff, J., Field, L., Milodowski, A., Holt, J., Taylor, S. & Read, D. (2016): The solubility of nickel and its migration through the cementitious backfill of a geological disposal facility for nuclear waste. Journal of Hazardous Materials 314, 211-219. DOI: 10.1016/j.jhazmat.2016.04.057.

Felipe-Sotelo, M., Hinchliff, J., Field, L.P., Milodowski, A.E., Preedy, O. & Read, D. (2017): Retardation of uranium and thorium by a cementitious backfill developed for radioactive waste disposal. Chemosphere 179, 127-138. DOI: 10.1016/j.chemosphere.2017.03.109.

Fröhlich, D.R., Koke, C., Maiwald, M.M., Chomyn, C., Plank, J. & Panak, P.J. (2019): A spectroscopic study of the complexation reaction of trivalent lanthanides with a synthetic acrylate based PCE-superplasticizer. Spectrochimica acta. Part A, Molecular and biomolecular spectroscopy 207, 270-275. DOI: 10.1016/j.saa.2018.09.025.

Fröhlich, D.R., Maiwald, M.M., Taube, F., Plank, J. & Panak, P.J. (2017): A thermodynamical and structural study on the complexation of trivalent lanthanides with a polycarboxylate based concrete superplasticizer. Dalton Transactions 46/12, 4093-4100. DOI: 10.1039/c7dt00200a.

Fröhlich, D.R. & Panak, P.J. (2018): A thermodynamical study on the complex formation of Cm(III) with methacrylate. Applied Geochemistry 92, 104-109.
DOI: 10.1016/j.apgeochem.2018.03.002.

Fröhlich, D.R. & Panak, P.J. (2019): The complexation of Eu(III) and Cm(III) with polyacrylate as a model compound for complex polycarboxylates studied by laser fluorescence spectroscopy. Journal of Luminescence 212, 166-170. DOI: 10.1016/j.jlumin.2019.04.037.

Fröhlich, D.R., Trumm, M., Skerencak-Frech, A. & Panak, P.J. (2016): The complexation of Cm(III) with succinate studied by time-resolved laser fluorescence spectroscopy and quantum chemical calculations. Inorganic Chemistry 55/9, 4504-4511. DOI: 10.1021/acs.inorgchem.6b00277.

Fujita, H., Haga, K., Shibata, M. & Mihara, M. (2008): Concentration and molecular weight of superplasticizer contained in pore solution extracted from hardened cement pastes. Journal of Advanced Concrete Technology 6/3, 389-395. DOI: 10.3151/jact.6.389.

Gaona, X., Dähn, R., Tits, J., Scheinost, A.C. & Wieland, E. (2011): Uptake of Np(IV) by C-S-H phases and cement paste: An EXAFS study. Environmental Science & Technology 45/20, 8765-8771. DOI: 10.1021/es2012897.

Gaona, X., Montoya, V., Colàs, E., Grivé, M. & Duro, L. (2008): Review of the complexation of tetravalent actinides by ISA and gluconate under alkaline to hyperalkaline conditions. Journal of Contaminant Hydrology 102/3-4, 217-227.
DOI: 10.1016/j.jconhyd.2008.09.017.

Gaona, X., Wieland, E., Tits, J., Scheinost, A.C. & Dähn, R. (2013): Np(V/VI) redox chemistry in cementitious systems: XAFS investigations on the speciation under anoxic and oxidizing conditions. Applied Geochemistry 28, 109-118.

García, D., Grivé, M., Duro, L., Brassinnes, S. & Pablo, J. de (2018a): Effect of superplasticizers on Ni behaviour in cementitious environments. Journal of Radioanalytical and Nuclear Chemistry 317, 397-407. DOI: 10.1007/s10967-018-5837-x.

García, D., Grivé, M., Duro, L., Brassinnes, S. & Pablo, J. de (2018b): The potential role of the degradation products of cement superplasticizers on the mobility of radionuclides. Applied Geochemistry 98, 1-9. DOI: 10.1016/j.apgeochem.2018.09.004.

García, D., Henocq, P., Riba, O., López-García, M., Madé, B. & Robinet, J.-C. (2020): Adsorption behaviour of isosaccharinic acid onto cementitious materials. Applied Geochemistry 118, 104625.

García-Gutiérrez, M., Missana, T., Mingarro, M., Morejón, J. & Cormenzana, J.L. (2018): Cesium diffusion in mortars from different cements used in radioactive waste repositories. Applied Geochemistry 98, 10-16. DOI: 10.1016/j.apgeochem.2018.09.001.

Ghosh, M., Devi, P., Verma, R. & Reddy, A. (2015): Sorption of niobium on colloidal silica and the effect of humic acid. Journal of Radioanalytical and Nuclear Chemistry 306, 147-153. DOI: 10.1007/s10967-015-4055-z.

Ghosh, M., Swain, K.K. & Verma, R. (2017): Interaction of niobium with iron-oxide colloids and the role of humic acid. Journal of Environmental Radioactivity 178-179, 101-109. DOI: 10.1016/j.jenvrad.2017.08.003.

Ghosh, M., Yadav, A.K., Devi, P.S., Swain, K.K., Verma, R., Jha, S.N. & Bhattacharyya, D. (2019): Thermodynamic and spectroscopic investigation of Nb(V) and Pa(V) sorption on colloidal silica. Environmental Earth Sciences 79, 32. DOI: 10.1007/s12665-019-8781-3.

Gillispie, E.C., Mergelsberg, S.T., Varga, T., Webb, S.M., Avalos, N.M., Snyder, M., Bourchy, A., Asmussen, R.M. & Saslow, S.A. (2021): Competitive TcO_4^-, IO_3^-, and CrO_4^{2-} incorporation into ettringite. Environmental Science & Technology 55/2, 1057-1066. DOI: 10.1021/acs.est.0c06707.

Glasser, F.P. (1992): Progress in the immobilization of radioactive wastes in cement. Cement and Concrete Research 22/2, 201-216. DOI: 10.1016/0008-8846(92)90058-4.

Glaus, M.A. & van Loon, L.R. (2008): Degradation of cellulose under alkaline conditions: new insights from a 12 years degradation study. Environmental Science & Technology 42/8, 2906-2911. DOI: 10.1021/es7025517.

González-Siso, M.R., Gaona, X., Duro, L. & Altmaier, M.: Jordi, B. (2017): Thermodynamic model of Ni(II) solubility, hydrolysis and complex formation with ISA. Radiochimica Acta 106, 31-45. DOI: 10.1515/ract-2017-2762.

Gougar, M., Scheetz, B.E. & Roy, D.M. (1996): Ettringite and C-S-H Portland cement phases for waste ion immobilization: A review. Waste Management 16/4, 295-303. DOI: 10.1016/S0956-053X(96)00072-4.

Grambow, B., López-García, M., Olmeda, J., Grivé, M., Marty, N., Grangeon, S., Claret, F., Lange, S., Deissmann, G., Klinkenberg, M., Bosbach, D., Bucur, C., Florea, I., Dobrin, R., Isaacs, M., Read, D., Kittnerová, J., Drtinová, B., Vopálka, D., Cevirim-Papaioannou, N., Mouheb, N.A., Gaona, X., Altmaier, M., Nedyalkova, L., Lothenbach, B., Tits, J., Landesman, C., Rasamimanana, S. & Ribet, S. (2020): Retention and diffusion of radio-active and toxic species on cementitious systems: Main outcome of the CEBAMA project. Applied Geochemistry 112, 104480. DOI: 10.1016/j.apgeochem.2019.104480.

Grangeon, S., Marty, N., Maubec, N., Warmont, F. & Claret, F. (2020): Selenate sorption by hydrated calcium aluminate (AFm): Evidence for sorption reversibility and implication for the modeling of anion retention. ACS Earth and Space Chemistry 4/2, 229-240. DOI: 10.1021/acsearthspacechem.9b00286.

Guérandel, C., Vernex-Loset, L., Krier, G., Lanève, M. de, Guillot, X., Pierre, C. & Muller, J.F. (2011): A new method to analyze copolymer based superplasticizer traces in cement leachates. Talanta 84/1, 133-140. DOI: 10.1016/j.talanta.2010.12.022.

Guillaumont, R., Fanghänel, T., Neck, V., Fuger, J., Palmer, D.A., Grenthe, I. & Rand, M.H. (2003): Update on the Chemical Thermodynamics of Uranium, Neptunium, Plutonium, Americium and Technetium. Chemical hermodynamics, 5. OECD/NEA, Paris.

Guillemot, T., Salazar, G., Rauber, M., Kunz, D., Szidat, S. & Wieland, E. (2022): Carbon-14 release and speciation during corrosion of irradiated steel under radioactive waste disposal conditions. The Science of the Total Environment 817, 152596. DOI: 10.1016/j.scitotenv.2021.152596.

Guo, B., Sasaki, K. & Hirajima, T. (2017): Selenite and selenate uptaken in ettringite: Immobilization mechanisms, coordination chemistry, and insights from structure. Cement and Concrete Research 100, 166-175. DOI: 10.1016/j.cemconres.2017.07.004.

Guo, B., Xiong, Y., Chen, W., Saslow, S.A., Kozai, N., Ohnuki, T., Dabo, I. & Sasaki, K. (2020): Spectroscopic and first-principles investigations of iodine species incorporation into ettringite: Implications for iodine migration in cement waste forms. Journal of Hazardous Materials 389, 121880. DOI: 10.1016/j.jhazmat.2019.121880.

Harfouche, M., Wieland, E., Dähn, R., Fujita, T., Tits, J., Kunz, D. & Tsukamoto, M. (2006): EXAFS study of U(VI) uptake by calcium silicate hydrates. Journal of Colloid and Interface Science 303/1, 195-204. DOI: 10.1016/j.jcis.2006.07.019.

Häussler, V., Amayri, S., Beck, A., Platte, T., Stern, T.A., Vitova, T. & Reich, T. (2018): Uptake of actinides by calcium silicate hydrate (C-S-H) phases. Applied Geochemistry 98, 426-434. DOI: 10.1016/j.apgeochem.2018.08.021.

Heberling, F., Metz, V., Böttle, M., Curti, E. & Geckeis, H. (2018): Barite recrystallization in the presence of ^{226}Ra and ^{133}Ba. Geochimica et Cosmochimica Acta 232, 124-139. DOI: 10.1016/j.gca.2018.04.007.

Heberling, F., Paulig, L., Nie, Z., Schild, D. & Finck, N. (2016): Morphology controls on calcite recrystallization. Environmental Science & Technology 50/21, 11735-11741. DOI: 10.1021/acs.est.6b04011.

Hellebrandt, S., Hofmann, S., Jordan, N., Barkleit, A. & Schmidt, M. (2016): Incorporation of Eu(III) into calcite under recrystallization conditions. Scientific Reports 6, 33137. DOI: 10.1038/srep33137.

Hoch, A.R., Baston, G.M.N., Glasser, F.P., Hunter, F.M.I. & Smith, V. (2012): Modelling evolution in the near field of a cementitious repository. Mineralogical Magazine 76/8, 3055-3069. DOI: 10.1180/minmag.2012.076.8.21.

Holland, T.R. & Lee, D.J. (1991): Radionuclide getters in cement : E-MRS 1991 Fall meeting, Strasbourg. AEA-D and R-0243. AEA Decommissioning and Radwaste, Harwell.

Hong, S.Y. & Glasser, F.P. (1999): Alkali binding in cement pastes: Part I. The C-S-H phase. Cement and Concrete Research 29/12, 1893-1903. DOI: 10.1016/S0008-8846(99)00187-8.

Hong, S.Y. & Glasser, F.P. (2002): Alkali sorption by C-S-H and C-A-S-H gels: Part II. Role of alumina. Cement and Concrete Research 32/7, 1101-1111. DOI: 10.1016/S0008-8846(02)00753-6.

Hummel, W. (2004): The influence of cyanide complexation on the speciation and solubility of radionuclides in a geological repository. Environmental Geology 45/5, 633-646. DOI: 10.1007/s00254-003-0928-5.

Hummel, W. (2008): Radioactive contaminants in the subsurface: the influence of complexing ligands on trace metal speciation. Monatshefte für Chemie 139/5, 459-480. DOI: 10.1007/s00706-008-0866-8.

Hummel, W. (2017): Chemistry of Selected Dose-Relevant Radionuclides. Nagra Technical Report NTB 17-05.

Hummel, W., Anderegg, G., Puigdomènech, I., Rao, L. & Tochiyama, O. (eds.) (2005): Chemical Thermodynamics of Compounds and Complexes of U, Np, Pu, Am, Tc, Se, Ni and Zr with Selected Organic Ligands. Chemical thermodynamics, 9. Elsevier Science & Technology, Amsterdam, Boston.

Hummel, W., Berner, U., Curti, E., Pearson, F.J. & Thoenen, T. (2002): Nagra/PSI chemical thermodynamic data base 01/01. Radiochimica Acta 90/9-11, 805-813. DOI: 10.1524/ract.2002.90.9-11_2002.805.

Hummel, W., Kulik, D.A. & Miron, G.D. (2022): Solubility of Radionuclides and Influence of EDTA for Use in the Development of the Cement Sorption Database. Nagra Arbeitsbericht NAB 22-38.

Hummel, W. & Thoenen, T. (2023): The PSI Chemical Thermodynamic Database 2020. Nagra Technical Report NTB 21-03.

Hummel, W. & van Loon, L.R. (1999): The effect of degradation products of strong acidic cation exchange resins on radionuclide speciation : A case study with Ni^{2+}. Nuclear Technology 128/3, 372-387. DOI: 10.13182/NT99-A3038.

Ipavec, A., Vuk, T., Gabrovšek, R. & Kaučič, V. (2013): Chloride binding into hydrated blended cements: The influence of limestone and alkalinity. Cement and Concrete Research 48, 74-85. DOI: 10.1016/j.cemconres.2013.02.010.

Isaacs, M., Hinchliff, J., Felipe-Sotelo, M. & Read, D. (2018): Factors affecting the suitability of superplasticiser-amended cement for the encapsulation of radioactive waste. Advances in Cement Research 30/5, 216-230. DOI: 10.1680/jadcr.17.00099.

Isaacs, M., Lange, S., Deissmann, G., Bosbach, D., Milodowski, A.E. & Read, D. (2020): Retention of technetium-99 by grout and backfill cements: Implications for the safe disposal of radioactive waste. Applied Geochemistry 116, 104580. DOI: 10.1016/j.apgeochem.2020.104580.

Iwaida, T., Nagasaki, S., Tanaka, S., Yaita, T. & Tachimori, S. (2002): Structure alteration of C-S-H (calcium silicate hydrated phases) caused by sorption of caesium. Radiochimica Acta 90/9-11, 677-681. DOI: 10.1524/ract.2002.90.9-11_2002.677.

Jacques, D., Wang, L., Martens, E. & Mallants, D. (2010): Modelling chemical degradation of concrete during leaching with rain and soil water types. Cement and Concrete Research 40/8, 1306-1313. DOI: 10.1016/j.cemconres.2010.02.008.

Jang, J.G., Park, S.M. & Lee, H.K. (2017): Cesium and strontium retentions governed by aluminosilicate gel in alkali-activated cements. Materials 10/4, 447. DOI: 10.3390/ma10040447.

Jo, Y., Garbev, K., Cevirim-Papaioannou, N., Dieste Blanco, O., de Blochouse, B., Altmaier, M. & Gaona, X. (2022): Solubility of niobium(V) in cementitious systems relevant for nuclear waste disposal: Characterization of the solubility-controlling solid phases. SSRN Journal. DOI: 10.2139/ssrn.4147151.

Johnson, C.A. & Glasser, F.P. (2003): Hydrotalcite-like minterals ($M_2Al(OH)_6(CO_3)_{0.5}.XH_2O$, where M = Mg, Zn, Co, Ni) in the environment: Symthesis, characterization and thermodynamic stability. Clays and Clay Minerals 51/1, 1-8. DOI: 10.1346/CCMN.2003.510101.

Kaplan, D.I., Xu, C., Li, D.E., Lin, P., Xing, W., Nichols, R.L., Schwehr, K.A. & Santschi, P.H. (2019): Iodine speciation in cementitious environments. Applied Geochemistry 103, 15-22. DOI: 10.1016/j.apgeochem.2019.02.007.

KEG (2003): Kernenergiegesetz (KEG), vom 21. März 2003, Stand am 01. Juli 2023. Systematische Sammlung des Bundesrechts SR 732.1, Schweiz.

Keith-Roach, M., Lindgren, M. & Källström, K. (2014): Assessment of Complexing Agent Concentrations in SFR. SKB Report R-14-03, Swedish Nuclear Fuel and Waste Management SKB, Stockholm.

Keith-Roach, M.J. (2008): The speciation, stability, solubility and biodegradation of organic co-contaminant radionuclide complexes: A review. Science of the Total Environment 396/1, 1-11. DOI: 10.1016/j.scitotenv.2008.02.030.

Keith-Roach, M.J. & Höglund, L. (2017): Review of the Long-term Risks Associated with the Use of Superplasticizers. Posiva Working Report 2017-52. Posiva Oy, Eurajoki, Finland.

Kitamura, A., Fujiwara, K., Mihara, M., Cowper, M. & Kamei, G. (2013): Thorium and americium solubilities in cement pore water containing superplasticiser compared with thermodynamic calculations. Journal of Radioanalytical and Nuclear Chemistry 298/1, 485-493. DOI: 10.1007/s10967-013-2618-4.

Kittnerová, J., Drtinová, B., Stamberg, K., Vopálka, D., Evans, N., Deissmann, G. & Lange, S. (2020): Comparative study of radium and strontium behaviour in contact with cementitious materials. Applied Geochemistry 122, 104713. DOI: 10.1016/j.apgeochem.2020.104713.

Kobayashi, T., Sasaki, T. & Kitamura, A. (2019): Thermodynamic interpretation of uranium(IV/VI) solubility in the presence of α-isosaccharinic acid. The Journal of Chemical Thermodynamics 138, 151-158. DOI: 10.1016/j.jct.2019.06.006.

Kobayashi, T., Teshima, T., Sasaki, T. & Kitamura, A. (2017): Thermodynamic model for Zr solubility in the presence of gluconic acid and isosaccharinic acid. Journal of Nuclear Science and Technology 54/2, 233-241. DOI: 10.1080/00223131.2016.1255573.

Kosakowski, G., Berner, U., Wieland, E., Glaus, M. & Degueldre, C. (2014): Geochemical Evolution of the L/ILW Near-Field. Nagra Technical Report NTB 14-11.

Kosakowski, G., Churakov, S.V., Glaus, M., Guillemot, T., Hummel, W., Kulik, D., Ma, B., Martin, L., Miron, D. & Prasianakis N. (2023): Geochemical Evolution of the L/ILW Near-Field. Nagra Technical Report NTB 23-03.

Kosakowski, G., Huang, Y. & Wieland, E. (2020): Influence of Material Heterogeneities, Process Couplings and Aggregate Reactivity on the Geochemical Evolution of the L/ILW Repository. Nagra Arbeitsbericht NAB 20-11.

Kremleva, A., Krüger, S. & Rösch, N. (2020): Uranyl(VI) sorption in calcium silicate hydrate phases. A quantum chemical study of tobermorite models. Applied Geochemistry 113, 104463. DOI: 10.1016/j.apgeochem.2019.104463.

Kuippers, G., Bassil, N.M., Boothman, C., Bryan, N. & Lloyd, J.R. (2015): Microbial degradation of isosaccharinic acid under conditions representative for the far field of radioactive waste disposal facilities. Mineralogical Magazine 79/6, 1443-1454.
DOI: 10.1180/minmag.2015.079.6.19.

Kuippers, G., Boothman, C., Bagshaw, H., Ward, M., Beard, R., Bryan, N. & Lloyd, J.R. (2018): The biogeochemical fate of nickel during microbial ISA degradation; implications for nuclear waste disposal. Scientific Reports 8/1, 8753. DOI: 10.1038/s41598-018-26963-8.

Kulik, D.A. (2011): Improving the structural consistency of C-S-H solid solution thermodynamic models. Cement and Concrete Research 41/5, 477-495.
DOI: 10.1016/j.cemconres.2011.01.012.

L'Hôpital, E., Lothenbach, B., Kulik, D.A. & Scrivener, K.L. (2016): Influence of calcium to silica ratio on aluminium uptake in calcium silicate hydrate. Cement and Concrete Research 85, 111-121. DOI: 10.1016/j.cemconres.2016.01.014.

L'Hôpital, E., Lothenbach, B., Scrivener, K.L. & Kulik, D.A. (2016): Alkali uptake in calcium alumina silicate hydrate (C-A-S-H). Cement and Concrete Research 85, 122-136. DOI: 10.1016/j.cemconres.2016.03.009.

Labbez, C., Jönsson, B., Pochard, I., Nonat, A. & Cabane, B. (2006): Surface charge density and electrokinetic potential of highly charged minerals: experiments and Monte Carlo simulations on calcium silicate hydrate. The Journal of Physical Chemistry. B 110/18, 9219-9230. DOI: 10.1021/jp057096.

Labbez, C., Nonat, A., Pochard, I. & Jönsson, B. (2007): Experimental and theoretical evidence of overcharging of calcium silicate hydrate. Journal of Colloid and Interface Science 309/2, 303-307. DOI: 10.1016/j.jcis.2007.02.048.

Lakshtanov, L.Z. & Stipp, S. (2004): Experimental study of europium (III) coprecipitation with calcite. Geochimica et Cosmochimica Acta 68/4, 819-827. DOI: 10.1016/j.gca.2003.07.010.

Lange, S., Klinkenberg, M., Barthel, J., Bosbach, D. & Deissmann, G. (2020): Uptake and retention of molybdenum in cementitious systems. Applied Geochemistry 119, 104630. DOI: 10.1016/j.apgeochem.2020.104630.

Lange, S., Kowalski, P.M., Pšenička, M., Klinkenberg, M., Rohmen, S., Bosbach, D. & Deissmann, G. (2018): Uptake of ^{226}Ra in cementitious systems: A complementary solution chemistry and atomistic simulation study. Applied Geochemistry 96, 204-216. DOI: 10.1016/j.apgeochem.2018.06.015.

Li, K. & Pang, X. (2014): Sorption of radionuclides by cement-based barrier materials. Cement and Concrete Research 65, 52-57. DOI: 10.1016/j.cemconres.2014.07.013.

Lidmann, F., Källström, K. & Kautsky, U. (2017): Mo-93 from the Grave to the Cradle. Report from a Workshop on Molybdenum in Radioactive Waste and in the Environment. SKB Report P-16-22, Swedish Nuclear Fuel and Waste Management SKB, Stockholm.

Locher, F.W. (2006): Cement. Principles of Production and Use. 1. Auflage. Verlag Bau+Technik, Erkrath.

Lothenbach, B., Kulik, D.A., Matschei, T., Balonis, M., Baquerizo, L., Dilnesa, B., Miron, G.D.& Myers, R. (2019): Cemdata18: A chemical thermodynamic database for hydrated Portland cements and alkali-activated materials. Cement and Concrete Research 115, 472-506. DOI: 10.1016/j.cemconres.2018.04.018.

Lothenbach, B. & Wieland, E. (2006): A thermodynamic approach to the hydration of sulphate-resisting Portland cement. Waste Management 26/7, 706-719. DOI: 10.1016/j.wasman.2006.01.023.

Ma, B., Charlet, L., Fernández-Martínez, A., Kang, M. & Madé, B. (2019): A review of the retention mechanisms of redox-sensitive radionuclides in multi-barrier systems. Applied Geochemistry 100, 414-431. DOI: 10.1016/j.apgeochem.2018.12.001.

Ma, B., Fernandez-Martinez, A., Grangeon, S., Tournassat, C., Findling, N., Carrero, S., Tisserand, D., Bureau, S., Elkaïm, E., Marini, C., Aquilanti, G., Koishi, A., Marty, N.C.M. & Charlet, L. (2018): Selenite uptake by Ca-Al LDH: A description of intercalated anion coordination geometries. Environmental Science & Technology 52/3, 1624-1632. DOI: 10.1021/acs.est.7b04644.

Ma, B., Fernandez-Martinez, A., Grangeon, S., Tournassat, C., Findling, N., Claret, F., Koishi, A., Marty, N.C.M., Tisserand, D., Bureau, S., Salas-Colera, E., Elkaïm, E., Marini, C. & Charlet, L. (2017): Evidence of multiple sorption modes in layered double hydroxides using Mo as structural probe. Environmental Science & Technology 51/10, 5531-5540. DOI: 10.1021/acs.est.7b00946.

Ma, B., Fernandez-Martinez, A., Wang, K., Madé, B., Hénocq, P., Tisserand, D., Bureau, S. & Charlet, L. (2020): Selenite sorption on hydrated CEM-V/A cement in the presence of steel corrosion products: Redox vs nonredox sorption. Environmental Science & Technology 54/4, 2344-2352. DOI: 10.1021/acs.est.9b06876.

Macé, N., Wieland, E., Dähn, R., Tits, J. & Scheinost, A.C. (2013): EXAFS investigation on U(VI) immobilization in hardened cement paste: Influence of experimental conditions on speciation. Radiochimica Acta 101/6, 379-389. DOI: 10.1524/ract.2013.2024.

Mäder, U. & Wersin, P. (2023): Reference porewaters for SGT Stage 3 of the Opalinus Clay for the siting regions Jura Ost (JO), Nördlich Lägern (NL) and Zürich Nordost (ZNO). Nagra Arbeitsbericht NAB 22-47.

Mancini, A., Wieland, E., Geng, G., Dähn, R., Skibsted, J., Wehrli, B. & Lothenbach, B. (2020): Fe(III) uptake by calcium silicate hydrates. Applied Geochemistry 113, 104460. DOI: 10.1016/j.apgeochem.2019.104460.

Mancini, A., Wieland, E., Geng, G., Lothenbach, B., Wehrli, B. & Dähn, R. (2021): Fe(II) interaction with cement phases: Method development, wet chemical studies and X-ray absorption spectroscopy. Journal of Colloid and Interface Science 588, 692-704. DOI: 10.1016/j.jcis.2020.11.085.

Mandaliev, P., Dähn, R., Tits, J., Wehrli, B. & Wieland, E. (2010): EXAFS study of Nd(III) uptake by amorphous calcium silicate hydrates (C-S-H). Journal of Colloid and Interface Science 342/1, 1-7. DOI: 10.1016/j.jcis.2009.06.011.

Mandaliev, P., Stumpf, T., Tits, J., Dähn, R., Walther, C. & Wieland, E. (2011): Uptake of Eu(III) by 11Å tobermorite and xonotlite: A TRLFS and EXAFS study. Geochimica et Cosmochimica Acta 75/8, 2017-2029. DOI: 10.1016/j.gca.2010.10.028.

Marchon, D., Sulser, U., Eberhardt, A. & Flatt, R.J. (2013): Molecular design of comb-shaped polycarboxylate dispersants for environmentally friendly concrete. Soft Matter 9/45, 10719-10728. DOI: 10.1039/c3sm51030a.

Märkl, V., Pflugmacher, S. & Stephan, D. (2017): Leaching of PCE-based superplasticiser from microfine cement: a chemical and ecotoxicological point of view. Water, Air, & Soil Pollution 228, 217. DOI: 10.1007/s11270-017-3373-x.

Märkl, V. & Stephan, D.A. (2016): Release behaviour of major elements and superplasticiser from cement suspensions. Water, Air, & Soil Pollution 227/1, 30. DOI: 10.1007/s11270-015-2730-x.

Marques Fernandes, M., Schmidt, M., Stumpf, T., Walther, C., Bosbach, D., Klenze, R. & Fanghänel, T. (2008): Site-selective time-resolved laser fluorescence spectroscopy of Eu^{3+} in calcite. Journal of Colloid and Interface Science 321/2, 323-331. DOI: 10.1016/j.jcis.2008.01.017.

Marques Fernandes, M., Stumpf, T., Rabung, T., Bosbach, D. & Fanghänel, T. (2008b): Incorporation of trivalent actinides into calcite: A time resolved laser fluorescence spectroscopy (TRLFS) study. Geochimica et Cosmochimica Acta 72/2, 464-474. DOI: 10.1016/j.gca.2007.10.015.

Martin, L., Kosakowski, G., Papafotiou, A. & Smith, P.A. (2023): Evolution of the Sealing System Porosity and its Impact on Performance. Nagra Arbeitsbericht NAB 23-21.

Marty, N.C.M., Grangeon, S., Elkaïm, E., Tournassat, C., Fauchet, C. & Claret, F. (2018): Thermodynamic and crystallographic model for anion uptake by hydrated calcium aluminate (AFm): An example of molybdenum. Scientific Reports 8/1, 7943. DOI: 10.1038/s41598-018-26211-z.

Matsuda, A. & Mori, H. (2014): A quantum chemical study on hydration of Ra(II): Comparison with the other hydrated divalent alkaline earth metal ions. Journal of Computer Chemistry, Japan 13/1, 105-113. DOI: 10.2477/jccj.2013-0011.

Mesbah, A., Cau-dit-Coumes, C., Renaudin, G., Frizon, F. & Leroux, F. (2012): Uptake of chloride and carbonate ions by calcium monosulfoaluminate hydrate. Cement and Concrete Research 42/8, 1157-1165. DOI: 10.1016/j.cemconres.2012.05.012.

Mesbah, A., Cau-dit-Coumes, D., Frizon, F., Leroux, F., Ravaux, J. & Renaudin, G. (2011): A new investigation of the Cl^{-}–CO_3^{2-} substitution in AFm phases. Journal of the American Ceramic Society 94/6, 1901-1910. DOI: 10.1111/j.1551-2916.2010.04305.x.

Missana, T., García-Gutiérrez, M., Alonso, U. & Ginestá, O.A. (2022): Nickel retention by calcium silicate hydrate phases: Evaluation of the role of the Ca/Si ratio on adsorption and precipitation processes. Applied Geochemistry 137, 105197.
DOI: 10.1016/j.apgeochem.2022.105197.

Missana, T., García-Gutiérrez, M., Mingarro, M. & Alonso, U. (2017): Analysis of barium retention mechanisms on calcium silicate hydrate phases. Cement and Concrete Research 93, 8-16. DOI: 10.1016/j.cemconres.2016.12.004.

Missana, T., García-Gutiérrez, M., Mingarro, M. & Alonso, U. (2018): Comparison between cesium and sodium retention on calcium silicate hydrate (C-S-H) phases. Applied Geochemistry 98, 36-44. DOI: 10.1016/j.apgeochem.2018.09.007.

Missana, T., García-Gutiérrez, M., Mingarro, M. & Alonso, U. (2019): Selenite retention and cation coadsorption effects under alkaline conditions generated by cementitious materials: The case of C-S-H Phases. ACS Omega 4/8, 13418-13425.
DOI: 10.1021/acsomega.9b01637.

Moir, G.K. & Glasser, F.P. (1992): Mineralisers modifiers and activators in the clinkering process, Proceedings of the 9th International Congress on the Chemistry of Cement. New Delhi, India, pp. 125-152.

Möschner, G., Lothenbach, B., Rose, J., Ulrich, A., Figi, R. & Kretzschmar, R. (2008): Solubility of Fe-ettringite ($Ca_6[Fe(OH)_6]_2(SO_4)_3 \cdot 26H_2O$). Geochimica et Cosmochimica Acta 72/1, 1-18. DOI: 10.1016/j.gca.2007.09.035.

Möschner, G., Lothenbach, B., Winnefeld, F., Ulrich, A., Figi, R. & Kretzschmar, R. (2009): Solid solution between Al-ettringite and Fe-ettringite ($Ca_6[Al_{1-x}Fe_x(OH)_6]_2(SO_4)_3 \cdot 26H_2O$). Cement and Concrete Research 39/6, 482-489. DOI: 10.1016/j.cemconres.2009.03.001.

Mouheb, N.A., Montoya, V., Schild, D., Soballa, E., Adam, C., Geyer, F. & Schäfer, T. (2017): Characterization and sorption properties of low pH cements. Proceedings of the Second Workshop of the HORIZON 2020 CEBAMA Project, 29-40.
DOI: 10.5445/IR/1000093176.

Müller, A.C.A., Scrivener, K.L., Gajewicz, A.M. & McDonald, P.J. (2013): Densification of C–S–H Measured by ^{1}H NMR Relaxometry. The Journal of Physical Chemistry C 117/1, 403-412. DOI: 10.1021/jp3102964.

Nagra (2002a): Project Opalinus Clay: Safety report: Demonstration of Disposal Feasibility for Spent Fuel, Vitrified High-level Waste and Long-lived Intermediate-level Waste (Entsorgungsnachweis). Nagra Technical Report NTB 02-05.

Nagra (2002b): Projekt Opalinuston: Konzept für die Anlage und den Betrieb eines geologischen Tiefenlagers: Entsorgungsnachweis für abgebrannte Brennelemente, verglaste hochaktive sowie langlebige mittelaktive Abfälle. Nagra Technischer Bericht NTB 02-02.

Nagra (2002c): Projekt Opalinuston: Synthese der geowissenschaftlichen Untersuchungsergebnisse - Entsorgunsnachweis für abgebrannte Brennelemente, verglaste hochaktive sowie langlebige mittelaktive Abfälle. Nagra Technischer Bericht NTB 02-03.

Nagra (2008): Vorschlag geologischer Standortgebiete für ein SMA- und ein HAA-Lager: Begründung der Abfallzuteilung, der Barrierensysteme und der Anforderungen an die Geologie (Bericht zur Sicherheit und Machbarkeit). Nagra Technischer Bericht NTB 08-05.

Nagra (2014): Modellhaftes Inventar für radioaktive Materialien – MIRAM 14. Nagra Technischer Bericht NTB 14-04.

Nagra (2023a): Chemical Criteria for Waste Group Classification: A Model Approach. Nagra Arbeitsbericht NAB 23-28.

Nagra (2023b): Modellhaftes Inventar radioaktiver Materialien MIRAM-RBG. Nagra Technischer Bericht NTB 22-05.

Nagra NTB 24-18 (*planned*): Consequence Analysis as Assessment Basis for the Evaluation of the Barrier Performance of a Combined Repository at Nördlich Lägern. Nagra Technical Report NTB 24-18.

NDA (2015): Solubility studies in the presence of polycarboxylate ether superplasticisers. Nuclear Decommissioning Authority NDA, Cumbria.

Neall, F. (1994): Modelling of the Near-Field Chemistry of the SMA Repository at the Wellenberg Site: Application of the Extended Cement Degradation Model. Nagra Technical Report NTB 94-03.

Nedyalkova, L. (2019): A structural and thermodynamic study of the intercalation of selenium, sulfur and iodine in AFm phases. PhD Thesis, Philosophisch-naturwissenschaftlichen Fakultät der Universität Bern. University of Bern, Switzerland.

Nedyalkova, L., Lothenbach, B., Geng, G., Mäder, U. & Tits, J. (2020): Uptake of iodide by calcium aluminate phases (AFm phases). Applied Geochemistry 116, 104559. DOI: 10.1016/j.apgeochem.2020.104559.

Nedyalkova, L., Tits, J., Bernard, E., Wieland, E. & Mäder, U. (2021): Sorption experiments with HTO, ^{36}Cl, ^{125}I and ^{14}C labeled formate on aged cement matrices retrieved from long-term in-situ rock laboratory experiments. Journal of Advanced Concrete Technology 19/7, 811-829. DOI: 10.3151/jact.19.811.

Nonat, A. (2004): The structure and stoichiometry of C-S-H. Cement and Concrete Research 34/9, 1521-1528. DOI: 10.1016/j.cemconres.2004.04.035.

Noshita, K., Takashi, N., Matsuda, M. & Izumida, T. (1995): Sorption mechanism of carbon-14 by hardened cement paste. MRS Symposium Proceedings 412, 435-442. DOI: 10.1557/PROC-412-435.

Ochs, M., Colàs, E., Grivé, M., Olmeda, J. & Campos, I., Bruno, J. (2014): Reduction of Radionuclide Uptake in Hydrated Cement Systems by Organic Complexing Agents: Selection of Reduction Factors and Speciation Calculations. SKB Report R-14-22. Swedish Nuclear Fuel and Waste Management SKB, Stockholm.

Ochs, M., Lothenbach, B. & Giffaut, E. (2002a): Uptake of oxo-anions by cements through solid-solution formation: experimental evidence and modelling. Radiochimica Acta 90/9-11, 639-646. DOI: 10.1524/ract.2002.90.9-11_2002.639.

Ochs, M., Mallants, D. & Wang, L. (2016): Radionuclide and Metal Sorption on Cement and Concrete. Topics in Safety, Risk, Reliability and Quality, vol. 29. Springer, Cham.

Ochs, M., Talerico, C., Lothenbach, B. & Giffaut, E. (2002b): Systematic trends and empirical modeling of lead uptake by cements and cement minerals. MRS Symposium Proceedings 757, 101. DOI: 10.1557/PROC-757-II10.1.

Ochs, M., Vielle-Petit, L., Wang, L., Mallants, D. & Leterme, B. (2011): Additional Sorption Parameters for the Cementitious Barriers of a Near-surface Repository. Project Near-surface Disposal of Category A Waste at Dessel. DATA-LT(NF) Version 1. NIROND-TR 2010-06 E. ONDRAF/NIRAS, Brussels.

Ochs, M., Vriens, B. & Tachi, Y. (2018): Retention of uranium in cement systems: Effects of cement degradation and complexing ligands. Progress in Nuclear Science and Technology 5/0, 208-212. DOI: 10.15669/pnst.5.208.

Olmeda, J., Missana, T., Grandia, F., Grivé, M., García-Gutiérrez, M., Mingarro, M., Alonso, U., Colàs, E., Henocq, P., Munier, I. & Robinet, J.C. (2019): Radium retention by blended cement pastes and pure phases (C-S-H and C-A-S-H gels): Experimental assessment and modelling exercises. Applied Geochemistry 105, 45-54.
DOI: 10.1016/j.apgeochem.2019.04.004.

Paikaray, S., Hendry, M.J. & Essilfie-Dughan, J. (2013): Controls on arsenate, molybdate, and selenate uptake by hydrotalcite-like layered double hydroxides. Chemical Geology 345, 130-138. DOI: 10.1016/j.chemgeo.2013.02.015.

Palmer, D.A. & Gamsjäger, H. (2010): Solubility measurements of crystalline β-$Ni(OH)_2$ in aqueous solution as a function of temperature and pH. Journal of Coordination Chemistry 63/14-16, 2888-2908. DOI: 10.1080/00958972.2010.492215.

Papafotiou, A. & Senger, R.K. (2016): Sensitivity Analyses of Gas Release from a L/ILW Repository in the Opalinus Clay including the Microbial Consumption of Hydrogen. Nagra Arbeitsbericht NAB 16-07.

Park, S.M. & Jang, J.G. (2018): Carbonation-induced weathering effect on cesium retention of cement paste. Journal of Nuclear Materials 505, 159-164.
DOI: 10.1016/j.jnucmat.2018.04.015.

Patten, J.T. & Byrne, R.H. (2017): Assessment of Fe(III) and Eu(III) complexation by silicate in aqueous solutions. Geochimica et Cosmochimica Acta 202, 361-373.
DOI: 10.1016/j.gca.2016.12.004.

Pavasars, I., Hagberg, J., Borén, H. & Allard, B. (2003): Alkaline degradation of cellulose: mechanisms and kinetics. Journal of Polymers and the Environment 11/2, 39-47. DOI: 10.1023/A:1024267704794.

Plusquellec, G. & Nonat, A. (2016): Interactions between calcium silicate hydrate (C-S-H) and calcium chloride, bromide and nitrate. Cement and Concrete Research 90, 89-96. DOI: 10.1016/j.cemconres.2016.08.002.

Pointeau, I., Coreau, N. & Reiller, P. (2003): Etude expérimentale et modélisation de la rétention de $^{14}CO_3^{2-}$ par les matériaux constituant le béton dans le cadre des études de faisabilité d'un stockage de déchets graphites. Andra Report FRP 18 CEA 03-001. Andra, Paris, France.

Pointeau, I., Coreau, N. & Reiller, P. (2008): Uptake of anionic radionuclides onto degraded cement pastes and competing effect of organic ligands. Radiochimica Acta 96, 367-374. DOI: 10.1524/ract.2008.1503.

Pointeau, I., Landesman, C., Coreau, N., Moisan, C. & Reiller, P. (2004a): Etude de la rétention chimique des radionucléides Cs(I), Am(III), Zr(IV), Pu(IV), NB(V), U(VI), et Tc(IV) par les matériaux cimentaires dégradés. Document externe C RP PSTR 04-0012 / RT DPC/SECR 03-037. ANDRA, Châtenay-Malabry.

Pointeau, I., Landesman, C., Giffault, E. & Reiller, P. (2004b): Reproducibility of the uptake of U(VI) onto degraded cement pastes and calcium silicate hydrate phases. Radiochimica Acta / Migration '03 92, 645-650.

Pointeau, I., Reiller, P., Macé, N., Landesman, C. & Coreau, N. (2006): Measurement and modeling of the surface potential evolution of hydrated cement pastes as a function of degradation. Journal of Colloid and Interface Science 300/1, 33-44.
DOI: 10.1016/j.jcis.2006.03.018.

Pourbaix, M. (1974): Atlas of Electrochemical Equilibria in Aqueous Solutions. NACE International, Houston, Texas.

Rai, D., Hess, N., Xia, Y., Rao, L., Cho, H., Moore, R. & van Loon, L. (2003): Comprehensive thermodynamic model applicable to highly acidic to basic conditions for isosaccharinate reactions with Ca(II) and Np(IV). Journal of Solution Chemistry 32, 665-689. DOI: 10.1023/B:JOSL.0000002988.99769.cb.

Rai, D. & Kitamura, A. (2017): Thermodynamic equilibrium constants for important isosaccharinate reactions: A review. The Journal of Chemical Thermodynamics 114, 135-143. DOI: 10.1016/j.jct.2017.02.012.

Rai, D., Rao, L. & Xia, Y. (1998): Solubility of crystalline calcium isosaccharinate. Journal of Solution Chemistry 27, 1109-1122. DOI: 10.1023/A:1022610001043.

Rai, D., Yui, M. & Moore, D.A. (2012): Isosaccharinate complexes of Fe(III). Journal of Solution Chemistry 41/11, 1906-1921. DOI: 10.1007/s10953-012-9911-7.

Ram, R., Vaughan, J., Etschmann, B. & Brugger, J. (2019): The aqueous chemistry of polonium (Po) in environmental and anthropogenic processes. Journal of Hazardous Materials 380, 120725. DOI: 10.1016/j.jhazmat.2019.06.002.

Richardson, I.G. (2004): Tobermorite/jennite- and tobermorite/calcium hydroxide-based models for the structure of C-S-H: applicability to hardened pastes of tricalcium silicate, β-dicalcium silicate, Portland cement, and blends of Portland cement with blast-furnace slag, metakaolin, or silica fume. Cement and Concrete Research 34/9, 1733-1777. DOI: 10.1016/j.cemconres.2004.05.034.

Rodriguez-Cruz, D., Jockusch, R. & Williams, R. (1999): Binding energies of hexahydrated alkaline earth metal ions, $M^{2+}(H_2O)_6$, M = Mg, Ca, Sr, Ba: evidence of isomeric structures for magnesium. Journal of the American Chemical Society 121/9, 1986-1987. DOI: 10.1021/ja983232v.

Rojo, H., Scheinost, A.C., Lothenbach, B., Laube, A., Wieland, E. & Tits, J. (2018): Retention of selenium by calcium aluminate hydrate (AFm) phases under strongly-reducing radioactive waste repository conditions. Dalton Transactions 47/12, 4209-4218. DOI: 10.1039/C7DT04824F.

Rose, J., Moulin, I., Hazemann, J.-L., Masion, A., Bertsch, P.M., Bottero, J.-Y., Mosnier, F., Haehnel, C., Rose, J., Moulin, I., Hazemann, J.-L., Masion, A., Bertsch, P.M., Bottero, J.-Y., Mosnier, F. & Haehnel, C. (2000): X-ray absorption spectroscopy study of immobilization processes for heavy metals in calcium silicate hydrates: 1. Case of lead. Langmuir 16/25, 9900-9906. DOI: 10.1021/la0005208.

Rout, S.P., Charles, C.J., Doulgeris, C., McCarthy, A.J., Rooks, D.J., Loughnane, J.P., Laws, A.P. & Humphreys, P.N. (2015a): Anoxic biodegradation of isosaccharinic acids at alkaline pH by natural microbial communities. PloS One 10/9, e0137682. DOI: 10.1371/journal.pone.0137682.

Rout, S.P., Charles, C.J., Garratt, E.J., Laws, A.P., Gunn, J. & Humphreys, P.N. (2015b): Evidence of the generation of isosaccharinic acids and their subsequent degradation by local microbial consortia within hyper-alkaline contaminated soils, with relevance to intermediate level radioactive waste disposal. PloS One 10/3, e0119164. DOI: 10.1371/journal.pone.0119164.

Saslow, S.A., Kerisit, S.N., Varga, T., Mergelsberg, S.T., Corkhill, C., Snyder, M., Avalos, N.M., Yorkshire, A.S., Bailey, D.J., Crum, J. & Asmussen, R.M. (2020): Immobilizing pertechnetate in ettringite via sulfate substitution. Environmental Science & Technology 54/21, 13610-13618. DOI: 10.1021/acs.est.0c03119.

Savoye, S., Macé, N., Lefèvre, S., Spir, G. & Robinet, J.C. (2018): Mobility of chloride through cement-based materials under partially saturated conditions. Applied Geochemistry 96, 78-86. DOI: 10.1016/j.apgeochem.2018.06.011.

Scheidegger, A.M., Wieland, E., Scheinost, A.C., Dähn, R. & Spieler, P. (2000): Spectroscopic evidence for the formation of layered Ni−Al double hydroxides in cement. Environmental Science & Technology 34/21, 4545-4548. DOI: 10.1021/es0000798.

Schindler, P.W. (1984): Surface complexation, in: Sigel, H. (Ed.), Metal Ions in Biological Systems. Marcel Dekker, New-York, USA.

Schwyn, B. (2008): Geochemische Nahfeld - Daten für die sicherheitstechnichen Betrachtungen zum Sachplan geologische Tiefenlager, Etappe 1. Nagra Arbeitsbericht NAB 08-51.

Serrano, S., Dimitris Vlassopoulos, D., Bessinger, B. & O'Day, P.A. (2012): Immobilization of Hg(II) by coprecipitation in sulfate-cement systems. Environmental Science & Technology 46, 6767-6775. DOI: 10.1021/es202939v.

Shi, Z., Geiker, M., Weerdt, K. de, Ostnor, T., Lothenbach, B., Winnefeld, F. & Skibsted, J. (2017): Role of calcium on chloride binding in hydrated Portland cement–metakaolin–limestone blends. Cement and Concrete Research 95, 205-216. DOI: 10.1016/j.cemconres.2017.02.003.

Stumpf, T. & Fanghänel, T. (2002): A time-resolved laser fluorescence spectroscopy (TRLFS) study of the interaction of trivalent actinides (Cm(III)) with calcite. Journal of Colloid and Interface Science 249/1, 119-122. DOI: 10.1006/jcis.2002.8251.

Stumpf, T., Marques Fernandes, M., Walther, C., Dardenne, K. & Fanghänel, T. (2006): Structural characterization of Am incorporated into calcite: A TRLFS and EXAFS study. Journal of Colloid and Interface Science 302/1, 240-245. DOI: 10.1016/j.jcis.2006.06.010.

Stumpf, T., Tits, J., Walther, C., Wieland, E. & Fanghänel, T. (2004): Uptake of trivalent actinides (curium(III)) by hardened cement paste: a time-resolved laser fluorescence spectroscopy study. Journal of Colloid and Interface Science 276/1, 118-124. DOI: 10.1016/j.jcis.2004.03.014.

Suda, Y., Saeki, T. & Saito, T. (2015): Relation between chemical composition and physical properties of C-S-H generated from cementitious materials. Journal of Advanced Concrete Technology 13/5, 275-290. DOI: 10.3151/JACT.13.275.

Tachi, Y. & Ochs, M. (2018): Sorption parameter setting approaches for radioactive waste disposal considering perturbation effects: Sorption reduction factors for organics. Progress in Nuclear Science and Technology 5, 229-232. DOI: 10.15669/pnst.5.229.

Talerico, C., Ochs, M. & Giffaut, E. (2004): Solubility of niobium(V) under cementitious conditions: Importance of Ca-niobate. MRS Symposium Proceedings 824, 414-419. DOI: 10.1557/PROC-824-CC8.31.

Tamura, N., Chida, T., Niibori, Y. & Kim, S.-Y. (2017): Sorption behavior of cesium on calcium silicate hydrate under high carbonate ion concentration conditions. Energy Procedia 131, 203-207. DOI: 10.1016/j.egypro.2017.09.428.

Tasi, A., Gaona, X., Fellhauer, D., Böttle, M., Rothe, J., Dardenne, K., Polly, R., Grivé, M., Colàs, E., Bruno, J., Källström, K., Altmaier, M. & Geckeis, H. (2018a): Thermodynamic description of the plutonium – α-d-isosaccharinic acid system I: Solubility, complexation and redox behavior. Applied Geochemistry 98, 247-264. DOI: 10.1016/j.apgeochem.2018.04.014.

Tasi, A., Gaona, X., Fellhauer, D., Böttle, M., Rothe, J., Dardenne, K., Polly, R., Grivé, M., Colàs, E., Bruno, J., Källström, K., Altmaier, M. & Geckeis, H. (2018b): Thermodynamic description of the plutonium – α–d–isosaccharinic acid system II: Formation of quaternary Ca(II)–Pu(IV)–OH–ISA complexes. Applied Geochemistry 98, 351-366. DOI: 10.1016/j.apgeochem.2018.06.014.

Tasi, A., Gaona, X., Rabung, T., Fellhauer, D., Rothe, J., Dardenne, K., Lützenkirchen, J., Grivé, M., Colàs, E., Bruno, J., Källstrom, K., Altmaier, M. & Geckeis, H. (2021): Plutonium retention in the isosaccharinate – cement system. Applied Geochemistry 126, 104862. DOI: 10.1016/j.apgeochem.2020.104862.

Taylor, H. (1997): Cement Chemistry. Thomas Telford Limited, London.

Telchadder, R., Smith, K. & Bryan, N.D. (2012): Europium interaction with a vault backfill at high pH. Mineralogical Magazine 76/8, 3083-3093. DOI: 10.1180/minmag.2012.076.8.23.

Tits, J., Curti, E., Laube, A. & Wieland, E. (2023): Sorption of ^{26}Al, ^{32}Si and ^{45}Ca by Isotopic Exchange during the Recrystallisation of Cement Phases. Nagra Arbeitsbericht NAB 23-03.

Tits, J., Fujita, T., Harfouche, M., Dähn, R., Tsukamoto, M. & Wieland, E. (2014a): Radionuclide Uptake by Calcium Silicate Hydrates: Case studies with Th(IV) and U(VI). PSI Bericht Nr. 14-03. Paul Scherrer Institut PSI, Villigen.

Tits, J., Gaona, X., Laube, A. & Wieland, E. (2014b): Influence of the redox state on the neptunium sorption under alkaline conditions: Batch sorption studies on titanium dioxide and calcium silicate hydrates. Radiochimica Acta 102, 385-400. DOI: 10.1515/ract-2013-2151.

Tits, J., Geipel, G., Macé, N., Eilzer, M. & Wieland, E. (2011): Determination of uranium(VI) sorbed species in calcium silicate hydrate phases: a laser-induced luminescence spectroscopy and batch sorption study. Journal of Colloid and Interface Science 359/1, 248-256. DOI: 10.1016/j.jcis.2011.03.046.

Tits, J., Iijima, K., Wieland, E. & Kamei, G. (2006): The uptake of radium by calcium silicate hydrates and hardened cement paste. Radiochimica Acta 94/9-11, 637-643. DOI: 10.1524/ract.2006.94.9-11.637.

Tits, J., Stumpf, T., Rabung, T., Wieland, E. & Fanghänel, T. (2003): Uptake of Cm(III) and Eu(III) by calcium silicate hydrates: a solution chemistry and time-resolved laser fluorescence spectroscopy study. Environmental Science & Technology 37/16, 3568-3573. DOI: 10.1021/es030020b.

Tits, J., Walther, C., Stumpf, T., Macé, N. & Wieland, E. (2015): A luminescence line-narrowing spectroscopic study of the uranium(VI) interaction with cementitious materials and titanium dioxide. Dalton Transactions 44/3, 966-976. DOI: 10.1039/c4dt02172j.

Tits, J. & Wieland, E. (2018): Actinide Sorption by Cementitious Materials. PSI Report 18-02. Paul Scherrer Institut PSI, Villigen.

Tits, J., Wieland, E. & Bradbury, M.H. (2005): The effect of isosaccharinic acid and gluconic acid on the retention of Eu(III), Am(III) and Th(IV) by calcite. Applied Geochemistry 20/11, 2082-2096. DOI: 10.1016/J.APGEOCHEM.2005.07.004.

Tits, J., Wieland, E., Müller, C.J., Landesman, C. & Bradbury, M.H. (2006b): Strontium binding by calcium silicate hydrates. Journal of Colloid and Interface Science 300/1, 78-87. DOI: 10.1016/j.jcis.2006.03.043.

Tritthart, J. (1989): Chloride binding in cement II. The influence of the hydroxide concentration in the pore solution of hardened cement paste on chloride binding. Cement and Concrete Research 19/5, 683-691. DOI: 10.1016/0008-8846(89)90039-2.

van Es, E., Evans, N., Felipe-Sotelo, M., Field, L.P., Hinchliff, J., Milodowski, A.E. & Read, D. (2015): Retention of chlorine-36 by a cementitious backfill. Mineralogical Magazine 79/6, 1297-1305. DOI: 10.1180/minmag.2015.079.6.05.

van Loon, L.R. & Glaus, M.A. (1998): Experimental and Theoretical Studies on Alkaline Degradation of Cellulose and its Impact on the Sorption of Radionuclides. Nagra Technical Report NTB 97-04.

van Loon, L.R., Glaus, M.A. & Vercammen, K. (2004): Stability of the ion pair between Ca^{2+} and 2-(hydroxymethyl)-3-deoxy-D-erythro-pentonate (α-isosaccharinate). Journal of Solution Chemistry 33/12, 1573-1583. DOI: 10.1007/s10953-004-1394-8.

van Loon, L.R., Glaus, M.A., Vercammen, K., Ghosh, S., Adersson, P.G., Mller, J., Senning, A., Yao, X.K., Wang, H.-G., Tuchagues, J.-P. & Örgen, M. (1999): Solubility products of calcium isosaccharinate and calcium gluconate. Acta Chemica Scandinavica 53, 235-240. DOI: 10.3891/acta.chem.scand.53-0235.

van Loon, L.R. & Hummel, W. (1995): The Radiolytic and Chemical Degradation of Organic Ion Exchange Resins under Alkaline Conditions: Effect on Radionuclide Speciation. Nagra Technical Report NTB 95-08.

van Loon, L.R. & Hummel, W. (1999a): Radiolytic and chemical degradation of strong acidic ion-exchange resins: Study of the ligands formed. Nuclear Technology 128/3, 359-371. DOI: 10.13182/NT99-A3037.

van Loon, L.R. & Hummel, W. (1999b): The degradation of strong basic anion exchange resins and mixed-bed ion-exchange resins: Effect of degradation products on radionuclide speciation. Nuclear Technology 128/3, 388-401. DOI: 10.13182/NT99-A3039.

Vercammen, K., Glaus, M.A., van Loon, L.R., Ghosh, S., Andersson, P.G., Møller, J., Senning, A., Yao, X.-K., Wang, H.-G., Tuchagues, J.-P. & Ögren, M. (1999): Complexation of calcium by alpha-isosaccharinic acid under alkaline conditions. Acta Chemica Scandinavica 53, 241-246. DOI: 10.3891/acta.chem.scand.53-0241.

Vespa, M., Dähn, R., Grolimund, D., Wieland, E. & Scheidegger, A.M. (2006): Spectroscopic investigation of Ni speciation in hardened cement paste. Environmental Science & Technology 40/7, 2275-2282. DOI: 10.1021/es052240q.

Viallis-Terrisse, H., Nonat, A. & Petit, J.-C. (2001): Zeta-potential study of calcium silicate hydrates interacting with alkaline cations. Journal of Colloid and Interface Science 244/1, 58-65. DOI: 10.1006/jcis.2001.7897.

Wang, L., Martens, E., Jacques, D., Canniere, P., Berry, J. & Mallants, D. (2012): Review of sorption values for the cementitious near field of a near-surface radioactive waste disposal facility. *In:* Radioactive Waste Management Committee: Cementitious materials in safety cases for radioactive waste: role, evolution and interactions. A workshop organised by the OECD/NEA Integration Group in the Safety Case and hosted by ONDRAF/NIRAS, NEA/RWM/R(2012)3/REV, 225-230.

Weerdt, K. de, Colombo, A., Coppola, L., Justnes, H. & Geiker, M.R. (2015): Impact of the associated cation on chloride binding of Portland cement paste. Cement and Concrete Research 68, 196-202. DOI: 10.1016/j.cemconres.2014.01.027.

Wersin, P., Johnson, L., Schwyn, B., Berner, U. & Curti, E. (2003): Redox Conditions in the Near-Field of Repository for SF/HLW and ILW in Opalinus Clay. Nagra Technical Report NTB 02-13.

Wieland, E. (2014): Sorption Database for the Cementitious Near Field of L/ILW and ILW Repositories for Provisional Safety Analyses for SGT-E2. Nagra Technical Report NTB 14-08.

Wieland, E. (2019): Sorption Values for Elements on Cement Paste. PSI Technical Report TM 44-19-08. Edited by Paul Scherrer Institut, Villigen PSI, Switzerland.

Wieland, E., Curti, E., Miron, D.G., Tits, J., van Loon, L.R. & Guillemot, T. (2023): Carbon-14 Source, Speciation and Release in the context of a Deep Geological Repository. Nagra Technical Report NTB 22-04.

Wieland, E. & Hummel, W. (2015): Formation and stability of ^{14}C-containing organic compounds in alkaline iron-water systems: preliminary assessment based on a literature survey and thermodynamic modelling. Mineralogical Magazine 79/6, 1275-1286. DOI: 10.1180/minmag.2015.079.6.03.

Wieland, E. & Kosakowski, G. (2020): Review of the Compositions of Hydrated Cements and Cement-type Pore Water at Differen Stages of the Cement Degradation. Nagra Arbeitsbericht NAB 20-12.

Wieland, E., Kosakowski, G., Lothenbach, B., Kulik, D.A. & Cloet, V. (2018): Preliminary Assessment of the Temporal Evolution of Waste Packages in the Near field of a L/ILW Repository. Nagra Arbeitsbericht NAB 18-05.

Wieland, E., Tits, J., Kunz, D. & Dähn, R. (2008): Strontium uptake by cementitious materials. Environmental Science & Technology 42/2, 403-409. DOI: 10.1021/es071227y.

Wieland, E., Tits, J., Ulrich, A. & Bradbury, M.H. (2006): Experimental evidence for solubility limitation of the aqueous Ni(II) concentration and isotopic exchange of ^{63}Ni in cementitious systems. Radiochimica Acta 94/1, 29-36. DOI: 10.1524/ract.2006.94.1.29.

Wieland, E. & van Loon, L.R. (2002): Cementitious Near-Field Sorption Database for Performance Assessment of ILW Repository in Opalinus Clay. Nagra Technical Report NTB 02-20.

Winnefeld, F., Becker, S., Pakusch, J. & Götz, T. (2007): Effects of the molecular architecture of comb-shaped superplasticizers on their performance in cementitious systems. Cement and Concrete Composites 29/4, 251-262. DOI: 10.1016/j.cemconcomp.2006.12.006.

Wolter, J.-M., Schmeide, K., Huittinen, N. & Stumpf, T. (2019a): Cm(III) retention by calcium silicate hydrate (C-S-H) gel and secondary alteration phases in carbonate solutions with high ionic strength: A site-selective TRLFS study. Scientific Reports 9/1, 14255. DOI: 10.1038/s41598-019-50402-x.

Wolter, J.-M., Schmeide, K., Weiss, S., Bok, F., Brendler, V. & Stumpf, T. (2019b): Stability of U(VI) doped calcium silicate hydrate phases in repository-relevant brines studied by leaching experiments and spectroscopy. Chemosphere 218, 241-251. DOI: 10.1016/j.chemosphere.2018.11.074.

Yamaguchi, T., Ohira, S., Hemmi, K., Barr, L., Shimada, A., Maeda, T. & Iida, Y. (2020): Consideration on modeling of Nb sorption onto clay minerals. Radiochimica Acta 108/11, 873-877. DOI: 10.1515/ract-2020-0006.

Yilmaz, V.T., Odabaǽoğlu, M., İçbudak, H. & Ölmez, H. (1993): The degradation of cement superplasticizers in a high alkaline solution. Cement and Concrete Research 23/1, 152-156. DOI: 10.1016/0008-8846(93)90146-Z.

Young, A.J., Warwick, P., Milodowski, A.E. & Read, D. (2013): Behaviour of radionuclides in the presence of superplasticiser. Advances in Cement Research 25/1, 32-43. DOI: 10.1680/adcr.12.00032.

Żak, R. & Deja, J. (2015): Spectroscopy study of Zn, Cd, Pb and Cr ions immobilization on C-S-H phase. Spectrochimica Acta Part A: Molecular and Biomolecular Spectroscopy 134, 614-620. DOI: 10.1016/j.saa.2014.06.069.

Zhang, M. & Reardon, E.J. (2003): Removal of B, Cr, Mo, and Se from wastewater by incorporation into hydrocalumite and ettringite. Environmental Science & Technology 37/13, 2947-2952. DOI: 10.1021/es020969i.

App. A Assessment of sorption reduction factors

A.1 List of abbreviations

R_d^0	Distribution ratio (R_d) for sorption on cement paste in the absence of colloids and aqueous complexing organic ligands
R_d^{compl}	R_d for sorption on cement paste in the presence of aqueous complexing organic ligands only
R_d^{coll}	R_d for sorption on cement paste in the presence of colloids only
R_d^{comp}	R_d for sorption on cement paste taking into account the effects of sorption competition
R_d^*	R_d for sorption on cement paste in the presence of colloids and aqueous complexing organic ligands
R_d^{eff}	R_d for sorption on cement paste taking into account the effects of colloids, complexing organic ligands and sorption competition
R_{coll}	R_d for sorption of metal ions on colloids
$\{M_s\}$	amount of metal ions sorbed on cement paste in the absence of colloids and aqueous complexing organic ligands
$\{M_s^*\}$	amount of metal ions sorbed on cement paste in the presence of colloids and aqueous complexing organic ligands
$\{M_{s,}^{compl}\}$	amount of metal ions sorbed on cement paste in the presence of aqueous complexing organic ligands
$\{M_s^{coll}\}$	amount of metal ions sorbed on cement paste in the presence of colloids and in the absence of organic complexing ligands
$\{M_{coll}\}$	amount of metal ions sorbed on colloids and in the absence of organic complexing ligands
$\{M_{coll}^{compl}\}$	amount of metal ions sorbed on colloids and in the presence of organic complexing ligands
$\{M_{coll}^{compl}\}$	the amount of metal sorbed onto colloids in the presence of organic complexing ligands
$[M_f]$	aqueous free metal concentration in the absence of colloids and aqueous complexing organic ligands
$[M_f^{compl}]$	aqueous free metal concentration in the presence of organic complexes
$[M_f^{coll}]$	aqueous free metal concentration in the presence of colloids only
$[M_f^{coll+compl}]$	$= [M_f^*]$: aqueous free metal concentration in the presence of colloids and complexing organic ligands
$[M]$	aqueous concentration of the metal and its inorganic complexes in the absence of colloids and aqueous complexing organic ligands
$[M^{compl}]$	aqueous concentration of the metal and its inorganic complexes in the presence of complexing organic ligands only
$[M^{coll}]$	aqueous concentration of the free metal and its inorganic complexes in the presence of colloids only

$[M^{coll+compl}]$ = $[M^*]$: aqueous concentration of the free metal cation and inorganic complexes in the presence of colloids and organic complexing ligands

$[M_c]$ = $[M_{s,coll}]$: concentration of M sorbed onto colloids

$[l^a]$ concentration of the inorganic ligand, l^a

b number of inorganic ligands, l^a, making up the complex Ml^a_b; $b \geq 1$

β^a_b thermodynamic stability constant of the aqueous inorganic metal – ligand complex, ML^a_b

$'\beta^k_n$ conditional stability constant of the aqueous metal – ligand complex, ML^k_n, corresponding to the thermodynamic stability constant of the metal-ligand complexation, β^a_b, divided by the side reaction factor A

$[L^k]$ aqueous concentration of an organic complexing ligand, L^k

n number of organic ligands, L^k, making up the complex ML^k_n. $n \geq 1$

A side reaction factor including metal complexation by inorganic ligands

$F_{red,2}$ reduction factor taking into account the effects of aqueous metal-organic ligand complexation on the radionuclide sorption onto cement paste

$F_{red,1}$ reduction factor taking into account the effects of radionuclide sorption on dispersed colloids on radionuclide uptake by cement paste in the absence of complexing ligands

F_{red,L^k_n} reduction factor taking into account the effect of aqueous complexation of a radionuclide with n ligands, L^k on the radionuclide sorption onto cement paste

$F_{red,3}$ reduction factor taking into account the effects of sorption competition

A.2 Derivation of reduction factors accounting for aqueous complexation, sorption onto dispersed colloids and sorption competition

The uptake of radionuclides by HCP can be reduced by the presence of dispersed colloids and organic complexing ligands due to the formation of water-soluble complexes in case of organics and the association of radionuclides with colloidal material. Competition with other metal cations for sorption sites can reduce the effective R_d values even further. These adverse effects can be described in terms of sorption reduction reactors, F_{red}, on the assumption of a reversible sorption process. The mathematical derivation of sorption reduction factors is described below.

In the absence of colloids and complexing organic ligands, the distribution ratio of M between cement and CPW, R_d^0, is defined as:

$$R_d^0 = \frac{\{M_s\}}{[M]} \qquad \text{(A-1)}$$

$\{M_s\}$ is the amount of metal cation sorbed on cement (mol/kg), and [M] is the aqueous metal concentration, including the free metal concentration, $[M_f]$ and the concentration of inorganic complexes such as hydroxy species, carbonates, sulphates, $\sum_a \sum_b \left[MI_b^a \right]$, in the absence of organic complexing ligands and colloids; i.e.:

$$\left[M\right] = \left[M_f\right] + \sum_a \sum_b \left[MI_b^a \right] \tag{A-2}$$

In this equation, b is the number of organic ligands, l^a, making up the inorganic complex ML^a_b.
Eq. A-2 can also be written as follows (van Loon & Glaus 1998):

$$\left[M\right] = \left[M_f\right] \cdot \left(1 + \sum_a \sum_b \beta_b^a \cdot \left[I^a \right]^b \right) \tag{A-3}$$

In a constant, well-defined cement porewater, the term $1 + \sum_a \sum_b \beta_b^a \cdot \left[I^a \right]^b$ is a constant value and is referred to as the side reaction factor, A.
Hence, Eq. A-3 can be simplified to:

$$\left[M\right] = \left[M_f\right] \cdot A \tag{A-4}$$

Combining Eq. A-1 with A-4 can be written as:

$$R_d^0 = \frac{\left\{M_s\right\}}{\left[M_f\right] \cdot A} \tag{A-5}$$

A real cement porewater contains not only free metal ions and inorganic complexes, but also organic complexes (ML^k_n) and metal-colloid complexes (M_c); the equation for the R_d value then becomes:

$$R_d^* = \frac{\left\{M_s^*\right\}}{[M_f^*] \cdot A + [M_c] + \sum_k \sum_n [ML_n^k]} \tag{A-6}$$

where $[M_f^*]$ and $\{M_s^*\}$ are the aqueous equilibrium concentration of the free metal cation (mol/L) and the amount of metal cation sorbed on cement (mol/kg) in the presence of organic complexing ligands and dispersed colloids, $[M_c]$ is the concentration of metals sorbed onto colloids (mol/L) in the presence of complexing ligands, and $\sum_k \sum_n [ML_n^k]$ is the sum of the concentrations of all metal complexes with all organic complexing ligands, L^k, in solution (mol/L).

A.2.1 Effect of complexation with aqueous organic ligands, L, on radionuclide uptake by cement paste

The effect of complexation with aqueous organic ligands can be described as given below.

The complexation of metal cation, M, with an organic complexing ligand, L^k, is defined by the following complexation reaction:

$$M + nL^k \Leftrightarrow ML^k_n \quad \text{with: } {}'\beta^k_n = \frac{\left[ML^k_n\right]}{\left[M^{compl}\right]\cdot\left[L^k\right]^n} \tag{A-7}$$

$[M^{compl}]$ is the sum of the aqueous concentration of the free metal cation and inorganic metal-complexes in the presence of organic complexing ligands; n is the number of organic ligands, L^k, making up the complex ML^k_n. Note that the value of n, is not necessarily the same for each organic complexing ligand, L^k. We use this notation to simplify the mathematics. $[ML_n{}^k]$ is the concentration of the metal-ligand complexes, $[L^k]$ is the concentration of the k^{th} ligand, ${}'\beta^k_n$ is the conditional metal-ligand complexation constant corresponding to the metal-ligand complexation constant (β^k_n) divided by the side reaction coefficient A.

$${}'\beta^k_n = \frac{\left[ML^k_n\right]}{\left[M^{compl}_f\right]\cdot\left[L^k\right]^n\cdot A} = \frac{\beta^k_n}{A} \tag{A-8}$$

The aqueous metal concentration is, in analogy to Eq. A-4, given by:

$$\left[M^{compl}\right] = \left[M^{compl}_f\right]\cdot A \tag{A-9}$$

$[M_f{}^{compl}]$ is the aqueous free metal concentration in the presence of organic complexes and A is the side reaction coefficient.

Combining Eqs. A-7 and A-9 and rewriting Eq. A-7 as a function of $\left[ML^k_n\right]$ and a summation over all metal organic ligand complexes in solution then gives:

$$\sum_k\sum_n\left[ML^k_n\right] = \sum_k\sum_n {}'\beta^k_n\cdot[M^{compl}_f]\cdot A\cdot[L^k]^n \tag{A-10}$$

In this case, the distribution ratio for sorption of M onto cement paste in the presence or organic ligands becomes:

$$R_d^{compl} = \frac{\{M_s^{compl}\}}{[M^{compl}] + \sum_k \sum_n [ML_n^k]} = \frac{\{M_s^{compl}\}}{[M_f^{compl}] \cdot A + \sum_k \sum_n {}'\beta_n^k \cdot [M_f^{compl}] \cdot A \cdot [L^k]^n} = \ldots$$
$$\ldots = \frac{\{M_s^{compl}\}}{[M_f^{compl}] \cdot A \cdot \left(1 + \sum_k \sum_n {}'\beta_n^k \cdot [L^k]^n\right)} \qquad \text{(A-11)}$$

With $\{M_s^{compl}\}$ as the amount of M sorbed on cement in the presence of complexing organic ligands.

Assuming linear and reversible sorption and a constant solution composition with regard to its inorganic ligand concentrations (A is constant), we can state that:

$$\frac{\{M_s\}}{[M_f] \cdot A} = \frac{\{M_s^{compl}\}}{[M_f^{compl}] \cdot A} = R_d^0 \qquad \text{(A-12a)}$$

A sorption process is called linear when the ratio of the amount of metal sorbed and the free metal concentration in solution are constant, independently of the free metal concentration in solution (e.g., Baeyens & Bradbury 1997); i.e.,

$$\frac{\{M_s\}}{[M_f]} = \text{constant} \qquad \text{(A-12b)}$$

Generally, this assumption is only valid at trace metal loadings.

Combining Eq. A-11 and Eq. A-12a leads to:

$$R_d^{compl} = \frac{R_d^0}{1 + \sum_k \sum_n {}'\beta_n^k \cdot [L^k]^n} \qquad \text{(A-13)}$$

We can now define a reduction factor, $F_{red,1}$, to express the effect of metal complexation in solution on the R_d value for sorption of M on cement:

$$F_{red,2} = \frac{R_d^0}{R_d^{compl}} = 1 + \sum_k \sum_n {}'\beta_n^k \cdot [L^k]^n \qquad \text{(A-14)}$$

where β_n^k / A equals ${}'\beta_n^k$ with β_n^k as the thermodynamic stability constant and A as the side reaction coefficient. Eq. A-14 is consistent with an earlier derivation by van Loon & Glaus (1998).

For strongly complexing ligands $\left('\beta_n^k \cdot [L^k]^n \gg 1\right)$, the combined effect of all complexing ligands on the radionuclide R_d values, ($F_{red,2}$) can be approximated as the sum of the reduction factors of each single complexing ligand. Indeed, Eq. A-14 says that

$$F_{red,2} = 1 + '\beta_1^1 \cdot \left[L^1\right]^1 + '\beta_2^1 \cdot \left[L^1\right]^2 + ... + '\beta_n^1 \cdot \left[L^1\right]^n + '\beta_1^2 \cdot \left[L^2\right]^1 + '\beta_2^2 \cdot \left[L^2\right]^2 + ... + '\beta_n^2 \cdot \left[L^2\right]^n + ...$$
$$... + '\beta_1^k \cdot \left[L^k\right]^1 + '\beta_2^k \cdot \left[L^k\right]^2 + ... + '\beta_n^k \cdot \left[L^k\right]^n \quad \text{(A-15)}$$

Defining the reduction factor for each single complexing ligand as:

$$F_{red,L_n^k} = 1 + '\beta_n^k \cdot \left[L^k\right]^n \quad \text{(A-16)}$$

Eq, A-15 can be written as:

$$F_{red,2} = F_{red,L_1^1} + \left(F_{red,L_2^1} - 1\right) + \ldots + \left(F_{red,L_n^1} - 1\right) + \left(F_{red,L_1^2} - 1\right) + \left(F_{red,L_2^2} - 1\right) + \ldots + \left(F_{red,L_n^2} - 1\right) + \ldots + \left(F_{red,L_1^k} - 1\right) + \left(F_{red,L_2^k} - 1\right) + \ldots + \left(F_{red,L_n^k} - 1\right) \quad \text{(A-17)}$$

For strongly complexing organic ligands, this equation can be approximated as follows:

$$F_{red,2} = F_{red,L_1^1} + F_{red,L_2^1} + ...F_{red,L_n^1} + F_{red,L_1^2} + F_{red,L_2^2} + ... + F_{red,L_n^2} + ... + F_{red,L_1^k} + F_{red,L_2^k} + ...$$
$$+ F_{red,L_n^k} = \sum_k \sum_n F_{red,L_n^k} \quad \text{(A-18)}$$

A.2.2 Effect of dispersed colloids on radionuclide uptake by cement paste in the presence and absence of complexing ligands

The effect of radionuclide sorption onto dispersed colloids on the uptake of the same radionuclide by cement in the absence of complexing ligands can be derived as described below.

The aqueous concentration of M sorbed onto colloids, $[M_{s,coll}]$, is:

$$[M_{s,coll}] = m_{coll} \cdot \{M_{,coll}\} \quad \text{(A-19)}$$

with m_{coll} as the mass of colloids (kg/L) and $\{M_{coll,}\}$ as the amount of M sorbed onto the colloids (mol/kg).

The distribution ratio describing the sorption of M onto colloids, R_{coll}, can be expressed in a similar way as in Eq. A-2 for metal sorption on cement paste, i.e., as the amount of metal sorbed on the colloids, $\{M_s^{coll}\}$ divided by the concentration of the aqueous free metal cations in solution $[M^{coll}]$:

$$R_{coll} = \frac{\{M_{coll}\}}{[M^{coll}]} \tag{A-20}$$

$[M^{coll}]$ is the sum of the aqueous concentration of the free metal cation and the inorganic metal-complexes in the presence of colloids; i.e., in analogy to equation A-4:

$$\left[M^{coll}\right] = \left[M_f^{coll}\right] \cdot A \tag{A-21}$$

Rewriting Eq. A-20 as a function of $\{M_{coll}\}$ and combining this with Eq. A-21, gives:

$$\{M_{coll}\} = R_{coll} \cdot [M_f^{coll}] \cdot A \tag{A-22}$$

Thus, by combining Eq. A-19 and Eq. A-22, the concentration of M sorbed onto the colloids, $[M_{s,coll}]$, can be described as follows:

$$\left[M_{s,coll}\right] = m_{coll} \cdot R_{coll} \cdot \left[M_f^{coll}\right] \cdot A \tag{A-23}$$

The sole effect of the sorption of M onto dispersed colloids on the R_d value for the sorption of M onto cement, R_d^{coll}, is:

$$R_d^{coll} = \frac{\{M_{s,coll}\}}{[M^{coll}] + [M_{s,coll}]} \tag{A-24}$$

$\{M_{s,coll}\}$ is the amount of metal sorbed on cement in the presence of dispersed colloids.

Combining Eq. A-24 with Eq. A-23 gives:

$$R_d^{coll} = \frac{\{M_{s,coll}\}}{\left[M_f^{coll}\right] \cdot A + m_{coll} \cdot R_{coll} \cdot \left[M_f^{coll}\right] \cdot A} \tag{A-25}$$

or:

$$R_d^{coll} = \frac{\{M_{s,coll}\}}{[M_f^{coll}] \cdot A \cdot (1 + m_{coll} \cdot R_{coll})} \tag{A-26}$$

Assuming, again, linear, reversible sorption and a constant value of A, we can state that:

$$\frac{\{M_s\}}{[M_f]\cdot A} = \frac{\{M_{s,coll}\}}{[M_f^{coll}]\cdot A} = R_d^0 \tag{A-27}$$

Thus, Eq. A-26 becomes:

$$R_d^{coll} = \frac{R_d^0}{1 + m_{coll}\cdot R_{coll}} \tag{A-28}$$

We can now define a reduction factor, $F_{red,1}$, to express the effect of metal sorption onto dispersed colloids on the R_d value for metal sorption on cement:

$$F_{red,1} = \frac{R_d^0}{R_d^{coll}} = 1 + m_{coll}\cdot R_{coll} \tag{A-29}$$

Equation A-28 is consistent with an earlier derivation by Wieland & van Loon (2002) and only holds in the absence of organic complexing ligands, L, therefore accounting for the effect of colloids on metal sorption on cement paste only.

In the presence of organic complexing ligands, metal sorption on colloids is given as:

$$R_{coll}^{comp} = \frac{\{M_{coll}^{compl}\}}{[M^{coll+compl}] + \sum_k \sum_n [ML_n^k]} \tag{A-30}$$

$\{M_{coll}^{compl}\}$ is the amount of metal sorbed onto colloids in the presence of organic complexing ligands. $[M^{coll+compl}]$ is the sum of the aqueous concentration of the free metal cations and the inorganic metal-complexes in the presence of colloids and organic complexing ligands given as:

$$[M^{coll+compl}] = [M_f^{coll+compl}]\cdot A \tag{A-31}$$

Assuming that the sorption process on colloids is linear and reversible, the sorption distribution ratio in the presence of complexing organic ligands, R_{coll}^{compl}, equals the sorption distribution ratio in the absence of complexing organic ligands, R_{coll}.

Combining Eq. A-30 and A-31 and replacing the metal-organic ligand complexes with their definition in Eq. A-10 gives:

$$R_{coll}^{comp} = R_{coll} = \frac{\left\{M_{coll}^{comp}\right\}}{\left[M_f^{coll+compl}\right]\cdot A + \sum_k \sum_n {}'\beta_n^k \cdot \left[M_f^{coll+compl}\right]\cdot A \cdot \left[L^k\right]^n} = \ldots$$
$$\ldots = \frac{\left\{M_{coll}^{comp}\right\}}{\left[M_f^{coll+compl}\right]\cdot A \cdot \left(1 + \sum_k \sum_n {}'\beta_n^k \cdot \left[L^k\right]^n\right)} \quad \text{(A-32)}$$

Assuming linear, reversible sorption on the colloids and a constant value of A, we can further state that:

$$\frac{\left\{M_{coll}\right\}}{[M_f^{coll}]\cdot A} = \frac{\left\{M_{coll}^{comp}\right\}}{[M_f^{coll+compl}]\cdot A} = R_{coll}$$

Rewriting Eq. A-32 as a function of $\{M_{coll}\}$ gives:

$$\left\{M_{coll}^{comp}\right\} = R_{coll} \cdot \left[M_f^{coll+compl}\right]\cdot A \cdot \left(1 + \sum_k \sum_n {}'\beta_n^k \cdot \left[L^k\right]^n\right) \quad \text{(A-33)}$$

The aqueous concentration of metals sorbed on colloids in the presence of complexing ligands then amounts to:

$$\left[M_{s,coll}\right] = \left[M_c\right] = m_{coll} \cdot R_{coll} \cdot \left[M_f^{coll}\right]\cdot A \cdot \left(1 + \sum_k \sum_n {}'\beta_n^k \cdot \left[L^k\right]^n\right) \quad \text{(A-34)}$$

A.2.3 Overall effect of metal complexation and metal sorption on dispersed colloids on radionuclide uptake by cement paste

The combined effects of aqueous complexation and sorption onto dispersed colloids can be described starting from Eq. A-6: the term $\sum_k \sum_n [ML_k^n]$ in this equation is replaced by its definition in Eq. A-9. $[M_c]$ corresponds to the concentration of metal sorbed on colloids in the presence of complexing ligands (Eq. A-34).

This gives the following expression for R_d^*:

$$R_d^* = \frac{\left\{M_s^*\right\}}{[M_f^*]\cdot A + m_{coll} \cdot R_{coll} \cdot \left([M_f^*]\cdot A + \sum_k \sum_n {}'\beta_n^k [M_f^*]\cdot A \cdot [L^k]^n\right) + \sum_k \sum_n {}'\beta_n^k [M_f^*]\cdot A \cdot [L^k]^n} \quad \text{(A-35)}$$

or:

$$R_d^* = \frac{\left\{M_s^*\right\}}{\left[M_f^*\right] \cdot A \cdot \left(1 + m_c \cdot R_{coll} \cdot \left(1 + \sum_k \sum_n {}'\beta_n^k \cdot [L^k]^n\right) + \sum_k \sum_n {}'\beta_n^k \cdot [L^k]^n\right)} \quad \text{(A-36)}$$

Here, $[M_f^*]$ and $\{M_s^*\}$ are the free aqueous concentration of M and the amount of M sorbed on cement in the presence of complexing ligands and dispersed colloids, respectively.

Assuming, linear, reversible sorption and a constant side-reaction coefficient, A, means that:

$$\frac{\{M_s\}}{[M_f] \cdot A} = \frac{\left\{M_s^*\right\}}{[M_f^*] \cdot A} = R_d^0 \quad \text{(A-37)}$$

Eq. A-36 can be rearranged giving:

$$R_d^* = \frac{R_d^0}{1 + m_c \cdot R_{coll} \cdot \left(1 + \sum_k \sum_n {}'\beta_n^k \cdot [L^k]^n\right) + \sum_k \sum_n {}'\beta_n^k \cdot [L^k]^n} \quad \text{(A-38)}$$

or

$$R_d^* = \frac{R_d^0}{1 + m_c \cdot R_d^{coll} + m_c \cdot R_{coll} \cdot \sum_k \sum_n {}'\beta_n^k \cdot \left[L^k\right]^n + \sum_k \sum_n {}'\beta_n^k \cdot \left[L^k\right]^n} \quad \text{(A-39)}$$

Using the expression for the sorption reduction factor by colloids (Eq. A-29) leads to:

$$R_d^* = \frac{R_d^0}{F_{red,1} + \left(F_{red,1} - 1\right) \cdot \left(\sum_k \sum_n {}'\beta_n^k \cdot \left[L^k\right]^n\right) + \sum_k \sum_n {}'\beta_n^k \cdot \left[L^k\right]^n} \quad \text{(A-40)}$$

Using the expression for the sorption reduction factor by complexing ligands (Eq. A-14) leads to

$$R_d^* = \frac{R_d^0}{F_{red,1} + \left(F_{red,1} - 1\right) \cdot \left(F_{red,2} - 1\right) + \left(F_{red,2} - 1\right)} \quad \text{(A-41a)}$$

and

$$R_d^* = \frac{R_d^0}{F_{red,1} + F_{red,1} \cdot F_{red,2} - F_{red,1} - F_{red,2} + 1 + F_{red,2} - 1} \quad \text{(A-41b)}$$

and eventually to

$$R_d^* = \frac{R_d^0}{F_{red,2} \cdot F_{red,1}} \quad \text{(A-42)}$$

$F_{red,1}$ values for sorption on colloids are taken from Wieland & van Loon (2002) and $F_{red,2}$ values accounting for complexation of the dose-relevant radionuclides have been derived in Section 6.3.

A.2.4 Overall effect of metal complexation, metal sorption on dispersed colloids and sorption competition on radionuclide uptake by cement paste

A further process that may decrease radionuclide sorption values is sorption competition. This effect is taken into account by applying a constant reduction factor, $F_{red,3}$ to the selected R_d values given in Tab. 7-1. This factor accounts for the reduction in the sorption capacity of C-S-H phases caused by competitive sorption of other ions and is discussed in more detail in App. B. For the sake of simplicity, it is assumed that sorption competition proportionally decreases the sorption capacity and therefore the overall sorption value.

The overall R_d value taking into account the effects of colloids, complexes and competition on the radionuclide uptake by cement paste, R_d^{eff}, is then obtained by dividing Eq. A-42 by the reduction factor, $F_{red,3}$,

$$R_d^{eff} = \frac{R_d^0}{F_{red,1} \cdot F_{red,2} \cdot F_{red,3}} \quad \text{(A-43)}$$

App. B Sorption competition

B.1 Introduction

The current design of an L/ILW repository implies that the inventory of metallic waste materials, in particular iron and steel, will be large. The metallic waste materials will be embedded in, and surrounded by, the cementitious materials of the engineered barrier. Current safety analysis is based on the assumption that HCP is the only sorbent in the near-field retarding the release of radionuclides (~ 14% of solid materials in the near-field). Hence, the barrier function of HCP in addition to impacts that could change the sorption properties of HCP have to be assessed adequately. The interaction of products resulting from the anoxic corrosion of iron and steel could have an adverse effect on the sorption properties of HCP. In the following sections, an attempt is made to assess the effect of the interaction of Fe(II,III) with C-S-H phases on radionuclide uptake by these phases (sorption competition). In addition to the effect of the presence of Fe(II,III), the presence of stable isotopes of the radionuclides considered for sorption competition in the cementitious near-field is also taken into account. It is assumed that C-S-H phases are largely responsible for the retention of metal cations by HCP.

B.2 Conceptual approach

The proposed approach aims at estimating the maximum loading of C-S-H phases with Fe(II,III) corrosion products and other metal cations present in the near-field and comparing this loading with the maximum sorption capacity of C-S-H phases under near-field conditions. With this approach, it is possible to assess whether or not sorption competition could influence retention of cationic radionuclides in the cementitious near-field of an L/ILW repository. The stepwise procedure is structured as follows:

1. define near-field parameters (App. B.3)
2. assess the potential and relevance of sorption competition on the various cement phases of HCP and for the radionuclides to be considered in the safety analysis for SGT-E3 (App. B.4)
3. outline the effect of Fe(II,III) uptake by C-S-H phases on sorption competition (App. B.5 and App. B.6)
4. estimate the maximum loadings of radionuclides on C-S-H phases (App. B.7)
5. compare radionuclide loadings with the sorption capacity of C-S-H phases (App. B.8)
6. conclude on an appraisal of sorption competition in the cementitious near-field of an L/ILW repository (App. B.9)

The current approach considers sorption competition on C-S-H phases, the most important sorbent for radionuclides in the cementitious near-field. The assessment of sorption competition is generally based on conservative estimates of those parameters required to estimate the maximum loading of the C-S-H phases. It should be noted that the current approach represents a gross simplification of the real near-field system and therefore constitutes a highly conservative overall view. For example, we do not consider additional sorbents for metal cations that can be expected in the cementitious near-field, such as iron corrosion products as well as cement phases present in smaller amounts (e.g., hydrotalcite, calcite) and products resulting from cement alteration (e.g., zeolites). These minerals also expose surface sites capable of coordinating metal cations (e.g., actinides), thereby reducing the cation loading of the C-S-H phases. Nevertheless, quantification of the sorption capacity in the real system is currently hardly possible due to the lack of quantitative information on the uptake of metal cations and anions by potential candidate minerals.

B.3 Near-field parameters

Information on the specific near-field parameters is required to carry out the following estimates of the radionuclide or metal cation loadings, respectively, on C-S-H phases in conditions relevant to a cementitious near-field. The near-field parameters have been derived based on the tentative design of the L/ILW repository (Kosakowski et al. 2023).

Tab. B-1: Characteristic parameters of the L/ILW repository

Kosakowski et al. (2023)

Parameter	**Notation**	**Value**
Average porosity [-]	ε	0.2
Mass of sorption-effective cement matrix [kg/m^3]	m_{cem}	350
Parameter (estimated)	**Notation**	**Value**
Total volume [m^3/m]	V_{tot}	144
Total volume of solution* [m^3/m]	V_{sol}	29
Volume of solid material** [m^3/m]	V_{solid}	115
Mass of solid material*** [kg/m]	M_{solid}	$2.88 \cdot 10^5$
Mass of sorption-effective cement matrix [kg/m]	M_{cem}	$4.02 \cdot 10^4$
Percentage of cement matrix of solid material [%]		13.9
Volume near-field porewater [m^3/m^3]	V_{sol}	0.2
Solid-to-liquid ratio for cement matrix [kg/m^3]	S/L	1,386

* $V_{sol} = \varepsilon V_{tot}$

** $V_{solid} = (1-\varepsilon)V_{tot}$

*** The average dry density is estimated at $2.5 \cdot 10^3$ kg/m^3 using the parameters given for the operational and decommissioning waste types in MIRAM 14 (Nagra 2014) and used for the modelling by Wieland et al. (2018).

The volume per metre of emplacement cavern is 144 m^3/m based on the description of the dead-end caverns in NTB 23-03 (Kosakowski et al. 2023) (internal width = ~ 11.5 m, height = 12.5 m. $11.5 \times 12.5 = 143.75$ m^3/m). The average porosity amounts to 20 volume percentage (vol.-%); the volume of solid materials corresponds to 115 m^3/m (Tab. B-1). The total mass of the sorption-effective cement matrix amounts to 13.9 wt.% of the total mass of solid material per metre of cavern length. HCP is considered the only sorbing material for radionuclides in the near-field of an L/ILW repository and accounts for less than 20 wt.% of the solid material disposed of in the cavern. The proportion of HCP seems plausible and therefore the amount of 350 kg/m^3 sorption-effective HCP is used for the assessment of sorption competition (Tab. B-1). The volume of near-field porewater amounts to 0.2 m^3 per m^3 cavern volume. The ratio of the two latter parameters results in an S/L ratio of the sorption-effective HCP of 1.39 kg/dm^3.

B.4 Cement phases and radionuclides involved

The uptake of metal cations and anions by HCP has to be assessed with a view to the radionuclides (species-sensitive) and the mineral phases involved (e.g., reviews by Cornelis et al. 2008, Evans 2008, Gougar et al. 1996). For this reason, assessment of the uptake process in the different stages of cement degradation and disturbances of the uptake process on HCP need to be discussed in terms of the dose-relevant radionuclides involved and those individual cement minerals with the potential to immobilise these radionuclides. This conceptual view has been applied in conjunction with the assessment of sorption competition on HCP.

i.) Calcium silicate hydrates (C-S-H)

C-S-H phases are the most abundant cement phase of HCP and have favourable sorption properties (e.g., high surface area and high sorption site densities (e.g., Churakov et al. 2014, Labbez et al. 2006, Ochs et al. 2016)). Therefore, they are among the most important sorbing materials present in the near-field of an L/ILW repository. Furthermore, C-S-H phases are among the most thermodynamically stable cement phases. They are found to persist in an evolving cementitious near-field over a very long period of time (e.g., Atkinson et al. 1987, Berner 1992, Wang et al. 2012, Kosakowski et al. 2014). The content of C-S-H phases in the HCP present in the L/ILW repository was estimated to vary between ~ 33 wt.% (DS-I) and ~ 67 wt.% (DS-III) (Tab. 2-3).

C-S-H phases are predominantly amorphous in nature with a high surface area (~ 148 m^2/g; Tits et al. 2006b, 192 $m^2/g \leq$ surface area $\leq$ 332 m^2/g, Suda et al. 2015), while the presence of microcrystalline domains cannot be excluded. The structure of amorphous C-S-H phases is related to 14-Å tobermorite, a crystalline C-S-H mineral with a low C/S ratio, and jennite, a crystalline C-S-H mineral with a high C/S ratio. C-S-H phases have a layered structure with central Ca-O layers and Si atoms arranged in “Dreierketten” sheets as structure building units (Fig. B-1). The oxygen atoms of the sevenfold coordinated calcium atoms of the CaO layers are thereby coordinated to silica atoms of the “Dreierketten” chains. The latter formation corresponds to silica dimers connected by bridging silica tetrahedra on both sides of the CaO_2 layers (e.g., Bonaccorsi et al. 2005, Chen et al. 2004, Richardson 2004).

The C/S ratio of the C-S-H phases varies between 1.5 (Fig. B-1a) and 0.66 (Fig. B-1b). These changes are attributable to progressive replacement of the interlayer protons neutralising the negative charges on the bridging Si tetrahedra by interlayer Ca^{2+} ions (e.g., Bonaccorsi et al. 2005, Nonat 2004, Richardson 2004). The C-S-H phases with a C/S ratio above 1.5 are envisaged either as a defect tobermorite-like structure interstratified with layers of $Ca(OH)_2$ or as a tobermorite-like structure intermixed with a jennite-like structure (Chen et al. 2004, Richardson 2004). Jennite is a layered crystalline C-S-H phase consisting of edge-sharing Ca octahedra and “Dreierketten” silica chains but at a much higher C/S ratio due to the presence of Ca-OH groups in the structure (Bonaccorsi et al. 2004, Richardson 2004).

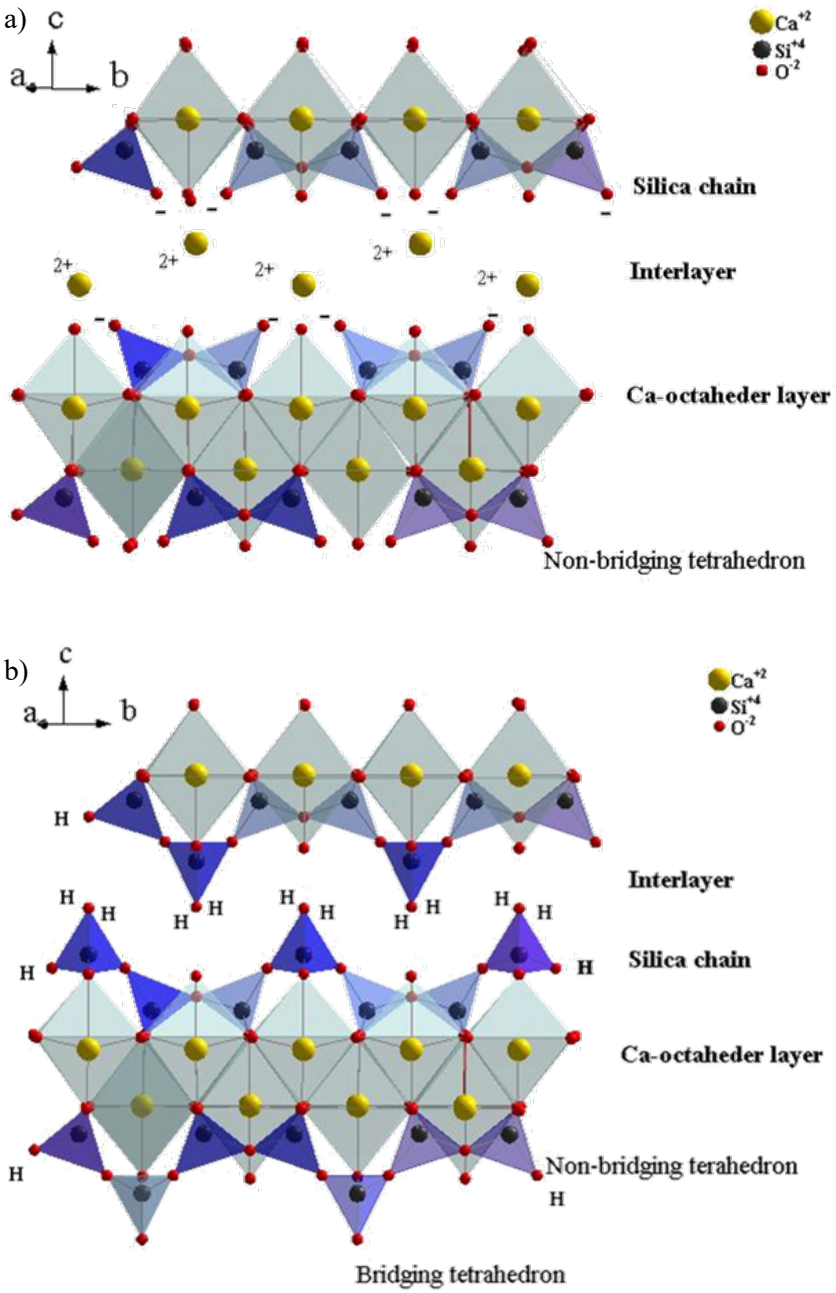

Fig. B-1: a) Schematic diagram of the tobermorite-based structure of a C-S-H phase with a C/S ratio of 1.5 obtained by removing the bridging tetrahedra and neutralising the negative charges of the silanol groups by Ca^{2+} ions. b) Schematic diagram of the tobermorite-based structure of a C-S-H phase with a C/S ratio of 0.66 and a maximum degree of protonation of the silica chains

Adapted from Richardson (2004) and modified from Tits et al. (2014a)

The uptake of metal cations by C-S-H phases is well documented (see, e.g., reviews by Cornelis et al. 2008, Evans 2008, Gougar et al. 1996, Ochs et al. 2016, Tits & Wieland 2018). Adsorption on the surface of C-S-H phases may often be an intermediate step in the uptake of metal cations by C-S-H phases. Nevertheless, there is ample evidence that metal cations can also be taken up into the structure of C-S-H phases (e.g., Cocke & Mollah 1993, Gaona et al. 2011, Glasser 1992, Mandaliev et al. 2011). In recent years, advanced spectroscopic techniques (e.g., synchrotron-based spectroscopy, laser-induced luminescence spectroscopy) have been increasingly used to develop a mechanistic picture of the uptake of metal cations by cementitious materials. To this end, the local coordination environment of metal cations by cementitious systems has been explored, thus allowing the type and number of neighbouring atoms as well as bond distances to be determined. The latter information is essential towards the aim of differentiating between adsorption and absorption processes (e.g., Gaona et al. 2011, Scheidegger et al. 2000, Tits et al. 2003, 2011, 2015, Vespa et al. 2006).

Uptake of anions into the C-S-H structure seems to be less important despite evidence suggesting that silicate substitution by chromate and arsenate could occur in C-S-H phases (Cornelis et al. 2008 and references therein).

ii.) Ettringite (AFt) and AFm phases

Ettringite, a calcium aluminate mineral, is the common AFt (Al_2O_3-Fe_2O_3-tri) phase in hydrated cement (Taylor 1997). Ettringite forms hexagonal prismatic or acicular crystals. Columns consisting of $Al(OH)_3$ octahedra alternating with triangular groups of edge-sharing CaO_8 polyhedra and columns occupied by SO_4^{2-} and H_2O molecules account for the main structural features. Incorporation of oxyanions, such as arsenate, chromate, selenate, selenite, etc., is the dominant retention process owing to partial or even full replacement of SO_4^{2-}. By contrast, adsorption of anions on the AFt surface is less likely due to the net negative surface charge of ettringite (Cornelis et al. 2008 and references therein). No evidence has been provided to indicate strong interaction of single-charged anions, such as chloride and iodide, with ettringite. Incorporation of monovalent anions is limited by the coordinative constraints imposed by the column structure of AFt.

AFm (Al_2O_3-Fe_2O_3-mono) phases, so-called hydrocalumites, naturally form under hydrothermal conditions. AFm phases belong to the family of layered double hydroxides (LDH). The minerals form flaky, hexagonal crystals in hydrated cement. However, they are often poorly crystalline. The AFm structure consists of positively charged structural units with the composition $[Ca_2(Al,Fe)OH)_6 \cdot 2H_2O]^+$. The overall positive structural charge of the octahedral layers is compensated by anions, which are bound in the interlayer space between two adjacent layers. Hence, the cavities formed in the interlayer space allow anionic contaminants to be accommodated. These cavities are often surrounded by three water molecules. AFm phases containing different types of anions in the interlayer are readily formed when the structure-forming ions are mixed in the appropriate stoichiometric amounts.

Overall, AFt and AFm phases have a stronger tendency to bind anions than C-S-H phases. Replacement of SO_4^{2-} by other two-fold negatively charged anions in the case of AFt and absorption of single and double negatively charged anions in the interlayer of AFm phases are considered to be the main processes immobilising anions in HCP, provided that the two cement phases are present in HCP. Adsorption of anions on the surfaces of AFt, AFm and C-S-H phases is unlikely to occur due to the dominance of negatively charged surface sites in the pH range 10 to 13.3, thus repelling the anions. However, locally isolated positively charged surface sites can cause weak anion adsorption, while the extent of surface sorption is expected to be small.

iii.) Relevance of sorption competition

Sorption competition on HCP in the cementitious near-field of an L/ILW repository is based on the notion that stable element impurities originating from the cementitious material and the waste could be important competitors to radionuclide uptake by HCP. Among these competitors, Fe(II) and Fe(III) could play an important role as they are produced in significant quantities over the course iron and steel corrosion in the L/ILW repository. Magnetite (Fe_3O_4) is the main iron phase produced during the anoxic corrosion of iron and steel (e.g., Wersin et al. 2003). Anoxic conditions are expected to prevail during the period under consideration for an L/ILW repository. Fe(II) and Fe(III) species are thus the soluble iron species in equilibrium with magnetite. In the following section, both oxidation states of iron are shown to interact with cement phases.

B.5 Interaction of corrosion products with C-S-H phases

i.) Fe(III) interaction with cement phases

Fe(III) was found to replace Al(III) in Al-containing cement phases, such as ettringite and AFm phases (e.g., Möschner et al. 2008, 2009, Dilnesa et al. 2011, 2012, 2014a, 2014b). Identical Fe(III)- and Al(III)-containing phases even form solid solutions, indicating a structural similarity of the Fe(III)- and Al(III)-containing end-members. For this reason, it is inferred that replacing Al(III) with Fe(III) in ettringite and AFm phases does not result in major structural changes and therefore has no impact on the uptake of anions by these cement phases. A recent study showed that Fe(III) is taken up by C-S-H phases (Mancini et al. 2020) as previously reported for Al(III)-forming C-A-S-H phases (L'Hôpital et al. 2016 2016, Barzgar et al. 2020). Fe(III) sorption on C-S-H phases was found to be significantly stronger than Al(III) sorption (Mancini et al. 2020). Furthermore, the effect of pH on Fe(III) uptake by C-S-H phases was found to be negligibly small or even absent as the sorption data for C-S-H phases with target C/S ratios of 0.8 and 1.5 agreed within the experimental uncertainty (Fig. B-2). This finding indicates that neither the C-S-H composition nor the pH (i.e., iron speciation) have any notable effect on Fe sorption, or that their effects counteract and compensate each other. Nonetheless, the finding suggests that, in addition to surface complexation, other uptake mechanisms may be important in the case of Fe(III). The effects of pH and Ca on Al(III) and Fe(III) uptake was found to be different, which suggests that Fe(III) is subject to a different binding mechanism in C-S-H as compared to Al(III). Al(III) is known to coordinate tetrahedrally and replace Si(IV) at the bridging positions of the "Dreierketten" silica chains. The extent of Fe(III) uptake, however, does not seem to depend strongly on the C/S ratio and, accordingly, not on the C-S-H structure (Fig. B-2).

Sorption isotherms of Fe(III) were determined on C-S-H phases with target C/S ratios of 0.8 and 1.5 (Fig. B-2). The sorption behaviour of Fe(III) was linear over the entire aqueous Fe concentration range for both C-S-H phases (slope = 1). In contrast to sorption onto TiO_2, Fe(III), uptake by C-S-H phases linearly increased over the entire investigated Fe(III) concentration range, implying that microcrystalline $Fe(OH)_3$ was not a solubility-limiting phase in these systems (Mancini et al. 2020). Precipitation of amorphous $Fe(OH)_3$(am) occurred at higher Fe concentrations in the C-S-H systems as indicated by EXAFS spectroscopy (Mancini et al. 2020). Presence of $Fe(OH)_3$(am) was observed at high Fe(III) loadings above 12,000 ppm for all C-S-H phases (C/S ratios = 0.8, 1.2 and 1.5) (Mancini et al. 2020).

For the assessment of sorption competition, we assume a K_d of 700 m^3/kg for Fe(III) sorption on C-S-H phases irrespective of the C/S ratio as reported elsewhere (Mancini et al. 2020). The maximum sorption capacity of Fe(III) is assumed to be the same for all C-S-H phases irrespective of the C/S ratio (= 0.70 mol/kg C-S-H; Fig. B-2). Furthermore, it is assumed that the maximum Fe(III) loading is reached at an aqueous Fe(III) concentration of ~ 10^{-6} M (Fig. B-2). Note, however, that the aqueous Fe(III) concentration in the cementitious near-field might be significantly lower due to solubility control by magnetite (Berner 2003, Wersin et al. 2003, Hummel et al. 2022). It should also be noted that Wersin et al. (2003) assumed 10^{-7} M as the maximum Fe(III) concentration in near-field porewater.

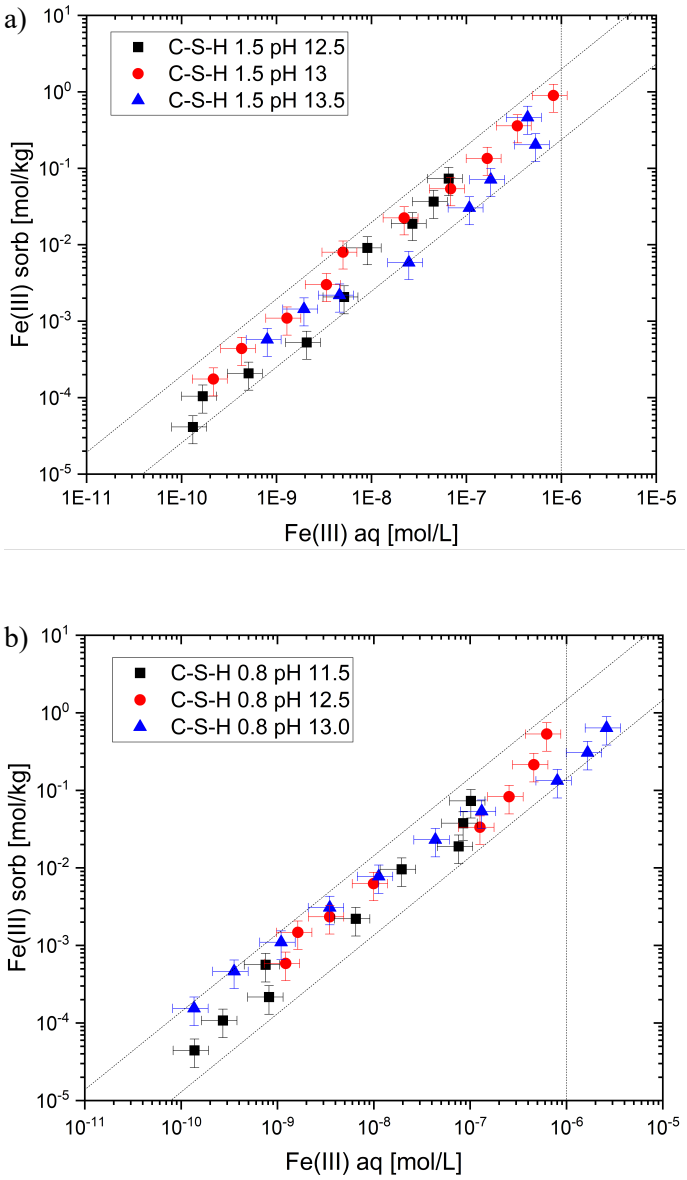

Fig. B-2: Sorption isotherms of Fe(III) on C-S-H with a target C/S ratio of 1.5 (a), and C-S-H with a target C/S ratio of 0.8 (b). The experimental data correspond to linear sorption

Mancini et al. (2020) further showed that Fe(III) coordination occurs in the interlayer of the C-S-H samples with target C/S ratios of 1.2 and 1.5. The proposed structural model was based on the structural parameters deduced from EXAFS spectroscopy and additional evidence by the ^{29}Si NMR data. The large number of neighbouring atoms of Fe(III) derived from EXAFS spectroscopy was interpreted in terms of coordination of Fe(III) in the interlayer rather than formation of Fe(III) species adsorbed on the C-S-H surface. Atomic distances and numbers of neighbouring atoms indicated that Fe(III) is directly bonded to Si tetrahedra of the "Dreierketten" silica chains adjacent to the interlayer space. The ^{29}Si NMR results further showed that Fe in C-S-H phases is directly connected to the silica chain (Mancini et al. 2020).

Identification of the interlayer position of Fe(III) further suggests that Fe(III) substitutes Ca coordinated to non-bridging Si tetrahedral in the interlayer of C-S-H phases.

Interpretation of Fe(III) coordination to C-S-H phases with a low C/S ratio was found to be more challenging based on the available EXAFS spectroscopy data and in combination with evidence from ^{29}Si NMR. The observed ^{29}Si NMR parameters, i.e., variations in centre-band linewidth, spinning sideband intensity, signal reduction (I/I0) and spin-lattice relaxation times, support a structural model of Fe(III) binding at a low C/S ratio, where Fe(III) is predominantly bonded to the surface of the C-S-H particles or present as clusters/separate particles, respectively, on the C-S-H surface (Mancini et al. 2020). Hence, the ^{29}Si NMR data did not support interlayer bonding of Fe(III) by C-S-H phases at a low C/S ratio. This conclusion was further supported by EXAFS spectroscopy. The EXAFS spectra could not be fitted with the same structural models used for the multi-shell fitting of the EXAFS data of the C-S-H phases with target C/S ratios of 1.2 and 1.5.

About four neighbouring Si atoms were determined at a distance of $R_{Fe\text{-}Si}$ of ~ 3.15 Å ± 0.07 and about three Ca atoms at $R_{Fe\text{-}Ca}$ of ~ 3.19 Å ± 0.05 in the case of the C-S-H phase with a target C/S ratio of 0.8. A third backscattering contribution resulted from two Fe(III) atoms located at a distance of $R_{Fe\text{-}Fe}$ ~ 3.34 Å ± 0.05. For the C-S-H phase with a low C/S ratio of 0.8, significant Fe(III) uptake by the interlayer can be excluded on the basis of the ^{29}Si NMR data. The model provided by the multi-shell fit of the EXAFS spectrum, however, supports the idea of the formation of a secondary phase or clusters on the surface of the C-S-H phase. Thus, for the current assessment of sorption competition, it is assumed that Fe(III) forms a separate secondary Ca-Si-rich phase (or clusters) on the surface of C-S-H phases with a low C/S ratio.

The current assessment of sorption competition is based on the following assumptions regarding Fe(III) uptake by C-S-H phases:

- K_d = 700 m^3/kg C-S-H for Fe(III) uptake by C-S-H phases (K_d = 350 m^3/kg HCP) and a maximum site occupancy of 0.70 mol/kg C-S-H for all C-S-H phases irrespective of the C/S ratio (= 0.35 mol/kg HCP). Maximum Fe(III) loading is achieved at an aqueous Fe(III) concentration between 10^{-6} M (Fig. 2) and 10^{-7} M (Wersin et al. 2003, Hummel et al. 2022) (see App. B-7).
- Fe(III) is preferentially taken up by the interlayer of C-S-H phases with a high C/S ratio (> 1) where it preferentially coordinates to non-bridging Si tetrahedra, substituting Ca and competing with dose-relevant, interlayer-bound radionuclides for sorption.
- Fe(III) is bonded on the surface of C-S-H phases with a low C/S ratio (< 1) where it coordinates to surface Si sites and competes with other dose-relevant, surface-bound radionuclides for sorption.
- Sorption competition between Fe(III) and dose-relevant radionuclides is only relevant to cationic species and can be ignored in the case of the uptake of anionic species by HCP.

ii.) Fe(II) interaction with cement phases

Mancini et al. (2021) investigated the interaction of Fe(II) with C-S-H phases (target C/S ratios = 0.8 and 1.5). The authors carried out co-precipitation experiments to explore to what extent Fe(II) can replace Ca(II) in C-S-H phases. To this end, C-S-H phases were synthesised by replacing a portion of CaO by FeO (10 mol%). The authors observed limited Fe(II)-Ca(II) replacement. About 2% Ca (on a mol basis) at best was replaced by Fe(II) as determined by linear combination fitting of the X-ray absorption near-edge spectroscopy (XANES) data. The replacement resulted in low Fe:Si ratios of ~ 0.02 in C-S-H 0.8 and ~ 0.05 in C-S-H 1.5. XRD of the phases further showed an increase in the basal spacing, i.e., a shift of the first peak at $2\theta \sim 9°$-$10°$ to lower values for both C-S-H phases. Hence, the assumption of interlayer binding of Fe(II) made in the current assessment is based on the evidence provided by XRD. The observed increase in the basal spacing has to be interpreted in terms of Fe(II) uptake into the interlayer.

Mancini et al. (2021) also investigated Fe(II)-loaded C-S-H phases by employing EXAFS spectroscopy. These investigations revealed the absence of $Fe(OH)_2(s)$ in the Fe(II) concentration range of the linear sorption isotherm of Fe(II) on the C-S-H phases, thus suggesting that precipitation of $Fe(OH)_2$ occurs only at Fe(II) loadings above 0.1 mol/kg. Hence, it is assumed that this Fe(II) loading corresponds to the maximum capacity that Fe(II) occupies in C-S-H phases. Furthermore, the same maximum Fe(II) loading has been assigned to C-S-H phases irrespective of their C/S ratio. Eventually, the maximum Fe(II) loading corresponds to an aqueous Fe(II) concentration of ~ 10^{-3} M (Fig. B-3). Note, however, that the aqueous Fe(II) concentration in the cementitious near-field might be significantly lower and depend on the type of Fe-containing solids used to estimate the Fe(II)-Fe(III) redox buffer (Wersin et al. 2003).

The wet chemistry measurements showed that Fe(II) sorption onto C-S-H phases is linear in the aqueous Fe(II) concentration range up to 10^{-3} M (Fig. B-3). $Fe(OH)_2(s)$ did not precipitate in the Fe(II) concentration range covered by the sorption isotherm, thus limiting the solubility of Fe(II), while precipitation cannot be excluded above aqueous Fe(II) concentrations of 10^{-3} M. The isotherm measurements further suggest that Fe(II) sorption does not depend on the pH or on the C/S ratio of C-S-H phases, respectively, in the pH range between 11.5 and 12.5, as the sorption data agree within the experimental uncertainty. Thus, the composition of a C-S-H phase (C/S ratio) and pH has no measurable effect on the uptake of Fe(II), although a reduction in Fe(II) uptake at a higher pH is expected due to the increasing concentration of the hydrolysis product $Fe(OH)_3^-$. The uptake of Fe(II) by C-S-H phases is much weaker compared to Fe(III) on the same C-S-H phases, resulting in a difference in the sorption value (K_d) of the two oxidation states of Fe by more than three orders of magnitude.

The spectroscopic investigations showed that Fe(II) is coordinated in octahedral geometry (i.e., 6 oxygen neighbours). Furthermore, Fe(II) was found to have a large number of neighbouring Ca (~ 2 and ~ 4 in C-S-H 0.8 and 1.5, respectively) and Si atoms (~ 4 and ~ 2 in C-S-H 0.8 and 1.5, respectively). This finding supports the idea that Fe(II) is bound either to surface sites of C-S-H or in the interlayer. Note that the number of neighbouring atoms would be significantly higher, i.e., typically resulting in ~ 10 neighbouring Ca and Si atoms as previously determined for Fe(III) in C-S-H phases (Mancini et al. 2020), if Fe(II) were taken up solely into the interlayer. The structural data derived from EXAFS spectroscopy also indicate that Fe(II) does not form solely mono- or bidentate Fe(II) surface complexes typically observed on stable oxide surfaces (e.g. oxides, clays) for which a maximum number of three neighbouring atoms (Ca + Si + O) is anticipated. For the current assessment, it is assumed that Fe(II) uptake occurs both by adsorption on the outer surface of the C-S-H phases and in the interlayer in a manner similar to Fe(III) bonding.

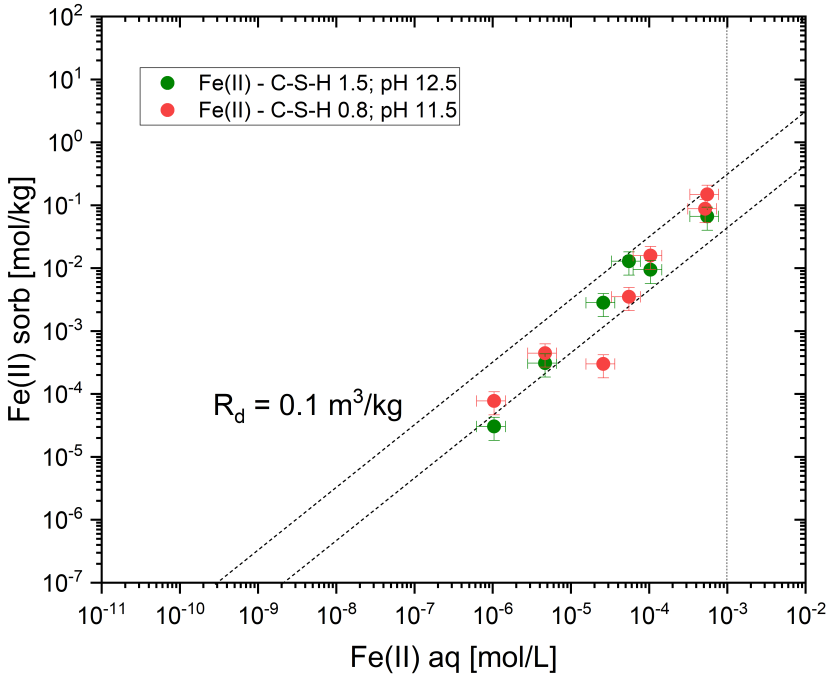

Fig. B-3: Fe(II) sorption isotherms on C-S-H phases (target C/S ratios = 0.8 and 1.5)

The experimental study of Mancini et al. (2021) shows that Fe(II) bonding in the interlayer cannot be the only mechanism of Fe(II) interaction with the C-S-H phases in the short-term sorption samples studied by EXAFS spectroscopy (i.e., up to 14 days equilibration), while the XRD data of the co-precipitation samples indicated an uptake into the interlayer. However, the presence of equal proportions of surface-bound and interlayer-bound Fe(II) species cannot be excluded on the basis of the EXAFS data. It should be noted that an alternative structure model allowing for a total of ~ 6 (Ca + Si) neighbours can be proposed based on Fe(II) incorporation into the near-surface structure, provided that the EXAFS spectra can be assigned to a single Fe(II) species. Presence of a single Fe(II) species is supported by linear sorption indicating that all sites have the same affinity towards Fe(II) binding. Nevertheless, this alternative structural model is not in line with the XRD data. In summary, the most plausible interpretation of the above findings from XRD, spectroscopy and wet chemistry is as follows: i) Fe(II) is bonded both on the surface (formation of surface complexes) and in the interlayer at about equal quantities, ii) both sites, i.e., surface and interlayer sites, have similar affinities for Fe(II). This assumption is supported by the large number of neighbouring atoms (~ 6 in total (Ca + Si)) of Fe(II) in C-S-H and the evidence for interlayer binding provided by XRD.

The current assessment of sorption competition is based on the following assumptions regarding Fe(II) uptake by C-S-H phases:

- K_d = 0.1 m³/kg C-S-H for Fe(II) uptake by C-S-H phases (K_d = 0.05 m³/kg HCP) and a maximum site occupancy of 0.1 mol/kg C-S-H for all C-S-H phases irrespective of the C/S ratio (= 0.05 mol/kg HCP).
- 50% of Fe(II) is bound on the surface of C-S-H phases (= 0.05 mol/kg C-S-H) while 50% is bound in the interlayer (= 0.05 mol/kg C-S-H).
- Maximum Fe(II) loading at an aqueous Fe(II) concentration of ~ 10^{-3} M (Fig. B-3) and 10^{-7} M (Wersin et al. 2003, Hummel et al. 2022) (see App. B.7).

B.6 Sorption competition of Fe(II,III) with dose-relevant radionuclides

In the current approach, we assess sorption competition in terms of maximum loadings estimated for the corrosion products Fe(II,III) and dose-relevant radionuclides in the interlayer and surface sites of C-S-H phases. To this end, preferential sorption sites must be assigned to each radionuclide considered.

i.) Radionuclides not subjected to sorption competition with Fe(II,III)

For the current assessment, it is assumed that sorption competition by Fe(II,III) has no effect on those dose-relevant radionuclides that are retarded by HCP in terms of an isotopic exchange mechanism, such as:

Al, Ca, $^{14}CO_3^{2-}$, Ni, Si

For the current assessment, it is further assumed that sorption competition by Fe(II,III) has no effect on the uptake of anionic, dose-relevant radionuclides, such as:

Cl, Se, Mo, Tc, I, ^{14}C-bearing organic compounds

ii.) Radionuclides subjected to sorption competition with Fe(II,III)

Sorption competition is taken into account for those cationic, dose-relevant radionuclides that could be taken up by C-S-H phases in all stages of cement degradation and include:

Ac, Ag, Am, Cf, Cm, Cs, Eu, Hg, Ho, Nb, Ni, Np, Pa, Pb, Po, Pu, Ra, Sn, Sr, Th, Ti, U, Zr

Spectroscopic studies have provided structural information on the uptake mechanism of some of the cationic, dose-relevant radionuclides listed above by C-S-H phases. Lanthanides and trivalent actinides, such as Cm(III) and Eu(III), can replace Ca(II) in C-S-H phases (e.g., Tits et al. 2003, Stumpf et al. 2004, Mandaliev et al. 2011, Wolter et al. 2019a). This finding implies the possibility of Ca replacement by lanthanides and trivalent actinides in the interlayer and the CaO layer of C-S-H phases. For the current assessment, sorption competition does not apply to the CaO layer of C-S-H phases because there is no evidence that Ca replacement by either Fe(II) or Fe(III) occurs in this layer. Spectroscopic studies further showed that Np(IV) is accommodated in the interlayer of C-S-H phases in a manner similar to that of Fe(III) (Gaona et al. 2011). This may also apply to other tetravalent actinides, such as U(IV) and Pu(IV), however, experimental evidence is presently lacking. The current assessment is thus based on the spectroscopic evidence that sorption competition between Fe(III) and lanthanides (Ln(III)) as well as tri- and tetravalent actinides (An(III, IV)) may occur in the interlayer of C-S-H phases. Sorption competition in the interlayer is further assumed for other tetra-, penta- and hexavalent metal cations, also including the actinides such as:

Nb(V), Np(V,VI), Pa(V), Pu(V,VI), Sn(IV), Ti(IV), U(V,VI) and Zr(IV)

The remaining dose-relevant radionuclides (Ag, Cs, Hg, Ni, Pb, Ra, Sr) are assumed to sorb only on the surfaces of the C-S-H particles, such as in the case of Sr and Ra (Tits et al. 2006, 2006b, Wieland et al. 2008) as well as Ni (Missana et al. 2022) and Pb (Rose et al. 2000, Ochs et al.

2002a). There is experimental evidence to suggest interlayer binding of Cs and other alkalis in C-(A)-S-H phases (Hong & Glasser 1999, 2002, Iwaida et al. 2002, L'Hôpital et al. 2016, 2016). Nevertheless, on the basis of sorption values, it is expected that bonding of Cs and alkalis uptake in the interlayer is weaker than that of Fe(II,III) and in particular also the lanthanides and actinides. This suggests that Cs and the alkalis are not able to compete with the latter metal cations for uptake into the interlayer.

iii.) Sorption competition in the different stages of cement degradation

Sorption competition is assessed for the different stages of cement degradation (DS-I through DS-III). In these stages, C-S-H phases with different C/S ratios dominate.

1. DS-I (pH > 12.5)

C-S-H phases with a C/S ratio of ~ 1.6 dominate in this stage of cement degradation. Fe(III) preferentially occupies interlayer sites, while Fe(II) is equally distributed among surface and interlayer sites (50%). The following modes of sorption competition are considered, including the radionuclides that compete for the same type of sites:

Interlayer sites: Fe(II,III), Ac, Am, Cf, Cm, Eu, Ho, Nb, Np, Pa, Po, Pu, Sn, Th, Ti, U, Zr

Surface sites: Fe(II), Ag, Cs, Hg, Ni, Pb, Ra, Sr

2. DS-II (pH ~ 12 – 12.5)

C-S-H phases with a C/S ratio of ~ 1.6 dominate in this stage of cement degradation. Also in this degradation stage, it is assumed that Fe(III) preferentially occupies interlayer sites, while Fe(II) is equally distributed among surface and interlayer sites (50%). The following modes of sorption competition are considered, including the radionuclides that compete for the same type of sites:

Interlayer sites: Fe(II,III), Ac, Am, Cf, Cm, Eu, Ho, Nb, Np, Pa, Po, Pu, Sn, Th, Ti, U, Zr

Surface sites: Fe(II), Ag, Cs, Hg, Ni, Pb, Ra, Sr

3. DS-III (pH < 12)

C-S-H phases with a C/S ratio between 0.7 and 1.1 dominate in this stage of cement degradation. Fe(III) preferentially occupies surface sites, while Fe(II) is equally distributed among surface and interlayer sites (50%). The following modes of sorption competition are considered, including the radionuclides that compete for the same type of sites.

Interlayer sites: Fe(II), Ac, Am, Cf, Cm, Eu, Ho, Nb, Np, Pa, Po, Pu, Sn, Th, Ti, U, Zr

Surface sites: Fe(II,III), Ag, Cs, Hg, Ni, Pb, Ra, Sr

B.7 Maximum loadings of dose-relevant radionuclides and stable isotopes

i.) Inventories and porewater concentrations

Maximum loadings were estimated based on the inventories of the stable isotopes of the element in HCP (Tab. B-2) or based on the porewater concentrations determined by solubility for those radionuclides for which no inventories have been reported, respectively (Tab. B-3). The solubility limits of radionuclides in the cementitious near-field were assessed based on thermodynamic calculations or expert judgement.

The maximum loadings of Fe(II,III) on C-S-H phases are known from measurements of the sorption isotherm and the solubility of Fe(II,III)-hydroxides in C-S-H systems (see Section B.3 to B.5; Fig. B-2 and Fig. B-3). For example, the maximum Fe(III) loading is reached at an aqueous Fe(III) concentration of 10^{-6} M (Fig. B-2). Accordingly, the maximum Fe(II) loading occurs at an aqueous Fe(II) concentration of 10^{-3} M Fe(II) (Fig. B-3). Precipitation of $Fe(OH)_2$ and $Fe(OH)_3$ is thus anticipated above these threshold concentrations.

Nevertheless, solubility limitation of the Fe(II,III) concentrations may be different under the conditions of the cementitious near-field. In the near-field situation, the Fe(II,III) concentrations are controlled by redox conditions in the anoxic state of the chemically heterogeneous near-field of the L/ILW repository (Wersin et al. 2003). The redox conditions will be affected by thermodynamic and kinetic factors, which are determined by the in-situ conditions, e.g., reactivity of waste forms, porewater compositions, etc.

In general, it is anticipated that redox conditions in the near-field are mainly controlled by steel corrosion due to the large inventory of iron and steel in the repository. The uncertainty of redox conditions results from the limited knowledge about the redox-active Fe(II,III)-containing compounds present in the course of the evolution of the cementitious near-field. Hummel et al. (2022) calculated solubility limits for Fe under anoxic (reducing) conditions equal to $3.2 \cdot 10^{-8}$ M (DS-I), $2.6 \cdot 10^{-8}$ M (DS-II) and $1.5 \cdot 10^{-9}$ M (DS-III). For the current assessment, we consider this Fe(II,III) concentration in addition to the maximum concentrations derived from the sorption isotherm measurements (Fig. B-2 and Fig. B-3). For this reason, two values are reported for the maximum Fe(II,III) loadings on C-S-H phases. They are listed in Tab. B-4 to Tab. B-6.

The maximum loadings by those radionuclides competing with Fe(II,III) for uptake by C-S-H phases, i.e., the radionuclides listed in Tab. B-2 and Tab. B-3, were estimated in two different ways, depending on the information that was available for a radionuclide.

On the one hand, maximum loadings of radionuclides were estimated based on the inventories of the stable counterparts of the radionuclides in the near-field of the L/ILW repository. The inventories of the stable isotope of a radionuclide associated with the various components in the near-field, such as the waste matrices (e.g., metallic waste materials, cement and aggregates used for the various applications in the disposal cavern, etc.) may be orders of magnitude larger than the inventories of the radionuclides associated with waste materials. As a result, only very low radionuclide concentrations are expected in the porewater of the cementitious near-field of the L/ILW repository (Bradbury & Sarott 1994), and therefore porewater concentrations of radionuclides may be controlled by the presence of stable isotope counterparts in the near-field rather than the radionuclide inventories themselves. Hence, knowledge of the inventories of stable elements in the near-field is imperative. For the current assessment of sorption competition, we assume that HCP is the main source of the stable isotopes of an element. The contents of the radionuclides in unhydrated cement are listed in Tab. B-2 (second column).

Tab. B-2: Concentrations of the stable counterparts of radionuclides present as impurities in unhydrated (Wieland 2014) and hydrated CEM I 52.5 N HTS and the porewater assuming DS-II, reducing conditions

Element	**Unhydrated cement concentration*** [ppm]	**HCP concentration**** [mol/kg]	**R_d value***** [m^3/kg HCP]	**Porewater concentration estimated based on inventory** [mol/L]	**Solubility-limited porewater concentration****** [mol/L]
Ac	-		100		$7.9 \cdot 10^{-11}$
Ag	-		$1.0 \cdot 10^{-4}$		$3.9 \cdot 10^{-7}$
Am	-		100		$5.2 \cdot 10^{-10}$
Cm	-		100		$1.0 \cdot 10^{-9}$
Cs	1.23	$7.1 \cdot 10^{-6}$	$1.0 \cdot 10^{-3}$	$5.9 \cdot 10^{-6}$	Unlimited
Eu	0.40	$2.0 \cdot 10^{-6}$	100	$2.6 \cdot 10^{-11}$	$5.8 \cdot 10^{-9}$
Hg	-		$1.0 \cdot 10^{-4}$		$3.4 \cdot 10^{-7}$
Ho	0.35	$1.6 \cdot 10^{-6}$	100	$2.1 \cdot 10^{-11}$	$6.2 \cdot 10^{-9}$
Nb	3.19	$2.6 \cdot 10^{-5}$	1	$3.4 \cdot 10^{-8}$	$1.0 \cdot 10^{-6}$
Ni	24.3	$3.2 \cdot 10^{-4}$	0.1	$1.3 \cdot 10^{-6}$	$1.0 \cdot 10^{-7}$
Np(IV)	-		100		$9.7 \cdot 10^{-10}$
Pa(V)	-		100		$3.0 \cdot 10^{-4}$
Pb	47.0	$1.7 \cdot 10^{-4}$	3	$7.6 \cdot 10^{-8}$	$6.3 \cdot 10^{-10}$
Po(IV)	-		0		$9.9 \cdot 10^{-8}$
Pu(IV)	-		100		$2.4 \cdot 10^{-12}$
Ra	-		$5.0 \cdot 10^{-2}$		$8.3 \cdot 10^{-6}$
Sn	3.47	$2.2 \cdot 10^{-5}$	20	$1.5 \cdot 10^{-9}$	$5.4 \cdot 10^{-7}$
Sr	1,576.0	$1.4 \cdot 10^{-2}$	$1.0 \cdot 10^{-2}$	$1.7 \cdot 10^{-3}$	$1.2 \cdot 10^{-3}$
Th	3.34	$1.1 \cdot 10^{-5}$	100	$1.4 \cdot 10^{-10}$	$1.2 \cdot 10^{-9}$
Ti	684.2	$1.1 \cdot 10^{-2}$	10	$1.4 \cdot 10^{-6}$	$5.6 \cdot 10^{-5}$
U(IV)	3.84	$1.2 \cdot 10^{-5}$	100	$1.6 \cdot 10^{-10}$	$4.4 \cdot 10^{-9}$
Zr	46.8	$4.0 \cdot 10^{-4}$	10	$5.1 \cdot 10^{-8}$	$3.1 \cdot 10^{-9}$

* Estimated uncertainty: ± 10%

** The concentration of stable elements in HCP was estimated as follows: 1 kg unhydrated cement is mixed with 0.4 kg water (w/c = 0.4). 75% of the water is bound by cement phases during hydration, which results in a total mass of 1.3 kg HCP (density ~ 2.2 g/cm^3) and 0.1 kg free water (porosity ~ 20%).

*** Distribution ratios (R_d) were taken from Tab. 7-1 assuming DS-II, reducing conditions. For Eu(III), the same R_d value as for Ho(III) and the trivalent actinides is taken.

**** Values correspond to those in Tab. B-3 except for Ni, which is based on the Ni concentration used for- the "shared solubility" calculations (Tab. 4-2). The solubility of Ra was determined in equilibrium with $(Ba,Ra)SO_4$ solid solution at $1 \cdot 10^{-6}$ mol Ra added per 1 dm^3 of concrete (0.107 dm^3 of cement porewater).

On the other hand, the maximum loadings of the radionuclides were estimated based on maximum porewater concentration controlled by solubility limitation in the near-field of the L/ILW repository (Tab. B-3) for those cases where the content of the stable isotope in cement was not reported (Tab. B-3, second column). The solubility limits of all dose-relevant radionuclides were taken from Hummel et al. (2022). Note that Hummel et al. (2022) assumed a cement porosity of 10 vol.-% for their solubility calculations, whereas for the calculations of the cement porewater compositions carried out in the framework of this SDB, a cement porosity of 20 vol.-% was assumed. Thermodynamic solubility calculations carried out assuming 20 vol.-% porosity showed that the influence of this difference in porosity on the radionuclide solubilities is negligible (Kulik, Pers. Comm). The solubility limits of all dose-relevant radionuclides, along with those of Fe(II, III) controlled by solubility limitation in the cementitious near-field, are listed in Tab. B-3.

For some of the stable isotopes in cement, the content is known, while information on the content of stable isotopes in other near-field components (e.g., waste materials) is often lacking. It was noted that HCP is an important source of stable elements in the cementitious near-field. Minor and trace elements are introduced to cement during clinker production by the raw materials used. Portland cements are ordinarily manufactured by heating raw mixes including limestone and clay, or materials with similar bulk composition and reactivity, ultimately to a temperature of about 1,450 °C. Non-volatile impurity elements inherently associated with the raw materials are accommodated in the clinker minerals, i.e., the products obtained through heat treatment. The impurity elements are then released by the dissolution of the clinker minerals and distributed among liquid and solid phases during cement hydration. The impurity elements inherently associated with the unhydrated cement determine their background inventory in the aqueous and solid phases of hydrated cements. Thus, hydrated cement is considered to be an important, maybe even the main source, of the majority of the impurity elements in the cementitious near-field of an L/ILW repository. For a few elements, such as Fe, Mn, Mo, Ni, and Cr, steel might be the main source due to their high concentrations in this material.

During the hydration process, the impurity elements are taken up by the structure of the cement phases of the hydrate assemblage or they may adsorb onto the surface of these phases. In contact with water, the elements associated with the hydrate assemblage of HCP are released to solution as a result of desorption from the surface or the interlayers of the cement phases, or as a result of the dissolution of small portions of the cement phases under non-equilibrium conditions. Hence, an aqueous solution in contact with HCP can contain significant concentrations of the impurity elements governed by the partitioning of the element between the liquid and solid phases.

The content of stable isotopes in unhydrated cement as listed in Tab. B-2 (second column) has been taken from Wieland (2014). These impurity elements are present at different concentration levels in unhydrated cement. For example, concentrations above 100 ppm (µg/g) were determined only for a few elements such as Sr and Ti. Most elements, however, are present at concentrations ranging between 1 and 100 ppm, while the concentration of a few elements (Eu, Ho) is even below 1 ppm, including, in particular, the rare earth elements. Furthermore, it is expected that the concentration of volatile elements, such as Hg, is negligibly small. The concentration of the elements in HCP was estimated by assuming that unhydrated cement is mixed with water at a w/c ratio of 0.4 to prepare the cement paste and, further, that 75% of the water is bound in HCP after hydration. As a consequence of this, the concentrations in hydrated cement are ~ 30% lower than reported for unhydrated cement (Tab. B-2, third column).

For the current assessment of sorption competition, it is further assumed that the partitioning of the stable isotopes between cement and porewater occurs according to the distribution ratios (R_d values) previously selected for the elements of interest. The R_d values have been taken from Tab. 7-1 on the assumption of reducing conditions in DS-II. The porewater concentration of each element was calculated with the help of the HCP concentrations and the R_d values listed in Tab. B-2 (column five).

Tab. B-3: Maximum aqueous concentrations of the elements in cementitious environments at pH 12.5 based on solubility limits calculated by taking into account the CPW composition under anoxic conditions in DS-II

Hummel et al. (2022)

Element	Maximum conc. [mol/L]	Element	Maximum conc. [mol/L]
Fe(II)*	$1.0 \cdot 10^{-7}/1.0 \cdot 10^{-3}$	Np(III,IV)	$9.7 \cdot 10^{-10}$
Fe(III)*	$1.0 \cdot 10^{-7}/1.0 \cdot 10^{-6}$	Pa(V)	$3.0 \cdot 10^{-4}$
Ac	$7.9 \cdot 10^{-11}$	Pb	$6.3 \cdot 10^{-10}$
Ag	$3.9 \cdot 10^{-7}$	Po(IV)	$9.9 \cdot 10^{-8}$
Am	$5.2 \cdot 10^{-10}$	Pu(III,IV)	$2.4 \cdot 10^{-12}$
Cm	$1.0 \cdot 10^{-9}$	Ra	$8.3 \cdot 10^{-6}$
Cs	Unlimited	Sn	$5.4 \cdot 10^{-7}$
Eu	$5.8 \cdot 10^{-9}$	Sr	$1.2 \cdot 10^{-3}$
Hg	$3.4 \cdot 10^{-7}$	Th	$1.2 \cdot 10^{-9}$
Ho	$6.2 \cdot 10^{-9}$	Ti	$5.6 \cdot 10^{-5}$
Nb	$1.0 \cdot 10^{-6}$	U(IV)	$4.4 \cdot 10^{-9}$
Ni	$5.7 \cdot 10^{-6}$	Zr	$3.1 \cdot 10^{-9}$

* The first value is assumed as an upper limit based on the modelling by Hummel et al. (2022) and Wersin et al. (2003). The second value is derived from sorption of isotherm measurements on C-S-H phases.

For some elements listed in Tab. B-2 such as Ag, however, the inventories of the stable isotopes in cement are not available, or some elements are not even present in pristine cement, such as most actinides. For those elements, we alternatively used porewater concentrations based on reported solubility limits in a cementitious environment (CPW with pH 12.5) (Tab. B-3 and Tab. B-2).

A comparison of the porewater concentrations estimated from elemental inventories in HCP and solubility limits (Tab. B-2, fifth and last column) shows that the aqueous concentrations estimated from the former are generally lower than the ones estimated from solubility limits, with the exception of Zr.

ii.) Estimate of maximum loadings of metal cations on HCP

The maximum loadings of the radionuclide on HCP were calculated based on the following equations:

Initial inventory per metre of cavern: $n_t = M_{Cem} \cdot c_{HCP}$ [mol/m] (B-1a)

Porewater inventory per metre of cavern: $n_{aq} = V_{sol} \cdot c_{aq}$ [mol/m] (B-1b)

Loading of HCP per metre of cavern: $n_{sorb} = n_t - n_{aq}$ [mol/m] (B-1c)

Partitioning: $R_d = \frac{n_t - n_{aq}}{n_{aq}} \left(\frac{V_{sol}}{M_{Cem}}\right)$ [m³/kg] (B-1d)

V_{sol} and M_{cem} are the near-field parameters listed in Tab. B-1. R_d values are listed in Tab. B-2.

The porewater concentrations listed in Tab. B-2 (column 5) were estimated by combining Eqs. B-1b and B-1d. The elemental loading on HCP results from the difference between total inventory and porewater inventory according to Eq. B-1c divided by M_{cem}. The elemental loadings on C-S-H phases were calculated by considering the wt.% contributions of C-S-H phases to HCP in the three degradation stages listed in Tab. 2-3, i.e., the loading on HCP was multiplied by a factor of 3, 2.8, and 1.5 for DS-I, DS-II and DS-III, respectively (Tab. B-4 to Tab. B-7, column 4). The elemental loading on HCP was estimated by combining Eqs. B-1c and B-1d for those radionuclides for which the porewater concentration was assumed to be controlled by solubility limits. Correction by the above-mentioned factors results in the elemental loadings on C-S-H phases.

The maximum loadings on interlayer and surface sites were estimated in accordance with the preferential sorption of each element as discussed in App. B.6 (Tab. B-4 to Tab. B-7, columns 6 and 7).

Sorption competition was estimated for two scenarios as follows:

Base case: For those elements, for which the porewater concentration could not be estimated on the basis of the impurity element inventory in HCP, the maximum concentrations based on solubility limits were used for the base case of sorption competition for DS-I through DS-III (Tab. B-4 to Tab. B-6).

Upper bound: For an extreme scenario (Tab. B-7), we used the solubility-limited porewater concentrations of all elements, irrespective of their inventory in HCP. It should be noted, however, that the solubility-limited concentration of an element in the porewater is only reached if the inventory of this element is sufficiently large in the cementitious near-field of the L/ILW repository. For example, the inventory of Fe(0) in the L/ILW repository is large due to the presence of metallic waste materials. However, the inventory may be very limited in the L/ILW repository for those elements, which are not associated with specific waste types or whose inventory in the waste is very low, such as the actinides.

The loading of C-S-H phases by dose-relevant radionuclides is assessed using the same approach as for Fe(II,III). For the base case, we estimated the loading of the C-S-H phases by the stable counterpart of a dose-relevant radionuclide on the basis of the partitioning of the element between HCP and CPW (Tab. B-2) or using the solubility-limited concentrations for those elements for which no stable element content has been reported (Tab. B-2, last column, and Tab. B-3). The loadings on C-S-H phases were calculated for DS-I through DS-III. Calculations account for DS-II and reducing conditions take a potential extreme scenario into consideration. The estimated loadings of the C-S-H phases for the base case are listed in Tab. B-4 to Tab. B-6. For the upper bound case, we estimated the loading of C-S-H phases on the assumption that the porewater concentration of all dose-relevant radionuclides is controlled by the solubility limits listed in Tab. B-3). The results of the calculations are listed in Tab. B-7.

The loadings of the C-S-H phases were estimated in accordance with the expected near-field conditions, i.e., $4.02 \cdot 10^4$ kg HCP per metre of cavern length in contact with 29 m^3 porewater per metre of cavern length (Tab. B-1), which corresponds to an S/L ratio of 1,386 kg/m^3. Tab. B-4 to Tab. B-6 show the results for the three stages of cement degradation. Differences in the loadings of C-S-H phases result from the different R_d values of some elements in the three stages, in particular Cs, Np(V), Pa(V), Pb, Pu(VI), Ra, Sr, and U(VI) (Tab. 7-1).

Tabs. B-4 to B-6 show the pronounced effect of Pa(V) on the interlayer loading of C-S-H phases due to its high solubility. The loadings range from ~ 41 to 51 mol/kg in the three stages of cement degradation. It is very unlikely that such a high porewater concentration of $3.4 \cdot 10^{-4}$ mol/L can be achieved in the near-field, as it is expected that the Pa inventory of the waste materials will be too low to reach saturation with the solubility-limiting Pa(V) phase Pa_2O_5. Therefore, it is assumed that the influence of Pa is greatly overestimated in the present assessment of sorption competition, and it is safe to ignore the high interlayer loading caused by Pa(V) sorption.

Neglecting the contribution of Pa(V) leads to total interlayer loadings ranging from 0.02 to 0.08 mol/kg for the best estimate (i.e., low Fe(II, III) loading) and 0.06 to 0.42 mol/kg for the worst case (i.e., high Fe(II,III) loading) in the three stages of cement degradation. The corresponding surface loadings of C-S-H phases are estimated to range in value between 0.03 and 0.05 mol/kg (best estimate) and between 0.11 and 0.20 mol/kg (worst case).

Besides Pa(V), Fe(II) and Fe(III) are important contributors to the surface and interlayer loadings of C-S-H phases (Tabs. B-4 to B-6). In addition, significant contributions arise from Ti for the interlayer loading and from Sr for the surface loading. All other metal cations contribute significantly less to the maximum loadings of interlayer and surface sites. In DS-I and DS-II, Fe(III) is assumed to be preferentially taken up by the interlayer of C-S-H with a C/S ratio ~ 1.6, indicating that Fe(III) is the main competitor for radionuclide uptake by the interlayer. In contrast, Fe(III) is the main competitor for surface sorption in DS-III, which is a consequence of the interpretation of the spectroscopic and ^{29}Si NMR data previously reported by Mancini et al. (2020). These data support the idea that Fe(III) is preferentially taken up by the interlayer of C-S-H phases at C/S ratios ≥ 1.2, while the evidence is that Fe(III) is preferentially surface-bound on C-S-H phase with a C/S ratio of 0.8 and below.

For the upper bound case, we calculated higher loadings for all elements as the porewater concentrations of the elements determined by solubility limits are generally higher than those estimated on the basis of HCP inventories.

In summary, the loadings on C-S-H phases for the base case can be estimated based on the assumption that HCP present in the cementitious near-field is the main source of impurity elements, with the exception of a few elements for which the concentration in the near-field porewater was estimated on the basis of solubility limits. The partitioning of radionuclides between HCP and porewater is expected to occur in the same manner as for the stable counterparts of the radionuclides. The current evaluation of the upper bound values implies that knowledge of the inventory of the stable isotopes of dose-relevant radionuclides in an L/ILW repository is essential as it has consequences on the assessment of sorption reduction by competing metal cations. The availability of elemental inventories suggests that the upper bound case, i.e., porewater concentrations controlled solely by solubility limits, leads to a very conservative assessment of sorption competition. The influence of Pa, in particular, could be greatly overestimated due to its high solubility limit. It should be noted that the upper bound loading of metal cations on the C-S-H phases in DS-II (Tab. B-7) decreases to 1.1 mol/kg instead of 48.4 mol/kg if the loading by Pa(V) is neglected.

Tab. B-4: Loading of C-S-H phases under near-field conditions in DS-I

Element (redox state)	**R_d value*** [m^3/kg HCP]	**Aqueous concentr.**** [mol/L]	**C-S-H loading***** [mol/kg]	**Sorption mode**	**Interlayer sites loading** [mol/kg]	**Surface sites loading** [mol/kg]
Fe(II)	0.05	$10^{-7}/10^{-3}$	$1.5\cdot 10^{-5}/0.15$	50% Int./ 50% Sur.	$7.5 \cdot 10^{-6}/0.075$	$7.5 \cdot 10^{-6}$/ 0.075
Fe(III)	100	$10^{-7}/10^{-6}$	0.03/0.3	Interlayer	0.03/0.3	
Ac	100	$7.9 \cdot 10^{-11}$	$2.4 \cdot 10^{-5}$	Interlayer	$2.4 \cdot 10^{-5}$	
Ag	$1.0 \cdot 10^{-4}$	$3.9 \cdot 10^{-7}$	$1.2 \cdot 10^{-7}$	Surface		$1.2 \cdot 10^{-7}$
Am	100	$5.2 \cdot 10^{-10}$	$1.6 \cdot 10^{-4}$	Interlayer	$1.6 \cdot 10^{-4}$	
Cm	100	$1.0 \cdot 10^{-9}$	$3.0 \cdot 10^{-4}$	Interlayer	$3.0 \cdot 10^{-4}$	
Cs	$5.0 \cdot 10^{-4}$	$8.6 \cdot 10^{-6}$	$1.3 \cdot 10^{-5}$	Surface		$1.3 \cdot 10^{-5}$
Eu	100	$2.6 \cdot 10^{-11}$	$7.9 \cdot 10^{-6}$	Interlayer	$7.9 \cdot 10^{-6}$	
Hg	$1.0 \cdot 10^{-4}$	$3.4 \cdot 10^{-7}$	$1.0 \cdot 10^{-7}$	Surface		$1.0 \cdot 10^{-7}$
Ho	100	$2.1 \cdot 10^{-11}$	$6.4 \cdot 10^{-6}$	Interlayer	$6.4 \cdot 10^{-6}$	
Nb	1	$3.4 \cdot 10^{-8}$	$1.0 \cdot 10^{-4}$	Interlayer	$1.0 \cdot 10^{-4}$	
Ni	0.1	$4.1 \cdot 10^{-6}$	$3.0 \cdot 1\,0^{-5}$	Surface		$3.0 \cdot 10^{-5}$
Np(V)	50	$9.7 \cdot 10^{-10}$	$1.5 \cdot 10^{-4}$	Interlayer	$1.5 \cdot 10^{-4}$	
Np(IV)	100	$9.7 \cdot 10^{-10}$	$2.9 \cdot 10^{-4}$	Interlayer	$2.9 \cdot 10^{-4}$	
Pa(V)	50	$3.0 \cdot 10^{-4}$	45.0	Interlayer	45.0	
Pb	0.5	$4.5 \cdot 10^{-7}$	$6.8 \cdot 10^{-4}$	Surface		$6.8 \cdot 10^{-4}$
Pu(V)	2	$5.0 \cdot 10^{-10}$	$3.0 \cdot 10^{-6}$	Interlayer	$3.0 \cdot 10^{-6}$	
Pu(IV)	100	$2.4 \cdot 10^{-12}$	$7.2 \cdot 10^{-7}$	Interlayer	$7.2 \cdot 10^{-7}$	
Ra	0.5	$8.3 \cdot 10^{-6}$	$1.25 \cdot 10^{-2}$	Surface		$1.25 \cdot 10^{-2}$
Sn	10	$2.9 \cdot 10^{-9}$	$8.8 \cdot 10^{-5}$	Interlayer	$8.8 \cdot 10^{-5}$	
Sr	0.1	$1.8 \cdot 10^{-4}$	$5.4 \cdot 10^{-2}$	Surface		$5.4 \cdot 10^{-2}$
Th	100	$1.4 \cdot 10^{-10}$	$4.3 \cdot 10^{-5}$	Interlayer	$4.3 \cdot 10^{-5}$	
Ti	10	$1.4 \cdot 10^{-6}$	$4.3 \cdot 10^{-2}$	Interlayer	$4.3 \cdot 10^{-2}$	
U(IV)	100	$1.6 \cdot 10^{-10}$	$4.8 \cdot 10^{-5}$	Interlayer	$4.8 \cdot 10^{-5}$	
U(VI)	2	$8.1 \cdot 10^{-9}$	$4.8 \cdot 10^{-5}$	Interlayer	$4.8 \cdot 10^{-5}$	
Zr	10	$5.1 \cdot 10^{-8}$	$1.5 \cdot 10^{-3}$	Interlayer	$1.5 \cdot 10^{-3}$	
Total			45.2/45.6		45.1/45.5	0.07/0.14

* R_d values relate to HCP as reported in Tab. 7-1 except for Ni, which is based on Missana et al. (2022).

** Porewater concentrations were calculated based on inventory (Tab. B-2) and R_d values from Tab. 7-1, or solubility-limited porewater concentrations when inventory is not known.

*** C-S-H loading was calculated on the basis of 33.3 wt.% C-S-H in HCP (see Section 2.2, Tab. 2-3).

Tab. B-5: Loading of C-S-H phases under near-field conditions in DS-II

Element (redox state)	**R_d value*** [m^3/kg HCP]	**Aqueous concentr.**** [mol/L]	**C-S-H loading** [mol/kg]	**Sorption mode**	**Interlayer sites loading** [mol/kg]	**Surface sites loading** [mol/kg]
Fe(II)	0.05	$10^{-7}/10^{-3}$	$1.4 \cdot 10^{-5}/0.14$	50% Int./ 50% Sur.	$7.0 \cdot 10^{-6}/0.07$	$7.0 \cdot 10^{-6}/0.07$
Fe(III)	100	$10^{-7}/10^{-6}$	0.03/0.27	Interlayer	0.03/0.27	
Ac	100	$7.9 \cdot 10^{-11}$	$2.2 \cdot 10^{-5}$	Interlayer	$2.2 \cdot 10^{-5}$	
Ag	$1.0 \cdot 10^{-4}$	$3.9 \cdot 10^{-7}$	$1.1 \cdot 10^{-7}$	Surface		$1.1 \cdot 10^{-7}$
Am	100	$5.2 \cdot 10^{-10}$	$1.4 \cdot 10^{-4}$	Interlayer	$1.4 \cdot 10^{-4}$	
Cm	100	$1.0 \cdot 10^{-9}$	$2.7 \cdot 10^{-4}$	Interlayer	$2.7 \cdot 10^{-4}$	
Cs	10^{-3}	$5.9 \cdot 10^{-6}$	$1.6 \cdot 10^{-5}$	Surface		$1.6 \cdot 10^{-5}$
Eu	100	$2.6 \cdot 10^{-11}$	$7.2 \cdot 10^{-6}$	Interlayer	$7.2 \cdot 10^{-6}$	
Hg	$1.0 \cdot 10^{-4}$	$3.4 \cdot 10^{-7}$	$9.3 \cdot 10^{-8}$	Surface		$9.3 \cdot 10^{-8}$
Ho	100	$2.1 \cdot 10^{-11}$	$5.8 \cdot 10^{-6}$	Interlayer	$5.8 \cdot 10^{-6}$	
Nb	1	$3.4 \cdot 10^{-8}$	$9.4 \cdot 10^{-5}$	Interlayer	$9.4 \cdot 10^{-5}$	
Ni	0.1	$4.1 \cdot 10^{-6}$	$2.7 \cdot 10^{-5}$	Surface		$2.7 \cdot 10^{-5}$
Np(V)	50	$9.7 \cdot 10^{-10}$	$1.3 \cdot 10^{-4}$	Interlayer	$1.3 \cdot 10^{-4}$	
Np(IV)	100	$9.7 \cdot 10^{-10}$	$2.6 \cdot 10^{-4}$	Interlayer	$2.6 \cdot 10^{-4}$	
Pa(V)	50	$2.4 \cdot 10^{-4}$	32.7	Interlayer	32.7	
Pb	3	$7.6 \cdot 10^{-8}$	$5.2 \cdot 10^{-6}$	Surface		$5.2 \cdot 10^{-6}$
Pu(V)	20	$5.0 \cdot 10^{-10}$	$2.7 \cdot 10^{-5}$	Interlayer	$2.7 \cdot 10^{-5}$	
Pu(IV)	100	$2.4 \cdot 10^{-12}$	$6.5 \cdot 10^{-7}$	Interlayer	$6.5 \cdot 10^{-7}$	
Ra	0.05	$8.3 \cdot 10^{-6}$	$1.3 \cdot 10^{-3}$	Surface		$1.3 \cdot 10^{-3}$
Sn	20	$1.5 \cdot 10^{-9}$	$8.0 \cdot 10^{-5}$	Interlayer	$8.0 \cdot 10^{-5}$	
Sr	0.01	$1.7 \cdot 10^{-3}$	$4.6 \cdot 10^{-2}$	Surface		$4.6 \cdot 10^{-2}$
Th	100	$1.4 \cdot 10^{-10}$	$3.9 \cdot 10^{-5}$	Interlayer	$3.9 \cdot 10^{-5}$	
Ti	10	$1.4 \cdot 10^{-6}$	$3.9 \cdot 10^{-2}$	Interlayer	$3.9 \cdot 10^{-2}$	
U(IV)	100	$1.6 \cdot 10^{-10}$	$4.4 \cdot 10^{-5}$	Interlayer	$4.4 \cdot 10^{-5}$	
U(VI)	20	$8.1 \cdot 10^{-10}$	$4.4 \cdot 10^{-5}$	Interlayer	$4.4 \cdot 10^{-5}$	
Zr	10	$5.1 \cdot 10^{-8}$	$1.4 \cdot 10^{-3}$	Interlayer	$1.4 \cdot 10^{-3}$	
Total			33.2/32.8		33.1/32.8	0.05/0.12

* R_d values relate to HCP as reported in Tab. 7-1 except for Ni, which is based on Missana et al. (2022).

** Porewater concentrations were calculated based on inventory (Tab. B-2) and R_d values from Tab. 7-1, or solubility-limited porewater concentrations when inventory is not known.

*** C-S-H loading was calculated on the basis of 36.7 wt.% C-S-H in HCP.

Tab. B-6: Loading of C-S-H phases under near-field conditions in DS-III

Element (redox state)	**R_d value*** [m^3/kg HCP]	**Aqueous concentr.**** [mol/L]	**C-S-H loading***** [mol/kg]	**Sorption mode**	**Interlayer sites loading** [mol/kg]	**Surface sites loading** [mol/kg]
Fe(II)	0.05	$10^{-7}/10^{-3}$	$7.4 \cdot 10^{-6}/0.074$	50% Int./ 50% Sur.	$3.7 \cdot 10^{-6}/0.037$	$3.7 \cdot 10^{-6}/0.037$
Fe(III)	100	$10^{-7}/10^{-6}$	0.015/0.15	Interlayer		0.015/0.15
Ac	100	$7.9 \cdot 10^{-11}$	$1.2 \cdot 10^{-5}$	Interlayer	$1.2 \cdot 10^{-5}$	
Ag	$1.0 \cdot 10^{-4}$	$3.9 \cdot 10^{-7}$	$5.8 \cdot 10^{-8}$	Surface		$5.8 \cdot 10^{-8}$
Am	100	$5.2 \cdot 10^{-10}$	$7.7 \cdot 10^{-5}$	Interlayer	$7.7 \cdot 10^{-5}$	
Cm	100	$1.0 \cdot 10^{-9}$	$1.5 \cdot 10^{-4}$	Interlayer	$1.5 \cdot 10^{-4}$	
Cs	$5.0 \cdot 10^{-4}$	$8.6 \cdot 10^{-6}$	$6.4 \cdot 10^{-6}$	Surface		$6.4 \cdot 10^{-6}$
Eu	100	$2.6 \cdot 10^{-11}$	$3.9 \cdot 10^{-6}$	Interlayer	$3.9 \cdot 10^{-6}$	
Hg	$1.0 \cdot 10^{-4}$	$3.4 \cdot 10^{-7}$	$5.0 \cdot 10^{-8}$	Surface		$4.3 \cdot 10^{-8}$
Ho	100	$2.1 \cdot 10^{-11}$	$3.1 \cdot 10^{-6}$	Interlayer	$3.1 \cdot 10^{-6}$	
Nb	1	$3.4 \cdot 10^{-8}$	$5.1 \cdot 10^{-5}$	Interlayer	$5.1 \cdot 10^{-5}$	
Ni	4.2	$9.9 \cdot 10^{-8}$	$6.1 \cdot 10^{-4}$	Surface		$6.1 \cdot 10^{-4}$
Np(V)	100	$9.7 \cdot 10^{-10}$	$1.4 \cdot 10^{-4}$	Interlayer	$1.4 \cdot 10^{-4}$	
Np(IV)	100	$9.7 \cdot 10^{-10}$	$1.4 \cdot 10^{-4}$	Interlayer	$1.4 \cdot 10^{-4}$	
Pa	100	$3.0 \cdot 10^{-4}$	44.4	Interlayer	44.4	
Pb	30	$7.5 \cdot 10^{-9}$	$2.8 \cdot 10^{-5}$	Surface		$2.8 \cdot 10^{-5}$
Pu(V)	100	$5.0 \cdot 10^{-10}$	$7.4 \cdot 10^{-5}$	Interlayer	$7.4 \cdot 10^{-5}$	
Pu(IV)	100	$2.1 \cdot 10^{-12}$	$3.1 \cdot 10^{-7}$	Interlayer	$3.1 \cdot 10^{-7}$	
Ra	0.1	$8.3 \cdot 10^{-6}$	$1.2 \cdot 10^{-3}$	Surface		$1.2 \cdot 10^{-3}$
Sn	20	$1.5 \cdot 10^{-9}$	$4.3 \cdot 10^{-5}$	Interlayer	$4.3 \cdot 10^{-5}$	
Sr	$1.0 \cdot 10^{-3}$	$1.1 \cdot 10^{-2}$	$1.7 \cdot 10^{-2}$	Surface		$1.7 \cdot 10^{-2}$
Th	100	$1.4 \cdot 10^{-10}$	$2.1 \cdot 10^{-5}$	Interlayer	$2.1 \cdot 10^{-5}$	
Ti	10	$1.4 \cdot 10^{-6}$	$2.1 \cdot 10^{-2}$	Interlayer	$2.1 \cdot 10^{-2}$	
U(IV)	100	$1.6 \cdot 10^{-10}$	$2.4 \cdot 10^{-5}$	Interlayer	$2.4 \cdot 10^{-5}$	
U(VI)	100	$1.6 \cdot 10^{-10}$	$2.4 \cdot 10^{-5}$	Interlayer	$2.4 \cdot 10^{-5}$	
Zr	10	$5.1 \cdot 10^{-8}$	$7.6 \cdot 10^{-4}$	Interlayer	$7.6 \cdot 10^{-5}$	
Total			44.5/44.7		44.5/44.5	0.03/0.2

* R_d values relate to HCP as reported in Tab. 7-1 except for Ni, which is based on Missana et al. (2022).

** Porewater concentrations were calculated based on inventory (Tab. B-2) and R_d values from Tab. 7-1, or solubility-limited porewater concentrations when inventory is not known.

*** C-S-H loading was calculated on the basis of 67.5 wt.% C-S-H in HCP.

Tab. B-7: Upper bound of the loading of C-S-H phases under near-field conditions in DS-II

Element (redox state)	**R_d value*** [m^3/kg HCP]	**Aqueous concentr.** ** [mol/L]	**C-S-H loading***** [mol/kg]	**Sorption mode**	**Interlayer sites loading** [mol/kg]	**Surface sites loading** [mol/kg]
Fe(II)	0.05	$1.0 \cdot 10^{-3}$	0.14	50% Interl./ 50% Surf.	0.07	0.07
Fe(III)	100	$1.0 \cdot 10^{-6}$	0.27	Interlayer	0.27	
Ac	100	$7.9 \cdot 10^{-11}$	$2.1 \cdot 10^{-5}$	Interlayer	$5.5 \cdot 10^{-3}$	
Ag	$1.0 \cdot 10^{-4}$	$3.9 \cdot 10^{-7}$	$1.5 \cdot 10^{-7}$	Surface		$1.5 \cdot 10^{-7}$
Am	100	$5.2 \cdot 10^{-10}$	$1.4 \cdot 10^{-4}$	Interlayer	$1.4 \cdot 10^{-4}$	
Cm	100	$1.0 \cdot 10^{-9}$	$2.7 \cdot 10^{-4}$	Interlayer	$2.7 \cdot 10^{-4}$	
Cs	$1.0 \cdot 10^{-3}$	$1.0 \cdot 10^{-5}$	$2.7 \cdot 10^{-5}$	Surface		$2.7 \cdot 10^{-5}$
Eu	100	$5.8 \cdot 10^{-9}$	$1.5 \cdot 10^{-3}$	Interlayer	$1.5 \cdot 10^{-3}$	
Hg	$1.0 \cdot 10^{-4}$	$3.4 \cdot 10^{-7}$	$1.3 \cdot 10^{-7}$	Surface		$1.3 \cdot 10^{-7}$
Ho	100	$6.2 \cdot 10^{-9}$	$1.7 \cdot 10^{-3}$	Interlayer	$1.7 \cdot 10^{-3}$	
Nb	1	$1.0 \cdot 10^{-6}$	$2.8 \cdot 10^{-3}$	Interlayer	$2.8 \cdot 10^{-3}$	
Ni	0.1	$5.7 \cdot 10^{-6}$	$1.5 \cdot 10^{-3}$	Surface		$1.5 \cdot 10^{-3}$
Np(V)	50	$9.7 \cdot 10^{-10}$	$1.32 \cdot 10^{-4}$	Interlayer	$1.32 \cdot 10^{-4}$	
Np(IV)	100	$9.7 \cdot 10^{-10}$	$2.6 \cdot 10^{-4}$	Interlayer	$2.6 \cdot 10^{-4}$	
Pa	50	$3.0 \cdot 10^{-4}$	46.3	Interlayer	46.3	
Pb	3	$6.3 \cdot 10^{-10}$	$5.5 \cdot 10^{-6}$	Surface		$5.5 \cdot 10^{-6}$
Pu(V)	20	$2.4 \cdot 10^{-12}$	$1.3 \cdot 10^{-7}$	Interlayer	$1.3 \cdot 10^{-7}$	
Pu(IV)	100	$2.4 \cdot 10^{-12}$	$6.3 \cdot 10^{-7}$	Interlayer	$6.3 \cdot 10^{-7}$	
Ra	0.05	$8.3 \cdot 10^{-6}$	$1.1 \cdot 10^{-3}$	Surface		$1.1 \cdot 10^{-3}$
Sn	20	$5.4 \cdot 10^{-7}$	$2.9 \cdot 10^{-2}$	Interlayer	$2.9 \cdot 10^{-2}$	
Sr	0.01	$1.2 \cdot 10^{-3}$	$3.3 \cdot 10^{-2}$	Surface		$3.3 \cdot 10^{-2}$
Th	100	$1.2 \cdot 10^{-9}$	$3.3 \cdot 10^{-4}$	Interlayer	$3.3 \cdot 10^{-4}$	
Ti	10	$5.6 \cdot 10^{-5}$	1.53	Interlayer	1.53	
U(IV)	100	$4.4 \cdot 10^{-9}$	$1.2 \cdot 10^{-3}$	Interlayer	$1.2 \cdot 10^{-3}$	
U(VI)	20	$1.0 \cdot 10^{-5}$	0.54	Interlayer	0.54	
Zr	10	$3.1 \cdot 10^{-9}$	$8.4 \cdot 10^{-5}$	Interlayer	$8.4 \cdot 10^{-5}$	
Total			48.4		48.2	0.2

* R_d values relate to HCP as reported in Tab. 7-1 except for Ni, which is based on Missana et al. (2022).

** Porewater concentrations were calculated based on inventory (Tab. B-2) and R_d values from Tab. 7-1, or solubility-limited porewater concentrations when inventory is not known.

*** C-S-H loading was calculated on the basis of 36.7 wt.% C-S-H in HCP.

B.8 Comparison of elemental loadings and sorption capacity on C-S-H phases

For an appraisal of sorption competition, the estimates for the maximum loadings of interlayer and surface sites of C-S-H phases have to be compared with the maximum sorption capacity of the two different sites on C-S-H phases.

i.) Estimate of the sorption capacity of C-S-H phases

The structure of tobermorite is used as an example to illustrate structural aspects of sorption competition. The "Dreierketten" structure of tobermorite, which has a low C/S ratio, consists of non-bridging silica tetrahedra connected by bridging silica tetrahedral (Fig. B-1b). The Si in each non-bridging silicate tetrahedron shares all its oxygen atoms with other Si ions or with Ca in the octahedral plane. The Si in the bridging silica tetrahedra, however, have two unshared oxygen atoms neutralised by H^+, thus forming a ($\equiv$Si-$(OH)_2$ group). Furthermore, the silicate end-groups, i.e., silicates connected to only one other silicate group ($Si[Q^1]$), also carry an unshared oxygen atom. With increasing pH, the silandiol groups in the interlayers and the silanol end-groups at the edges become dissociated and form potential sorption sites for Ca^{2+} or other cations (Richardson 2004). With an increase of the C/S ratio, the bridging silica tetrahedra are removed from the "Dreierketten" structure, resulting in the formation of additional $Si[Q^1]$ groups on the remaining non-bridging silica tetrahedra, which carry one unshared oxygen atom. In terms of negatively charged sites, an increase in the C/S ratio results in the replacement of a silandiol site carrying two unshared oxygen atoms with two silanol sites that each carry one unshared oxygen atom.

Synchrotron-based spectroscopic studies showed that the local coordination environment of cations sorbing in the C-S-H interlayer is typically characterised by the presence of three (high C/S ratio) to five (low C/S ratio) neighbouring Si atoms from the silica tetrahedral chains forming the C-S-H interlayer (e.g., Mandaliev et al. 2010, Gaona et al. 2011, Mancini et al. 2020). Hence, three to five Si atoms form one interlayer sorption site (Fig. B-4). The uncertainties on the Si coordination numbers (N_{Si}) in the EXAFS studies is always rather high ($\pm$ 1). For the current estimate of the number of interlayer sorption sites, we therefore assume an average value of $N_{Si} = 4$ irrespective of the C/S ratio. The four Si atoms in the C-S-H structure form one interlayer sorption site.

Synchrotron-based spectroscopic studies further indicated that cations sorbing on the surface of C-S-H phases generally form monodentate bonds to only one silanol site (e.g., Rose et al. 2000, Wieland et al. 2008). Thus, we assume that each surface silanol group forms one potential surface sorption site.

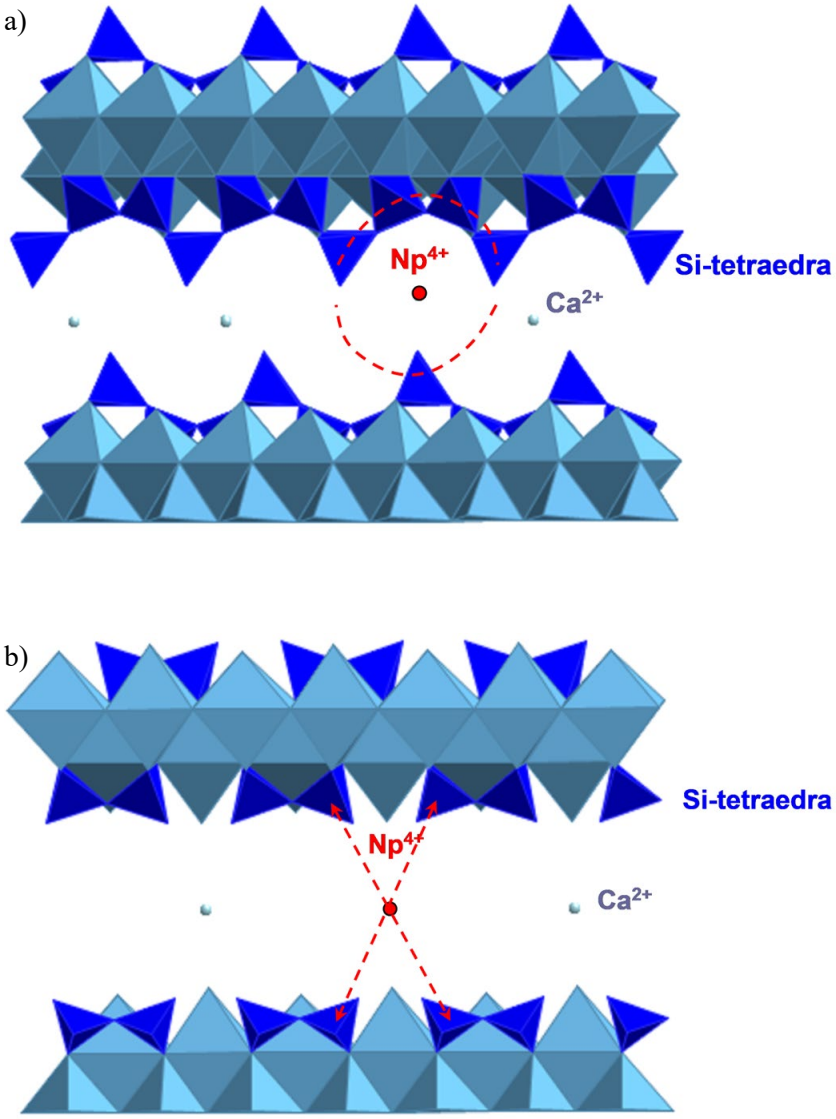

Fig. B-4: Np(IV) sorption into the interlayers of C-S-H phases with low (a) and high (b) C/S ratios

Figure taken from Gaona et al. (2011)

Both the number of interlayer sorption sites and the number of surface sorption sites are related to the amount of silica tetrahedra associated with the C-S-H structure. This value can be calculated from the C-S-H composition, i.e., the CaO, SiO_2 and H_2O contents of the C-S-H phases. This composition is defined by the C/S ratio of the C-S-H phases and varies depending on the cement degradation stage. For the calculation of the composition, we take a C/S of 1.58 (DS-I and DS-II), and a C/S of 0.77 (DS-III). In the case of DS-II and DS-III, the selected C/S ratios correspond to the C-S-H phases at the end of the degradation stage. The H_2O content was quantified in view of the C-S-H structure. Müller et al. (2013) distinguished between interlayer water and gel water in C-S-H phases. Including the gel water, C-S-H phases contain 4 – 6 H_2O molecules per Si atom,

two of which are positioned in the C-S-H interlayer and, depending on the degree of hydration, 2 – 4 are positioned in the gel pores. For the present assessment, we assume 4 moles H_2O per mole C-S-H. The molecular weight of C-S-H phases (m_W) is defined as follows:

$$m_W\text{C-S-H} = (\text{C/S}) \cdot m_W\text{CaO} + m_W\text{SiO}_2 + 4\ m_W\text{H}_2\text{O}\ [\text{kg/mol}] \quad \text{(B-2)}$$

with m_WCaO, $m_W$$SiO_2$ and $m_W$$H_2O$ as the molecular weights of CaO (= 0.05608 kg/mol), SiO_2 (= 0.06009 kg/mol) and H_2O (= 0.01802 kg/mol), respectively. This definition means that one mole C-S-H phase contains one mole Si atoms.

Using Eq. B-2, the m_W values of C-S-H phases with C/S ratios of 1.58 and 0.7 were calculated to be 0.2205 kg/mol and 0.1712 kg/mol, respectively.

The above considerations allowed us to calculate the Si content (c_{Si}) of the C-S-H phases for different C/S ratios:

$$c_{Si} = 1/m_W\text{C-S-H}\ [\text{mol/kg}] \quad \text{(B-3)}$$

Applying Eq. B-3 results in C_{Si} values of 4.54 mol/kg and 5.84 mol/kg, for the C-S-H phases with C/S ratios of 1.58 and 0.70, respectively.

The sorption capacity of the surfaces of C-S-H particles (c_{Si}^{surf}) was estimated based upon the measured surface area after Brunauer et al. (1938) (BET surface area) (~ 148 m^2/g; Tits et al. 2006b) and accepting a density of 4.8 silanol groups per nm^2 previously calculated by Labbez et al. (2006) on the assumption that the C-S-H structure closely resembles the structure of 14-Å tobermorite. This latter value is comparable to the density of surface hydroxyl groups on amorphous SiO_2 (5 sites per nm^2) reported earlier by Schindler (1984). The combination of the silanol surface density with the BET surface area reported by Tits et al. (2006) results in a surface sorption site density per unit mass of 1.2 mol/kg. Note that the sample treatment applied prior to a BET measurement (2 hours under vacuum at 80 °C) can change the C-S-H structure dramatically and thus the BET surface area. Hence, the surface area reported by Tits et al. (2006) and used in this study is taken as a lower bound. This implies that a surface sorption site density per unit mass of 1.2 mol/kg can be used as a lower limit.

The interlayer sorption capacity of C-S-H phases (c_{Si}^{int}) was estimated as follows: the amount of Si-forming interlayer sorption sites (c_{Si}^{int}) was obtained from the difference between the total amount of Si of C-S-H phases (c_{Si}) and the amount of Si-forming surface sorption sites (c_{Si}^{surf}):

$$c_{Si}^{int} = c_{Si} - c_{Si}^{surf}\ \ [\text{mol/kg}] \quad \text{(B-4)}$$

On the assumption that four interlayer Si atoms form one interlayer sorption site, the interlayer sorption capacity was obtained by dividing c_{Si}^{int} by 4. This results in the following interlayer sorption capacities: 0.83 mol/kg (C/S = 1.58) and 1.16 mol/kg (C/S = 0.7). Note that the interlayer sorption capacities estimated above are absolute maximum capacities based on the total number of dissociated silanol and silandiol sites per kg of C-S-H phase. Under real conditions, the maximum sorption capacity could be lower because not every interlayer sorption site might accommodate one radionuclide cation, for example due to steric constraints, charge compensation (electroneutrality), etc.

II.) Comparison

The elemental loadings on C-S-H phases estimated based on the inventories of the stable isotopes and their maximum sorption capacity were compared for the three stages of cement degradation (Tab. B-8). The results show that loadings of all stable isotopes and radionuclides competing for sorption are much higher than the maximum sorption capacity of the C-S-H phases. The reason for this is the extremely high Pa(V) loading caused by the high solubility of Pa(V) under alkaline conditions ($3 \cdot 10^{-4}$ M) along with the high R_d value (40 – 100 m^3/kg) for this element in Tab. 7-1. These high Pa(V) loadings seem very unlikely. Therefore, the table also shows values for the C-S-H loadings in which the contribution of Pa(V) is ignored. The latter, more realistic, values are generally lower than the maximum sorption capacity both of the interlayer and the surface sites in all stages of cement degradation. In the further discussion, only the loadings without the Pa(V) contribution will be considered. In the case of the interlayer sites, the maximum occupancies depend on the scenario considered for Fe(II,III) uptake. Maximum occupancies are as follows: DS-I: 7.8/54.5%, DS-II: 9.1/49.3%, DS-III: ~ 1.4/4.2%. The lower site occupancies in DS-I and DS-II were estimated by assuming that, at best, the Fe(III) concentration reaches 10^{-7} M by solubility limitation. The calculations imply that loading of the interlayer sites by impurity elements is not negligibly small. In the case of the surface sites, less than 20% of the sites are expected to be occupied by metal cations in all degradation stages, predominately to Fe(III) by assuming the higher Fe loadings. However, site occupancy reduces to less than 10% on the assumption that the Fe(III) concentration reaches 10^{-7} M by solubility limitation.

The above findings reveal that structural information on the Fe(II,III) uptake by C-S-H phases and maximum Fe(II,III) loadings on the C-S-H phases are essential with a view to the current assessment of sorption competition. The maximum sorption capacities on the surface of C-S-H phases and in the interlayer are comparable. Thus, it is essential to identify the binding mechanisms of radionuclides on C-S-H phases, i.e., whether or not a metal cation of interest is preferentially bonded to interlayer sites, CaO layer sites or surface sites, respectively.

Tab. B-8: Comparison of C-S-H loadings in the three stages of cement degradation with the maximum sorption capacity of interlayer and surface sites for the base case

	Total sites [mol/kg]	**Interlayer sites** [mol/kg]	**Surface sites** [mol/kg]
Stage I			
Maximum sorption capacity	2.03	0.83	1.2
Estimated loading (Tab. B-4)*	0.2/0.6*	0.1/0.5*	0.07/0.14*
Stage II			
Maximum sorption capacity	2.03	0.83	1.2
Estimated loading (Tab. B-5)*	0.1/0.5*	0.1/0.4*	0.05/0.12*
Stage III			
Maximum sorption capacity	2.36	1.16	1.2
Estimated loading (Tab. B-6)*	0.1/0.3*	0.1/0.1*	0.03/0.2*

* C-S-H loadings neglecting the contribution of Pa(V) (see text) and referring to low (first value) and high (second value) Fe loadings.

In the case of the upper bound estimate, it emerges that the maximum sorption capacities of the interlayer sites are significantly lower than the maximum loadings of metal cations, e.g., compare 48.2 mol/kg (Tab. B-7) with 0.83 – 1.16 mol/kg (Tab. B-8). In the case of the surface sites, the maximum loading is lower than the maximum sorption capacity, e.g., compare 0.2 mol/kg (Tab. B-7) with 1.2 mol/kg (Tab. B-8). However, it should again be noted that the main contributions are related to Pa(V) (40.9 mol/kg) in the case of interlayer loading. The current estimate supports our previous conclusion that a more detailed assessment would be required on the basis of elemental inventories in the near-field. The availability of elemental inventories would allow us to assess the upper bound case with regard to the underlying assumption that the porewater concentration of an impurity element is controlled solely by solubility limits if the elemental inventory is sufficiently large.

B.9 Recommendation for an appraisal of sorption competition in the cementitious near-field of an L/ILW repository

The current appraisal of sorption competition has been based on the assumption that HCP present in the cementitious near-field is the main source of impurity elements ("base case"), with the exception of a few elements for which their content in cement is not known. This assumption implies that the inventories of the impurity elements in waste are much smaller. It should be noted that HCP is the major component of the L/ILW near-field. Therefore, it is anticipated that the partitioning of the impurity elements between HCP and porewater determines the maximum loading of most elements on C-S-H phases. Nevertheless, for some impurity elements, the content in HCP is not known, while they could be present in the waste in significant amounts. For this reason, the maximum concentration in CPW determined by solubility limitation was considered as input parameter for those elements with unknown content in HCP. This approach implies that i) the inventory of an impurity element controlled by solubility is sufficiently large in the near-field in order to actually reach the solubility of the element considered, and ii) a solid phase precipitates above the threshold concentration, which limits the loading on C-S-H phases of the element considered. It should be noted that the above assumption of the maximum concentration of the impurity elements to be controlled by solubility can be expected to contribute a high level of conservatism to the current assessment and increase the safety margin. For example, Tab. B-2 shows that the concentration of the elements calculated on the basis of HCP inventories is, in most cases, much lower than the maximum concentration estimated on the basis of solubility limits (Tab. B-3). For example, the porewater concentration of Cs was estimated to be $5.9 \cdot 10^{-6}$ M on the basis of its content in HCP, while its solubility is not limited under cementitious near-field conditions. Comparison of maximum metal loading with maximum sorption capacities of C-S-H phases shows that the underlying assumptions regarding elemental inventories in the near-field is important for a more refined and more precise appraisal of sorption competition, i.e., by considering impurity elements associated with HCP and the waste.

The current assessment of sorption competition implies the possibility of a sorption competition between dose-relevant radionuclides and Fe(II,III). In particular, Fe(III) at maximum loadings may occupy a significant portion of the interlayer sites or surface sites, respectively, of C-S-H phases. The maximum loading, however, depends on the Fe(III) concentration expected in the porewater of the cementitious near-field. It should be noted that the latter concentration was estimated to be much higher on the basis of laboratory studies (Mancini et al. 2020, 2021) as compared to estimated solubility limits under near-field conditions (Wersin et al. 2003, Hummel et al. 2022). In addition to Fe(II,III), the presence of stable isotopes may also contribute to sorption competition and reduce the uptake of the dose-relevant radionuclides by C-S-H phases. In the current appraisal of sorption competition, HCP is considered as the main source of the stable isotopes of a radionuclide in the cementitious near-field.

The current assessment is further based on a simplified consideration of the sorption capacity for the retention of metal cations in the real cementitious near-field. C-S-H phases are considered as the main sorbent for metals cations, thus neglecting additional sorbents that can be expected in the cementitious near-field, such as iron corrosion products as well as cement phases present in smaller amounts (e.g., hydrotalcite, calcite) and cement alteration products (e.g., zeolites). It should be noted that sorption onto these minerals could reduce the cation loading of the C-S-H phases.

On the basis of the above considerations, we conclude that, for the base case, sorption competition can be neglected as the loading of metal cations does not exceed the maximum sorption capacity of C-S-H phases. However, sorption reduction factors related to sorption competition could be considered for pessimistic scenarios. In this case, a sorption reduction factor of 10 is recommended for all radionuclides preferentially taken up into the interlayer of C-S-H phases. The recommended value is based on expert judgement. The same reduction factor has been assigned to surface-bound radionuclides in DS-III.

The pessimistic value is based on the following appraisal:

- Site occupancies on C-S-H phases by Fe(II,III) could be significant in all stages of cement degradation and irrespective of the C/S ratio of C-S-H phases, which may result in maximum loadings ranging between 10 and 20% of the total sorption capacity of C-S-H phases.
- Impurity elements present in the near-field (stable isotopes) could additionally occupy sorption sites on C-S-H phases.
- Sorption capacities estimated for both surface and interlayer sites are maximum capacities based on the total number of dissociated silanol and silandiol sites per g C-S-H phase. In reality, the maximum sorption capacities could be lower because not every dissociated Si-O- site of C-S-H might accommodate one radionuclide cation. The reasons are steric constraints, charge compensation, etc. This means that sorption sites may have different affinities with regard to metal binding, and subsets of sites may exist.

The sorption reduction factors due to sorption competition are listed in Tab. 7-6.

App. C Influence of EDTA on radionuclide speciation

C.1 Database and code

The calculations of the EDTA "solubility enhancement factors" discussed in Section 6.3.3 were performed with the most recent version of the GEM Software (GEMS, https://gems.web.psi.ch/) using the PSI Chemical Thermodynamic Database 2020 (TDB 2020, Hummel & Thoenen 2023) imported by G.D. Miron into GEMS format and combined with the CEMDATA18 TDB adjusted to TDB 2020 (Lothenbach et al. 2019; https://www.empa.ch/web/s308/cemdata). TDB 2020 contains thermodynamic data for all radionuclides considered in this modelling study, and thus no additional thermodynamic data were needed from other sources.

C.2 Porewater compositions

The solubility calculations were performed in a cement porewater representing cement degradation stage II under reducing conditions (DS-II) (Tab. 2-3).

C.3 Operational approach for deriving "EDTA solubility enhancement factors"

"EDTA solubility enhancement factors" were calculated for a total EDTA concentration of 0.025 M, the maximum concentration in certain waste forms (Tab. 6-1). The calculation procedures followed and the database used for EDTA complexation calculations are described in Hummel et al. (2022). Solubilities were first calculated without EDTA as described in Hummel et al (2022) followed by an "all-in-one" recalculation in the presence of EDTA, meaning that the speciation several radionuclides of interest is calculated in a cement-type porewater in the presence of EDTA (Tab. C-1) (see Hummel et al. 2022 for details on the calculation procedure). The GEMS recipe is described in Tab. C-1. The predefined composition objects (compos) "CEMIPWDS2ZrE20" and "RedoxMtpy" are defined in Tab. C-2 and Tab. C-3.

After calculating the porewater composition without EDTA, 0.048 mol Na_2H_2EDTA were added as described in composition object "CEMIPWDS2ZrE20" (Tab. C-2). To obtain the desired total concentration of 0.025 M EDTA, half the amount introduced in the composition object "CEMIPWDS2ZrE20" was subtracted again in the GEMS recipe described in Tab. C-1.

Reducing conditions were obtained by adding 0.3 g of a magnetite – pyrite FeS_2 redox buffer defined in composition object "RedoxMtPy".

The resulting porewater compositions for selected elements in the absence and presence of 0.025 M EDTA can be found in Tab. 6-3.

Tab. C-1: GEMS recipe of the anoxic all-in-one system in the presence of 0.025 M EDTA

Recipe:	**PW_SGT3:G:DS2ZreSLhAll:21:0:1:25:1:**						
Property	**Compos. name**	**Quantity**	**Units**	**Property**	**Compos name**	**Quantity**	**Units**
xa_	$BaSO_4$	1E-5	Mol	bi_	Cm	3E-9	Mol
xa_	CEMIPWDS2ZrE20	1	Mol	bi_	Cs	1E-9	Mol
xa_	$Ca(OH)_2$	0.1	Mol	bi_	Eu	1E-8	Mol
xa_	HCl	7.72182E-05	Mol	bi_	Hg	3E-6	Mol
xa_	Na_2H_2Edta	-0.0242535	Mol	bi_	Ho	1E-8	Mol
xa_	NaOH	1E-9	Mol	bi_	Nb	1E-6	Mol
xa_	$Ni(OH)_2$	0.1	Mol	bi_	O	0.0045	Mol
xa_	NpO_2	3E-5	Mol	bi_	Pa	0.001	Mol
xa_	PuO_2	1E-6	Mol	bi_	Pb	1E-9	Mol
xa_	RedoxMtPy	0.3	g	bi_	Po	1E-6	Mol
				bi_	Ra	4E-5	Mol
xa_	$SrCO_3$	0.001	Mol	bi_	Sn	1E-6	Mol
xa_	UO_2	0.003	Mol	bi_	Th	1E-8	Mol
bi_	Ac	3E-9	Mol	bi_	Ti	0.001	Mol
bi_	Ag	1E-6	Mol	bi_	Zr	1E-8	Mol
bi_	Am	1E-9	Mol	dul_	$Am(OH)_3$ (cr)	0	Mol

xa_: Compos object quantity to add
bi_: IComp object quantity to add
dul_: Upper on amount of DComp

Tab. C-2: Composition of composition object “CEMIPWDS2ZrE20”

symIC	PCO	Units
Al e	1.55E-05	Mol
Ba e	2.91E-05	Mol
Br e	9.84E-10	Mol
e	1.62E-05	Mol
Ca e	0.06523348	Mol
Cl e	0.1965899	Mol
Edta a	0.04846979	Mol
F e	0.00017399	Mol
Fe e	2.51E-08	Mol
H h	107.3644	Mol
K e	0.06507773	Mol
Mg e	5.45E-09	Mol
Mn e	6.47E-07	Mol
N_atm a	9.98E-10	Mol
Na e	0.2619995	Mol
O o	53.71747	Mol
S e	0.00084123	Mol
Si e	2.63E-05	Mol
Sr e	0.00202777	Mol

Tab. C-3: Composition of composition object “RedoxMtPy” equivalent to 1 mol of magnetite and 1 mol of pyrite

symIC	PCO
Fe e	4
O o	4
S e	2

App. D Cement sorption values for the cement-based near-field for Nagra's safety analysis

Lukas Martin (Nagra), Erich Wieland (CWL Solutions)

D.1 Introduction

D.1.1 Data basis for deriving the cement sorption values

Nagra will consider the sorption of radionuclides in the cement-based near-field in its models as part of the safety analysis (Nagra NTB 24-18 *planned*).

For this purpose, the compositions of cement porewaters and the cementitious materials for cement degradation stages I to III were calculated (see Kosakowski et al. 2023, Appendix A) and used to derive the current cement sorption database (SDB). In addition, based on the derived porewater composition for cement degradation stage II, which is considered to be the most representative stage for the cement-based near-field (see Nagra 2023a), Hummel et al. (2022) calculated the solubility limits for the to be considered dose-relevant radionuclides for safety analysis under oxidising and reducing conditions. The solubility limits derived by Hummel et al. (2022) serve to ensure that the measured concentrations in solution analysed in the cement sorption experiments compiled in this report are related to sorption processes and not to solubility limitations.

Based on the calculated solid phase and porewater compositions in the different cement degradation stages (Kosakowski et al. 2023), cement sorption data were extracted and tabulated for the following conditions:

- sorption values for unperturbed hardened cement paste (HCP) in cement degradation stages I – III under oxidising (oxid.) and reducing (red.) conditions including uncertainty factors for experimental data (Tab. 7-1)
- sorption values for cement degradation stage IV under oxidising (oxid.) and reducing (red.) conditions including uncertainty factors for experimental data (Tab. 7-7) to calculate the "what-if scenario" based on the assumption that the cement is completely degraded in the near-field

The species distribution of the dominating complexes in the aqueous solutions as calculated by Hummel et al. (2022) indicates which redox state dominates for multivalent radionuclides, i.e., whether the radionuclides are present as reduced species, as expected due to the H_2-rich atmosphere in the L/ILW repository (Kosakowski et al. 2023), or whether they occur in a more oxidised state. On this basis, the corresponding sorption value can be selected from Tab. 7-1 for the consequence analysis according to the procedure described below (cf. Sections D.2 and D.3).

In general, it must be assumed that the waste in the cement-based near-field is heterogeneous in composition (Nagra 2023a, Nagra NTB 24-18 *planned*), leading to locally different chemical conditions for the retention of radionuclides. Most radionuclides are retained by sorption on cement minerals or by the low solubilities in the corresponding high-pH environment (Nagra 2023a). However, according to the MIRAM-RBG database (Nagra 2023b), some waste types contain substances (i.e., complexing ligands) that can increase the mobility of radionuclides by complexation. This may result in a sorption reduction of radionuclides by the cement. According to Cloet et al. (2014), Nagra (2023a) and Kosakowski et al. (2023), the most important substances

in terms of their concentration in the porewater of the near-field and their complex-forming properties are:

- isosaccharinic acid (ISA)
- gluconic acid (GLU)
- ethylenediaminetetraacetic acid (EDTA)
- nitriloacetic acid (NTA)
- cyanide
- nitrate/nitrite

To account for the possibility of increased mobility of radionuclides and/or the potentially unfavourable retention of the radionuclides by these substances in the case of increased cement degradation that affects sorption, waste is to be classified into two groups as implemented in the approach presented in Nagra (2023a). For this purpose, the following data were extracted as part of this report:

- sorption reduction factors for the complexation of radionuclides in waste group 1 (WG 1) (Tab. 7-4)
- sorption reduction factors for the complexation of radionuclides in waste group 2 (WG 2) (Tab. 7-5)

In addition, adsorption of radionuclides onto colloids could also increase their mobility, similarly to complexing ligands, which is accounted for by:

- colloid factors considered to account for the mobilisation of radionuclides by colloids (Tab. 7-3).

In Stage 2 of the Sectoral Plan for Deep Geological Repositories, a reference sorption value was only derived for waste groups 1 and 2, as well as an upper guideline value for each (see Nagra 2014, Tab. A3.4-3). However, for the probabilistic analyses for the safety analysis (Nagra NTB 24-18 *planned*), sorption values are to be derived for a reference scenario for waste groups 1 and 2, as well as optimistic and pessimistic sorption values, respectively.

The methodology described in Nagra (2023a) for classifying the waste group and deriving the cement sorption values is based on the so-called mixing tank approach with a homogenised, fully saturated near-field, as also used for the abstraction in the consequence analysis calculations (Nagra NTB 24-18 *planned*). It is to be noted that partially saturated conditions within the L/ILW near-field are expected to dominate for at least about 100,000 years, as shown by Papafotiou et al. (2016), explained in Martin et al. (2023) and documented in Nagra NTB 24-18 (*planned*). However, as robust calculations of chemical thermodynamic equilibrium can only be performed for fully saturated conditions and these conditions represent a conservative abstraction of the conditions within a repository, a full mixing tank is considered for the waste group classification, cement degradation as well as for the derivation of the cement sorption values. In fact, the lack of availability of water within the upper part of the L/ILW caverns (see Fig. 7-4 in Martin et al. 2023, Nagra NTB 24-18 *planned*) limits the mobility of colloids (Martin et al. 2023), the degradation of cement (Kosakowski et al. 2023) and the release of complexing ligands. Therefore, the mobility of radionuclides will be significantly lower, which means that a consequence analysis performed with the cement sorption values derived here can be considered very conservative.

D.1.2 Influence of the composition of C-S-H phases on the sorption behaviour of HCP

Sorption of radionuclides onto cement in the L/ILW near-field is primarily determined by the mineralogy of the HCP. The recalculation of cement mineral equilibria with cement porewaters based on the recently published, revised PSI-Nagra thermodynamic database (Hummel & Thoenen 2023) showed that AFm phases, which were considered particularly responsible for anion sorption in earlier cement SDBs (e.g. Wieland 2014), are not stable in the long term. This is a consequence of new thermodynamic data determined experimentally for iron-containing hydrogarnet. The high thermodynamic stability of this phase (incorporation of Fe and Al) leads to thermodynamic instability of the AFm phases (Al is preferentially bound in hydrogarnet). As a consequence, the C-S-H phases, which are considered to be responsible for cation sorption, are also considered to be responsible for anion sorption. Therefore, the presence of C-S-H phases is particularly decisive for both cation and anion sorption. As indicated in Section 3.3.4, C-S-H phases with a higher Ca/Si molar ratio have a higher anion sorption capacity compared to C-S-H phases with a Ca/Si ratio < 1.1. The reason is that the latter C-S-H phases have a negative surface charge due to negatively charged silanol groups, which strongly reduces anion sorption. If the Ca/Si ratio of the C-S-H phases is > 1.1, Ca^{2+} ions sorb on these negatively charged silanol groups and cause a reversal of the surface charge, i.e., a positive instead of a negative surface charge dominates, which favours anion sorption.

In Nagra (2023a), it is shown that the molar Ca/Si ratio of the calculated cement paste agrees well with that of the C-S-H phases with a Ca/Si ratio of 1.1. For this reason, this criterion was applied as the limit for cement sorption in the waste group allocation (see Nagra 2023a, Section 2.3), which is also consistent with the experimentally determined sorption values in this report.

For cement degradation stage II, the investigated C-S-H has a Ca/Si ratio of ~ 1.5 and for cement degradation stage III, the Ca/Si ratio is 1.1. It should be noted that the differences in the values extracted for degradation stages II and III for the RBG are very small for most radionuclides (see Tab. 7-1). Mostly minor differences occur only for Ca, Al, Si, Sr, Ra, $^{14}CO_3^{2-}$, Mo and Pb. This does not apply to Al, Si and Pb, which show significantly higher sorption in cement degradation stage III.

D.1.3 Complexing ligands

Complexing ligands, i.e., substances that can increase the mobilisation of radionuclides by complex formation after their release from the waste, are present in elevated concentrations in various types of waste binders. In Cloet et al. (2014) and in Nagra (2023a), waste package types have been divided into waste groups 1 and 2 based on concentration limits of complexing ligands in the cement pore solution (see Section 2.4 in Nagra 2023a). For waste in waste group 2 with elevated concentrations of complexing ligands, sorption reduction factors were derived for the corresponding reference sorption values (Tabs. 7-4 and 7-5). It is to be noted that with the update of the PSI-Nagra thermodynamic database (Hummel & Thoenen 2023), quality-checked data for EDTA have been added to the thermodynamic database. Work by DiBlasi et al. (2021) has shown that strong quaternary Ca-Pu(IV)-OH-EDTA complexes could form in cement porewaters, which, according to the calculations by Hummel et al. (2022), could lead to a strong increase in the solubilities of Ni, Np, Pu and U. Based on the assumption that an increase in solubility could also lead to a reduction in sorption of the corresponding radionuclide on HCP, sorption reduction factors corresponding to the increase in solubility were defined. However, it should be noted that this assumption has not yet been verified and may be very conservative. The quaternary complexes for waste group 2 are currently assumed to reduce radionuclide sorption by the inverse factor affecting solubility (factors of 811, 7,800 and 31,900 for Np, Pu and U, respectively). For

this reason, the resulting cement sorption values for waste group 2 used for the pessimistic case in the safety analysis for the RBG (Nagra NTB 24-18 *planned*) are much lower than those previously used in Stage 2 of the Sectoral Plan (Wieland 2014, Nagra 2014).

D.2 Derivation of the sorption values for the cement-based near-field for the safety analysis

D.2.1 Approach

The derivation of the sorption coefficients for the cement-based near-field is based on the broad set of data documented in the present cement SDB, derived through careful analysis and taking into account the specific conditions of the cement-based near-field. These data form the basis for the derivation of the sorption values used in the safety analysis. Chapter 7 presents the databases based on which the sorption values have been calculated:

- The sorption coefficients for cement degradation stages I to III (DS-I to DS-III) for oxidising (ox.) and reducing conditions (red.) are documented in Tab. 7-1.
- Sorption reduction factors for colloids are documented in Tab 7-3.
- Sorption reduction factors for waste group 1 (WG 1) are documented in Tab 7-4.
- Sorption reduction factors for waste group 2 (WG 2) are documented in Tab 7-5.
- Sorption coefficients for cement degradation stage IV are documented in Tab 7-7. These values are used for the "what-if scenario" assuming "no cement sorption present in the near-field".
- Waste group assignments are documented in Nagra (2023a) and in the associated spreadsheet.
- The corresponding valences of radionuclides have been assigned based on the species distributions obtained from the calculations of solubility limits in the cementitious near-field according to Hummel et al. (2022).

The sorption coefficients (R_d^{eff}) were calculated with Eq. D-1 (Eq. 2 in this report):

$$R_d^{eff} = \frac{R_d^0}{F_{Colloid\ sorpt.\ red.fact.} \cdot F_{Complexation\ sorpt.red.fact.} \cdot F_{Sorption\ Comp.red.\ fact.}} \quad \text{(D-1)}$$

R_d^0: Reference sorption value of radionuclides on HCP

$F_{Colloid\ sorpt.red.fact.}$: Factor to account for sorption reduction of radionuclides through the presence of colloids

$F_{Complexation\ sorpt.red.fact.}$: Factor to account for sorption reduction of radionuclides through the presence of complexing ligands

$F_{Sorption\ comp.\ red\ fact.}$: Reduction factor due to possible sorption competition, which can be set to one (= 1), since the sorption capacity of the HCP is not exceeded

For waste group 1, the sorption values were calculated as follows:

- For the reference sorption values, the reference sorption values for DS-II (red.) were selected as initial values (Tab. 7-1) and modified according to Eq. D-1 by taking into account the colloid factors (Tab. 7-3) and the sorption reduction factors for waste group 1 (Tab. 7-4).
- For the optimistic sorption values, the calculated reference sorption values were multiplied with the associated uncertainty factor from Tab. 7-1.
- For the pessimistic sorption values, the reference sorption values for DS-III (red.) were selected as initial values and modified according to Eq. D-1 by taking into account the colloid factors (Tab. 7-3) and the sorption reduction factors for waste group 1 (Tab. 7-4) and finally dividing the result by the uncertainty factors (Tab. 7-1). The lower solubility limits were used for Ni, CO_3^{2-}, Ca, Al and Si (see Section D.4).

For waste group 2, the sorption coefficients were calculated as follows:

- For the reference sorption values, the reference values for DS-II (red.) were chosen as initial values (Tab. 7-1) and modified according to Eq. D-1 by taking into account the colloid factors (Tab. 7-3) and the sorption reduction factors for waste group 2 (Tab. 7-5).
- For the optimistic sorption values, the optimistic sorption values derived for waste group 1 were chosen as initial values and modified according to Eq. D-1 by taking into account the sorption reduction factors for waste group 2 (Tab. 7-5). Note that in the case of the optimistic sorption values for waste group 1, the colloid factors and uncertainty factors have already been considered.
- For the pessimistic sorption values, the reference sorption values for DS-III (red.) were chosen as initial values and modified according to Eq. D-1 by taking into account the colloid factors (Tab. 7-3), the sorption reduction factors for waste group 2 (Tab. 7-5) and finally dividing the result by the uncertainty factors (Tab. 7-1). The lower solubility limits were used for Ni, CO_3^{2-}, Al and Si (see Section D.4).

For the "what-if scenario" (no cement in the near-field; DS-IV), the sorption values were calculated as follows:

- For the optimistic sorption values, the column "Degraded near-field in DS-IV (70 wt.% calcite)" was selected as the initial values from Tab. 7-7 and multiplied with the uncertainty factors (Tab. 7-7).
- For the pessimistic sorption values, the column "Degraded near-field in DS-IV (70 wt.% calcite)" was selected as the initial values from Table 7-7 and divided by the uncertainty factors (Table 7-7).

It should be noted that sorption values assigned to DS-IV do not account for sorption reduction by colloids and complexing ligands.

D.3 Extended assumptions for the derivation of the sorption values

The following extended assumptions were made:

- For U and Pa, the values under oxidising conditions in DS-II (ox.) were used to derive the reference and optimistic values due to the mixed solubilities and speciation reported by Hummel et al. (2022). Under these conditions, U(VI) and Pa(V) are the predominant redox states. For the pessimistic values, the values under reducing conditions in DS-II (red.) were used with the appropriate sorption reduction factors.
- For Al, Si, and Pb, the pessimistic values were calculated for both waste groups using an alternative approach regarding the conservatism of the values. Since for these elements, the initial values for DS-III (red.) were found to be substantially higher than the initial values for DS-II (red.), the pessimistic values were higher than the reference values in each case. Therefore, for the calculation of the pessimistic values, the reference values were divided by the uncertainty factors.
- For Pu, a sorption reduction factor of 1 was used for waste group 1 because all EDTA-containing wastes have been assigned to waste group 2 (see Nagra 2023a).
- For Pa, no experimental and modelled solubility and speciation data are available. Because of the uncertainty regarding the redox state, the initial values assigned to oxidising conditions in DS-II (ox.) were used for conservatism.
- As previously mentioned, there are no EDTA-containing wastes in waste group 1. Therefore, no sorption reduction factors involving EDTA were taken into account in the case of waste group 1. For the other complexing ligands to which sorption reduction factors were assigned, these factors were taken into account accordingly.
- According to Nagra (2023a), GLU is only present in waste package types assigned to waste group 1. For this waste group, sorption reduction by GLU has to be considered only in the case of tetravalent actinides (Th(IV), Np(IV), Pu(IV)). Thus, the corresponding sorption reduction factors for waste group 1 were used. When calculating the optimistic sorption values for waste group 2 from the optimistic sorption values for waste group 1, the sorption reduction due to GLU was not taken into account, since GLU is not present in the binder types of waste group 2.
- In Stage 2 of the Sectoral Plan for Deep Geological Repositories (Nagra 2014), the values for DS-I were chosen for Cl, Cs, and Se because they were lower (more pessimistic) than the values for DS-II. For the RBG, the values for DS-II (red.) are lower (more pessimistic) in the case of Cl and Se and were selected accordingly.
- In the case of Se, for the sake of conservatism, the lowest (pessimistic) sorption values for DS-II were chosen for the reference and optimistic cases, and for the pessimistic case for DS-III, in each case under reducing conditions.
- In Stage 2 of the Sectoral Plan, so-called “shared solubilities” were used for C_{inorg}, Co, and Ni because experimental data did not support the idea of a sorption process on HCP. It was shown that cobalt is not a dose-relevant nuclide, and therefore no values are selected for the RBG. In the case of C_{inorg} and Ni, the values for DS-II (red) are based on a “shared solubility” approach.
- For dissolved organic carbon compounds, the reference R_d value of 0 m^3/kg was set for waste group 1 and waste group 2. For the pessimistic and optimistic case, the following values were selected for both waste groups: pessimistic value $R_d = 0$; optimistic value $R_d = 10^{-3}$ m^3/kg.

D.4 Derivation of lower pessimistic limits for waste groups 1 and 2 based on the solubility calculations of dose-relevant nuclides in the cement porewater

In the case of Ni, CO_3^{2-}, Ca, Al, and Si, whose retention in the cementitious near-field is assumed to be based on "shared solubility", the lowest ranges of solubility limits derived by Hummel et al. (2022) were considered as an alternative approach to determining the lowest sorption values for pessimistic calculation cases for waste groups 1 and 2 (see excerpt from Tab. 4-3 and 4-5 of this report):

Tab. D-1: Estimated R_d values for $^{59,63}Ni$ and $^{14}CO_3^{2-}$ for the three stages of cement degradation in the L/ILW repository (accessibility factors f = 0.1 for $^{59,63}Ni$ and f = 0.01 for $^{14}CO_3^{2-}$)

Alias Tab. 4-3

Radionuclide	**R_d value** [m^3/kg]	
	Best estimate*	**Lower bound****
$^{59,63}Ni$ – all stages	0.41	0.01
$^{14}CO_3^{2-}$		
Stage I	$4.6 \cdot 10^{-1}$ (suboxic)	10^{-1}
Stage II	1.55 (anoxic)	1.0
Stage III	2.04 (anoxic)	1.0

* Estimated with Eq. (3) using the parameters given in Tab. 4-2.
** Estimated based on uncertainty ranges of the parameters.

To ensure that the conservative sorption coefficients for the pessimistic case of the safety analysis are used nonetheless, the calculated sorption coefficients were compared to the lower solubility limits for the elements Ni, CO_3^{2-}, Ca, Al and Si and the lowest values from Tabs. D-1 and D-2 were used (see Tab. D-3).

In the implemented approach to derive the pessimistic sorption values, mostly the sorption values for DS-III (red.) were used and accounted for the sorption reduction by complexing ligands and colloids as well as sorption competition according to Eq. D-1. It should be noted that the calculated sorption reduction factors for EDTA (Tabs. 7-4 and 7-5) are based on the calculated solubility limits reported by Hummel et al. (2022). In case these calculated (pessimistic) values were higher than the reference sorption values, the sorption values for DS-III were divided by the uncertainty factors to estimate the lowest (pessimistic) sorption values.

As previously mentioned, the sorption reduction factors in the presence of EDTA for waste group 2, especially those for the actinides, are associated with a large uncertainty because full sorption reduction is considered, while possible adsorption of the quaternary complexes to cement phases, where Ca is the surface-bound counterpart, is excluded. In this regard, Hummel et al. (2022) writes: "Note that although the mentioned Ca-Pu(IV)-OH-EDTA complex completely dominates the aqueous cementitious Pu system, there is no experimental data yet whether and to what extent this and chemically analogous complexes may sorb to cement solid phases."

Tab. D-2: Estimated operational R_d values for ^{41}Ca, ^{26}Al and ^{32}Si for the three stages of cement degradation in the L/ILW repository (accessibility factor f = 0.1 for all radionuclides)

Alias Tab. 4-5

Radionuclide	R_d value [m^3/kg]	
	Best estimate*	**Lower bound****
^{41}Ca		
Stage I	$3.2 \cdot 10^{-1}$	$1.0 \cdot 10^{-1}$
Stage II	$5.8 \cdot 10^{-2}$	$1.0 \cdot 10^{-2}$
Stage III	$1.0 \cdot 10^{-2}$	$1.0 \cdot 10^{-3}$
^{26}Al		
Stage I	2.5	0.5
Stage II	0.1	0.02
Stage III	45	10
^{32}Si		
Stage I	5.2	1
Stage II	0.2	0.05
Stage III	1.5	0.5

* Estimated with Eq. (3) using the near-field parameters given in Tab. 4-4.
** Estimated based on the uncertainty ranges of the parameters

Tab. D-3: Comparison of the sorption values calculated according to the above procedure (Eq. D-1) or alternatively taking into account the solubility limits in the cement porewater (m^3/kg)

The pessimistic values used are marked in bold.

Element	Waste group 1		Waste group 2	
	Calculated according to Eq. D-1	**Solubility-limited concentrations**	**Calculated according to Eq. D-1**	**Solubility-limited concentrations**
Ni	0.29	**0.01**	0.014	**0.01**
CO_3^{2-}	1.41	**1.0**	1.41	**1.0**
Ca	$7.14 \cdot 10^{-3}$	$\mathbf{1.00 \cdot 10^{-3}}$	$\mathbf{7.14 \cdot 10^{-4}}$	$1.00 \cdot 10^{-3}$
Al	$7.14 \cdot 10^{-2}$	$\mathbf{2.00 \cdot 10^{-2}}$	$7.14 \cdot 10^{-2}$	$\mathbf{2.00 \cdot 10^{-2}}$
Si	0.143	**0.05**	0.143	**0.05**

D.5 Derived sorption values for the safety analysis

The cement sorption values have been calculated according to the approach outlined in Sections D.2 to D.4. The values are listed in Tab. D-4.

Tab. D-4: Extracted sorption values (R_D) for the cementitious near-field for use in the safety analysis

optimistic value (optim.), pessimistic value (pess.)

	Waste group 1			**Waste group 2**			**What-if scenario DS IV**	
m^3/kg	**reference**	**optim.**	**pess.**	**reference**	**optim.**	**pess.**	**optim.**	**pess.**
Ca	$5.80 \cdot 10^{-2}$	$8.12 \cdot 10^{-2}$	$1.00 \cdot 10^{-3}$	$5.80 \cdot 10^{-3}$	$8.12 \cdot 10^{-3}$	$7.14 \cdot 10^{-4}$	$1.16 \cdot 10^{-4}$	$1.06 \cdot 10^{-5}$
Al	0.10	0.14	$2.00 \cdot 10^{-2}$	0.10	0.14	$2.00 \cdot 10^{-2}$	$1.16 \cdot 10^{-4}$	$1.06 \cdot 10^{-5}$
Si	0.20	0.28	0.05	0.20	0.28	0.05	0	0
Cs	$5.00 \cdot 10^{-4}$	$1.65 \cdot 10^{-3}$	$1.52 \cdot 10^{-4}$	$5.00 \cdot 10^{-4}$	$1.65 \cdot 10^{-3}$	$1.52 \cdot 10^{-4}$	0	0
Sr	$1.00 \cdot 10^{-2}$	$1.40 \cdot 10^{-2}$	$7.14 \cdot 10^{-4}$	$1.00 \cdot 10^{-2}$	$1.40 \cdot 10^{-2}$	$7.14 \cdot 10^{-4}$	$1.16 \cdot 10^{-4}$	$1.06 \cdot 10^{-5}$
Ra	$5.00 \cdot 10^{-2}$	$7.00 \cdot 10^{-2}$	$3.57 \cdot 10^{-2}$	$5.00 \cdot 10^{-2}$	$7.00 \cdot 10^{-2}$	$3.57 \cdot 10^{-2}$	$1.16 \cdot 10^{-4}$	$1.06 \cdot 10^{-5}$
$^{14}CO_3^{2-}$	1.60	2.24	1.00	1.60	2.24	1.00	$2.94 \cdot 10^{-3}$	$1.50 \cdot 10^{-3}$
Organics	0	$1.00 \cdot 10^{-3}$	0	0	$1.00 \cdot 10^{-3}$	0	0	0
Cl	$1.00 \cdot 10^{-4}$	$3.30 \cdot 10^{-4}$	$3.03 \cdot 10^{-5}$	$1.00 \cdot 10^{-4}$	$3.30 \cdot 10^{-4}$	$3.03 \cdot 10^{-5}$	0	0
I	$1.00 \cdot 10^{-4}$	$3.30 \cdot 10^{-4}$	$3.03 \cdot 10^{-5}$	$1.00 \cdot 10^{-4}$	$3.30 \cdot 10^{-4}$	$3.03 \cdot 10^{-5}$	0	0
Se	$1.00 \cdot 10^{-4}$	$3.30 \cdot 10^{-4}$	$3.03 \cdot 10^{-5}$	$1.00 \cdot 10^{-4}$	$3.30 \cdot 10^{-4}$	$3.03 \cdot 10^{-5}$	0	0
Mo	$2.50 \cdot 10^{-2}$	$3.50 \cdot 10^{-2}$	$1.43 \cdot 10^{-2}$	$2.50 \cdot 10^{-2}$	$3.50 \cdot 10^{-2}$	$1.43 \cdot 10^{-2}$	0	0
Tc	1.0	1.40	0.71	1.0	1.40	0.71	0	0
Fe	$5.00 \cdot 10^{-2}$	$7.00 \cdot 10^{-2}$	$3.57 \cdot 10^{-2}$	$4.76 \cdot 10^{-4}$	$6.67 \cdot 10^{-4}$	$3.40 \cdot 10^{-4}$	$4.90 \cdot 10^{-4}$	$2.50 \cdot 10^{-4}$
Ni	0.41	0.57	0.01	$2.73 \cdot 10^{-2}$	$3.83 \cdot 10^{-2}$	$4.76 \cdot 10^{-4}$	$4.90 \cdot 10^{-4}$	$2.50 \cdot 10^{-4}$
Ti	9.80	32.35	2.83	0.98	3.24	0.28	$8.33 \cdot 10^{-4}$	$4.25 \cdot 10^{-4}$
Zr	9.80	32.35	2.83	0.98	3.24	0.28	$8.33 \cdot 10^{-4}$	$4.25 \cdot 10^{-4}$
Nb	1.0	1.40	0.71	1.0	1.40	0.71	0	0
Ag	$1.00 \cdot 10^{-4}$	$3.30 \cdot 10^{-4}$	$3.03 \cdot 10^{-5}$	$1.00 \cdot 10^{-4}$	$3.30 \cdot 10^{-4}$	$3.03 \cdot 10^{-5}$	0	0
Hg	$1.00 \cdot 10^{-4}$	$3.30 \cdot 10^{-4}$	$3.03 \cdot 10^{-5}$	$1.00 \cdot 10^{-4}$	$3.30 \cdot 10^{-4}$	$3.03 \cdot 10^{-5}$	0	0
Sn	19.23	63.46	5.41	1.92	6.35	0.54	$3.72 \cdot 10^{-4}$	$1.90 \cdot 10^{-4}$
Pb	3.0	4.20	2.14	0.60	0.84	0.43	$1.96 \cdot 10^{-2}$	0.01
Po	0	0	0	0	0	0	$9.24 \cdot 10^{-5}$	$8.48 \cdot 10^{-6}$
Ho	83.33	275	15.15	$8.25 \cdot 10^{-2}$	$2.72 \cdot 10^{-1}$	$1.49 \cdot 10^{-2}$	$1.27 \cdot 10^{-1}$	$6.50 \cdot 10^{-2}$
Ac	83.33	275	15.15	$8.25 \cdot 10^{-2}$	$2.72 \cdot 10^{-1}$	$1.49 \cdot 10^{-2}$	$1.27 \cdot 10^{-1}$	$6.50 \cdot 10^{-2}$
Th	9.80	32.35	1.52	$4.17 \cdot 10^{-2}$	$1.62 \cdot 10^{-1}$	$7.58 \cdot 10^{-3}$	$4.41 \cdot 10^{-2}$	$2.25 \cdot 10^{-2}$
Pa	44.64	147.32	15.15	4.17	14.73	$7.58 \cdot 10^{-3}$	$4.51 \cdot 10^{-3}$	$2.30 \cdot 10^{-3}$
U	19.23	63.46	15.15	1.67	6.35	$4.59 \cdot 10^{-4}$	$9.31 \cdot 10^{-2}$	$4.75 \cdot 10^{-2}$
Np	9.80	32.35	1.52	$4.17 \cdot 10^{-2}$	$1.62 \cdot 10^{-1}$	$7.58 \cdot 10^{-3}$	$5.39 \cdot 10^{-2}$	$2.75 \cdot 10^{-2}$

Tab. D-4: Cont.

	Waste group 1			Waste group 2			What-if scenario DS IV	
m^3/kg	**reference**	**optim.**	**pess.**	**reference**	**optim.**	**pess.**	**optim.**	**pess.**
Pu	9.80	32.35	1.52	$9.26 \cdot 10^{-3}$	$3.59 \cdot 10^{-2}$	$1.68 \cdot 10^{-3}$	1.96	1.00
Am	83.33	275	15.15	$8.25 \cdot 10^{-2}$	$2.72 \cdot 10^{-1}$	$1.49 \cdot 10^{-2}$	0.98	0.50
Cm	83.33	275	15.15	$8.25 \cdot 10^{-2}$	$2.72 \cdot 10^{-1}$	$1.49 \cdot 10^{-2}$	$8.53 \cdot 10^{-1}$	$4.35 \cdot 10^{-1}$
Cf	83.33	275	15.15	$8.25 \cdot 10^{-2}$	$2.72 \cdot 10^{-1}$	$1.49 \cdot 10^{-2}$	$8.53 \cdot 10^{-1}$	$4.35 \cdot 10^{-1}$